

FLUID FLOW PROBLEMS IN HOT MOLDS FOR INVESTMENT CASTINGS OF THIN SECTIONS AND THE DESIGN IMPACT ON METROLOGICAL PROPERTIES

THESIS SUBMITTED

By

SOUMYAJIT ROY

Index no.-296/21/E

Registration no: 1012112001, Dated: 09/08/2021

DOCTOR OF PHILOSOPHY (ENGINEERING)

Department of Metallurgical and Material Engineering

Faculty of Engineering and Technology

Jadavpur University

Kolkata: 700 032, INDIA

2024

1. Title of the thesis:

**FLUID FLOW PROBLEMS IN HOT MOLDS FOR INVESTMENT CASTINGS
OF THIN SECTIONS AND THE DESIGN IMPACT ON METROLOGICAL
PROPERTIES**

2. Name, Designation & Institution of the Supervisor/s :

Name: Prof. (Dr.) AKSHAY KUMAR PRAMANICK

Designation: Professor

Department: Metallurgical and Material Engineering Department

Institution of the Supervisor: Jadavpur University

3. List of Publication

- I. Negative Shrinkage of Thin-walled Investment Brass Castings, **Soumyajit Roy, Akshay Kumar Pramanick**, Prasanta Kumar Datta, Archives of Foundry Engineering (ISSN 1897-3310, eISSN 2299-2944), Vol.-23, issue 1/2023, 2023, Publisher: The Katowice Branch of the Polish Academy of Sciences, [DOI: 10.24425/afe.2023.144274] (**ESCI**)
- II. Investigation of Dhokra Casting in Light of Modern Engineering Technique, **Soumyajit Roy**, Sourav Debnath, **Akshay Kumar Pramanick**, Prasanta Kumar Datta, Journal of Mines, Metals and Fuels (ISSN:0022-2755), 71(11): 2348-2357; 2023, Publisher: Books & Journals Private Ltd. DOI: 10.18311/jmmf/2023/36037, (**Scopus**)
- III. Precise Filling Time Calculation of Thin-Walled Investment Casting in Hot Mold, Soumyajit Roy, Akshay Kumar Pramanick, Prasanta Kumar Datta, Journal of the Brazilian Society of Mechanical Science and Engineering (ISSN: 16785878), Vol.-42, issue 10, Oct 2020, Springer Nature Publication [doi.org/10.1007/s40430-020- 02634-6](**SCIE**)
- IV. Quality Analysis of Tribal Casting Products by TOPSIS for Different Gating System, **Soumyajit Roy, Akshay Kumar Pramanick**, Prasanta Kumar Datta, IOP Conference Series: Materials Science and Engineering, (ISSN:1757-8981), Vol.-1080,2021, p.-1-5, IOP Publishing Ltd. (doi:10.1088/1757-899X/1080/1/012014) (**Scopus**)
- V. The Effect of Gating System on Quality of Traditional Rural Metal Castings of India, **Soumyajit Roy, Akshay Kumar Pramanick**, Prasanta Kumar Datta, Recent Trends in Industrial and Production Engineering, Print ISBN 978-981-16-3134-4; Online ISBN 978-981-16-3135-1, July 2021, pp-267-278, Lecture Notes in Mechanical Engineering, Book Series, Springer Publication (Doi.org/10.1007/978-981-16-3135-1_27) (**Scopus Book Chapter**)
- VI. Kinetics of liquid metal flow in gating design of investment casting production, **Soumyajit Roy**, Utpal Kumar Maity, **Akshay Kumar Pramanick**, Prasanta Kumar

Datta, Slévárenství (ISSN: 22788719), Issue No 5– 6/2017, pp-149-153, Publisher:
The Association of Czech Foundries

- VII.** The Technology Inherent in Indian Traditional Craft Metal Casting Process, **Soumyajit Roy**, Barun Kumar Das, **Akshay Kumar Pramanick**, Prasanta Kumar Datta, Indian Foundry journal (ISSN: 03795446) Vol.-65, Issue-8, Aug 2019, pp:27-37, The Institute of Indian Foundrymen

4. List of Patents :NIL

5. List of Presentations in National/ International/ Conferences/ Workshops

- I.** Investigation of Ancient Indian Metal Casters through Modern Engineering, **Soumyajit Roy**, **Akshay Kumar Pramanick**, Prasanta Kumar Datta, 1st International Virtual Conference on “Recent Advances in Material Science and Organic Synthesis” (RAMSOS 2021)” Department of Chemistry National Institute of Technology Raipur Raipur, India, 20th - 21st December 2021
- II.** Development of Mold Filling Time for Metal Casting using Kinetic Energy Correction Factor, **Soumyajit Roy**, **Akshay Kumar Pramanick**, Prasanta Kumar Datta, International Conference on Industry 5.0: Revolution, Innovation and Efficiency, Department Of Mechanical Engineering Swami Vivekananda Institute of Science & Technology , Kolkata, 4th & 5th March, 2023, Kolkata,
- III.** The Technology of Ancient Craft Metal Casting Process Of India, **Soumyajit Roy**, **Akshay Kumar Pramanick**, Prasanta Kumar Datta, 4th International ‘Communication in New World’ Congress, 19-21 February 2021, Tokyo, Japan
- IV.** Metrological Analysis Of Thin Walled Hollow Cylindrical Investment Castings For Different Gating System, Soumyajit Roy, Akshay Kumar Pramanick, Prasanta Kumar Datta, 1st International conference of Physics, 17th August, 2021, Ankara, Turkey, Organization: Institute of Economic Development and Social Researches.

“Statement of Originality”

I, **Soumyajit Roy**, registered on **9th August, 2021** do hereby declare that this thesis entitled **“Fluid flow problems in Hot molds for Investment castings of Thin sections and the Design Impact on metrological properties”** contains literature survey and original research work done by the undersigned candidate as part of Doctoral studies.

All information in this thesis have been obtained and presented in accordance with existing academic rules and ethical conduct. I declare that, as required by these rules and conduct, I have fully cited and referred all materials and results that are not original to this work.

I also declare that I have checked this thesis as per the “Policy on Anti Plagiarism, Jadavpur University, 2019”, and the level of similarity as checked by iThenticate software is 6%.

Soumyajit Roy

Signature of Candidate:

Date: *21/03/2024*

Ajmanu/03/24

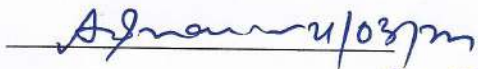
Certified by Supervisor:

Date:

Dr. Akshay Kr. Pramanick
Professor
Department of Metallurgical &
Material Engineering
Jadavpur University, Kolkata-700 032

CERTIFICATE FROM THE SUPERVISOR

This is to certify that the thesis entitled "Fluid flow problems in Hot molds for Investment castings of Thin sections and the Design Impact on metrological properties" submitted by Shri Soumyajit Roy, who got his/her name registered on 9th August, 2021 for the award of Ph.D. (Engineering) degree of Jadavpur University is absolutely based upon his/her own work under the supervision of Prof. (Dr.) Akshay Kumar Pramanick and that neither his/her thesis nor any part of the thesis has been submitted for any degree/diploma or any other academic award anywhere before.



Signature of the Supervisor
and date with Office Seal

Dr. Akshay K. Pramanick
Professor
Department of Metallurgical &
Material Engineering
Jadavpur University, Kolkata-700 032

ACKNOWLEDGEMENT

Completing this PhD thesis has been a profound journey, and I am deeply indebted to the individuals and institutions whose support has been fundamental to this accomplishment.

Foremost, I extend my profound gratitude to Prof. (Dr.) Prasanta Kumar Datta, the pivotal figure in this research, whose invaluable guidance and wisdom has been the cornerstone of my academic journey. My sincere appreciation goes to Prof. (Dr.) Akshay Kumar Pramanick, my supervisor, for his unwavering support, scholarly guidance, and mentorship throughout this research endeavor. His insights have been instrumental in shaping the trajectory of this work.

I extend my gratitude to Prof. (Dr.) Pravash Chandra Chakraborty, HOD of the Metallurgical and Materials Engineering Department at Jadavpur University, and Prof. Gautam Majumdar and Prof. Gautam Nandi from the Mechanical Engineering Department, for fostering an academic environment conducive to research and innovation.

Special thanks to Prof. (Dr.) Pallab Roy (HOD BBIT, Kolkata), Prof. (Dr.) Jhumpa Dey (Professor, AOT, Kolkata), and Mr. Rik Goswami, my childhood teachers and professors, for enduring influence on my intellectual development. To my seniors, Prof. Utpal Maity (Met. and mat. Engg. Dept., Jadavpur University), Barun Kumar Das (JTO (Scientific), Ministry of Defence, GoI), and Prof. Barnali Maji (Met. and mat. Engg. Dept. NIT Durgapur), your mentorship has been inspiring and has significantly contributed to my academic growth.

I appreciate the camaraderie and support from my friends in various capacities - Dr. Subhasis Sarkar (Assistant Engineer, WB Govt.), Prof. Sourav Debnath (Prof., SVIST, Kolkata), Dr. Ujjwal Ghosh (Scholar, Jadavpur University), Mr. Subrata Das (Assistant Manager (P&E), Haldia Post trust, GoI), and Mr. Rupam Mandal (Scholar, Jadavpur University). Your friendship has been a source of strength.

I extend my thanks to the laboratories at Jadavpur University (Metallography Lab and Mechanical testing Lab of Met. and mat. Engg. Dept., Metrology Lab and Metallography Lab of Mechanical engg. Dept.), IEST Shibpur (Metallography Lab, Met. and mat. Engg. Dept.), and CRNN, University Of Calcutta for providing essential facilities for my research.

A heartfelt acknowledgment to Gopan Karmakar from Bankura for graciously permitting me to conduct experiments in his workshop, exemplifying the essence of collaborative spirit.

I express my gratitude to all the colleagues and staff of the Metallurgical and Materials Engineering Department at Jadavpur University for their support. My heartfelt thanks go to my family for their unwavering encouragement and understanding throughout this academic journey.

Finally, I acknowledge the financial support from AICTE through the ADF (AICTE Doctoral Fellowship) scholarship, which has played a pivotal role in enabling my research endeavors.

Thank you all for being integral parts of this academic odyssey.

Sourmyajit Ray
21/03/2024

Content

Topic	Page No.
<u>Chapter-1</u>	
Introduction	1.1-1.4
<u>Chapter-2</u>	
Literature Survey	2.1-2.23
2.1 Investment Casting	2.1
2.2 Type of Investment Casting	2.2
2.3 Constraints of Thin-section Investment casting	2.4
2.3.1 Liquid metal flow problem through thin section investment casting	2.4
2.3.1.1 Boundary-Layer Concept: Introduction of Kinetic Energy Correction Factor	2.5
2.3.1.1.1 Velocity Distribution	2.6
2.3.1.1.2 Kinetic-Energy Correction Factor for flow through Parallel Plate	2.8
2.3.1.2 Friction head loss for Flow through Wide Channel	2.9
2.3.1.2.1. Determine the Friction Factor for Flow through Noncircular Ducts	2.10
2.3.1.2.2. Flow through Parallel Plates	2.11
2.3.1.2.3. The hydraulic diameter of a wide channel	2.13
2.3.1.3 Capillary Action in Thin Annular Hot Mold	2.14
2.3.1.3.1. Surface Tension of Liquid Metal inside a Capillary Mold	2.14
2.3.1.3.2. Pressure due to Capillary action	2.16
2.3.1.4 Limitations of 'Mold Filling time' equation using Bernoulli's Principle	2.18
2.3.1.5 Effect of Gating Design on Mold Filling Behavior	2.19
2.3.2 Metrological challenges for investment casting product	2.21
2.3.2.1. Casting quality and dimensional accuracy	2.21
2.3.2.2. Factors influencing dimensional accuracy	2.22
2.3.2.3. Dimensional variation at different stage due to Shrinkage	2.22

Chapter-3

Analytical Model for Mathematical Expression of Filling Time Estimation	3.1-3.11
3.1 Assumptions for Annular Thin Cylindrical Sections	3.1
3.2 Incorporation of the factors into the analytical model	3.4
3.2.1. Effect of Friction Head Loss (z_f)	3.4
3.2.2. Kinetic Energy Correction Factor (α)	3.5
3.2.3. Pressure due to Capillary action ($\Delta P\gamma$)	3.5
3.2.4. Bernoulli's Equation for Fluid Flow Through a Annular Mold	3.6
3.3 Filling Time Calculation of Thin-Section Annular Cylindrical Hot Mold by Top Gating	3.7
3.4 Flow area for $d_g \leq w$ and $d_g > w$	3.9
3.5 Pressure Inside Hot Mold	3.10

Chapter-4

Experimental Framework	4.1 - 4.17
4.1. Plan of work	4.1
4.1.1. Simulation experiments	4.1
4.1.2. Metrological analysis of thin walled investment casting	4.1
4.1.3. Confirmation through actual industrial application	4.3
4.2. Mathematical expressions and Numerical Techniques	4.4
4.2.1. Filling Time Calculation	4.4
4.2.2. Gating Design Calculation	4.5
4.2.3. Dimensional variation and Shrinkage analysis	4.6
4.2.4. Procedure of calculation to determine the Rank of the Casting using TOPSIS	4.8
4.3. Instruments and testing procedure	4.11
4.3.1. Instruments used for Dimensional Analysis	4.11
4.3.2. Experimental Procedure for Surface Roughness	4.12
4.3.3. Experimental Procedure for Characterization of Metals	4.12
4.3.3.1. Chemical Analysis	4.12
4.3.3.2. Vickers Hardness Test	4.12
4.3.3.3. Metallography of Cast Metal Sample	4.13
4.3.3.4. SEM and EDX	4.14
4.3.4. Analysis of the Clay used for Experiment	4.14

4.3.5.	Temperature Measuring Instrument	4.15
4.4.	Physical property of Liquid Metals	4.15

Chapter-5

Simulation Experiments	5.1 - 5.12
5.1 Simulation Experiments with Water and Mercury	5.1
5.1.1 Experimental procedure	5.1
5.1.2 Results	5.3
5.2 Experiment to Determine the Suction Pressure inside Hot Clay Mold	5.9
5.2.1 Experimentation:	5.9
5.2.2 Result	5.11
5.3 Discussion	5.11

Chapter-6

Metrological Analysis of Clay Molded Thin Walled Investment Casting	6.1 - 6.21
6.1 Quality Evaluation of Investment Casting	6.1
6.1.1 Design of Experiment	6.1
6.1.2 Shrinkage analysis	6.6
6.1.3 Dimensional Variation	6.7
6.1.4 Sectional Quality by Visual Inspection and Surface Roughness	6.8
6.1.5 Summary of the experimentation	6.9
6.2 Investigation of anomalous Expansion of Metal for Thin-walled Investment Brass Castings	6.11
6.2.1 Theoretical aspects	6.11
6.2.2 Shrinkage Analysis of Mold Material	6.12
6.2.2.1 Experimentation	6.13
6.2.2.2 Result	6.13
6.2.2.3 Reasons behind the expansion of mold material	6.14
6.2.3 Shrinkage Analysis of Cast Metal	6.15
6.2.3.1 Experimentation	6.15
6.2.3.2 Results	6.15
6.2.3.3 Reasons behind the expansion of cast metal	6.17
6.3 Metallographic study	6.19
6.4 Discussion	6.20

Chapter-7

Confirmation through Actual Industrial Practice	7.1 - 7.27
7.1 Confirmation of Analytical Model for Mold Filling Time	7.1
Estimation through Actual Casting	
7.1.1 Experimental Framework	7.1
7.1.2 Production Procedure	7.2
7.1.3 Result	7.8
7.2 Metrological analysis of Industrial Clay Molded thin-walled investment casting	7.11
7.2.1. Experimental Framework	7.11
7.2.2 Shrinkage Analysis of Wax-Based Hot Walled Brass Castings in Mold Thin	7.16
7.2.3 Effect of Gating System for Thin Walled Investment Castings	7.18
7. 2.3.1 The Eccentricity of the Lip and Base	7.18
7. 2.3.2 Uniformity of Thickness of Metal Width	7.18
7. 2.3.3 Surface Quality	7.18
7. 2.3.4 Surface Roughness	7.19
7.2.4 Ranking by TOPSIS	7.20
7.3 Metallurgical Characterization of Castings Products	7.21
7. 3.1 Chemical Compositions	7.21
7.3.2 Hardness of the Cast Samples	7.21
7.3.3 Microstructures with SEM-EDX Analyses	7.22
7.4 Discussion	7.25

Chapter-8

Conclusion	8.1-8.2
-------------------	----------------

Bibliography	B.1-B.6
---------------------	----------------

List of Symbols	B.7
------------------------	------------

Appendix	A.1-A.48
-----------------	-----------------

List of Appendix

	Description	Page No.
I	Investigation details by researcher on Investment casting	A.1
II	Fluid flow patterns through the mold: Water Simulation	A.2
III	Fluid flow patterns through the mold: Mercury Simulation	A.4
IV	Calculation of Simulation experiment using Mercury for 0.7mm Thick plate at vertical position (zm=140mm)	A.7
V	Calculated Data Chart for Simulation Experiments and Actual Metal casting	A.8
VI	Mercury Simulation experiments using in Annular Cylindrical glass mold with two different position	A.9
VII	Comparison of Calculated and Actual Filling Time and Gating Design of Few other thin-walled investment castings in hot clay mold	A.10
VIII	Detailed Dimension, Volume and Area of Model “Saraswati” part by part	A.15
IX	Calculation of Filling Time and Gating Design of Brass Icon ‘Saraswati’	A. 17
X	Variation of length, breadth and width of the plates	A.18
XI	Shrinkage/ Expansion of length, breadth, metal thickness and the holes	A.20
XII	Surface roughness graphs of Thin (w<2mm) Rectangular Plate Castings	A.21
XIII	Surface roughness graphs of Thick (w>3mm) Rectangular Plate Castings	A.25
XIV	Analysis of Clay	A.27
XV	Procedure of Calculation Zn Equivalent	A.28
XVI	SEM-EDX Analysis of Thick and Thin plate followed by Horacek Model	A.29
XVII	Data chart of Dimensional Shrinkage (%) of Cast Samples at different stages	A.31
XVIII	Data chart of average variation of Metal width for different plane and different section for cosmetic case and cap for different gating system	A.32
XIX	Calculation to determine the Rank of the Casting using TOPSIS of Thin (w<2) Plate	A.35
XX	Calculation to determine the Rank of the Casting using TOPSIS of Cosmetics Case	A.37
XXI	Calculation to determine the Rank of the Casting using TOPSIS of Cosmetics Cap	A.38
XXII	The Indian Traditional Investment Casting Technology	A.39

List of Tables

	Description	Page No.
Chapter-2		
2.1	Dimensional Changes during the Investment Casting Process	2.25
Chapter-4		
4.1	Payoff Matrix	4.9
4.2	Normalized Payoff Matrix	4.9
4.3	Weighted Normalized Payoff Matrix	4.10
4.4	Details of Measuring Instruments	4.11
4.5	Pouring Temperature and Physical property of Liquid Metals	4.15
Chapter-5		
5.1	Experimental framework for Simulation Experiment	5.2
Chapter-6		
6.1	Details of the Sample for various factors	6.2
6.2	Materials used for mold and pattern	6.2
6.3	Chemical composition and Nomenclature and property of metal used	6.2
6.4	Surface and Sectional Quality of the Plate	6.8
6.5	Dimensions of Fiber Die, Wax Pattern and Cast Product in different Gating	6.10
6.6	Ranking of the Casting Samples Based on Quality using the TOPSIS method	6.10
6.7	Transformation details of Kaolinite clay and silica sand	6.12
6.8	Expansion percentage of Mold	6.14
6.9	Cast metal thickness Expansion	6.17
6.10	Shrinkage / expansion of clay Mold at different stages	6.18
Chapter-7		
7.1	Experimental framework	7.2
7.2	Experiments for Dimension Analysis	7.12
7.3	Shrinkage Analysis of Cast Product with respect to Wax Pattern and	7.17

	Shrinkage of Internal dimensions with respect to Die	
7.4	Surface and Sectional Quality of the Cosmetics Case	7.20
7.5	Preferable and Rejected Gating System with Ranking	7.20
7.6	Chemical Composition of Cast Samples	7.23

List of Figures

	Description	Page No.
	Chapter-2	
2.1	Block diagram of Production sequences of investment casting	2.3
2.2	Velocity Profile and Shear Stress Distribution for a viscous fluid flow between two Parallel planes	2.5
2.3	Viscous Flow between Parallel Plate	2.6
2.4	Control volume of steady fully developed Stress Channel the flow between two sections in an inclined non- circular pipe-flow	2.10
2.5	Flow through Parallel Wide Channel	2.12
2.6	Flow of liquid metal through a Circular Channel and a Parallel Plate	2.14
2.7	Liquid Flow through a Thin Hot Clay Mold from Sprue	2.18
2.8	Mold filling behaviour in the top gating system with mold thickness	2.20
	Chapter-3	
3.1	Sectional View of an Annular Cylinder during filling	3.6
3.2	Gating System for Thin Molds	3.9
3.3	Temperature wise Pressure difference (ΔP) inside a mold along with air density	3.11
	Chapter-4	
4.1	Block Diagram of Experimental Framework	4.2
4.2	Measuring Instrument:	4.16
4.3	Surface Roughness Measuring Machine	4.16
4.4	Vickers Indentation Instrument	4.16
4.5	Optical Microscope	4.17
4.6	Pictorial View of SEM-EDX Machine	4.17
4.7	Instruments used for analysis of Clay	4.17

4.8	K-Type Thermocouple with Digital indicator	4.17
-----	--	------

Chapter-5

5.1	Details of (a) Mold volume and (b) Gate Area	5.2
5.2	Schematic diagram of the molds at different position with Gating System, Pictorial representation of the molds: front view and side view	5.4
5.3	Flow pattern of Water and Liquid Mercury through various mold thickness and mold position at different time frame	5.6
5.4	Simulated actual filling time (tact) and calculated filling time (tf) for the molds with varying positions. Working fluid: Water	5.7
5.5	The error (%) between the simulated actual filling time (tact) and the calculated filling time (tf), as well as the error between the conventional filling time and tact, for molds with varying positions. Working fluid: Water	5.7
5.6	Simulated actual filling time (tact) and calculated filling time (tf) for the molds with varying positions. Working fluid: Liquid mercury	5.8
5.7	The error (%) between the simulated actual filling time (tact) and the calculated filling time (tf), as well as the error between the conventional filling time and tact, for molds with varying positions. Working fluid: Liquid mercury	5.8
5.8	Comparison of Filling time among molds with the same mold height ($z_m=140\text{mm}$), gating design, and mold volume, based on the molds' volume fractions.	5.9
5.9	Experiment to estimate the suction pressure inside clay during firing	5.10
5.10	Details of Pressure inside the Mold:	5.11

Chapter-6

6.1	Schematic diagram and Fibre model of Die, Schematic diagram of three Gating System, and Dimension Nomenclatures of Cast Plate	6.3
6.2	Procedure of plate making	6.4
6.3	Cast Plates of "Horacek Model" with Both Side Surface	6.5
6.4	Shrinkage/ Expansion of the Plate dimension	6.6
6.5	Root mean square deviation (R.M.S.D) (mm) of (a) Length, (b) Breadth and (c) Thickness of the Plate	6.7
6.6	Surface Roughness (Ra) for the thin and thick plate	6.9
6.7	Experiment to estimate the shrinkage and expansion of mold material	6.13

6.8	Casting procedure of the sheets: (a) side view of all dies, (b) side view of all wax sheets, (c) side view of the metal sheet.	6.16
6.9	Cast metal thickness distribution along with wax pattern thickness	6.16
6.10	Microstructure (SEM) of Brass Casting (500X) with SEM- EDX analysis for (a) 0.5mm, (b) 1.75mm and (c) 3.6mm thick cast metal. (d) ASTM Grain size number of all the microstructure	6.19

Chapter-7

7.1	Schematic diagram of Model-1 along with clay mold	7.2
7.2	Pictorial representation of Model-1 (Mann): Cast by Three different Alloy	7.3
7.3	The schematic diagram of Model-1, featuring two Gating systems, Volume and Surface Area, illustrating the different parts involved	7.5
7.4	Pictorial representation of Model-2: Cast by two different gating system	7.6
7.5	Physical Parameters of the cast samples	7.7
7.6	Gating Details of the castings	7.8
7.7	Calculated Parameters	7.9
7.8	Comparison among the calculated filling time, actual (experimented) filling time, and the conventional filling time	7.10
7.9	Comparison of the error (%) between calculated filling time and actual filling time as well as between conventional filling time and actual filling time	7.10
7.10	Schematic diagram of Cosmetic Cap and case. with gating system:	7.12
7.11	Production Steps of Cosmetics Case and its Cap	7.13
7.12	Pictorial View of casting with gating system	7.14
7.13	Surface Quality of Finished Product	7.15
7.14	Dimensional Shrinkage (%) of Cast Samples	7.16
7.15	Schematic diagram of different Stage of Cosmetic Case and cap	7.17
7.16	Eccentricity of Cosmetics Case and Cap	7.19
7.17	Percentage of Mean Variation (R.M.S) of Metal Thickness	7.19
7.18	Surface Roughness of Cosmetics Case and Cap	7.19
7.19	Vickers (Bulk) Hardness and Micro Hardness of Cast Samples	7.23
7.20	SEM Microstructure of Auminium Cast Sample	7.24
7.21	Microstructure (SEM) of Brass Casting	7.24
7.22	SEM Microstructure of Gunmetal Cast Sample	7.25

Chapter-1

Introduction

1. Introduction

In many countries of Asia (India, China and Thailand), Africa (Benin) and Pacific Islands (Papua, New Guinea), traditional silica molded thin-walled investment castings are produced. From the ancient time Investment Casting has matured into a modern manufacturing process to produce precision component and unmachinable machine parts of electronic and computer industry, Boeing engines and spacecrafts. This is one of the most advanced technologies of the world, so much so, no country wants to share the technique. This technology requires very much individual initiatives to develop investment casting production parameters. One of which is gating system based on fluid mechanics principle of actual mold condition.

Using Bernoulli's energy conservation equation the filling time of the mold is generally estimated in sand molds and other kind of molds using mass flow rate. The actual filling time often comes overshooting the predicted values. The problem of investment molds arises because of a very small opening in the annular mold during fluid flow which generates considerable fictional head loss as described by many authors like Spurk, Aksel [1], Schaschke [2] et al. The second problem as referred by White [3], Çengel, Cimbala [4] et al., is the kinetic energy correction factor due to non-unidirectional velocity encountered from the fluid dynamics. According to Stefanescu [5], the flow between the narrow channels introduces a negative pressure head due to the capillary action of its liquid and its vapor in terms of surface tension. Much mathematics has been developed on the basis of fluid flow but no specific models have been encountered in text books for investment casting process, in general. Even though there is an abundant development of software for the solution of fluid flow problems by mechanical engineers, there are few

developments in fluid mechanics principles derived from rules of physics. The obvious reason is quite apparent as all the software are basically man-made mathematical tools using numerical techniques, whereas, the rules of physics are guided by Mother Nature and limited in expression. In case of fluid flow, those are manifested by Torricellian principle, Pascal's derivation, and Bernoulli's theorem. But all the software basically originated from the above rule of physics using digital techniques enumerated in mechanical engineer's textbooks.

In this respect, the important thing of principle derivation of Bernoulli's theorem has been modified for the kinetic energy factor by mechanical engineers for fluid flow through parallel plates having capillary openings. This modification must have to be incorporated for liquid metal flow in case of investment molds which resemble the stated problem of fluid flow through parallel plates.

This project makes an attempt to develop an analytical model on theoretical basis for the solution overcoming these physical constraints. Hopefully, the new analytical solution of the mathematical problem of investment mold filling time could be taken as a basic or primary solution to solve this kind of problem by software developers.

The real-time simulation experimentations utilizing two fluids, one Water and one Mercury, were executed to validate the proposed analytical model as well as to determine the nature of fluid flow patterns within parallel plates having capillary dimensions. Again, the validation of the proposed analytical model described above was conducted using actual castings produced in hot silica molds.

Investment castings, generally of thin ($\sim\mu\text{m}$) sections, also demands a high level of dimensional accuracy from producers to achieve their objective. The present thesis attempts to propose to quantify the metrological solutions of investment castings produced in hot silica mold. Furthermore, a rudimentary metallurgical investigation was undertaken to assess the quality of thin-section investment castings.

Objective

Investment casting produces complex metal parts of Superalloys and other unmachinable alloys used in jet engines and spacecrafts. The production process has been a time consuming operation which lacks productivity sustainable in modern time. On the other hand Investment casting has been used commercially in the manufacture of precision components of modern electronics competitive with die casting and shell molding processes. In this case also the productivity is a paramount importance for sustenance of the industry, as far as designers and assemble engineers are concerned. With these two perspectives in mind the objective of the thesis has been visualized.

One of the important design aspects during foundry operations has been prescribed as gating design. The purpose of gates basically implies streamline flow of metals at shortest filling time to fill the mold cavity in order to produce defect free castings. The problem at hand therefore, becomes a study of the available theoretical and experimental expressions and observations so that one can make an intelligent choice of gating system design for a given combination of metal, mold and mold graphics. So, any good gating system design will make many engineering compromises, necessary for achieving the result. For an example, the annular fluid mechanics deviates from classical fluid flow models familiar

to mechanical engineers. This necessitates the modification of classical equation developed by fluid flow engineers to suit the actual condition of investment mold system. Thus, the primary objective to increase the productivity boils down to the development of a system of equations for easy and uninterrupted metal flow to fill the mold cavity at the shortest filling time compromising the thermodynamic production of 'dross' as well as thermographical temperature loss occurred due to physical losses of conduction, convection and radiation.

After the derivation of the filling time of the mold, the emphasis of the objective proceeded towards the validation of the model involving a group of simulation experiments using water and mercury as experimental fluids. The water-plastic combination model has been a familiar experimental combination used by many fluid flow engineers and the mercury-plastic combination has been used to understand the actual liquid metal flow within the imaginary mold graphics without wetting the mold surface. Attempts were made to get an understanding of the gating system design in case of actual castings using Copper alloys and Aluminum alloys produced in hot silica molds.

Mechanical design engineers exert a lot of emphasis on metrological characteristics and systematic accuracy of the designed product. Therefore, a further objective of the thesis attempted a basic discussion on metrological assessment of the experimental castings. Generally, the experiments have been conducted based on the principle commonly adopted by investment casting engineers to express the accuracy of the precision cast products. To extend the objective further, a limited metallurgical assessment of the produced castings was conducted in form of metallographic analysis.

Chapter-2

Literature Survey

2. Literature Survey

The increasing demand for near-net shape components is stimulating the use of investment casting methods because of its ability to produce thin section castings with very smooth and detailed surface finishes with excellent dimensional tolerances and also for its inherent capability to reduce or minimize secondary operations, such as machining. Although the lost-wax investment casting technique was used for produce thin-walled intricate shaped cast items from the time of Bronze Age [2.1].

2.1. Investment Casting

Investment casting is described in ‘ASM handbook (vol.-15-Casting)’ as [2.2], “the Investment casting process has been known for at least 6000 years, but its use for the production of commercial castings has grown considerably during the second half of the 20th century. The process is also referred to as the lost wax process and as precision casting. The term precision implies high accuracy of dimensions and tight tolerances. Investment casting also yields smoother, high-integrity surfaces that require little or no machining, depending on the application”. “In Investment Casting, a ceramic slurry is applied around a disposable pattern, usually wax, and allowed to harden to form a disposable casting mold. The term disposable means that the pattern is destroyed during its removal from the mold and that the mold is destroyed to recover the casting.

Although it has a wide variety of applications, investment casting is particularly favored for the production of parts for gas turbine blades and vanes (nickel and cobalt alloys) and aircraft structural components (titanium, super-alloys, and 17-4 PH stainless steel). The

application of directional solidification (DS) and single-crystal (SC) technology to investment casting has also increased interest and use.” [2.2]

In modern time, investment casting technique is used to produce high precision product in the sectors of aerospace, automobile, bio-medical, chemical and defense [2.3]. The most precious items produced by Investment castings are turbine blade [2.4], engine component, surgical tools, orthopedic implants [2.5] firearms component, various machine parts, jewelry and sculpture [2.6]. In recent past productivity of investment casting industry getting improved by adopting additive manufacturing (3D Printing) and rapid prototyping technique [2.7, 2.8].

2.2. Type of Investment Casting

As illustrated in ASM Handbook “A major advantage of investment casting is its ability to cast very thin walls. This results from the use of a hot mold, but is further enhanced by specific casting methods, such as vacuum-assist casting, pressurized casting and counter-gravity casting. Both air and vacuum casting are important in investment casting. Most vacuum casting is investment casting”. [2.8] The Investment casting process falls into two distinct categories, based on expendable and permanent patterns”. [2.9]

The production sequences of the investment casting by lost wax (or expendable pattern) technique are illustrated in figure-2.1 [2.8]. Generally wax patterns or polystyrene patterns and are used for this technique.

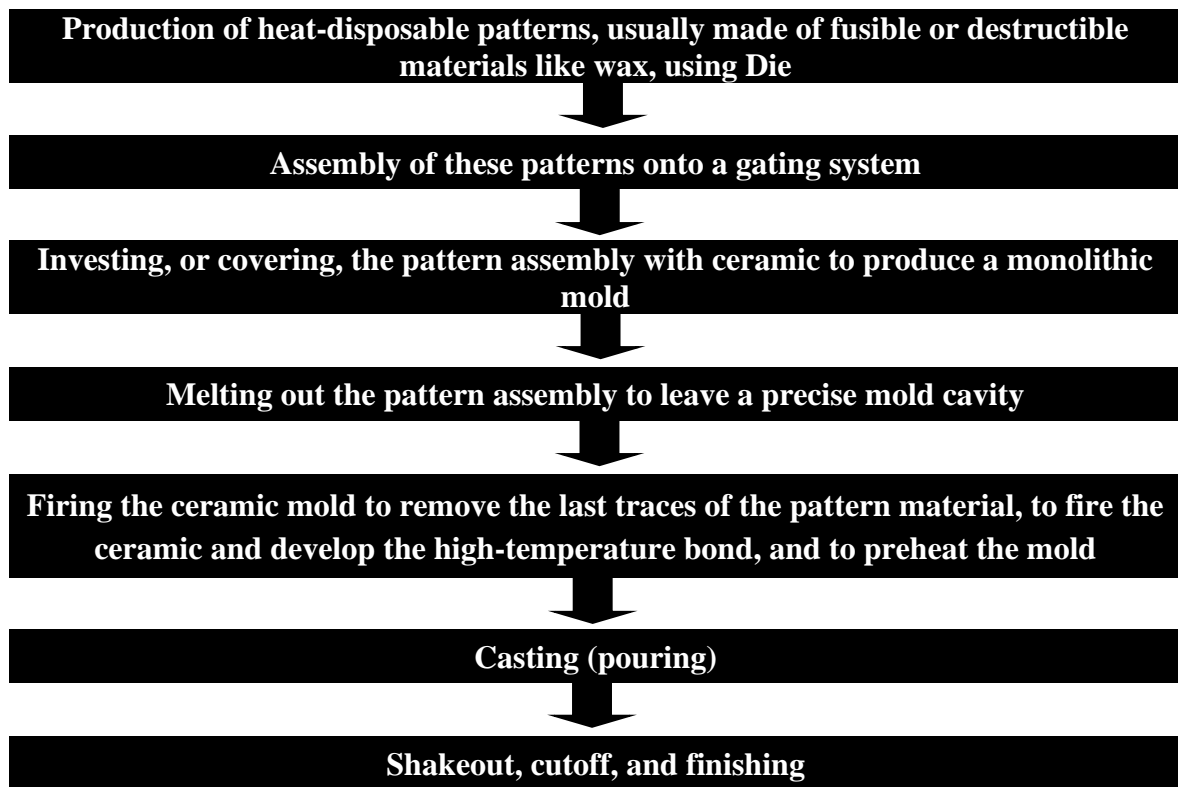


Figure 2.1: Block diagram of Production sequences of investment casting
(Expendable pattern technique)

The Investment casting from permanent patterns as illustrated by Peter Beeley in the book 'Foundry technology' as, [2.9] "The advantages of liquid investments, with their close conformity to the pattern and smooth mold surfaces, can be utilized in a simpler and less costly sequence involving direct molding from patterns of metal, plaster or wood. Various processes use this principle and all produce multipart rather than one piece molds. The castings have a high standard of accuracy and finish, although the degree of precision is second to that of castings produced from expendable patterns because of the need to align the separate mold parts and cores. The errors are nevertheless small because of the precise mold components. Plaster of Paris investments have long been established for the production of non-ferrous castings, especially in aluminium and copper base alloys. Although orthodox pattern materials are used, flexible rubber patterns can also be employed to facilitate the production of undercut features in intricate components."

“Permanent pattern investment castings are capable of accuracies within the range $\pm 0.5\% - 1.5\%$ ”. [2.9]

2.3. Constraints of Thin-section Investment casting

The problems of thin-walled investment castings were noticed and analyzed by many researchers like J. Campbell [2.10], X. Yang, Weng-Sing Hwang, R. A. Stoehr [2.11], D.M. Stefanescu [2.12], M. Horáček [2.13], Adrian S. Sabau [2.14, 2.15] and many others.

Beeley [2.16] in ‘Foundry technology’ suggests that, “The minimum feasible section thickness for metal flow depends on alloy fluidity, extent of section, and moulding process and material”. A. J. Clegg [2.17] recommends in his research article that the wall thickness of Investment castings are generally 0.6mm to 1.3 mm. “Under the special conditions of investment and die casting, where flow is assisted by hot molds or by pressure, sections as thin as 0.4mm (≈ 0.015 in) can be attained over short distances” [2.16]. Based on the experiments, Kondic [2.18] reaches to a conclusion that “a mold cavity with a large surface area to volume ratio is used to provide an analogous mold filling problem to that encountered in investment castings of thin section”.

2.3.1. Liquid metal flow problem through thin section investment casting

The complications of Liquid metal flow, through narrow channels are influenced by the physical properties of liquid metal such as surface tension, viscosity and other fluid dynamic factors like head loss due to friction, uneven shear stress, capillary action and

also gas pressure. The mathematical expressions adopted for the analytical analysis of the fluid flow problem is discussed here.

Ragone et al. [2.19] investigated the flow of molten tin in channels of various diameters down to 3mm in vacuum, finding subsequently extended by Barlow [2.20], carried out the experiment to 0.5mm channels for various alloys. The importance of surface tension with respect to flow in small passages was demonstrated by Hoar and Atterton [2.21]. T. A Baruch et al. [2.22] and M. C. Flemings et al. [2.23] discovered that “There is wide agreement that the surface tension factor becomes significant in the channel size range 0.5–5mm”.

2.3.1.1. Boundary-Layer Concept: Introduction of Kinetic Energy Correction Factor

Liquid metal is viscous and obeys Newton’s Law of Viscosity [2.24]. Due to viscosity, the flow, between two planes suffers maximum shear stresses at the surfaces and minimum at the centre [2.25]. The velocity distribution (Figure.-2.2) will not be constant throughout the section, maximum at centre and minimum at surfaces [2.26]. Therefore a Kinetic Energy Correction should be introduced [2.27].

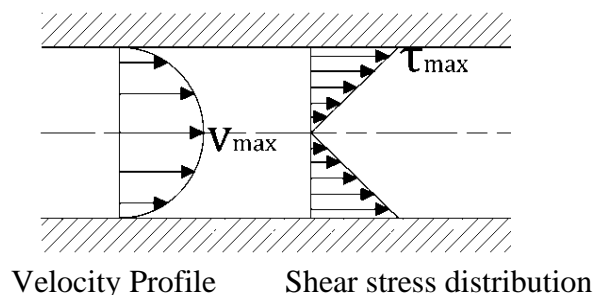


Figure 2.2: Velocity Profile and Shear Stress Distribution for a viscous fluid flow between two Parallel planes (considered as fully developed flow region)

2.3.1.1.1. Velocity Distribution [2.17]

Consider a unit breadth fluid element of length ' Δx ' and width ' Δy ' at a distance ' y ' from the lower surface (Figure 2.3). The resultant Pressure force between two opposite faces of the element in the direction perpendicular to flow is $\left(\frac{\delta p}{\delta x} \cdot \Delta x \cdot \Delta y\right)$. Also, the resultant Shear force between two opposite faces of the element in the direction parallel to flow is $\left(\frac{\delta \tau}{\delta y} \cdot \Delta x \cdot \Delta y\right)$.

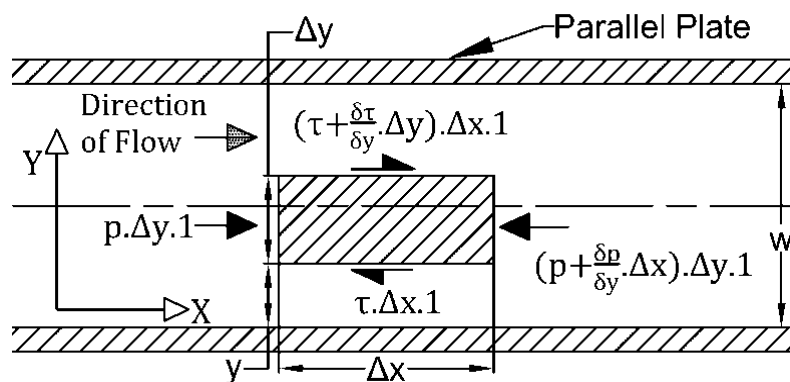


Figure.2.3: Viscous Flow between Parallel Plate

For uniform and steady flow,

$$\frac{\delta p}{\delta x} = \frac{\delta \tau}{\delta y} \quad (2.1)$$

From Newton's law of viscosity,

$$\tau = \mu \frac{\delta v}{\delta y} \quad (2.2)$$

[τ =Shear stress (N/ m²), μ =Viscosity (Pa.s), p = pressure ((N/ m²))]

From Eq.2.1 and 2.2, it can be derived,

$$\frac{\delta^2 v}{\delta y^2} = \frac{1}{\mu} \cdot \frac{\delta p}{\delta x} \quad (2.3)$$

Integrating both sides and calculates the integrating constant,

$$v = -\frac{1}{2\mu} \left(\frac{\delta p}{\delta x} \right) (wy - y^2) \quad (2.4)$$

Maximum velocity is at $y = \frac{w}{2}$, therefore,

$$v_{\max} = -\frac{1}{8\mu} \cdot \frac{\delta p}{\delta x} \cdot w^2 \quad (2.5)$$

To determine average velocity, first, calculate the flow rate 'Q',

$$dQ = \text{Velocity at distance } y \times \text{Area of Strip} = v \cdot dy \cdot 1$$

$$Q = \int_0^t dQ = \int_0^t -\frac{1}{2\mu} \left(\frac{\delta p}{\delta x} \right) (wy - y^2) dy = -\frac{1}{12\mu} \left(\frac{\delta p}{\delta x} \right) w^3 \quad (2.6)$$

As average velocity, $v_{avg} = \frac{Q}{Area} = \frac{Q}{w \times 1}$ therefore

$$v_{avg} = -\frac{1}{12\mu} \cdot \frac{\delta p}{\delta x} \cdot w^2 \quad (2.7)$$

2.3.1.1.2. Kinetic-Energy Correction Factor for flow through Parallel Plate

Frequently, the flow entering or leaving a port is not strictly one-dimensional; thus, velocity may vary over the cross-section (Figure 2.2). To account for this, a dimensionless correction factor ' α ' is employed to adjust the kinetic energy term in Equation-2.3 for a specific port. This modification ensures that the integral is proportional to the square of the average velocity through the port.

$$\alpha = \frac{\text{K. E./ sec based on Actual velocity}}{\text{K. E./ sec based on Average velocity}} \quad (2.8)$$

Actual Kinetic Energy of fluid flowing through the unit breadth fluid element of length ' Δx ' and width ' Δy ' per second is KE_{act} .

$$KE_{act} = \frac{1}{2} \times mass \times v^2 = \frac{1}{2} \rho \cdot dQ \cdot v^2 = \rho v^3 \cdot dy \quad (2.9)$$

Total actual Kinetic Energy of flow per second

$$KE_{act} = \int_0^R \frac{\rho}{2} v^3 \cdot dy = \int_0^R \frac{\rho}{2} \left[\frac{1}{2\mu} \left(-\frac{\partial p}{\partial x} \right) (wy - y^2) \right]^3 \cdot dy \quad (2.10)$$

$$KE_{act} = \frac{\rho}{16\mu^3} \left(-\frac{\partial p}{\partial x} \right)^3 \frac{w^7}{140} \quad (2.11)$$

Kinetic energy based on average velocity;

$$KE_{avg} = \frac{1}{2} \times mass \times v_{avg}^2 = \frac{1}{2} \rho \cdot A \cdot v_{avg} \cdot v_{avg}^2 = \frac{1}{2} \rho \cdot A \cdot v_{avg}^3 \quad (2.12)$$

Substituting the value, $A = w \times 1$

$$KE_{avg} = \frac{\rho}{2} \cdot w \cdot \left[\frac{1}{12\mu} \cdot \left(-\frac{\partial p}{\partial x} \right) \cdot w^2 \right]^3 = \frac{\rho}{2\mu^3} \left(-\frac{\partial p}{\partial x} \right)^3 \frac{w^7}{12^3} \quad (2.13)$$

Determine the Kinetic Energy Correction Factor by Dividing Equation 2.11 to Equation. 2.13

$$\alpha = 1.54 \approx 2.0 \quad (2.14)$$

The value of Kinetic Energy Correction Factor is taken 2.0 for the flow through thin annular hot mold considering the flow is Laminar”.

2.3.1.2. Friction head loss for Flow through Wide Channel

Friction between liquid and the surface of the channel hinders the flow. The flow through the wide channel is similar to the fluid flow through the thin-walled castings, so understanding of Friction head loss for this type of flow is important to design optimum gating system.

2.3.1.2.1. Determine the Friction Factor for Flow through Noncircular Ducts

To analysis the fully developed flow in the non-circular duct, the Hydraulic Diameter approximation is taken [2.29]. For a noncircular duct (Figure. 2.4), considering control volume system, the momentum equation is, Where, “A” cross-sectional area, “ ξ ” is wetted perimeter,

$$\Delta p A + \rho g A \Delta L \sin \phi - \overline{\tau_w} \xi \Delta L = 0 \quad (2.15)$$

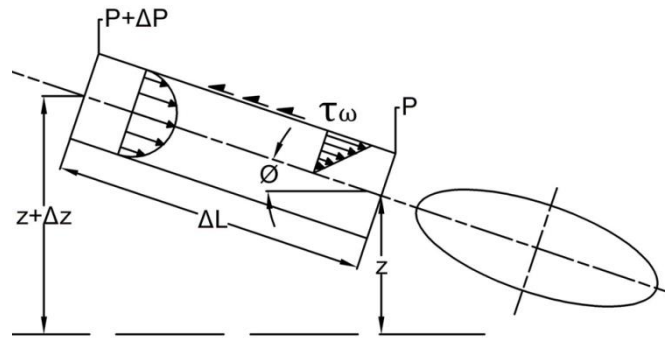


Figure.-2.4: Control volume of steady fully developed flow between two sections in an inclined non- circular pipe flow with Stress distribution (Left), Cross-sectional view (Right),

This equation relates to friction head loss (z_f) to the wall shear stress

$$\frac{\Delta p}{\rho g} + \Delta z = \frac{\overline{\tau_w}}{\rho g} \frac{\Delta L}{A/\xi} = z_f \quad [\Delta z = \Delta L \sin \phi] \quad (2.16)$$

To solve the problem of head loss in pipe flow, functionally, it is assumed that

$$\tau_w = F(\rho, V, d, \mu, \epsilon) \quad (2.17)$$

Where ϵ is the wall-roughness height. From dimensional analysis

$$\frac{8\tau_w}{\rho V^2} = f = F(\text{Re}_d, \frac{\epsilon}{d}) \quad (2.18)$$

The dimensionless parameter f is called the *Darcy friction factor* [2.30]. From the equation (2.16) and (2.18) the expression of pipe head loss is

$$z_f = f \frac{L}{4r_h} \frac{V^2}{2g} = f \frac{L}{d_h} \frac{V^2}{2g} \quad (2.19)$$

This is equivalent to the equation for circular pipe flow, with the only difference being the replacement of the diameter by $4r_h$. Therefore, the hydraulic diameter [2.29] is defined as.

$$d_h = \frac{4A}{\xi} = \frac{4 \times \text{Cross sectional Area}}{\text{Wetted Perimeter}} = 4r_h \quad (2.20)$$

2.3.1.2.2. Flow through Parallel Plates [2.29]

The fluid flow between parallel plates at a distance 'w' can be viewed as the limiting case of flow through a very wide rectangular channel (Figure 2.5). In fully developed flow, the velocity profile $u=u(y)$, satisfying continuity identically. Subject to no-slip conditions, for $u=0$ at $y=\pm w/2$, the momentum equation in Cartesian coordinates becomes

$$0 = \frac{dp}{dx} + \rho g_x + \frac{d\tau}{dy}$$

$$\tau_{lam} = \mu \frac{du}{dy} \quad (2.21)$$

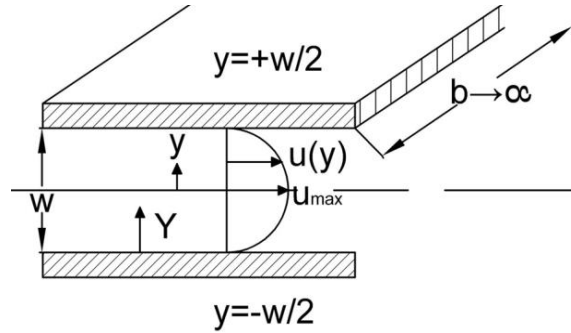


Figure 2.5: Flow through Parallel Wide Channel

For the sloping channel, with a pressure gradient due to gravity, the laminar-flow solution is

$$u = \frac{1}{2\mu} \left[-\frac{d}{dx} (p + \rho g z) \right] \left[\left(\frac{w}{2} \right)^2 - y^2 \right] \quad (2.22)$$

If the channel has breadth b , the volume flow is

$$Q = \int_{-w/2}^{+w/2} u(y) b \cdot dy = \frac{bw^3}{24\mu} \left[-\frac{d}{dx} (p + \rho g z) \right] \quad (2.23)$$

or,

$$v = \frac{Q}{bw/2} = \frac{w^2}{12\mu} \left[-\frac{d}{dx} (p + \rho g z) \right] = \frac{2}{3} u_{\max} \quad (2.24)$$

The wall shear stress in developed channel flow is a constant:

$$\tau_{lam} = \mu \left| \frac{du}{dy} \right|_{y=+w/2} = \frac{w}{2} \left[-\frac{d}{dx} (p + \rho g z) \right] \quad (2.25)$$

Therefore, the friction factor,

$$f = \frac{8\tau_w}{\rho V^2} = \frac{24\mu}{\rho v(w/2)} \quad (2.26)$$

2.3.1.2.3. The hydraulic diameter of a wide channel [2.29]

The hydraulic diameter of a wide channel is

$$d_h = \frac{4A}{\xi} = \lim_{b \rightarrow \infty} \frac{4 \times (w \times b)}{(2b + 2w)} = 2w \quad (2.27)$$

Therefore hydraulic diameter of a wide channel is twice the distance between the plates.

Substituting the value into Equation (2.26) the friction factor for a wide channel is

$$f_{lam} = \frac{96\mu}{\rho V(4h)} = \frac{96}{\text{Re}_{d_h}} \quad (2.28)$$

2.3.1.3. Capillary Action in Thin Annular Hot Mold

Capillary action is caused by the free energy gained by wetting the internal surfaces of the capillary walls. It is a natural phenomenon caused due to the surface energy of liquid, distance between plates (or channel diameter) and contact angle between liquid and mold. As Thin Walled casting is a Surface dominated system, therefore the Capillary action has an important role in it.

2.3.1.3.1. Surface Tension of Liquid Metal inside a Capillary Mold [2.12]

To understand the Surface Tension of Liquid Metal inside a Capillary Mold; let, consider liquid metal moving through a cylindrical conduit having radius is ' r ' and length ' L ' as shown in figure 2.6. The change in interface energy within the system if the metal moves from the position ' L ' to position ' $L-x$ ' is:

$$\Delta G_\gamma = \Delta G_\gamma^{L-x} - \Delta G_\gamma^L \quad (2.29)$$

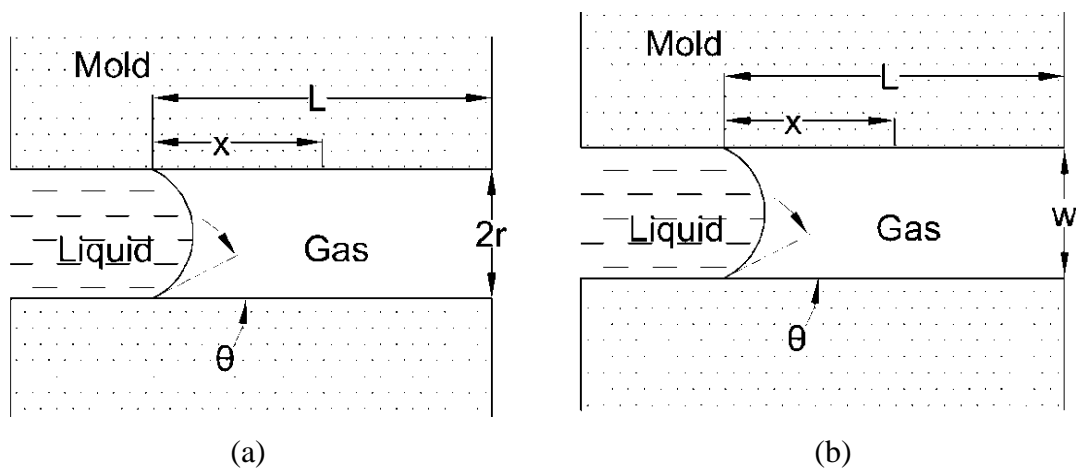


Figure 2.6: Flow of liquid metal through (a) a Circular Channel and (b) a Parallel Plate.

Before the liquid moves from L to $L-x$, the total interface energy of the system can be described as:

$$\Delta G_{\gamma}^L = \pi^2 \phi \gamma_{LV} + 2r\pi L \gamma_{SV} + A_{LS}^0 \gamma_{LS} \quad (2.30)$$

Where A_{LS}^0 is the interface area of contact of the melt and the mold, γ_{LS} , γ_{LV} and γ_{SV} are the interfacial energies between the corresponding phases (L : liquid, S : solid, V : vapour), and $\phi > 1$ is a parameter showing the difference between the surface area of the curved and of the flat meniscus of the melt. Similarly, the total interface energy of the system when the liquid is at position $L-x$ is:

$$\Delta G_{\gamma}^{L-x} = \pi^2 \phi \gamma_{LV} + 2r\pi(L-x) \gamma_{SV} + (A_{LS}^0 + 2\pi x) \gamma_{LS} \quad (2.31)$$

The disparity between the two interfacial energies in equation 2.30 and 2.31 can be considered as the energy change corresponding to the flow:

$$\Delta G_{\gamma} = \Delta G_{\gamma}^{L-x} - \Delta G_{\gamma}^L = 2\pi x (\gamma_{LS} - \gamma_{SV}) \quad (2.32)$$

ΔG_{γ} is the work done during flow through the capillary by the average force F_{γ} over the penetration path x . The pressure difference required for this force is:

$$\Delta P_{\gamma} = \frac{F_{\gamma}}{\pi r^2} = \frac{\Delta G_{\gamma}}{\pi r^2 x} = \frac{2}{r} (\gamma_{LS} - \gamma_{SV}) \quad (2.33)$$

The Young equation gives a relationship between the three interfacial energies and the contact angle if the drop of a melt and the solid phase are in mechanical equilibrium:

$$\gamma_{SV} - \gamma_{LS} = \gamma_{LV} \cos \theta \quad (2.34)$$

Substituting in the preceding equation, the outside pressure that must be applied to push the melt through the conduit of radius r is obtained”.

2.3.1.3.2. Pressure due to Capillary action

The pressure drop along the mold, attributed to the resistance to flow due to metal-mold interaction, involves the resistance to flow through a channel of radius ' r ', as well as the flow between narrow parallel plates separated by a distance ' w ' (see Figure 2.6). This can be calculated with [2.31, 2.32]

$$\Delta P_r = -\frac{2}{r} \gamma_{LV} \cos \theta \quad (2.35)$$

$$\Delta P_w = -\frac{2}{w} \gamma_{LV} \cos \theta \quad (2.36)$$

Where γ_{LV} is the surface energy between the liquid metal and its vapour phase, and θ is the contact angle between the metal and the mold.

When the melt wets the mold (i.e., $\theta < 90^\circ$), $\Delta P_\gamma < 0$, no external pressure is required for flow. However, if the melt does not wet the mold (i.e., $\theta > 90^\circ$), $\Delta P_\gamma > 0$, indicating that external pressure is necessary for flow. This equation characterizes the pressure drop during flow through capillary interstices. In general, for the liquid metal flow through the capillary mold, it is necessary that the external pressure acting on the metal be higher than ΔP_γ i.e., $\Delta P_{ext} > \Delta P_\gamma$. The external pressure would be:

$$\Delta P_{ext} = P_{met} - P_{mold} = (P_{atm} + P_{st} + P_{dyn}) - (P_{atm} + P_{gas}) = \rho g z + \rho v^2 - P_{gas} \quad (2.37)$$

Where P_{met} and P_{mold} are the pressures on the liquid-air interface on the metal and mold side respectively, $P_{st} = \rho g h$ is the metallostatic pressure, $P_{dyn} = \rho v^2$ is the dynamic pressure, and P_{gas} is the pressure exercised by the gas in the mold. Thus, to have flow it is necessary that [2.10, 2.12]

$$\rho g z + \rho v^2 - \rho_{gas} \geq -\frac{2\gamma}{r} \cos \theta \quad (2.38)$$

$$\rho g z + \rho v^2 - \rho_{gas} \geq -\frac{2\gamma}{w} \cos \theta \quad (2.39)$$

It is apparent from these equations that if the metal wets the mold ($0 < 90^\circ$), $\cos \theta < 1$ and the metal will flow even if $\Delta P_{ext} = 0$ (spontaneous flow). However, in most cases, the metal does not wet the mold and external pressure is required for flow. To maximize ΔP_{ext} one needs to minimize P_{gas} . Thus, **the Porosities present in Hot Clay Mold are an accelerating factor for liquid metal flow.**

2.3.1.4. Limitations of ‘Mold Filling time’ equation using Bernoulli’s Principle

Bernoulli’s Equation is used in traditional Mold Filling Time calculation [2.33, 2.34], which deals with ideal fluid, i.e., viscosity is zero [2.35], but liquid metal is a real fluid [2.36] and in thin-walled hot mold, liquid metal flow affects by many other factors like viscosity, surface tension, gas pressure inside mold [2.12] etc., therefore some modification is needed.

The Bernoulli’s Equation [2.37] for a steady incompressible flow (Figure-2.7) considering the friction head loss is

$$\frac{P_0}{\rho g} + \frac{v_0^2}{2g} + z_0 = \frac{P_1}{\rho g} + \frac{v_1^2}{2g} + z_1 + z_{friction} \quad (2.40)$$

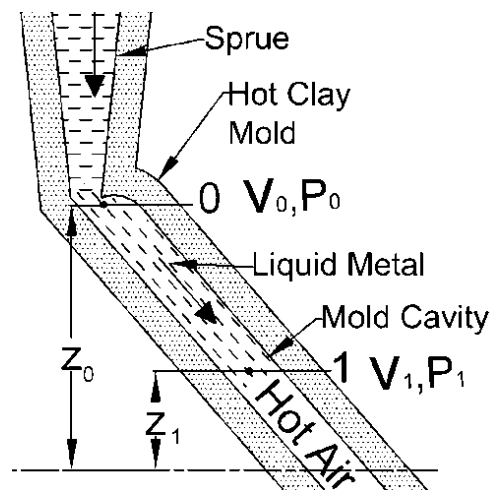


Figure.2.7: Liquid Flow through a Thin Hot Clay Mold from Sprue

Accounting the Kinetic Energy Correction Factor, Bernoulli's equation would generalized to

$$\frac{P_0}{\rho g} + \alpha \frac{v_0^2}{2g} + z_0 = \frac{P_1}{\rho g} + \alpha \frac{v_1^2}{2g} + z_1 + z_{friction} \quad (2.41)$$

For steady viscous flow through a Parallel Plate (Figure.2.3), Kinetic Energy Correction Factor for Laminar flow, $\alpha = 2.0$ (From equation 2.14)

Finally, The Modification of Bernoulli's Equation is

$$\frac{P_0}{\rho g} + \frac{v_0^2}{g} + z_0 = \frac{P_1}{\rho g} + \frac{v_1^2}{g} + z_1 + z_{friction} \quad (2.42)$$

2.3.1.5. Effect of Gating Design on Mold Filling Behavior

Different techniques are used for prediction of liquid metal flow patterns like Computational Fluid Dynamics Technique, Numerical simulation and different software but real time simulations of actual liquid metal flow pattern is very effective to understand the nature flow pattern. The flow patterns are observed by visual inspection, X-ray, Infrared and many other techniques. X. Yang [2.3], J. Campbell [2.10, 2.38], describes the real time simulation experiments. Y. H. K. Kharrazi [2.39], et al. studied the effect of gating system on mold filling behaviour by Aluminum alloy (A413) using lost foam casting (LFC) (Figure-2.8). Weng-Sing Hwang [2.11] and Mohsin Raza [2.40] also simulate the molten metal flow pattern for near net shape castings. All The experiments

identified that the liquid metal flow is highly influence by gating design such as gate diameter, sprue height and also thickness of mold.

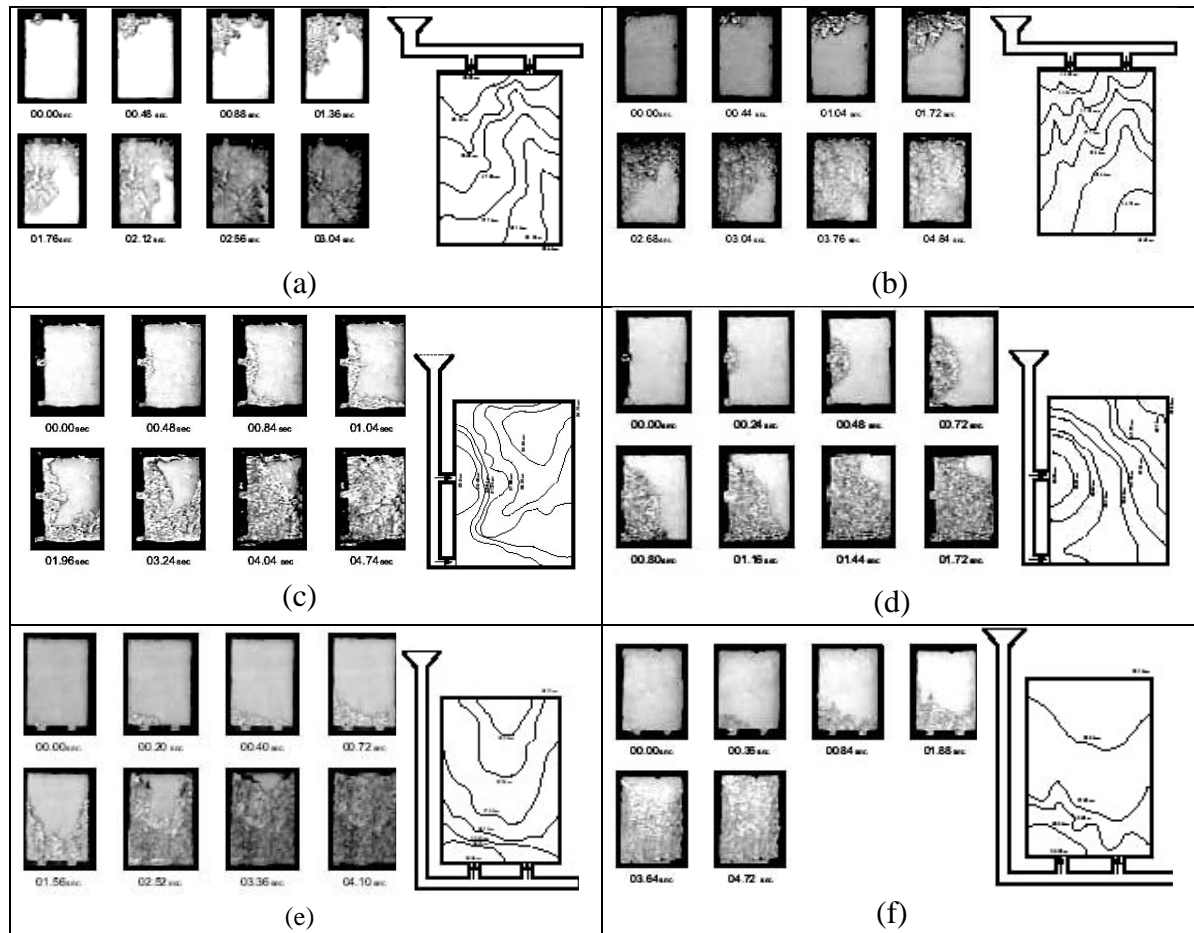


Figure- 2.8: Mold filling behaviour in the top gating system with mold thickness (a) 5 mm and (b) 10 mm, Mold filling behaviour in the side gating system with mold thickness (c) 5 mm and (d) 10 mm, Mold filling behaviour in the bottom gating system with mold thickness (e) 5 mm and (f) 10 mm, [Y. H. K. Kharrazi et. al.]

All the “contributions have employed mathematical modelling and simulation. This aspect is embodied in some of the commercial software designed to provide comprehensive pictures of events occurring in the mould throughout the casting process” [2.41].

2.3.2. Metrological challenges for investment casting product

The quality of precision encompasses not only the accuracy of individual dimensions but surface finish and general appearance. An exemplary casting not only fits within specified dimensional limits but also exhibits sharply defined outlines and a flawless surface. On the other hand, increased accuracy can minimize or eliminate machining expenses, particularly in scenarios involving intricate shapes, challenging access, or resilient alloys, thus potentially reducing overall costs [2.42].

2.3.2.1. Factors influencing dimensional accuracy

Factors contributing to the dimensional accuracy of castings are summarized below. According to Beeley [2.42] “They are:

1. Accuracy of the pattern or die equipment,
2. The accuracy with which the mold reproduces the pattern shape: important sources of error include pattern rap, distortion by sagging, and inexact mutual fit of mold parts,
3. The accuracy with which the casting confirms to the original shape of the mold, depending on the degree of filling and dimensional stability of the mold cavity on pouring,
4. The contraction factor, which determines the predictability of dimensional changes during cooling,
5. Finishing operations.

Increased precision must be based upon improvement in one or more of these fields”.

2.3.2.2. Casting quality and dimensional accuracy

According to the ‘Designers’ Handbook for Investment Casting’ published by British Investment Casting Trade Association (1990), “The minimum metal thickness that can be run depends partly upon the area of the section concerned. Although thicknesses of 0.75mm or even less can be achieved over small areas of casting wall, 1–1.5mm is seen as a reasonable minimum for large areas. Tolerances of around ± 0.15 mm are commonly accepted as feasible for linear dimensions up to 25 mm, extending to ± 1.5 mm for sizes around 250 mm. Allowances in the range 0.5–2.5mm are recommended depending on the size of the casting”. [2.43, 2.44]

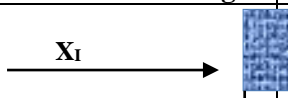


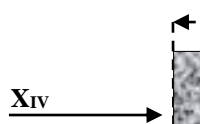
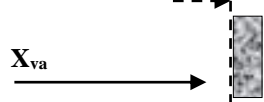

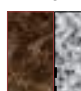

2.3.2.3. Dimensional variation at different stage due to Shrinkage

The stages of Investment casting Production were studied by M. Horáček [2.7], Adrian S. Sabau [2.45], Nick Cannell [2.46], Y.W. Donga [2.9] and many other researchers [Appendix-I]. It was noteworthy that the prediction of change of dimension in different stages of production is the key to the Economic casting production with dimension accuracy. An experiment was carried out by M. Horáček [2.7] to understand the problem. The influences investigated by M. Horáček were elaborated in Table- 2.1. The study is so important for Modeling of shrinkage during investment casting of thin-walled hollow turbine [2.9].

India has its own ancient investment casting technique [2.47, 2.48] [Appendix-XXII]. Many Indian researchers already investigated on this technique. According to these research works, Pattern allowances and distortion were widely varied from height to

width directions depending on type of castings due to complex distortion in thin section investment casting process. Distortion analysis was done for of thin-section investment castings which is the barriers to achieve the dimensional accuracy for the curved section [2.49, 2.50] or extended parts of a casting.

Table-2.1: Dimensional Changes during the Investment Casting Process [2.34]

	Technology Phase	Illustration of Dimensional changes	Short Process description
I	Die		X_I = DIMENSION OF DIE - Accuracy depending on die manufacturing method used
II	Wax pattern		X_{II} = WAX PATTERN DIMENSION - Contraction of injected wax $\Delta T: \sim 70^{\circ}\text{C} \rightarrow 20^{\circ}\text{C}$ ΔT = temperature range
III	Shell (Including wax)		X_{III} = SHELL DIMENSION - INTERNAL - Practically no dimensional changes $\Delta T: \sim 30^{\circ}\text{C} \rightarrow 20^{\circ}\text{C}$
IV	Shell cavity (After de-waxing + 24 hrs drying time)		X_{IV} = SHELL CAVITY DIMENSION - Contraction during process of shell binder system $\Delta T: \sim 25^{\circ}\text{C} \rightarrow 20^{\circ}\text{C}$
V(a)	a) SHELL CAVITY - After firing		X_{Va} = SHELL CAVITY AFTER FIRING Shell expansion during firing process $\Delta T: \sim 20^{\circ}\text{C} \rightarrow 1000^{\circ}\text{C}$
V(b)	a) SHELL CAVITY - After cooling (when applicable – i.e. Al ₂ O ₃ shell)		X_{Vb} = “COOLED” SHELL CAVITY - Shell contraction during its cooling after firing $\Delta T: \sim 1000^{\circ}\text{C} \rightarrow 20^{\circ}\text{C}$
VI(a)	METAL POURING - Into “hot” mould - Metal pouring + Solidification + cooling		X_{VIa} = CASTING DIMENS. – HOT MOULD - Initial slight shell expansion and final metal contraction after metal pouring $\Delta T: \sim 800 \rightarrow 1500 \rightarrow 20^{\circ}\text{C}$
VI(b)	METAL POURING - Into “cold” mould - Metal pouring + Solidification + cooling		X_{VIb} = CASTING DIMENS. – COLD MOULD - Initial slight shell expansion and final metal contraction after metal pouring $\Delta T: \sim 20 \rightarrow 1500 \rightarrow 20^{\circ}\text{C}$

Chapter-3

Analytical Model for Mathematical Expression of Filling Time Estimation

3. Analytical Model for Mathematical Expression of Filling Time Estimation

Employing Bernoulli's energy conservation equation, the mold's filling time is usually predicted in sand molds and other mold types through mass flow rate calculations. However, real filling times often exceed these forecasts. This discrepancy arises due to the minuscule aperture in the annular mold, resulting in significant frictional head loss (Z_f), as elucidated by authors like Spurk, Aksel [3.1], and Schaschke [3.2]. Another challenge highlighted by White [3.3], Çengel, Cimbala [3.4], and others is the kinetic energy correction factor (α) stemming from non-unidirectional fluid velocity in the dynamic process.

As Stefanescu [3.5] points out, flow within narrow channels introduces negative pressure head (ΔP_γ) due to capillary action between liquid and vapor, influenced by surface tension. The amalgamation of these three factors shapes the mathematical framework for filling time.

The estimation of filling time in conventional mold has been worked out using Bernoulli's principle by different authors like Elliott [3.6], J.Green Sylvia[3.7], Richard A. Flinn [3.8], Serope Kalpakjian, Steven R. Schmid [3.9] etc.

Empirical expressions [3.10] are generally used for precise time calculation but Conventional Filling Time (t_{conv}) used for top gating system [3.7, 3.8, 3.9] is given below

$$t_{conv} = \frac{Vol_{mold}}{A_g v_g} \quad (3.1)$$

where,
$$v_g = c_D \sqrt{2gz_s} \quad (3.2)$$

where, Gate Area is A_g , velocity of liquid metal at gate is v_g , sprue height is z_s , and co-efficient of discharge is C_D . The value of co-efficient of discharge is (C_D) is generally taken as 0.8 [3.11]. The Mathematical Modelling of Filling Time calculation for thin section casting, in hot clay mold was derived.

3.1.Assumptions for Annular Thin Cylindrical Sections

Improving the conventional Filling time in thin walled investment casting in hot mold the following assumptions have been postulated.

i. Stream Line Flow:

The liquid has been assumed to be Newtonian fluid [3.12, 3.13], with steady and streamline motion.

ii. Friction Head Loss (z_f):

The flow through Thin Mold or Capillary Mold ($\sim \mu\text{m}$) experienced severe resistance force due to friction head (z_f) and the resistance has been taken .

iii. Kinetic Energy Correction Factor (α):

A velocity distribution through the thin mold width over cross section occurs. Therefore Kinetic Energy Correction Factor (α) has been introduced due to non-one dimensional flow.

iv. Pressure due to Capillary action ($\Delta P\gamma$):

The pressure drop ($\Delta P\gamma$) along the capillary mold (resistance to flow) because of the resistance to flow between narrow parallel plates (w) for the surface energy between the liquid and its vapour phase.

v. Flow through Wide Channel:

The concept of Flow through Wide Channel (Flow through Plate) has been adapted as considering the diameter of the cylinder is too large with respect to the very small mold opening (in μm range). Based on this friction head loss has been calculated.

vi. Negligible Heat Loss:

The temperature of the mold is more or less equal to the liquid metal temperature, so the heat loss from the liquid metal during pouring has been considered negligible.

vii. Effect of Hot Clay Mold:

A Torricellian vacuum has been created within the red hot mold by the differential pressure head- negative air pressure between the hot mold interior and the ambient outside atmospheric pressure. The reason is in hot clay mold, the density of the air inside the mold is less; therefore the air pressure inside the mold is always lesser than the atmospheric pressure. The gas pressure difference [3.14] is calculated in segment-3.5, considering the air as an ideal gas. The negative gas pressure factor changes the filling time result very negligibly in numerical terms.

viii. Bottom Gating System:

The gating system resembles top gating but for the annular mold, the liquid metal reaches the bottom first and then starts rising from the bottom, filling the mold like Bottom Gating. Therefore the liquid velocity varies with rising height of the fluid in the mold. So the flow rate of the liquid has not been constant throughout the filling time.

3.2.Incorporation of the factors into the analytical model

The Factors, taken into account to modify the Gating Design of Thin-Section Hot Mold Castings are given below

3.2.1. Effect of Friction Head Loss (z_f)

Assuming, flow through parallel plates (wide channel) in thin walled hot metal the hydraulic diameter (d_H) has been calculated for W =width or thickness [equation-2.27]:

$$d_H=2w \quad (3.3)$$

Friction factor has been calculated for flow through parallel plates in equation-2.28:

$$f = \frac{96}{Re} \quad (3.4)$$

The Reynolds No (Re) is:

$$Re = \frac{\rho v d_H}{\mu} \quad (3.5)$$

Where, W =width or thickness, v =velocity of flow , ρ =density of liquid, μ = viscosity.

The Friction Head loss for Flow through Parallel Plates (wide channel), is given by [equation -2.19], Where, L_m = Length of path of Flow inside mold, f = Friction factor

$$z_f = f \frac{L_m}{d_H} \frac{v^2}{2g} \quad (3.6)$$

The Friction Head Loss due to flow through Thin Annular Section becomes (using equation 3.3,3.4, 3.5 and 3.6):

$$z_f = \frac{48\mu L_m v}{\rho g d_H^2} \quad (3.7)$$

3.2.2. Kinetic Energy Correction Factor (α)

The Kinetic Energy Correction Factor (α) for the flow through a channel considering the flow is Laminar is taken by [3.15] [from equation-2.14]

$$\alpha=2 \quad (3.8)$$

3.2.3. Pressure due to Capillary action ($\Delta P\gamma$)

Because of metal-mold interaction the pressure drop along the capillary mold (resistance to flow) has been considered as a fluid flow between narrow capillary thickness 'w' parallel plates, as follows [3.16] [from equation-2.36]

$$\Delta P_\gamma = -\frac{2}{w} \gamma_{LV} \cos \theta \quad (3.9)$$

Where, γ_{LV} is the surface energy between the liquid metal and its vapour phase, and ' θ ' is the contact angle between the metal and the mold ($90^\circ < \theta < 180^\circ$).

3.2.4. Bernoulli's Equation for Fluid Flow Through a Annular Mold

Neglecting all other factors, for ideal condition Bernoulli's energy balance equation between the point 1 and 2 of figure-3.1 will be

$$\frac{P_1}{\rho} + \frac{v_g^2}{2} + gz_m = \frac{P_2}{\rho} + \frac{v^2}{2} + gz \quad (3.10)$$

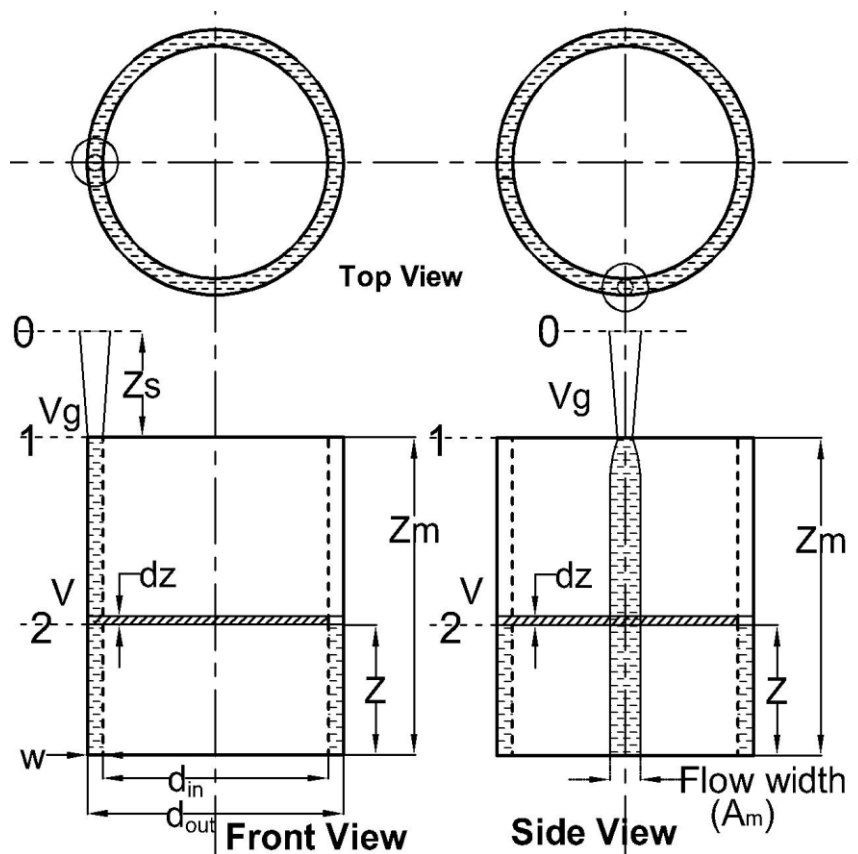


Figure-3.1: Sectional View of an Annular Cylinder during filling

3.3. Filling Time Calculation of Thin-Section Annular Cylindrical Hot Mold by Top Gating

Considering an annular cylindrical mold filled by liquid metal with a top gating system (Figure-3.1), having Mold height ' Z_m ', Sprue Height ' Z_s ', and width ' w ', the Bernoulli's energy balance equation between 1 and 2 with putting all the incorporations of the factors becomes

$$\frac{P_1}{\rho} + \frac{\alpha v_g^2}{2} + gz_m = \frac{P_2}{\rho} + \frac{\alpha v^2}{2} + gz + gz_f + \frac{\Delta P_\gamma}{\rho_{liq}} \quad (3.11)$$

From equation 3.7, 3.8, 3.9, and 3.10 by neglecting Gas Pressure effect (i.e., $P_1=P_2$), the velocity becomes

$$v^2 + \left[\frac{48\mu L_m}{\rho d_H^2} \right] v - [gz_m - gz + v_g^2 - \frac{\Delta P_\gamma}{\rho_{liq}}] = 0 \quad (3.12)$$

Putting: $b = \frac{24\mu L_m}{\rho d_H^2}$ the derived equation for velocity ' v ' becomes

$$v = -b \pm \sqrt{g \left[\frac{1}{g} (b^2 + z_m + \frac{v_g^2}{g} - \frac{\Delta P_\gamma}{\rho_{liq} g}) \right] - z} \quad (3.13)$$

Putting, $k = \frac{1}{g} [b^2 + gz_m + v_g^2 - \frac{\Delta P_\gamma}{\rho_{liq}}]$ and neglecting negative term, the equation for velocity ' v ' simplifies and Equation (3.13) becomes

$$v = \sqrt{g(k - z)} - b \quad (3.14)$$

If ' dt ' time is taken for filling of infinitely small height ' dz ', then it can be written as:
[Where; A_f = Cross-sectional area of liquid flow inside the mold. A_m = Cross-sectional area of mold filled by liquid metal]

$$v \cdot A_f \cdot dt = A_m \cdot dz \quad (3.15)$$

$$\Rightarrow \frac{A_f}{A_m} dt = \frac{dz}{v} \quad (3.16)$$

$$\Rightarrow \frac{A_f}{A_m} \int_0^{t_f} dt = \int_0^{Z_m} \frac{dz}{-b + \sqrt{g(k - z)}} \quad (3.17)$$

By Integrating both sides and Putting: $\lambda = \left[\frac{\sqrt{k} - \frac{b}{\sqrt{g}}}{\sqrt{k - Z_m} - \frac{b}{\sqrt{g}}} \right]$

[Considering, λ = Filling Time Factor for Thin Walled Casting. It is a Unit less quantity.]

Filling time becomes

$$t_f = \frac{A_m}{A_f} \left[\frac{2}{\sqrt{g}} (\sqrt{k} - \sqrt{k - Z_m}) + \frac{2b}{g} \ln(\lambda) \right] \quad (3.18)$$

This is the modified Filling Time Equation for Thin walled casting in hot mold [3.17].

3.4. Flow area for $d_g \leq w$ and $d_g > w$ [d_g = gate diameter (m), w = mold thickness (m)]

Two types (Figure-3.2) of gating systems are often used for thin-walled casting. The gate area modified as (A_f) depending upon the relationship between the gate diameter (d_g) and the width (w) of the thin mold cavity where Gate diameter (d_g) is less or equal to Mold cavity thickness (w) or greater than w :

Case-I: Gate diameter (d_g) is less or equal to Mold cavity thickness (w) [$d_g \leq w$]

$$A_f = \frac{\pi}{4} \times d_g^2 \quad [\text{For } d_g \leq w] \quad (3.19a)$$

Case-II: Gate diameter (d_g) is greater than Mold cavity thickness (w) [$d_g > w$]

$$A_f = W \times d_g \quad [\text{For } d_g > w] \quad (3.19b)$$

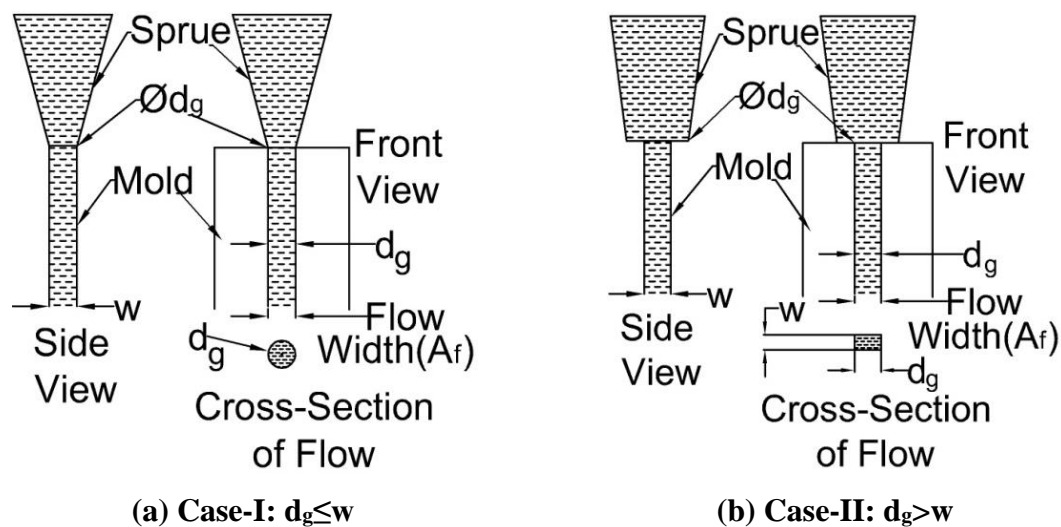


Figure-3.2: Gating System for Thin Molds [3.17]

3.5. Pressure Inside Hot Mold [3.13, 3.18]:

In hot mold, the density of the air inside the mold is less; therefore the air pressure inside the mold is always lesser than the atmospheric pressure. The gas pressure difference is calculated below, considering the air as an ideal gas.

Inside the hot mold at high temperature $=T_h$ (K), Pressure inside hot mold $= P_h$ (Pa), ρ_h = Air density (kg/m³) inside hot mold at temperature T_h (K), P_{atm} = Atmospheric air pressure (Pa), Atmospheric Air density (kg/m³) at ambient temperature T_a (K). R_C = Characteristics Gas Constant for air [3.19]=287 J.kg⁻¹.K⁻¹

$$P_{atm} = \rho_{air} R_C T_a \quad (3.20)$$

$$P_h = \rho_h R_C T_h \quad (3.21)$$

The gas pressure difference between inside and outside of the a red hot mold is:

$$\therefore \Delta P_{gas} = P_h - P_a \quad (3.22)$$

The pressure difference is in terms of Gauge Pressure, as according to convention [3.20]

$$P_{gauge} = P_{absolute} - P_{atm}$$

To understand the pressure difference (in gauge) between ambient air pressure and the inner pressure of hot clay mold a graph was plotted by considering air density [5.6] at

various temperatures between 500⁰C to 1100⁰C. The calculations were done after converting the temperature into Kelvin from degree centigrade (⁰C). Ambient temperature was considered as 300K.

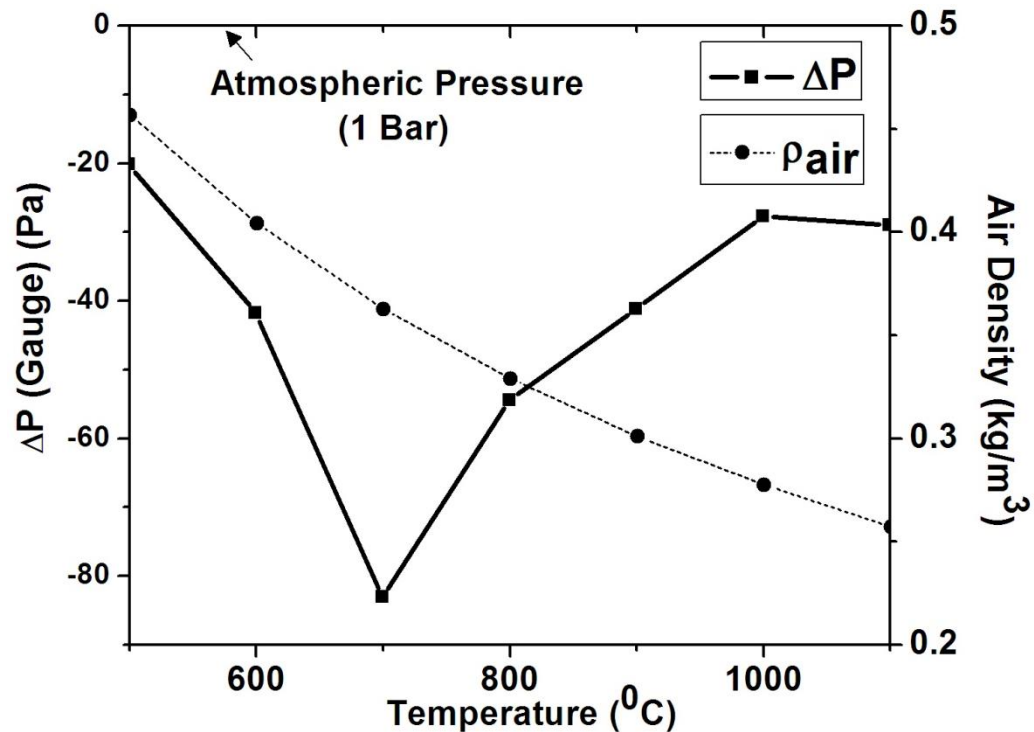


Figure-3.3: Temperature (⁰C) wise Pressure difference (ΔP) (Gauge pressure) (Pa) inside a mold along with air density (kg/m³)

The pressure inside the hot mold is less than external ambient air pressure with a negligibly low value, but it will act as a suction pressure (negative gauge pressure). During the pouring of liquid metal inside a thin section mold for gravity investment casting the suction pressure plays a very vital role in overcoming the constraints and initiating the entrance of liquid metal in very thin section mold comfortably; like, High initial torque during the start of an IC engine or High No-Load current during the start of an Induction motor or the friction threshold required to set a stationary object in motion.

Chapter-4

Experimental Framework

4. Experimental Framework

The Experimental framework as well as the calculation procedure and the instruments used for all the experiments are discussed here.

4.1. Plan of work

The Experimental Framework has been shown in figure-4.1 and elaborated.

4.1.1. Simulation experiments

The analytical model was validated by simulation experimentation using liquid Mercury and water at room temperature. Transparent molds having various thickness but same geometrical sections were used with different position. The real time flow patterns of the liquids were studied and the actual mold filling time compared using the error calculation. Errors were calculated for 'tradition mold filling time' and 'analytical model for mold filling time' with respect to actual mold filling time.

The suction pressure inside a hot clay mold investigated and compared with the proposed model which was already discussed in chapter-3.

4.1.2. Metrological analysis of thin walled investment casting

Thin section investment casting in hot clay molds were investigated by a laboratory experiment. The patterns were designed by the influence of M. HORÁČEK's [4.1]

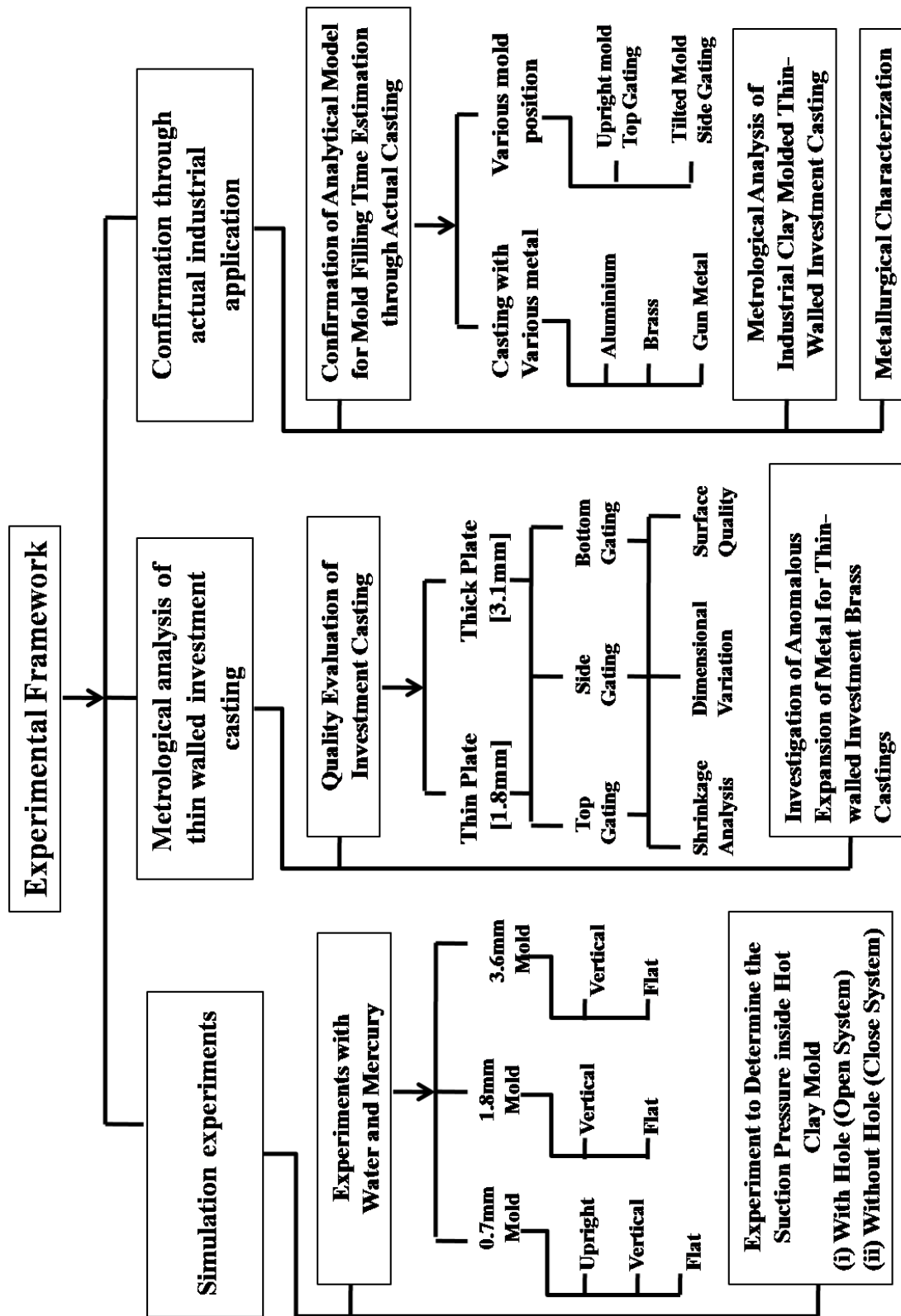


Figure-4.1: Block Diagram of Experimental Framework

experiment but at Indian environment and using Indian materials, like Indian Bee's wax as pattern material, Indian Kaolinite clay and Silica sand mixture as mold material.

The samples were designed to cast by the following parameters

- (i) Pattern Thickness: Thin [$1.8^{+0.08}_{-0.0}$ mm] and Thick [$3.6^{+0.05}_{-0.0}$ mm]
- (ii) Presence of Core: With Core [Restricted] and Without Core [Un-Restricted]
- (iii) Type of Gating: Top, side and Bottom gating

In addition to Shrinkage analysis, assessment of Casting Quality was done by the following metrological analysis.

- (i) Dimensional Variation: [Root mean square deviation (R.M.S.D) of Length, Breadth and Thickness]
- (ii) Surface quality and surface Roughness

Based on the result of experimentation the samples were ranked by TOPSIS (Technique for Order Preference by Similarity to Ideal Solution). TOPSIS is a scientific numerical technique of the multi-criteria decision making (MCDM).

The discrepancies found in the experimentation were further investigated by other tests and discussed elaborately in other section.

4.1.3. Confirmation through actual industrial application

All the derived and adopted analytical or numerical models was confirmed through actual industrial application. As it was difficult to conduct the investigation inside an

industrial investment casting workshop, an Indian traditional rural small scale casting industry was chosen.

Analytical model for mold filling time was vindicated with actual casting thin section investment casting in hot clay mold. Metrological study and shrinkage analysis was done for a product and its parts.

4.2.Mathematical expressions and Numerical Techniques used for calculations

The Mathematical expressions and Numerical Techniques for evaluation of mold filling time, gating design and ranking method were illustrated in this segment.

4.2.1. Filling Time Calculation

Mold Filling Time was calculated according to the derived ‘Analytical Model for Mathematical Expression of Filling Time Estimation’.

Velocity of the liquid metal at the Gate, $v_g = C\sqrt{2gz_t}$, m/s

[C= co-efficient of Discharge=0.8,

z_t = Total height (m) = Sprue height (z_s) + Cup height (z_c)]

Equivalent Mold Area, $A_m = \left(\frac{V}{z_m}\right)$, $\times 10^3$, m²

[V= mold volume (m³), z_m = mold height (m)]

Time of Filling, (sec) [Symbols were already mentioned in chapter-3] [4.2]

$$t_f = \frac{A_m}{A_f} \left[\frac{2}{\sqrt{g}} (\sqrt{k} - \sqrt{k - Z_m}) + \frac{2b}{g} \ln \left(\frac{\sqrt{k} - \frac{b}{\sqrt{g}}}{\sqrt{k - Z_m} - \frac{b}{\sqrt{g}}} \right) \right] \quad [\text{Equation-3.18}]$$

$$b = \frac{24\mu L}{\rho d_H^2}, \quad k = \left[\left(\frac{24\mu L_m}{\rho d_H^2} \right)^2 + g z_m + v_g^2 + \frac{\Delta P_{Gas}}{\rho_{liq}} - \frac{\Delta P_\gamma}{\rho_{liq}} \right]$$

Checked by Reynolds's No.: $R_e = \frac{v_g \rho w}{\mu}$ [Equation-3.5]

Error Calculation:

Compare with proposed mold filling time (t_f):

$$Error(\%) = \left(\frac{t_f - t_{actual}}{t_f} \right) \times 100 \quad (4.1-a)$$

Compare with Conventional Filling Time (t_{conv}):

$$Error(\%) = \left(\frac{t_{conv.} - t_{actual}}{t_{conv.}} \right) \times 100 \quad (4.1-b)$$

4.2.2. Gating Design Calculation [4.3]

The following method was used to design a Gating system for simulation experiments and metal castings.

Sprue Design: [By Aspiration Correction] Cup Diameter, d_c , (m);

$$\frac{d_c}{d_g} = \sqrt[4]{\frac{z_t}{z_c}} \quad (4.2)$$

Riser Design [4.4]: [By Modulus Method] Riser diameter, (m) = d_r ;

$$\text{Modulus of the casting, (m),} = M_c \quad M_c = \left(\frac{\text{Vol}}{\text{Area}} \right)_{\text{Casting}} \quad (4.3)$$

$$M_r = \text{Modulus of riser} \quad M_c = \left(\frac{\text{Vol}}{\text{Area}} \right)_{\text{Riser}} \quad (4.4)$$

$M_r = 1.2 M_c$ [By Modulus Method] also assume, Cylindrical Riser, $d_r = h_r$

$$M_r = \frac{d_r}{4} \quad (4.5)$$

Hot metal required (kg) [considering, 20% extra metal for drossing and spilling]

$$W_{\text{Total}} = (V_{\text{Casting}} + V_{\text{Gating}}) \times \rho_{\text{liquid Metal}} \quad (4.6)$$

$$\text{Yield of the Casting, (\%)} \quad \text{Yield} = \frac{W}{W_{\text{Total}}} \cdot 100 \quad (\%) \quad (4.7)$$

4.2.3. Dimensional variation and Shrinkage analysis

The following expression was used to determine the shrinkage analysis of the two dimensional castings (plate) with respect to wax pattern (Chapter-5) [4.5, 4.6].

$$\text{Shrinkage (\%)} = \frac{\text{Wax pattern dimension} - \text{Cast dimension}}{\text{Wax pattern dimension}} \times 100 \quad (4.8)$$

The following expressions were used to determine the shrinkage analysis of the three dimensional castings (Circular section) with respect to die and wax pattern (Chapter-6).

$$\text{Clay Core Shrinkage (\%)} = \frac{\text{Die dimension} - \text{Clay Core dimension}}{\text{Die dimension}} \times 100 \quad (4.9)$$

Shrinkage of Internal and External Dimension of Cast Product:

$$\text{Avg. diameter} = \frac{\text{Major Diameter} + \text{Minor Diameter}}{2} \quad (4.10)$$

$$\text{External Shrinkage (\%)} = \frac{\text{Wax Pattern dia} - \text{External Dia}}{\text{Wax Pattern dia}} \times 100 \quad (4.11)$$

$$\text{Internal Shrinkage (\%)} = \frac{\text{Clay core dia} - \text{Internal Dia}}{\text{Clay Core dia}} \times 100 \quad (4.12)$$

Metal Thickness Shrinkage:

$$\text{Wax Thickness} = (\text{Mean Wax Pattern Radius} - \text{Mean Clay Core Radius}) \quad (4.13)$$

$$\text{Wax Thickness Shrinkage (\%)} = \frac{\text{wax thickness} - \text{metal thickness}}{\text{wax thickness}} \times 100 \quad (4.14)$$

➤ *According to calculation Positive (+) value is for SHRINKAGE and Negative (-) value is for EXPANSION.*

The following calculations were performed to analyze the dimensional variations of the castings by Root mean square method (RMSD) [4.7, 4.8]. If x_1, x_2, \dots, x_n is a sample of a population with true mean value x_0 , then the RMSD of the sample is

$$\text{RMSD} = \sqrt{\frac{1}{n} \sum_{i=1}^n (x_i - x_0)^2} \quad (4.15)$$

The eccentricity of Outer and Inner diameter of Lip and Base positions were calculated by measured Major and Minor Diameters [4.9].

$$\text{Eccentricity} = \sqrt{1 - \frac{(\text{Minor Diameter})^2}{(\text{Major Diameter})^2}} \quad (4.16)$$

4.2.4. Procedure of calculation to determine the Rank of the Casting using TOPSIS

The evaluation of cast product quality posed a challenge due to the non-commensurability of the parameters [4.10], making it intricate to establish a ranking based on quality. Addressing this complexity, the utilization of MCDM [4.11] (multi-criteria decision-making) techniques emerges as a crucial approach for analyzing intricate real-world problems, given its inherent capacity to assess diverse alternatives, be it choices, strategies, and so forth.

Among the array of scientific numerical methods within the realm of MCDM, TOPSIS [4.12] (Technique for Order Preference by Similarity to Ideal Solution) stands out as a popular choice. The subsequent section delves into the application of TOPSIS [4.13] as a solution method for addressing problems.

Step-1:

Let's consider a set of m alternatives, denoted as $X_1, X_2, \dots, X_{m-1}, X_m$. Each alternative X_i is evaluated against n criteria, $C_1, C_2, C_3, \dots, C_n$ where the criteria are represented by positive numbers C_{ij} . Among these criteria $C_1, C_2, C_3, \dots, C_k$ are considered as benefit criteria, indicating a monotonically increasing preference, while the remaining criteria are classified as non-benefit, reflecting a monotonically decreasing preference. The criteria Weights C_j are assigned weights, denoted as w_j , satisfying the condition $\sum_{j=1}^n w_j = 1$. The objective is to identify the most optimal alternative based on these criteria and their assigned weights. To enhance clarity, a tabular representation (Table- 4.1) is provided, outlining the alternatives, criteria, and their respective weights.

Step-2:

Ensuring a balanced payoff matrix is crucial, especially when the numbers c_{ij} representing different criteria possess varying measuring units. The provided weights, denoted as w_j , for each criterion must be duly considered. To address this, an initial step involves replacing the measurement values c_{ij} associated with the criteria c_j . This replacement involves the use of normalized or relative numbers, denoted as r_{ij} .

$$r_{ij} = \frac{c_{ij}}{\sqrt{\sum_{i=1}^m x_{ij}^2}} \quad (4.17)$$

The Normalized Payoff Matrix has been shown in Table- 4.2.

Table-4.1: Payoff Matrix [4.14]

Criteria	C ₁	C ₂	C _{n-1}	C _n
Weights	w ₁	w ₂	w _{n-1}	w _n
Alternatives			
X ₁	c ₁₁	c ₁₂	c _{1n}
X ₂	c ₂₁	c ₂₂	c _{2n}
⋮	⋮	⋮	⋮	⋮	⋮
X _{m-1}			
X _m	c _{m1}	c _{m2}	c _{mn}

Table-4.2: Normalized Payoff Matrix

C ₁	C ₂	C _{n-1}	C _n
w ₁	w ₂	w _{n-1}	w _n
r ₁₁	r ₁₂	r _{1n}
r ₂₁	r ₂₂	r _{2n}
⋮	⋮	⋮	⋮	⋮
		
r _{m1}	r _{m2}	r _{mn}

Step-3:

The normalized numbers (r_{ij}) belong to open interval $<0,1>$. Subsequently, in accordance with the share $w_i c_j$ of the criteria c_j , these normalized numbers (r_{ij}) are substituted with the weighted normalized numbers, denoted as:

$$a_{ij} = w_j r_{ij} = w_j \frac{c_{ij}}{\sqrt{\sum_{i=1}^m x_{ij}^2}} \quad (4.18)$$

Determining the ideal (f_i^*) value which is maximum and the negative ideal (f_i^{**}) value which is minimum for each criterion j . The Weighted Normalized Payoff Matrix, ideal (f_i^*), negative ideal (f_i^{**}) values are tabulated in Table-4.3.

Table-4.3: Weighted Normalized Payoff Matrix, ideal (f_i^*), negative ideal (f_i^{**}) values

Criteria	C_1	C_2	C_{n-1}	C_n
Alternatives			
X_1	a_{11}	a_{12}	a_{1n}
\vdots	\vdots	\vdots	\vdots	\vdots	\vdots
X_m	a_{m1}	a_{m2}	a_{mn}
f_j^*					
f_j^{**}					

Step-4:

Parameters needed for computing the separation measure include the ideal (f_j^*) and negative ideal (f_j^{**}) value for each criterion j . Subsequently, the separation measures D_a^+ and D_a^- , representing J -dimensional Euclidean distances, are calculated for each alternative.

(i) The separation measures of each alternative 'a' from the ideal solution and negative ideal solution are determined by calculating the distance of each criterion from its ideal value as well as negative ideal value and summing these distances across all criteria for the specified alternative 'a' i.e.,

$$D_a^+ = \sqrt{\sum_{j=1}^j (f_j(a) - f_j^*)^2} \quad (4.19)$$

$$D_a^- = \sqrt{\sum_{j=1}^j (f_j(a) - f_j^{**})^2} \quad (4.20)$$

(ii) Computation of relative closeness of each alternative 'a' with reference to negative ideal measure D_a^- is

$$C_a = \frac{D_a^-}{D_a^+ + D_a^-} \quad (4.21)$$

Rank of the alternative base on the C_a value The Lower the C_a value, the better the alternative.

4.3. Testing procedure and Instruments used

The description of the instruments used for metrological analysis is illustrated and the testing procedure techniques are elaborated here.

4.3.1. Instruments used for Dimensional Analysis

Metrological Instruments [4.15] used to measure the dimension of different samples were mentioned in Table-4.4 and shown in figure-4.2.

Table-4.4: Details of Measuring Instruments

	Instruments	Used to Measure
i.	Digital Vernier Caliper	Thickness, Diameter
ii.	Micrometer	The thickness of Complex Section
iii.	Screw Thread Micrometer	The thickness of the Curved Section
iv.	Depth Vernier Caliper	Depth of the Samples
v.	Height Gauge	Height of the Wax and Cast Models
vi.	Dial Indicator	Eccentricity
vii.	Inside and Outside caliper	Inside and Outside Dimension of the profound part

4.3.2. Experimental Procedure for Surface Roughness

Surface Roughness [4.16] of the cast samples were measured by Taylor Hobson instrument; model- Sutronic 3+ (figure-4.3). The plane and straight surface part of the samples collected from the Field Experiment were being cut for surface roughness measurement. Samples made in the Laboratory were measured directly. The machine was calibrated before measurement using the test sample.

4.3.3. Experimental Procedure for Characterization of Metals

The following experimental procedures were followed for characterization for different metals.

4.3.3.1. Chemical Analysis

Chemical Analyses of cast metals were done by Spectroscopy using the standard- IS 4027. Cu-alloy and Detailed calculation of 'Zn equivalent' of the Brass Samples [4.17, 4.18]. was given in Appendix-XV.

4.3.3.2. Vickers Hardness Test

The Hardness of the cast samples were measured by Vickers Hardness [4.19]. The pictorial view of the Vickers Indentation machine (model no. VM 50, Sr. No. 02/2006–815) has been shown in figure- 4.4.

The Vickers Hardness indenter comprising a diamond square-based pyramid with a face angle of 136° between faces [4.20]. was utilized under a consistent load (5 kgf) for a fixed duration (10 sec). Microscopic measurement of square indentation diagonals yielded an averaged value. The Vickers Hardness Number (VHN) was then determined [4.23], with parameters: P (Applied Load, Kg), d (Average Length of Diagonals, mm), and ϕ (Face Angle, 136°).

$$VHN = \frac{2P \sin(\theta/2)}{L^2} = \frac{1.854P}{L^2} \quad (4.22)$$

4.3.3.3. Metallography of Cast Metal Sample

A metallurgical microscope is an optical instrument distinguished from other microscopes by its approach to specimen illumination. Due to the opaque nature of metals, frontal lighting is imperative. Consequently, the light source is internally situated within the microscope tube, facilitated by a plain glass reflector installed in a tube (figure-4.5) [4.20].

The procedures to develop microstructure were as described sequentially

- i. Samples were ground by a belt grinder to make a flat surface
- ii. Emery paper was used with a sequence of 120, 180, 1/0, and 2/0 to remove the scratches as well as smoothing the plane
- iii. The samples were then cloth polished for the final mirror polishing.
- iv. Etched with FeCl_3 (1 gm. FeCl_3 , 10 ml HCl , 100 ml H_2O) or 2% Nital solution followed by drying with alcohol ($\text{C}_2\text{H}_5\text{OH}$).

4.3.3.4. SEM and EDX

The scanning electron microscopy [4.21, 4.22] of specimens was done by Oxford, JEOL JSM-6360 (figure-4.6). This microscope utilizes electrons instead of light to create images. Compared to traditional light microscopes, SEM offers numerous advantages, such as a substantial depth of field, enabling a broader sample area to be in focus simultaneously. Additionally, SEM EM produces high-resolution images, enabling meticulous examination of closely spaced features at elevated magnification. Sample preparation is generally straightforward, given that most SEMs necessitate conductive samples.

Energy Dispersive X-ray analysis (EDX Analysis), also known as EDS or EDAX analysis, is a technique integrated with a scanning electron microscope (SEM). It determines the elemental composition of specimens by detecting X-rays emitted during electron interactions, offering valuable insights into material makeup. The EDX system cannot operate independently and requires integration with an SEM.

4.3.4. Analysis of the Clay used for Experiment

Grain Fineness Number of the clay used for experiments were determined by Sieve analysis [4.24] and also Sodium equivalent [4.25] for the same clays were determined by calculation from the pH measured. The instrument and tools used for sieve analysis and pH measurement were shown in figure-4.7.

4.3.5. Temperature Measuring Instrument

K-Type Thermocouple with Digital indicator and Steel Probe used to measure the temperature of the mold and liquid metal during the experiments were given below (figure-4.8).

4.4. Physical property of Liquid Metals

The Pouring Temperature and Physical properties [Density (ρ_{liq} , kg/m³), Viscosity (μ , mPa.s), Surface Energy (γ , mN/m), Contact Angle, (θ , rad)] of the Liquid Metals [Aluminium (LM6), Bronze (Gunmetal), Brass (60/40), Mercury (99.9%)] used for the experiments are tabulated in table-4.5.

Table-4.5: Pouring Temperature and Physical property of Liquid Metals

Metal/Alloy (with Grade)	Aluminium (LM6)	Bronze (Gunmetal)	Brass (60/40)	Mercury (99.9%)
Pouring Temp. (°C)	780	1120	1080	30
Density (ρ_{liq} , kg/m ³)	2700 [4.26]	8719 [4.28]	8400 [4.33]	13150 [4.37]
Viscosity (μ , mPa.s)	1.3 [4.27]	4.3 [4.30]	4 [4.34]	0.0016 [4.38]
Surface Energy (γ , mN/m)	500 [4.28]	480 [4.31]	8400 [4.35]	476 [4.39]
Contact Angle (θ , rad)	2.11 [4.29]	2.23 [4.32]	2.37 [4.36]	2.27 [4.40]

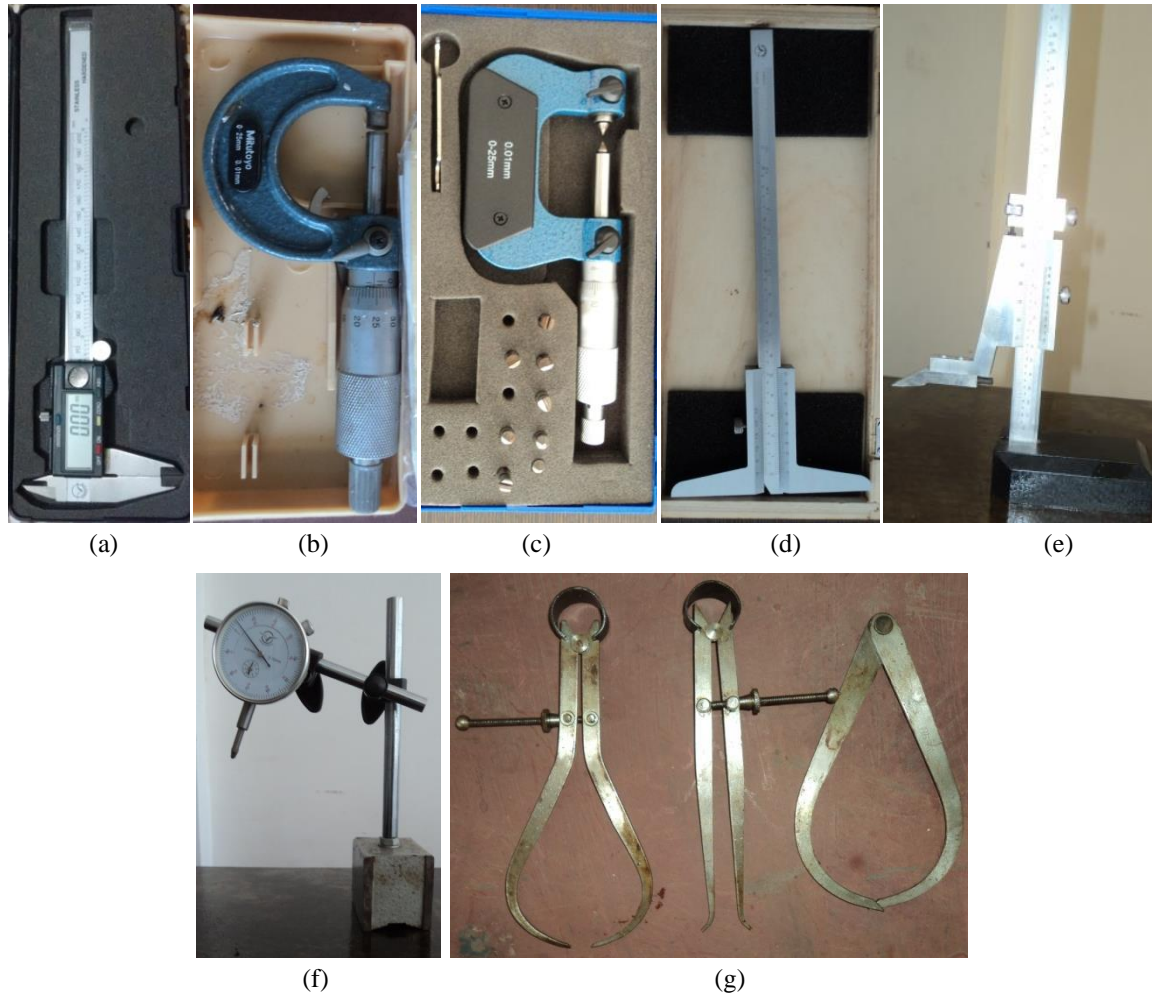


Figure-4.2: Measuring Instrument: (a) Digital Vernier Caliper, (b) Micrometer, (c) Screw Thread Micrometer, (d) Depth Vernier Caliper, (e) Height Gauge, (f) Dial Indicator, (g) Inside and Outside caliper.



Figure-4.3: Surface Roughness Measuring Machine: Taylor-Hobson instrument



Figure-4.4: Vickers Indentation Instrument



Figure-4.5: Optical Microscope



Figure-4.6: Pictorial View of SEM-EDX Machine



Weight Machine



pH meter



Sieve Shaker with Sieves

Figure--4.7: Instruments used for analysis of Clay



Figure-4.8: K-Type Thermocouple with Digital indicator: The steel probe of the thermocouple put in the crucible at the Furnace to measure the temperature

Chapter-5

Simulation Experiments

5. Simulation Experiments

The Analytical Model for Mathematical Expression of Filling Time Estimation was verified by the following simulation experimentations. Fluid engineers commonly consider water as the principle fluid on which most of the fluid mechanics derivations are made.

Mercury has got non-wetting characteristics because of wide contact angles, similar to many metal-mold combinations of investment castings and very easy to observe at room temperature which cannot be observed in opaque hot molds. So, an attempt was made to predict or imagine the flow pattern in case of opaque hot silica mold.

5.1 Simulation Experiments with Water and Mercury

Simulation Experiments with Water and Liquid Mercury were done under constant flow rate to validate the proposed filling time (t_f) [Equation-3.18]. The Water and Liquid Mercury was poured into some rectangular narrow section plastic molds. Justification was made by error (%) calculation.

5.1.1 Experimental procedure

Fluid flow engineers generally operate with parameters like liquid head, inlet diameter, flow through parallel plates and similar parameters to understand friction loss, capillary head loss and others energy losses. Incidentally the derived filling time model was developed with perspective of fluid flow engineers and therefore, the experimental set up

was designed to determine the resultant observations and the validation of the derived model.

To account for variation, each mold was simulated with different positions. The experimental framework was shown in Table 5.1. A detailed depiction of the molds, including the accompanying gating system, along with elaborate dimensions, can be observed in Figure 5.1. For additional parameters, a graphical representation can be found in Figure 5.2 showing the mold volume and gate area.

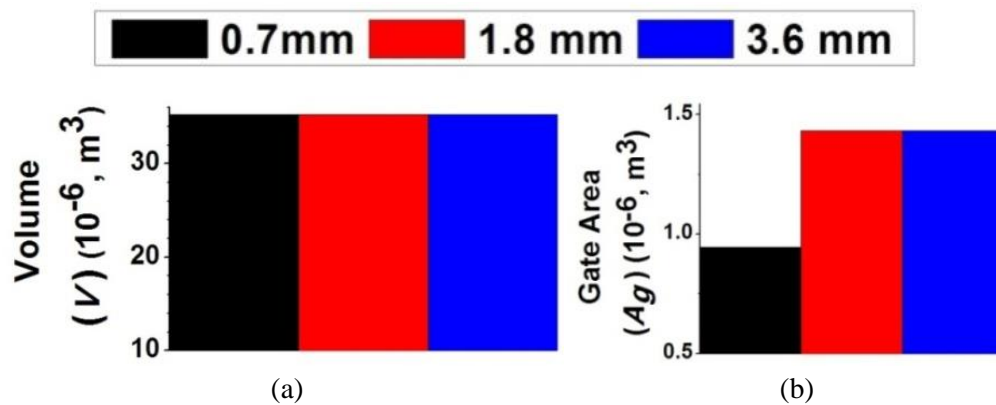


Figure- 5.1: Details of (a) Mold volume and (b) Gate Area

Table-5.1: Experimental framework for Simulation Experiment

(Gating Design same for each experiment)

Mold Thickness (w)		0.7 mm			1.8 mm		3.6 mm	
Water	Mold Position	Upright	Vertical	Flat	Vertical	Flat	Vertical	Flat
	(z_m) (mm)	360	140	0.7	140	1.8	140	3.6
Mercury	Mold Position	Upright	Vertical	Flat	Vertical	Flat	Vertical	Flat
	(z_m) (mm)	360	140	0.7	140	1.8	140	3.6

z_m = Mold Height

5.1.2 Results

Fluid flow patterns of the liquids for selected time frames were shown in figures 5.3. For a more extensive analysis, please refer to Appendix II for the water simulation and Appendix III for the mercury simulation, where a comprehensive examination of the flow patterns is provided.

In Figure 5.4, a comprehensive record of the filling time for all molds and positions is presented for the water simulation. Similarly, Figure 5.6 provides the same detailed information for the mercury simulation. For a comparison of errors between the conventional and proposed filling time in relation to the actual filling time, figure-5.5 illustrates this analysis for the water simulation, while Figure 5.7 showcases the comparison for the mercury simulation.

Figure 5.8 (a) illustrates the relationship between filling time and the percentage of mold filling for the upright and vertical mold position across all molds in the water simulation. On the other hand, Figure 5.8 (b) showcases the same relationship for the same mold positions across all molds in the mercury simulation.

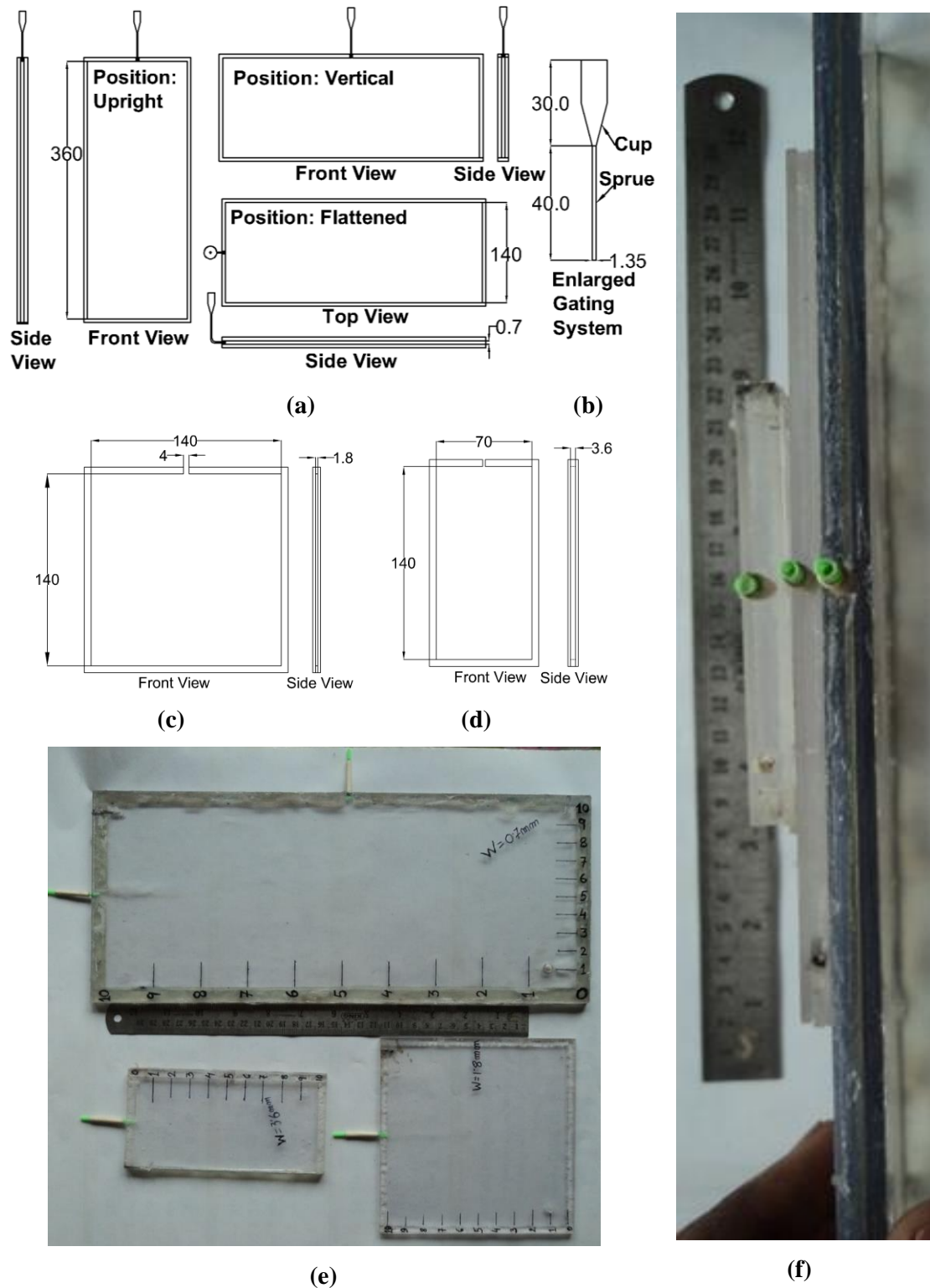
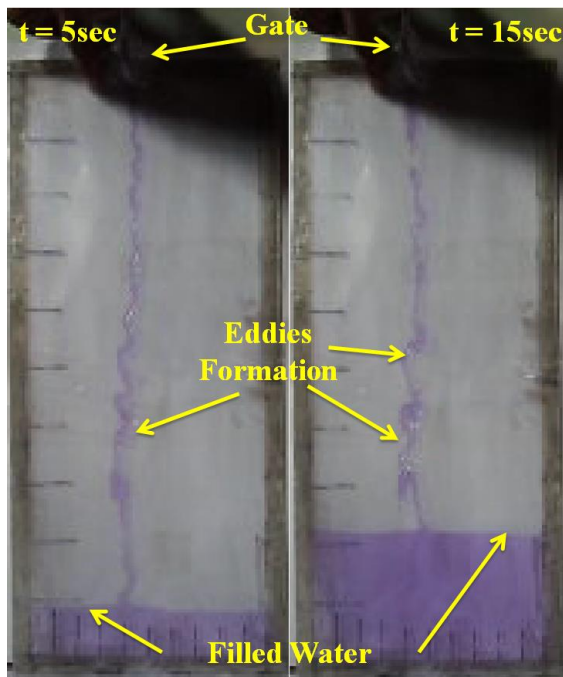
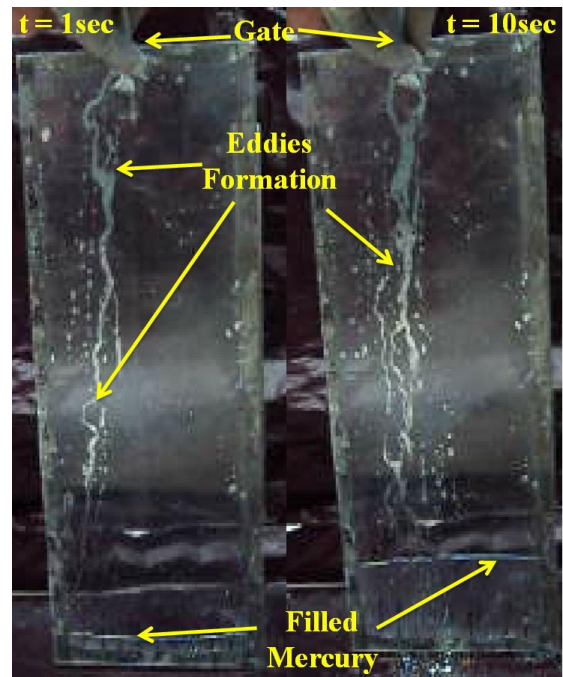


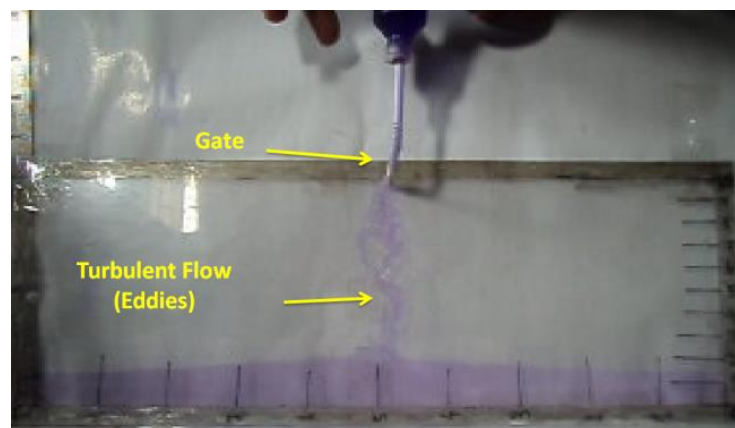
Figure- 5.2: Schematic diagram of (a) 0.7mm thin mold at different position with Gating System, (b) Enlarged Gating System, (c) 1.8 mm and (d) 3.6 mm thick mold; Pictorial representation of the molds: (e) front view and (f) side view (All dimensions are in mm)



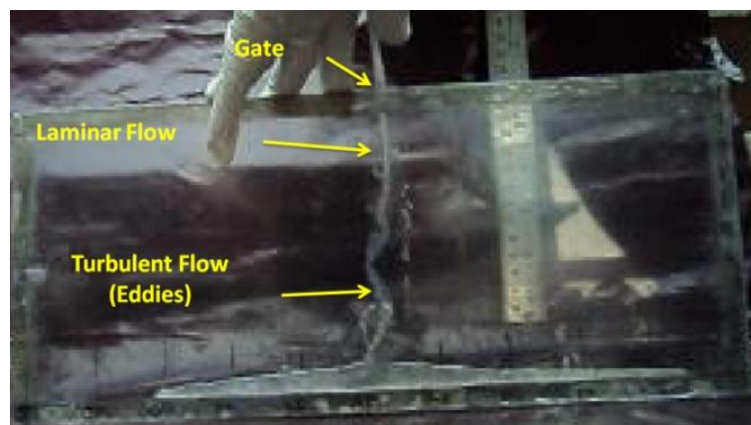
(a) Flow pattern of Water, inside 0.7 mm Mold, at upright position



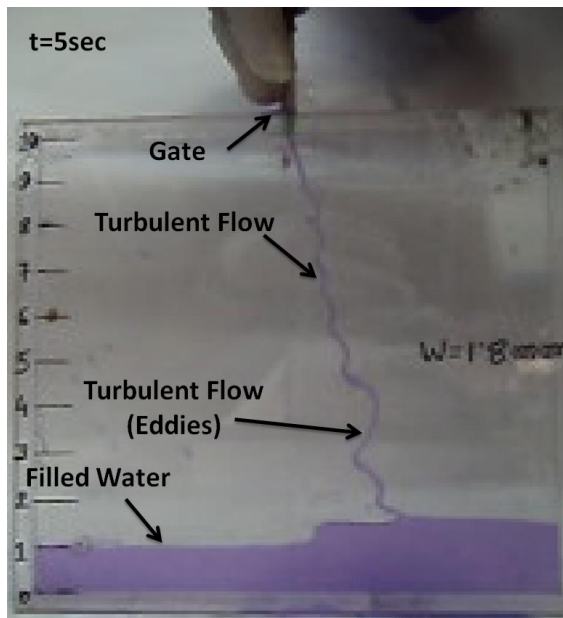
(b) Flow pattern of Liquid Mercury, inside 0.7 mm Mold, at upright position



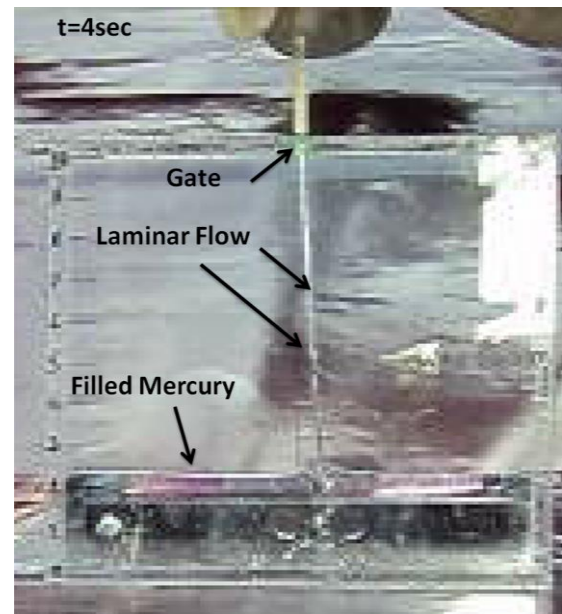
(c) Flow pattern of Water inside 0.7 mm Mold at Vertical Position



(d) Flow pattern of Liquid Mercury inside 1.8 mm Mold at Vertical Position



(e) Flow pattern of Water inside 1.8 mm Mold at Vertical Position



(f) Flow pattern of Liquid Mercury inside 1.8 mm Mold at Vertical Position



(g) Flow pattern of Water inside 3.6 mm Mold at Vertical Position



(h) Flow pattern of Liquid Mercury inside 3.6 mm Mold at Vertical Position

Figure- 5.3: Flow pattern of Water and Liquid Mercury through various mold thickness and mold position at different time frame

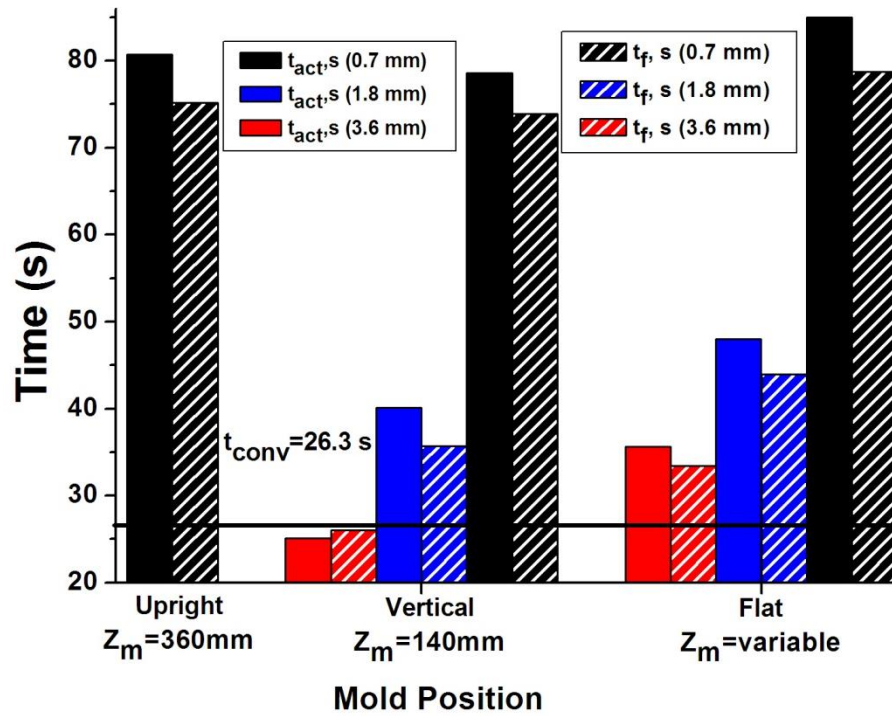


Figure- 5.4: Simulated actual filling time (t_{act}) and calculated filling time (t_f) for the molds with varying positions. Working fluid: Water.

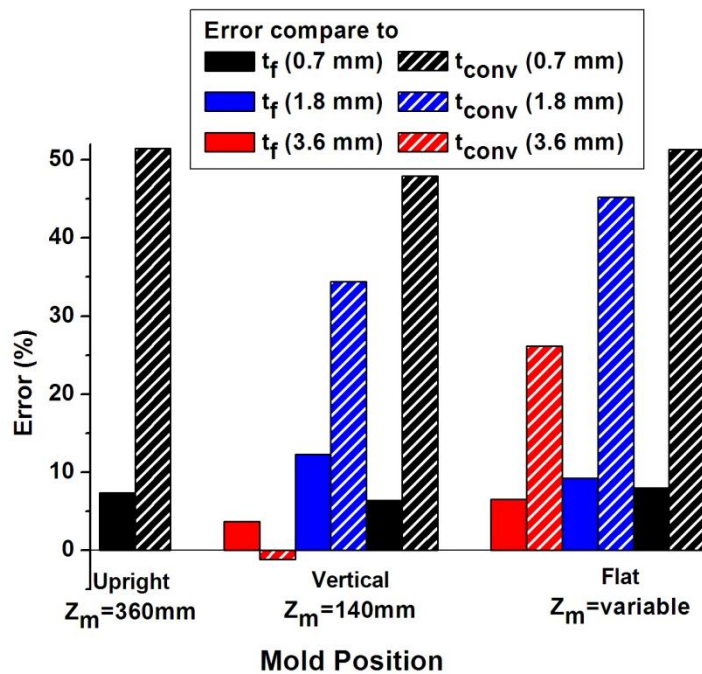


Figure- 5.5: The error (%) between the simulated actual filling time (t_{act}) and the calculated filling time (t_f), as well as the error between the conventional filling time and t_{act} , for molds with varying positions. Working fluid: Water

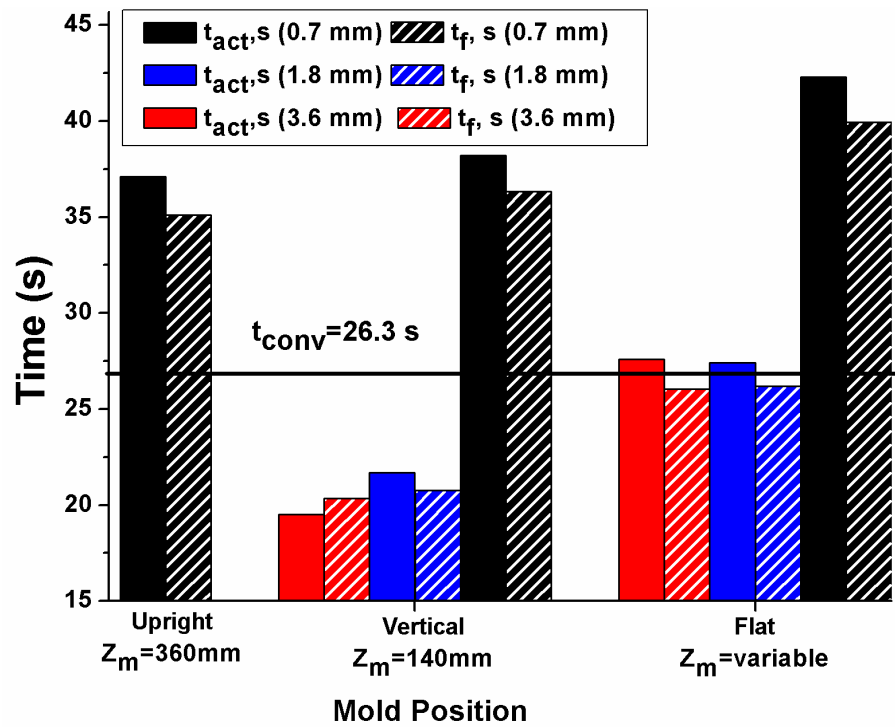


Figure- 5.6: Simulated actual filling time (t_{act}) and calculated filling time (t_f) for the molds with varying positions. Working fluid: Liquid mercury

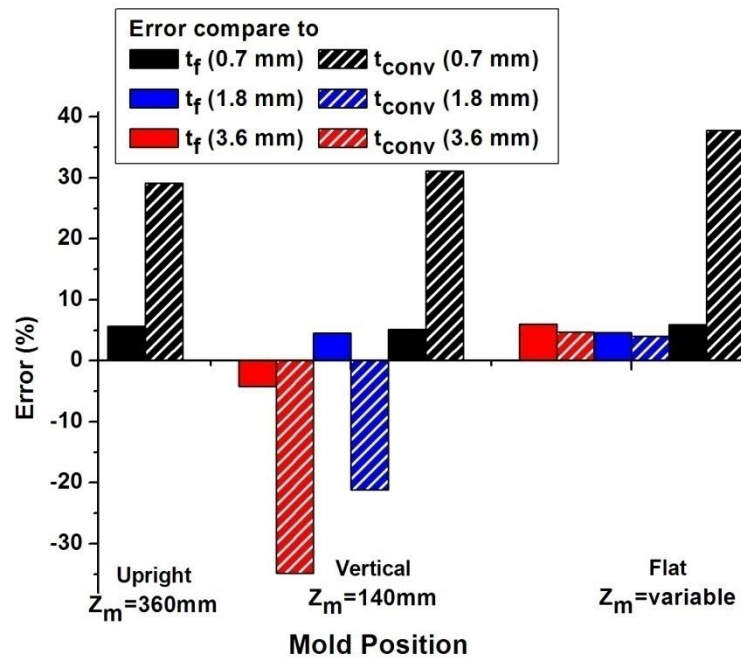


Figure- 5.7: The error (%) between the simulated actual filling time (t_{act}) and the calculated filling time (t_f), as well as the error between the conventional filling time and t_{act} , for molds with varying positions. Working fluid: Liquid mercury

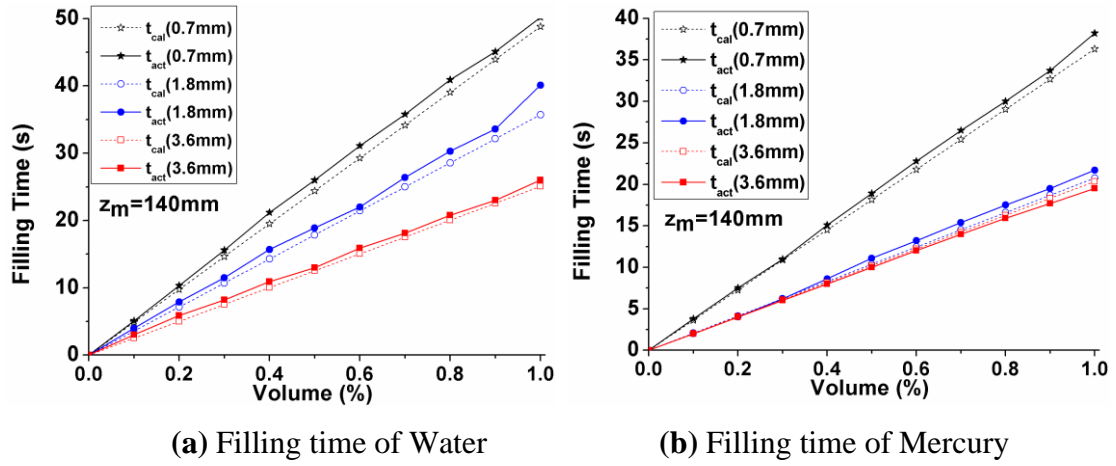


Figure- 5.8: Comparison of Filling time among molds with the same mold height ($z_m=140\text{mm}$), gating design, and mold volume, based on the molds' volume fractions. All three molds were used for the comparison.

5.2 Experiment to Determine the Suction Pressure inside Hot Clay Mold

To ascertain the negative gas pressure (gauge) (suction pressure) within a heated clay mold, two field experiments were conducted. Two hollow cylindrical clay molds were made according to the set up shown in figure-5.9 to measure the internal pressure by water column height. Subsequently, one cylinder having a 5mm hole through the wall functioned as a Closed System, while the other operated as an Open System. Both cylinders were linked to a slanted single-column manometer [5.2, 5.3]. The mold's interior pressure was gauged using a water column.

5.2.1 Experimentation:

Initially air and water vapour got out from the mold and then the water column was start to fluctuating. Both the clay molds were heated to a red-hot state (Temperature: 1273K). The highest water column pressure was documented during the trial and converted to gauge pressure.

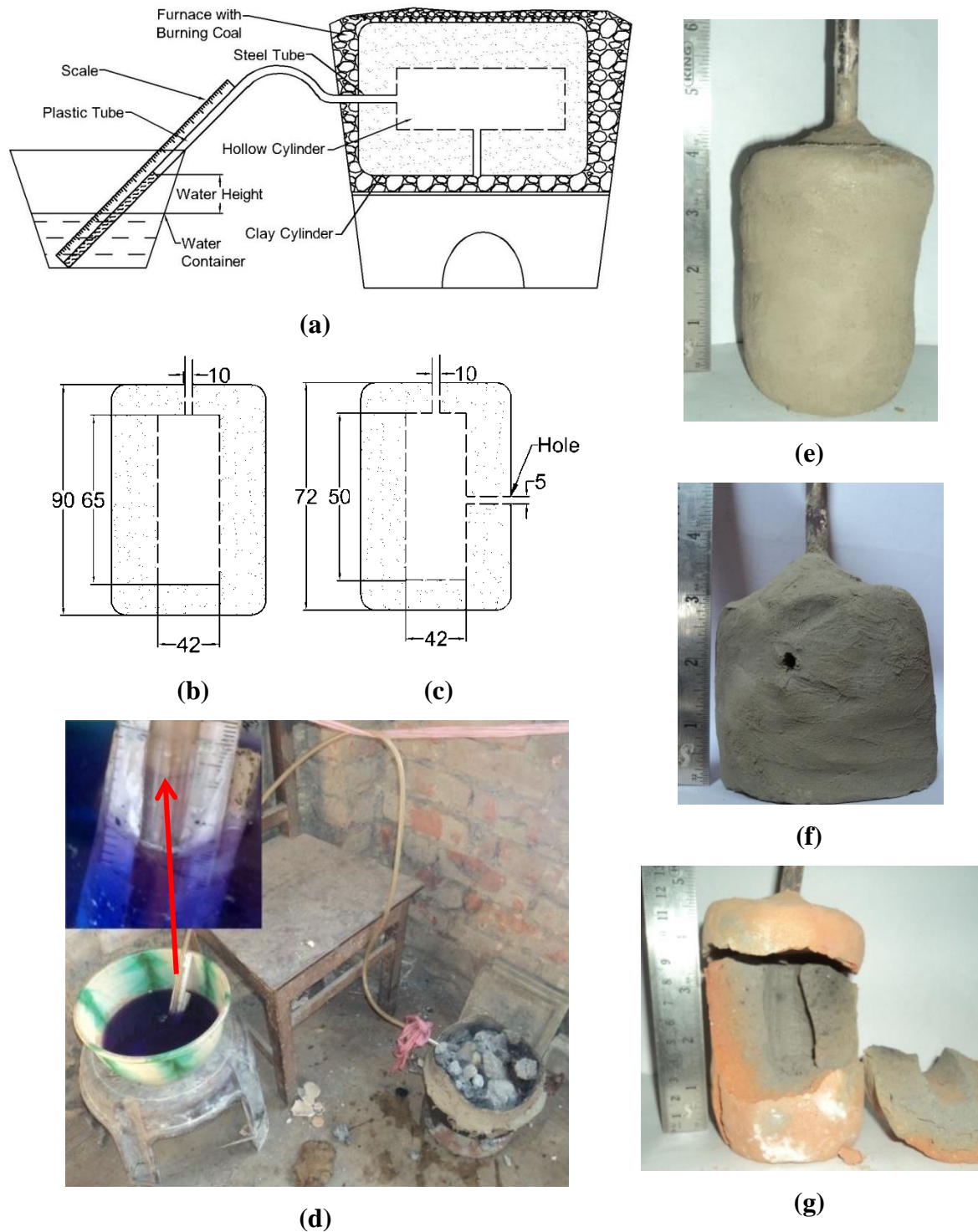


Figure-5.9: Experiment to estimate the suction pressure inside clay during firing. (a) schematic diagram of experimental set up, schematic diagram of hollow clay cylinders: (b) without hole and (c) with hole (5mm), (d) pictorial view of experimental set up inset: height of water column in inclined pipe, pictorial view of the fired clay cylinders (e) without hole and (f) with Hole, (g) Sectional View of a Cylinder after Firing

5.2.2 Result

Figure 5.10 illustrates the vacuum pressure generated within both molds. The vacuum pressure produced in a heated mold induced a suction effect during the pouring of liquid metal into a heated clay mold.

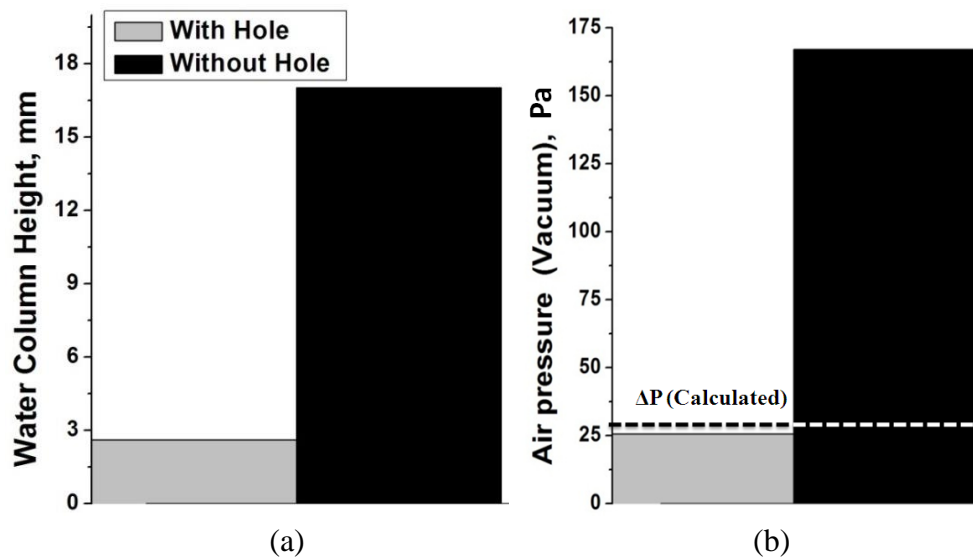


Figure-5.10: Details of Pressure inside the Mold: in terms of (a) Water column (mm), (b) Air Pressure (vacuum) (Pa)

5.3 Discussion

According to the conventional mold filling time calculation technique, factors such as fluid characteristics, mold thickness, and mold position are not considered to affect the mold filling time. However, in real-time experimentation or simulation, it has been proven that these factors do indeed have an impact on the mold filling time. The results from simulation experiments provide further justification for the inclusion of these factors in the mathematical model.

- i. **Flow Patterns:** Eddies Formation [5.4, 5.5] in fluid flow was observed for the entire water simulation, but for mercury simulation it was found only in 0.7mm thick mold.

- ii. **Effects of Fluid on Mold Filling Time:** Mold filling time for Water was more compare to Mercury, which was similar to the proposed model.
- iii. **Effects of Mold Thickness on Mold Filling Time:** Remaining the other entire factors constant the mold filling time of a thinner mold is longer compared to that of a thicker mold. This is due to the Eddies formation caused by capillary action, friction between the mold surface and the liquid.
- iv. **Effects of Mold Position on Mold Filling Time:** Mold filling time varies with the change of mold position. It was observed that, the simulation for flat positions requires a longer mold filling time compared to the other mold position, as the effective head was lowest for flat position among all position.
- v. **Error calculation:** The calculation of error reveals a significant discrepancy in the conventional mold filling time estimation for thin section molds. However, the proposed model provides more accurate predictions that closely align with the actual filling time.
- vi. **The suction pressure experiment** affirms the pivotal role of a heated mold in yielding high-quality outcomes in the Investment Casting Process. Mathematically it was derived earlier. Investment casting is preferable to cast thin, intricate, and complex shapes, though the narrow passage applies a resistance due to many factors even for hot clay mold. Despite that, liquid metal overcomes the constraints because the suction pressure effectively draws the liquid metal into the mold and obviously with the help of gravity.

Chapter-6

Metrological Analysis of Clay Molded Thin- Walled Investment Casting

6. Metrological Analysis of Clay Molded Thin-Walled Investment Casting

Metrological inspection was done for Clay Molded thin walled investment casting using Indian Bee's wax as wax pattern and Indian Silica sand and Kaolinite clay as mold material. Dimensional discrepancy and Surface quality was checked along with shrinkage analysis. All the dimensions were measured followed by the ISO standard- ISO 1:2022 [6.1].

6.1 Quality Evaluation of Investment Casting

To understand the effect of Gating System on Thickness and presence of Core, few rectangular plates were made followed by Horáček model [6.2].

6.1.1 Design of Experiment

The factors' details alongside sample numbers are cataloged in table-6.1. Figure 6.1 illustrates schematic diagrams of various Gating Systems [6.3], with labeled dimensions for each section. As per the design (Figure 6.1a), fiber dies were made (Figure 6.2b) using laser cutting to ensure nominal dimensional deviation. In all samples, the gate was affixed at the same position [Figure 6.1]. The details of Mold and pattern materials were tabulated in table-6.2 and the chemical analysis of the used metal [6.4, 6.5] was tabulated in table-6.3. The entire manufacturing stages, from pattern making to clay mold formation, are depicted in figure-6.2. Cast samples, along with observed defects, are shown in figure-6.3.

Table-6.1: Details of the Sample for various factors

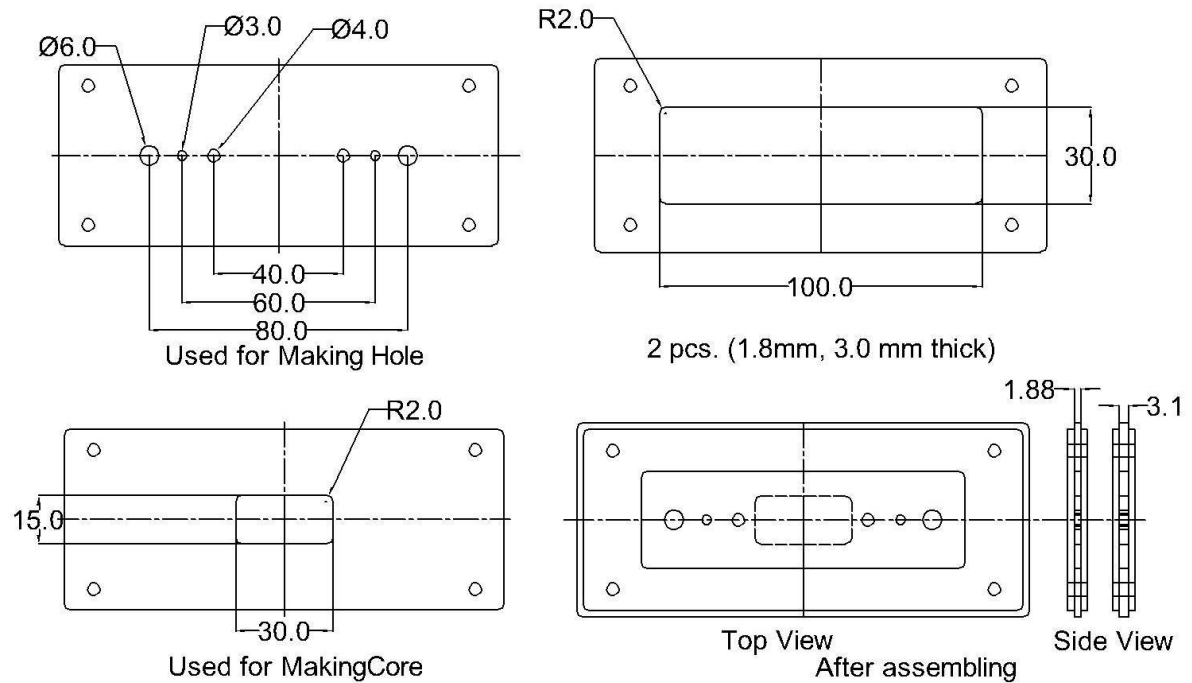
Thin Plate (Thickness<2mm)			Thick Plate (Thickness>3mm)		
Sample No.	Type of Pattern	Gating System	Sample No.	Type of Pattern	Gating System
1	Solid	Side	7	Solid	Side
2	Solid	Top	8	Solid	Top
3	Solid	Bottom	9	Solid	Bottom
4	Cored	Side	10	Cored	Side
5	Cored	Top	11	Cored	Top
6	Cored	Bottom	12	Cored	Bottom

Table-6.2: Materials used for mold and pattern

Materials	Components
Wax Pattern	Sal Dammar resin (40%) + Bees wax (60%)
Clay	Local Kaolinite Clay [3Al ₂ O ₃ 2SiO ₂ 2H ₂ O or Al ₂ Si ₂ O ₅ (OH) ₄]
Sand	Silica Sand [SiO ₂] [GFN=61]
Primary Coating (Facing clay)	Very fine Kaolinite (100%) [GFN=125; pH=7.2, Base Exchange Capacity= 0.37]
Secondary Coating (Backing clay)	Fine and Medium Silica Sand (60%-70%) + Kaolinite (20% - 30%) + Rice husk + Cow Dung + Jute Cuttings (10%) [GFN=61; pH=7.87, Base Exchange Capacity= 1.7]

Table 6.3: Chemical composition and Nomenclature and property of metal used

Cu%	Zn%	Pb%	Fe%	Sn%	Zn Equivalent	Cu: Zn
60.6	33.86	2.85	0.92	0.77	38.41	61.59: 38.41
Common Name: Engraving brass (2% Pb): [ISO No.: CuZn39Pb2] Cu%: 59.0-64, Zn%: ~ 39, Pb%: 2.0-3.0						
Thermal expansion co-efficient (μm/m°C)					Melting point (°C)	
20.5 (within the range of 20°C -300°C)					885	



(a) Design of Die

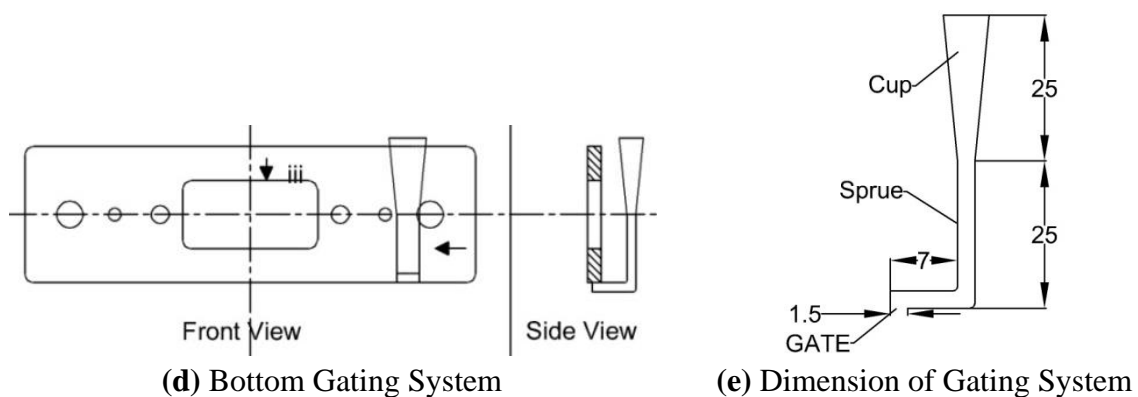
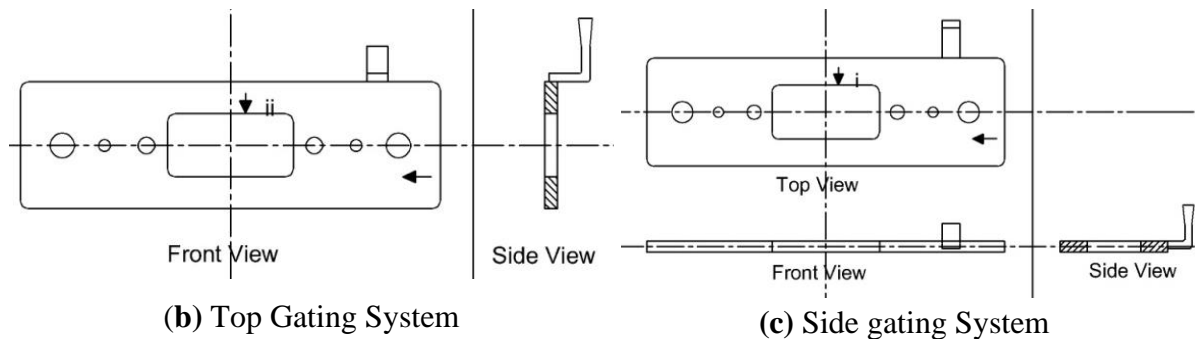
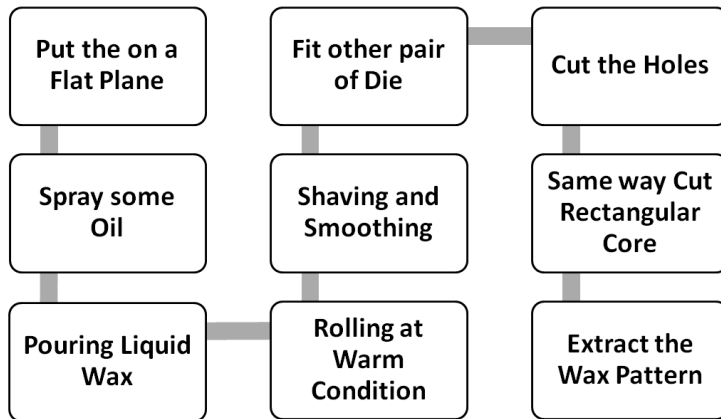


Figure- 6.1.: (a) Schematic diagram of Fibre Die, (b) (c) and (d) Schematic diagram of Cast Plates with three Gating System, (e) The Gating System [All Dimensions are in mm]



(a) Flow diagram for Making of Wax Pattern



(b) Laser cut fiber die



(c) Liquid wax pouring



(d) Rolling at warm condition



(e) Shaving and smoothing



(f) Cutting of hole



(g) Three gating hystem of solid plate

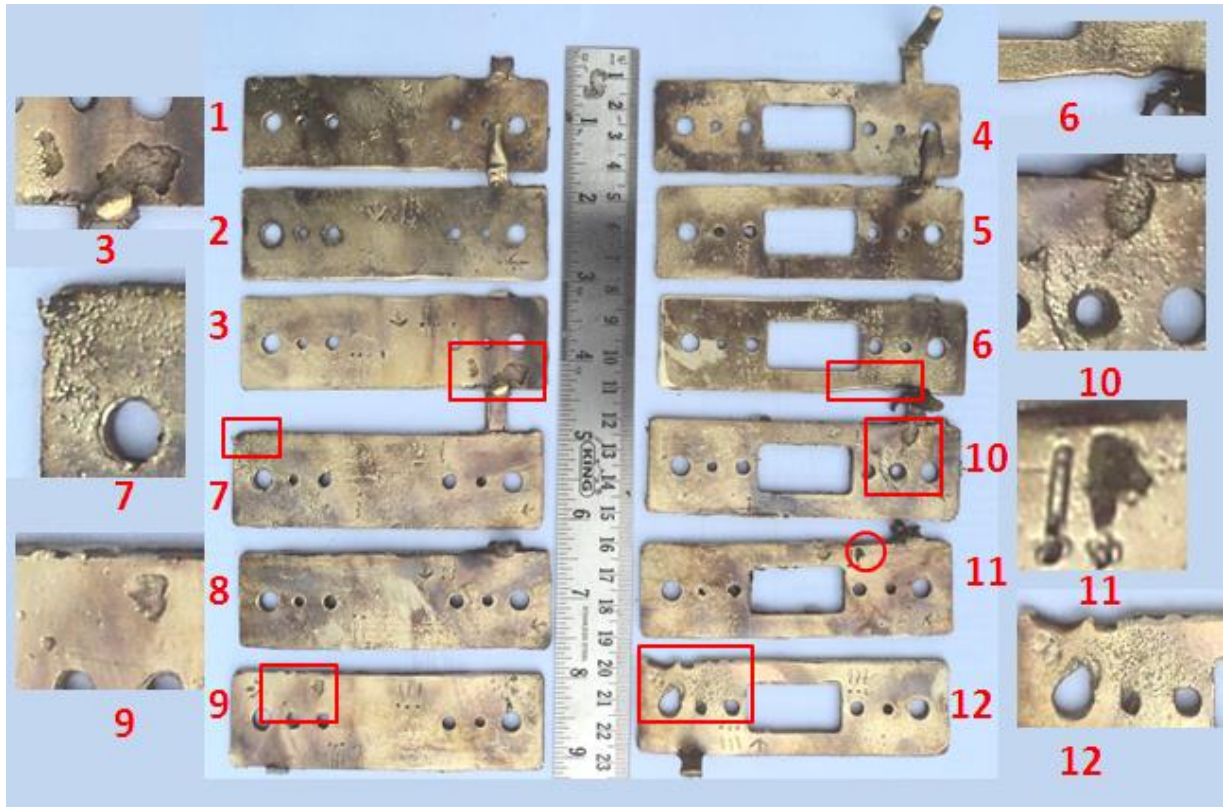


(h) Three gating system of cored plate



(i) Clay mold of all plates with gating

Figure 6.2: Procedure of plate making



(a) Front Surface of the Cast Samples



Back Surface of the Cast Samples

Figure 6.3- : Cast Plates of “Horacek Model” with Both Side Surface; Solid (Left), Cored (Right).

6.1.2 Shrinkage analysis

Position-specific shrinkage/expansion details for length, breadth, and metal thickness are presented in Appendix- XI according to the nomenclature described there. An overview of shrinkage or expansion analysis for length, breadth, metal thickness, and clay core was visualized in figure- 6.4.

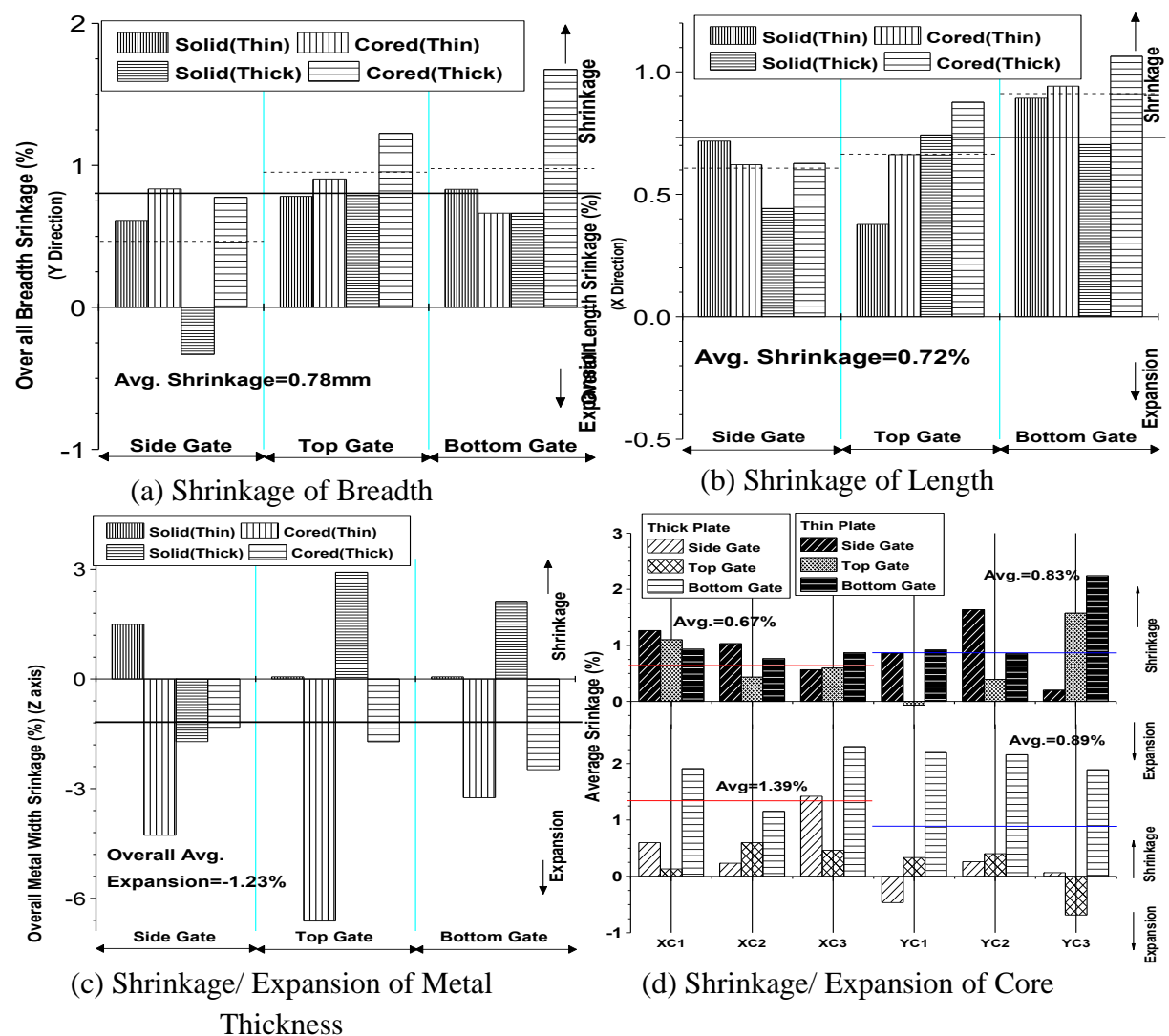


Figure 6.4: Shrinkage/ Expansion of the Plate dimension

6.1.3 Dimensional Variation

The average variation of Metal Thickness at different positions and the Variation of Breadth and Length are illustrated in Appendix-X. Furthermore, the Root mean square deviation (R.M.S.D) (mm) of the Plates has been visualized in Figure 6.5.

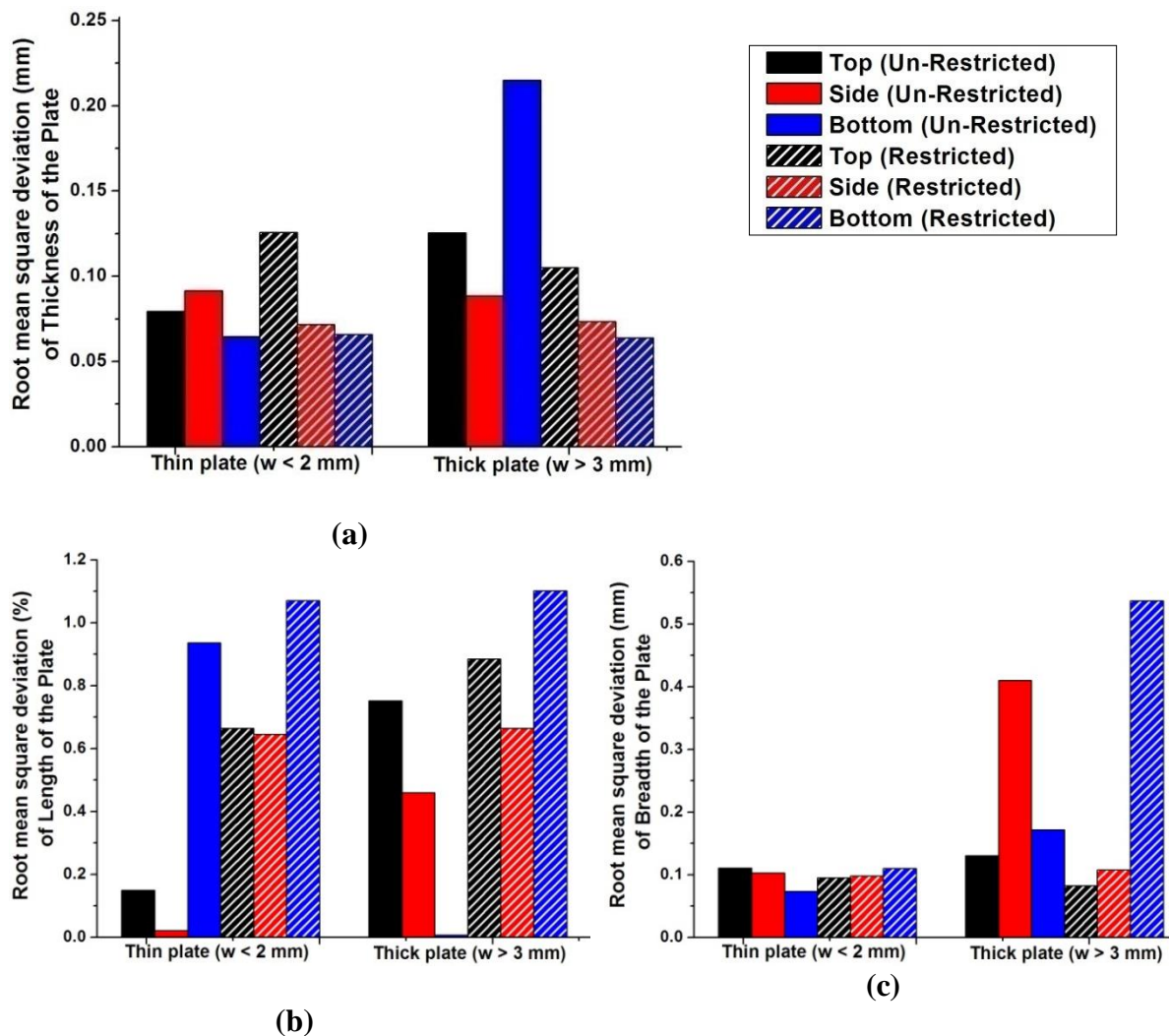


Figure-6.5 Root mean square deviation (R.M.S.D) (mm) of (a) Thickness of the Plate (b) Length, (c) Breadth and

6.1.4. Sectional Quality by Visual Inspection and Surface Roughness

Surface quality observation involved both Visual and Instrumental inspections, detailed extensively. Figure 6.3 depicted the surfaces of the plates, including the gating system and defects. During Visual Inspection, surface quality was categorized as ‘Accepted’, ‘Salvaged’, or ‘Damaged’ areas. Unfilled sections were assessed and quantified, with the outcomes presented in Table- 6.4.

Surface roughness measurements were conducted using the Taylor Hobson instrument model Sutronic 3+. A sampling length (Lc) of 2.5 mm was selected for these measurements. Ra values (Arithmetic mean of the profile departures from the mean line) were obtained for various points on the samples, categorized based on the distance from the Gate. Additionally, the average of the Best and Worst Surface Roughness was computed. This information is illustrated in Figure 6.6. The surface profiles are available in Appendix-XII and XIII for thin and thick plate respectively.

Table-6.4: Surface and Sectional Quality of the Plate

	Gating Type	Thin plate (w< 2 mm)				Thick Plate (w> 3 mm)			
		Surface Quality (%)			Un-Filled section (%)	Surface Quality (%)			Un-Filled section (%)
		Accepted	Salvaged	Damaged		Accepted	Salvaged	Damaged	
Solid	Side	100	0	0	0	100	0	0	0
	Top	100	0	0	0	99.93	0.07	0	0
	Bottom	98.45	1.55	0	0	97.43	2.57	0	0
Cored	Side	100	0	0	0	97.45	2.55	0	0
	Top	100	0	0	0	99.9	0.01	0	0
	Bottom	94.93	2.81	2.24	2.24	94.84	2.92	2.24	2.24

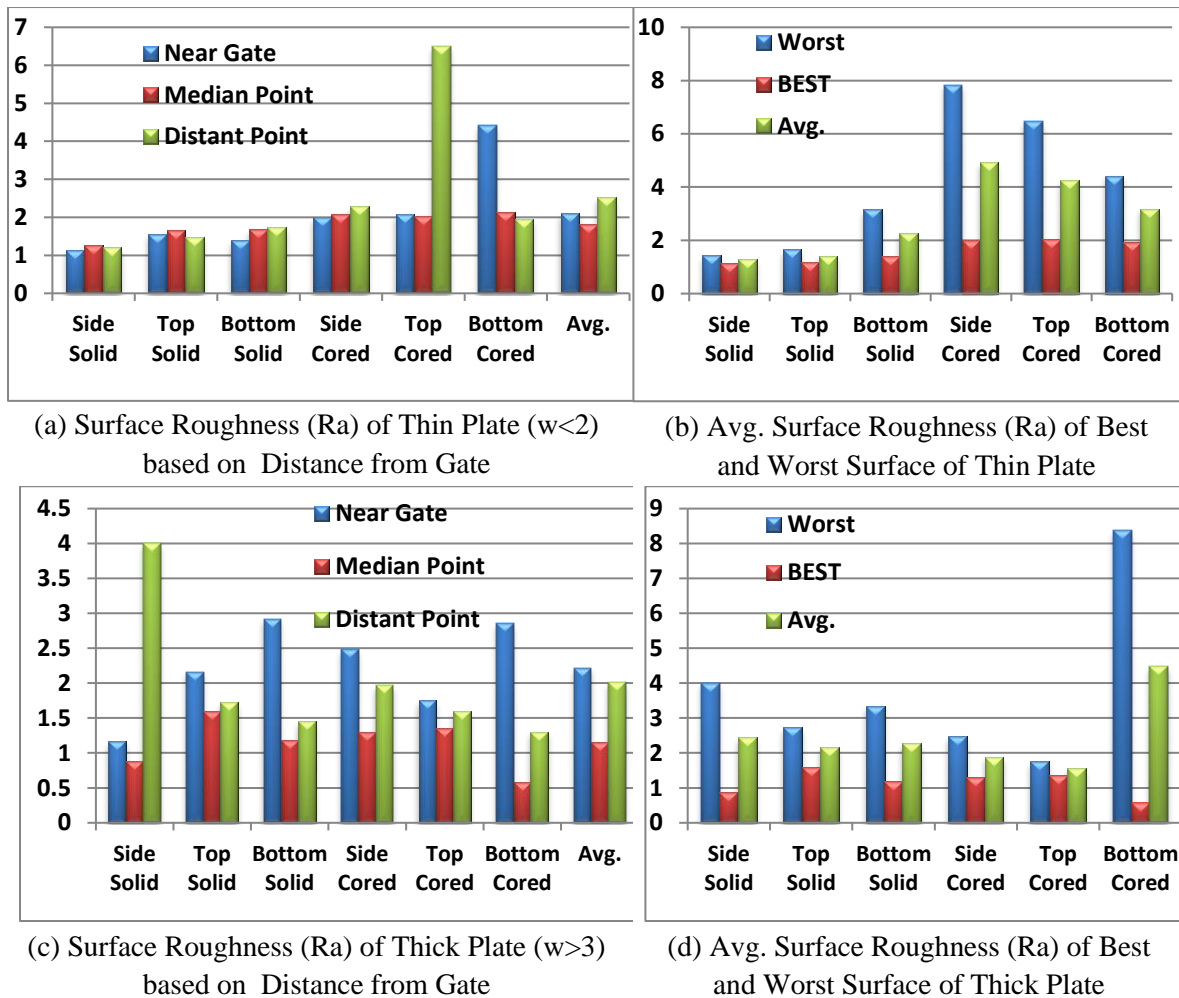


Figure 6.6 Surface Roughness (Ra) for the thin (Top) and thick plate (Bottom)

6.1.5 Summary of the experimentation

The summarized dimensions at different stages for various gating systems were presented in Table 6.5. The ranking by TOPSIS method based on the dimensional variation and casting quality was illustrated in Table 6.6. The calculation was shown in Appendix-XIX. It was observed that, the cast metal thickness expanded compared to wax pattern thickness for sections less than 3 mm, metal thickness exhibited expansion instead of shrinkage. This anomalous expansion was investigated and elaborated in subsequent section.

Table 6.5: Dimensions of Fiber Die, Wax Pattern and Cast Product in different Gating

		External Dimension				Width		Internal Dimension		
Phase		Longitudinal (X direction)		Lateral (Y direction)		Thickness (Z direction)		Longitudinal (X axis)	Lateral (Y axis)	
Presence of core		Solid	Cored	Solid	Cored	Solid	Cored			
Die		100 ⁺¹⁵ _{+0.0}		30 ⁺³⁰ ₊₂₀		1.8 ^{+0.08} _{-0.0} & 3.6 ^{+0.05} _{-0.0}		30 ⁺¹² _{+0.0}	15 ⁺¹ _{+0.0}	
Wax pattern		Thin	99.95 ^{+0.24} _{-0.23}	100.04 ^{+0.15} _{-0.15}	30.3 ^{+0.17} _{-0.17}	30.3 ^{+0.38} _{+0.15}	2.0 ^{+0.12} _{-0.1}	1.95 ^{+0.2} _{-0.1}	30.03 ^{+0.21} _{-0.09}	15.2 ^{+0.07} _{-0.07}
		Thick	100.36 ^{+0.18} _{-0.24}	100.46 ^{+0.12} _{-0.15}	30.54 ^{+0.58} _{-0.21}	30.58 ^{+0.15} _{+0.14}	3.1 ^{+0.3} _{-0.13}	3.08 ^{+0.17} _{-0.18}	30.2 ^{+0.36} _{-0.14}	15.06 ^{+0.25} _{-0.44}
Cast	Top Gating	Thin	99.46 ^{+0.21} _{-0.14}	99.46 ^{+0.01} _{-0.04}	30.07 ^{+0.16} _{-0.18}	29.99 ^{+0.15} _{-0.13}	2.03 ^{+0.13} _{-0.11}	2.11 ^{+0.2} _{-0.16}	29.87 ^{+0.19} _{-0.2}	15.16 ^{+0.11} _{-0.14}
		Thick	99.74 ^{+0.03} _{-0.05}	99.48 ^{+0.07} _{-0.09}	30.43 ^{+0.22} _{-0.23}	30.14 ^{+0.17} _{-0.13}	3.1 ^{+0.17} _{-0.23}	3.14 ^{+0.21} _{-0.14}	29.99 ^{+0.05} _{-0.05}	14.8 ^{+0.05} _{-0.08}
	Side Gating	Thin	99.2 ^{+0.02} _{-0.05}	99.3 ^{+0.14} _{-0.2}	30.16 ^{+0.13} _{-0.18}	29.95 ^{+0.19} _{-0.1}	1.98 ^{+0.22} _{-0.14}	1.95 ^{+0.12} _{-0.14}	29.75 ^{+0.05} _{-0.07}	15.02 ^{+0.03} _{-0.02}
		Thick	99.72 ^{+0.12} _{-0.1}	99.86 ^{+0.16} _{-0.26}	30.5 ^{+0.33} _{-0.49}	30.37 ^{+0.25} _{-0.15}	3.12 ^{+0.21} _{-0.15}	3.17 ^{+0.15} _{-0.19}	29.94 ^{+0.1} _{-0.14}	15.2 ^{+0.05} _{-0.07}
	Bottom Gating	Thin	99.16 ^{+0.23} _{-0.2}	99.15 ^{+0.53} _{-0.4}	30.01 ^{+0.13} _{-0.07}	30.15 ^{+0.19} _{-0.11}	2.03 ^{+0.11} _{-0.11}	2.07 ^{+0.11} _{-0.09}	29.72 ^{+0.06} _{-0.04}	14.98 ^{+0.1} _{-0.14}
		Thick	99.74 ^{+0.25} _{-0.23}	99.47 ^{+0.38} _{-0.31}	30.36 ^{+0.21} _{-0.28}	30.12 ^{+0.11} _{-0.1}	3.05 ^{+0.18} _{-0.75}	3.1 ^{+0.2} _{-0.09}	29.79 ^{+0.19} _{-0.11}	14.88 ^{+0.14} _{-0.2}

Table-6.6: Ranking of the Casting Samples Based on Quality using the TOPSIS method

Ranking	Thin plate (width <2 mm)						Thick plate (width >3 mm)					
	Un-Restricted			Restricted			Un-Restricted			Restricted		
	Side	Top	Bottom	Side	Top	Bottom	Side	Top	Bottom	Side	Top	Bottom
Sample No	1	2	3	4	5	6	7	8	9	10	11	12
Individual	2	1	5	4	3	6	2	1	4	5	3	6
Overall	2	1	5	7	6	11	4	3	9	10	8	12

6.2. Investigation of Anomalous Expansion of Metal for Thin-walled Investment Brass Castings

The dimensional analysis revealed an intriguing anomaly: the cast metal thickness expands compared to the wax pattern, contrary to typical casting shrinkage. The experiments were designed to understand the nature of shrinkage or expansion of the Cast metal as well as mold materials.

6.2.1. Theoretical aspects

The dilation of cast metal sheets compared to wax patterns is quite an unusual phenomenon. To explain the phenomenon the study of the ingredient of clay mold material is required.

Kaolinite [6.6, 6.7, 6.8] and Silica Sand mixtures were used for making the mold. The study on Kaolinite clay [6.9] on changes in length from room temperature to 1000⁰C was explored by Hyslop, McMurdo (1938) [6.10] and Heindl and Meng (1939) [6.11] by using differential thermal expansion apparatus and interferometer respectively.

One of the most important ingredients of mold materials is silica sand. It is already mentioned in table-6.2 that fine and medium Silica sand is present (60%-70%) in the exterior coating of the mold which actually takes 95% of the total mold. According to J. Thiel [6.12], Silica sand expands by approximately 4.74% to 12.44 by volume at different temperature ranges. The details of the expansion and contraction of Kaolinite clay and Silica sand along with an explanation are documented in table-6.7.

The research of the scientists illustrates that Kaolinite clay contracts and Silica sand expand at a high-temperature range. Clay molded investment casting involves both the ingredients in a certain percentage for different stages, so, it is essential to estimate the shrinkage and expansion nature of clay mold separately.

Table 6.7: Transformation details of kaolinite clay and silica sand

	Temperature (⁰ C)	Expansion/ Contraction by volume (%)	Explanation
Kaolinite Clay	470 ⁰ C –550 ⁰ C	0.3% Expansion	---
	550 ⁰ C -650 ⁰ C	1.0–1.8 % Contraction	Dehydroxylation
	650 ⁰ C –920 ⁰ C	1.5–2.3 % Contraction	Escape of OH groups as water/steam
	930 ⁰ C –980 ⁰ C	1.0–1.4 % .Contraction	Formation of Mullite (mullitization)
	Above 1000 ⁰ C	Contraction	Formation of a molten phase
Silica Sand	573 ⁰ C	4.74% Expansion	Alpha-quartz to beta-quartz
	870 ⁰ C	12.44% Expansion	Beta-quartz to beta-tridymite
	1470 ⁰ C	2.27% Expansion	Beta-tridymite to beta-cristobalite
		14.71% Expansion	Beta-quartz to beta-cristobalite

6.2.2. Shrinkage Analysis of Mold Material

The experiment was designed [6.13] to understand the shrinkage or expansion behavior of clay mold during heating.

6.2.2.1. Experimentation

A few solid cylinders of the same size and shape were made using the mold materials (i) facing-clay (primary clay) and (ii) backing-clay (secondary clay). The dimensions and weights were measured after getting completely dry. The samples were heated at 1000°C (figure-6.7). The temperature for the experiment was chosen based on the data from the previous experiments.

6.2.2.2. Result

The result shows that both the radial and the longitudinal dimensions of all molding materials had expanded. The weight of the dried clay at room temperature and the fired clay samples along with the loss of weight percentage has shown in table-6.8.

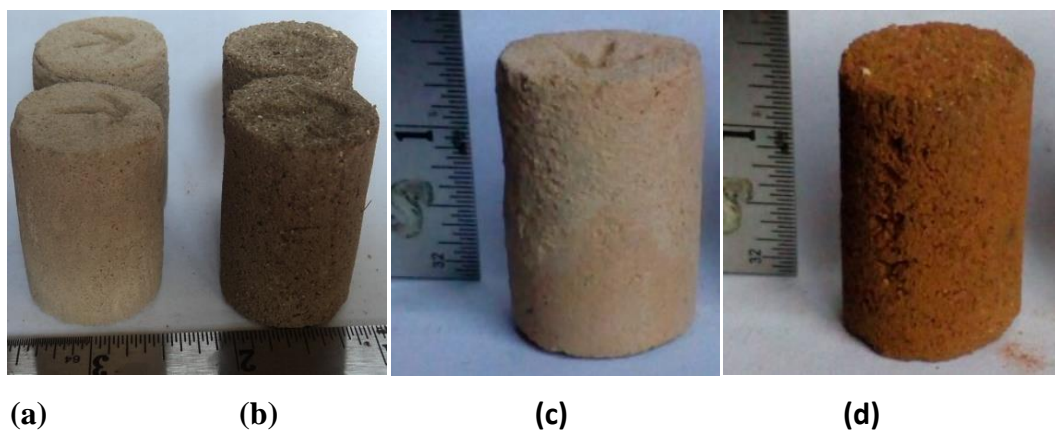


Figure-6.7: Experiment to estimate the shrinkage and expansion of mold material. At room temperature: (a) Primary clay, (b) Secondary clay; At 1000°C : (c) Primary clay, (d) Secondary clay

Table 6.8. Expansion percentage of Mold

	Expansion (%)		Weight (gm)		Weight loss (%)
	Diameter	length	Dried at 35 ⁰ C	Fired at 1000 ⁰ C	
Primary mold clay	1.44%	1.36%	39.9	38.4	(-3.75%)
Secondary mold clay	0.63%	0.46%	39.4	37	(-6.09%)

6.2.2.3.Reasons behind the expansion of mold material

The explanations for the expansion of mold materials are as follows

- i.Silica generally expands by 4.74% to 12.4% by volume (table-6.7) at the temperature of 573⁰C and 870⁰C respectively. The amount of shrinkage of Kaolinite at different temperature zone is very low (maximum 1.8%) compared to silica sand.
- ii.The shrinkage or expansion of the mold is mostly controlled by the Silica Sand because of its adequacy (60%-70%) in the clay mold, especially in secondary coating clay (backing clay mold) which occupies 95%-98% of the total mold.
- iii.The thickness of Primary coating clay (Facing clay) over the wax pattern is not used more than 1.0 mm in regular practice. Whereas the secondary coating clay (backing clay) is 20 to 50 times thicker than facing clay based on the volume of casting. So, the primary layer has a negligible effect on the shrinkage or expansion of the mold.

iv.Secondary mold clay expanded at all temperatures compared to others, which signifies that the volume of mold cavity increases for the investment casting in the hot clay mold.

6.2.3. Shrinkage Analysis of Cast Metal

The experiment was designed to understand the shrinkage or expansion behavior of Cast metal thickness only compared to the wax pattern thickness.

6.2.3.1.Experimentation

The experiment was designed to cast five different thicknesses of sheets of 0.5mm, 1mm, 1.75mm 2.5mm, and 3.25mm. The production steps of the sheets were same the Figure-6.2. The dies, wax patterns and cast metals were shown in figure -6.8. The wax thickness of the patterns and metal thickness of the castings were measured at similar positions and then shrinkage percentage or expansion percentage was determined.

6.2.3.2.Results

The dimensional distributions of the thicknesses of cast metal parts were shown in figure-6.9 and the expansion percentage (compared to wax pattern thickness) was shown in table-6.9. It was observed that the amount of dilation cast metal thicknesses decreases with the increase in metal thickness.

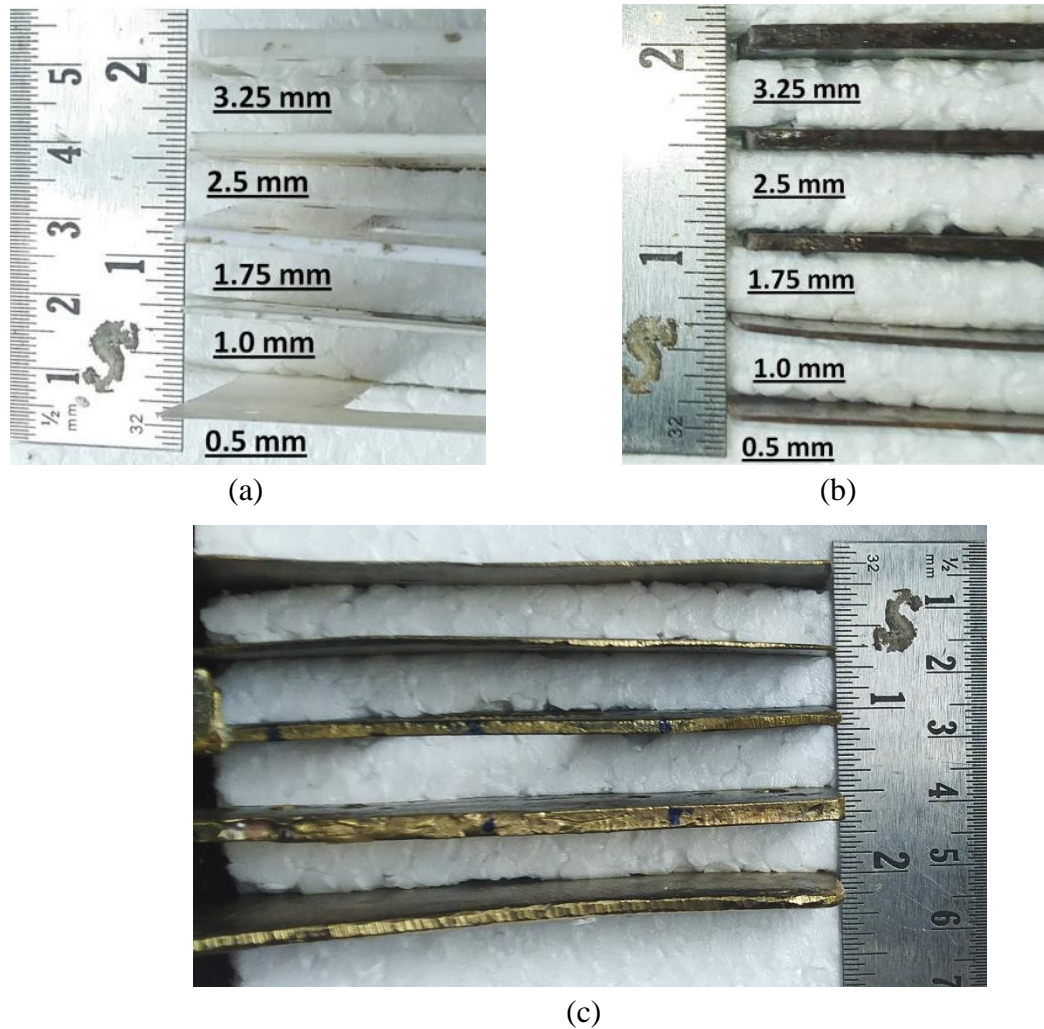


Figure- 6.8: Casting procedure of the sheets: (a) side view of all dies, (b) side view of all wax sheets, (c) side view of the metal sheet.

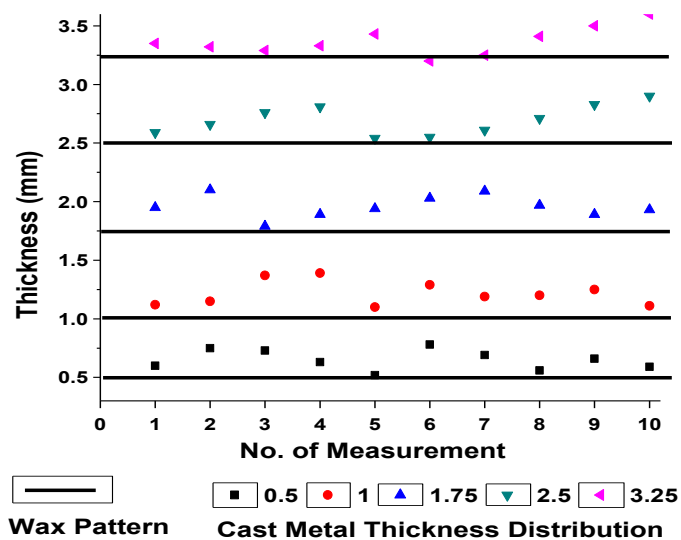


Figure- 6.9: Cast metal thickness distribution along with wax pattern thickness

Table 6.9: Expansion of Cast metal thickness ('-ve' sign symbolised the expansion)

Wax Pattern Thickness (mm)	$0.5^{+0.05}_{-0.05}$	$1.0^{+0.1}_{-0.1}$	$1.75^{+0.1}_{-0.1}$	$2.5^{+0.1}_{-0.1}$	$3.25^{+0.1}_{-0.1}$
Avg. Metal Thickness (mm)	0.65	1.21	1.95	2.69	3.36
Avg. Expansion (%)	-30.2	-21.7	-11.88	-7.84	-3.63

6.2.3.3.Reasons behind the expansion of cast metal

The shrinkage or expansion of clay mold based on heating and cooling sequences at different stages has been shown in table-6.10. The explanations are as follows

- i.** In previous experiment, it was proven that the volume of mold cavity increases for the investment casting specially at high temperature and liquid metal is poured at that condition. So, liquid metal has more space than the wax pattern thickness.
- ii.** To understand the mechanism, the stages of heating and cooling sequence of clay mold was shown in table-6.10, based on the experimental and theoretical analysis [6.14, 6.15].
- iii.** Metal thickness expansion percentage getting gradually decrease with the increase in thickness. Mold thicknesses are usually same for all the sections. So, the expansion of mold was approximately the same at every point. But on another side solid-solid contraction is more for thicker sections. So, the thicker sections can overcome the mold cavity dilation phenomenon more than thinner sections.

Table- 6.10: Shrinkage / Expansion of clay Mold at different stages

	<u>Mold side</u>	<u>Pattern</u> or <u>Mold Cavity</u>	<u>Mold side</u>
Stage-I Molding	Mold (wet clay)	Wax Pattern	Mold (wet clay)
Stage-II Drying of mold	Drying (Shrink) → →	Wax Pattern	← ← Drying (Shrink)
Stage-III Heating in furnace	← ← Expansion	Wax vapoured	→ → Expansion
Stage-IV Molten metal pouring	← ← Expansion	Metal Filling	→ → Expansion
Stage-V Cooling	No Change	L -L & L -S Shrinkage Liquid Metal Supply from Cup/ Riser	No Change
Stage-VI Cooling and Solidification	<u>Initial Mold</u> <u>Wall</u> →	S-S Shrinkage	← <u>Final Mold</u> <u>Wall</u>

Symbols and abbreviation

----- Initial mold wall

———— Intermediate mold wall

———— Final mold wall

L-L: Liquid-Liquid

L-S: Liquid-Solid

S-S: Solid-Solid

6.3. Metallographic study

Preliminary metallographic study was carried out for 0.5mm, 1.75mm and 3.25 thick cast metal samples (Figure-6.10) of 60:40 brass. The ASTM (American Society for Testing and Materials) grain size number [6.16] was also studied and coarseness of the grains was observed. [Appendix-XVI] The grains of the microstructures are not resolvable because these are the cast structures and cast structures are heterogeneous and non-equilibrium in nature. Higher the ASTM value, lower the grain size.

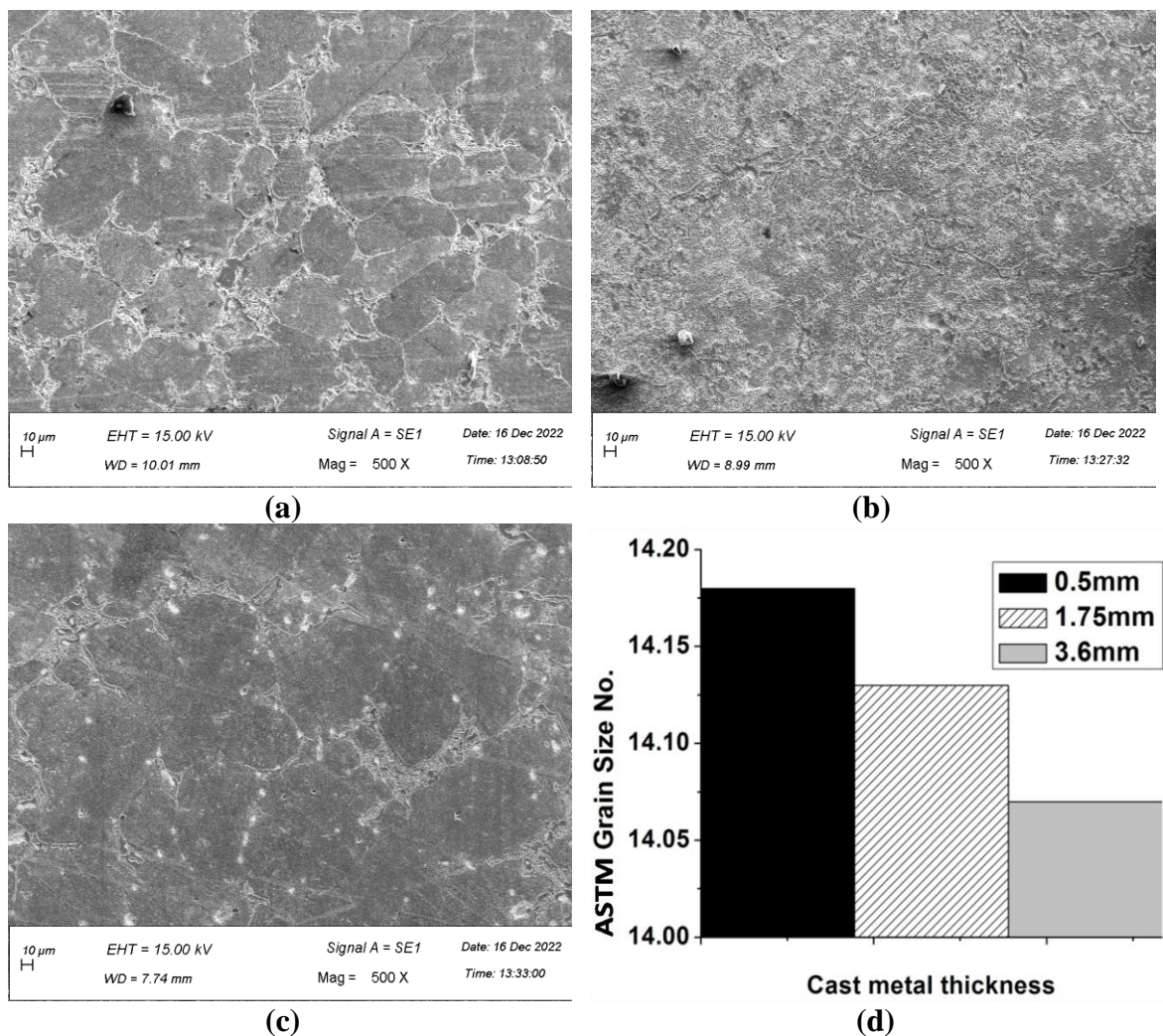


Figure-6.10: Microstructure (SEM) of Brass Casting (500X) (Etchant: FeCl_3 in HCl) with SEM- EDX analysis for (a) 0.5mm, (b) 1.75mm and (c) 3.6mm thick cast metal. (d) ASTM Grain size number of all the microstructure

6.4. Discussion

The following observations were done on the basis of the investigation.

- i. The percentage of shrinkage (or expansion) of cast metals at different direction (viz. thickness, longitudinal and lateral) elucidate that all the dimensions were shrunk except the thickness of metal.
- ii. The major part of the mold was silica rich containing 60%-70% silica sand. At 870⁰C silica sand expand approximately 12.44% by volume. This is the main cause behind the expansion of the mold. Solidification is very slow inside the red hot clay mold. The Engraving Brass (2% lead) has a very small shrinkage allowance (thermal expansion co-efficient 20.5 $\mu\text{m/m } ^\circ\text{C}$) [6.4]. The solid-solid metal shrinkage may not overcome the increased amount of mold cavity volume for thin section casting. Whereas thicker section of cast metal does not show anomalous expansion.
- iii. Surface acceptability was higher for Side and Top Gating Systems compared to the Bottom Gating System. Cores significantly impacted thin section plates (<2mm), correlating with increased surface roughness (Ra) in their presence. Sections closer to the gate displayed inferior surface quality compared to other parts in the Side and Top Gating Systems.
- iv. The metallographic study confirms the coarseness of the grains, as castings were performed in hot clay mold. Solidification rate is very slow due to slow cooling rate inside the red hot mold. As the liquid metal was poured into a red hot mold which was even hotter than liquid metal, so, the sprue and cup fulfilled the function of the riser.

v. Thinner castings have high value of S/V (surface: volume) ratio. High Faster cooling (chilling) is occurred due to this reason. Hence, Nucleation rate is higher, so number of nucleation site is more. Higher the nucleation site is the cause of fine grain. A finer grain means high ASTM number.

Chapter-7

Confirmation through Actual Industrial Practice

7. Confirmation through Actual Industrial Practice

The Analytical Model for Filling Time Estimation and metrological observations were validated through industrial applications. There is a small-scale, traditional clay-molded lost wax investment casting industry in rural India, where thin-section ($\sim\mu\text{m}$) hollow investment castings with intricate shapes like jewelry, utensils, hollow models, artifacts, etc are produced in batches and pieces [Appendix-XXII]. All experiments were conducted in this industrial setting.

7.1. Confirmation of Analytical Model for Mold Filling Time Estimation through Actual Casting

A few thin-section wax-based investment casting items in hot clay mold were done to vindicate the proposed model by varying the parameters. The filling time as well as the gating design of the thin-walled castings was compared with the actual simulated value.

7.1.1. Experimental Framework

The experimental framework was tabulated in table-1 and described below [7.1]

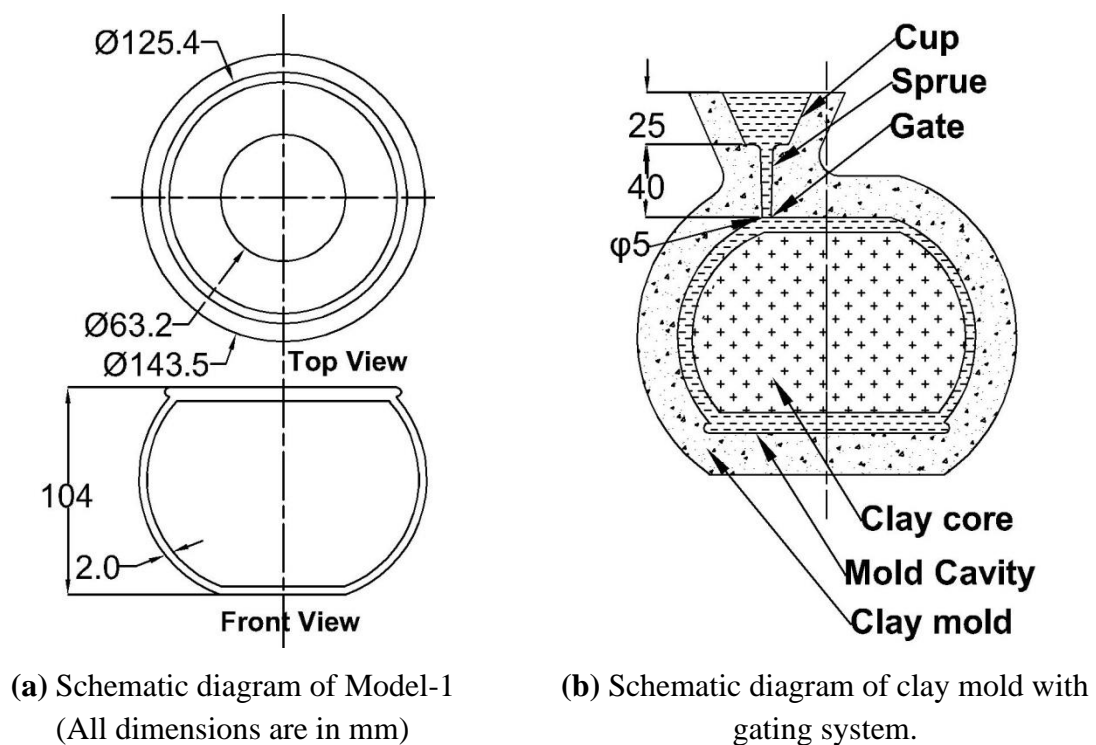
- (i) **Casting with various metals:** The molds (Model-1) having the same shape and dimension were cast with various metals but same mold position and same gating design; the metals were Aluminium (LM6), Brass (Cu/Zn-60/40) and Bronze (Gun Metal).
- (ii) **Varying mold position:** In the second experiment (Model-2) the molds having the same shape and dimension were cast with different mold positions. Each of the models was cast by Brass and had the same gating design.

Table-7.1: Experimental framework

	Simulation Experimentation with Actual Casting				
	Experiment-1			Experiment-2	
Model	Model-1 (Mann)			Model-2 (Ganesha)	
Factor	Variation with Metals			Variation with Mold Position	
Variation	Aluminium	Brass	Bronze	Top Gating	Side Gating

7.1.2. Production Procedure

The schematic diagrams of the items were shown in Figures- 7.1 and 7.3 for model-1 and model-2 respectively. A pictorial representation of the manufacturing stages of the products was shown in Figures- 7.2 and 7.4 for both models. The graphical representation of the physical parameters of the items and the gating details were shown in Figures 7.5 and 7.6 respectively.





(a) Wax Pattern



(b) Clay Mold



(c) Cast Model with Gating System



(d) Finished Mann of Aluminium

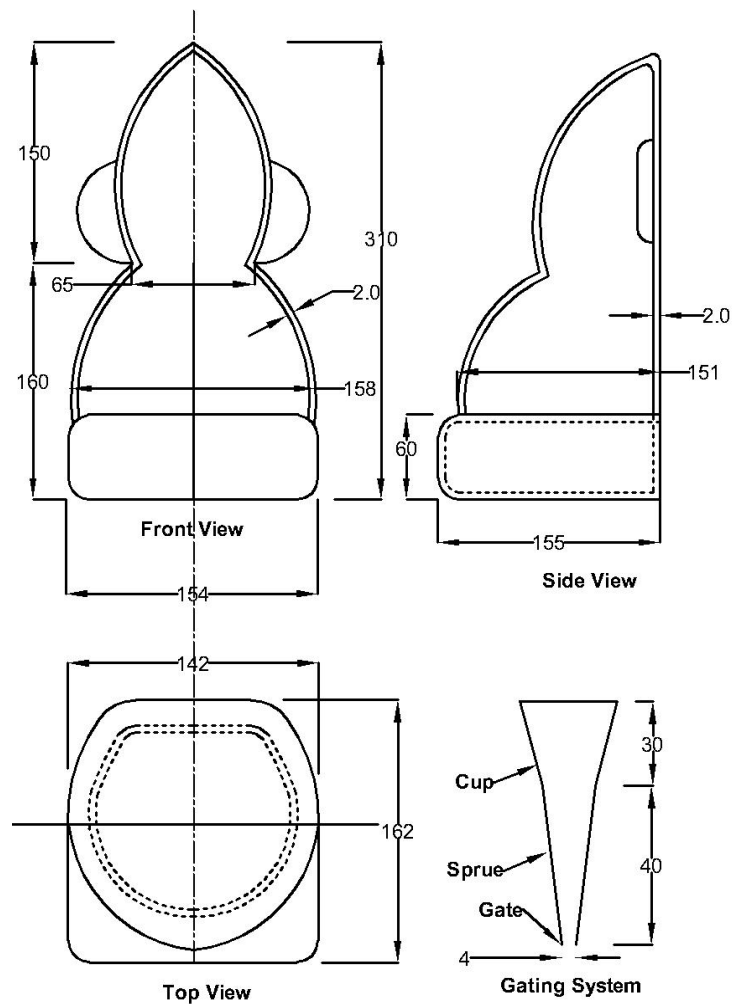


(e) Finished Mann of Bronze
(Gunmetal)

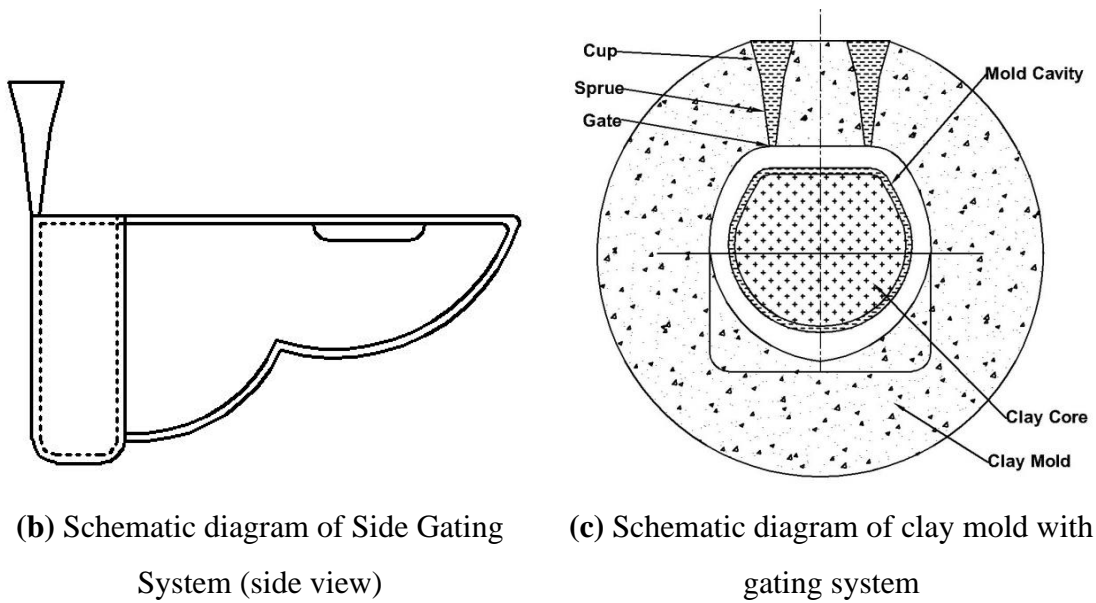


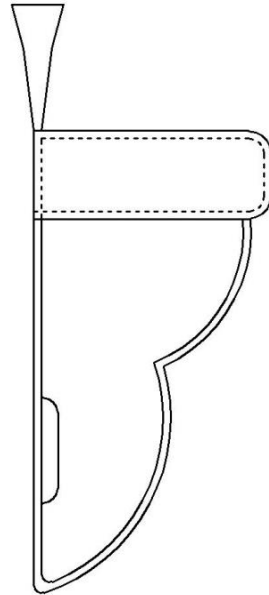
(f) Finished Mann of Brass

Figure 7.2: Pictorial representation of Model-1 (Mann):
Cast by Three different Alloy

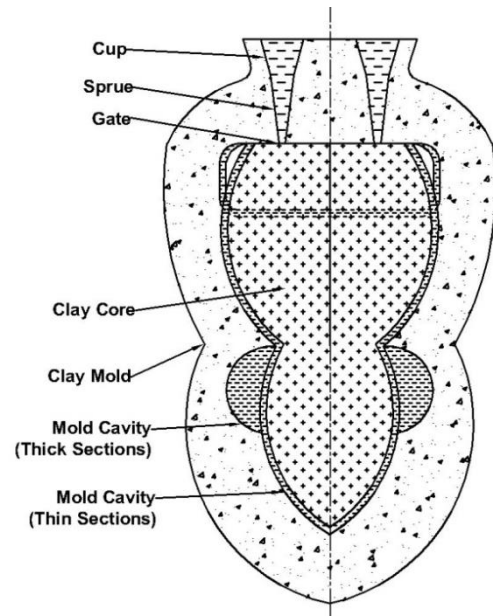


(a) Schematic diagram of Model-1 along with dimension. Gating dimension also given in bottom left corner. (All dimensions are in mm)

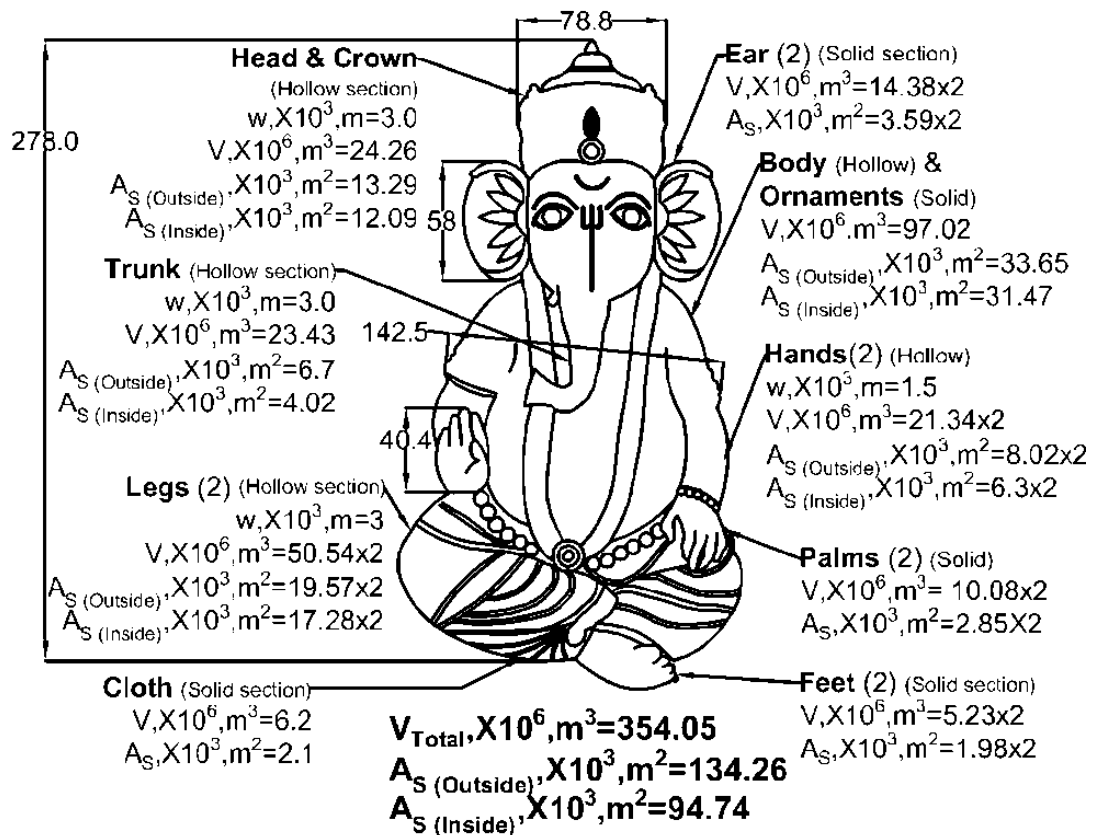




(d) Schematic diagram of Top Gating System (side view)



(e) Schematic diagram of clay mold with gating system



(f) Schematic Diagram with Dimension and Partwise Volume and Surface area

Figure- 7.3 The schematic diagram of Model-1, featuring two Gating systems, Volume and Surface Area, illustrating the different parts involved

(All dimensions are in mm).



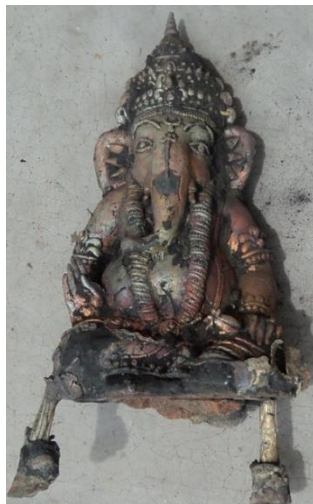
(a) Wax Patten



(b) Clay Mold with Top Gating System



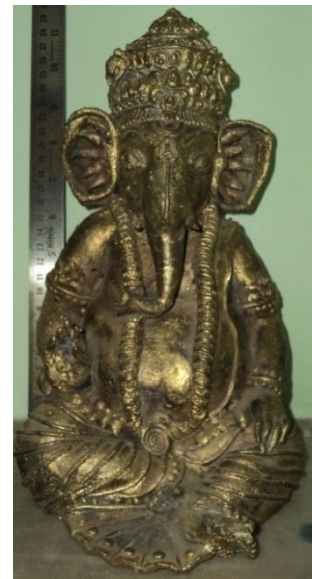
(c) Clay Mold with Side Gating System



(d) Unfinished Cast Model with Top Gating System

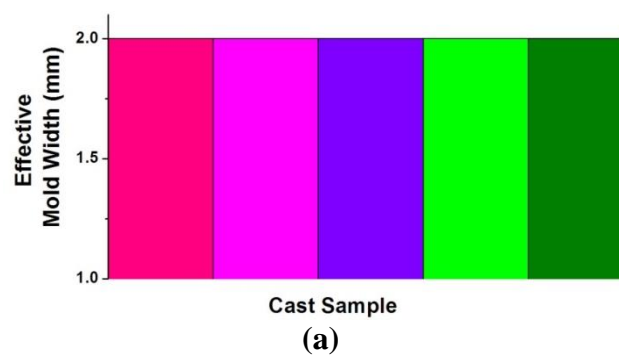


(e) Unfinished Cast Model with Side Gating System



(f) Finished Model,

Figure- 7.4: Pictorial representation of Model-2: Cast by two different gating system



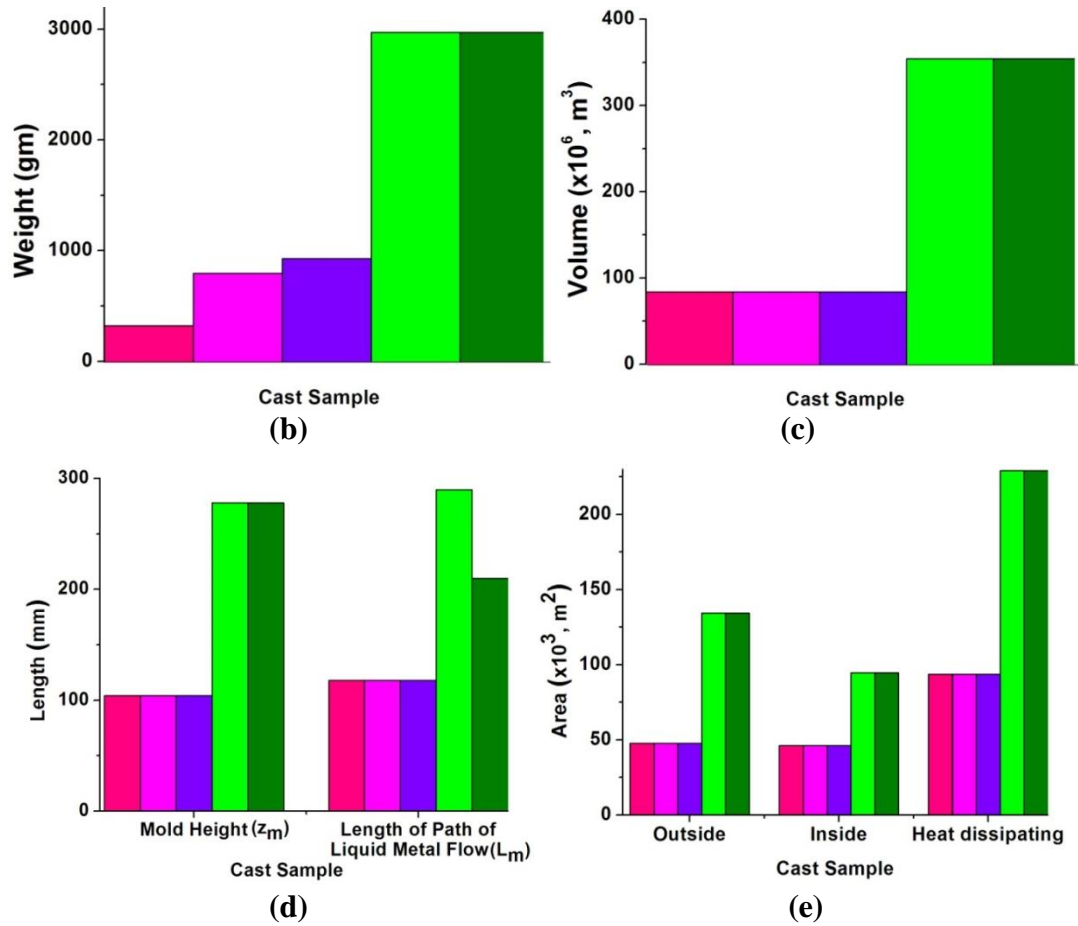
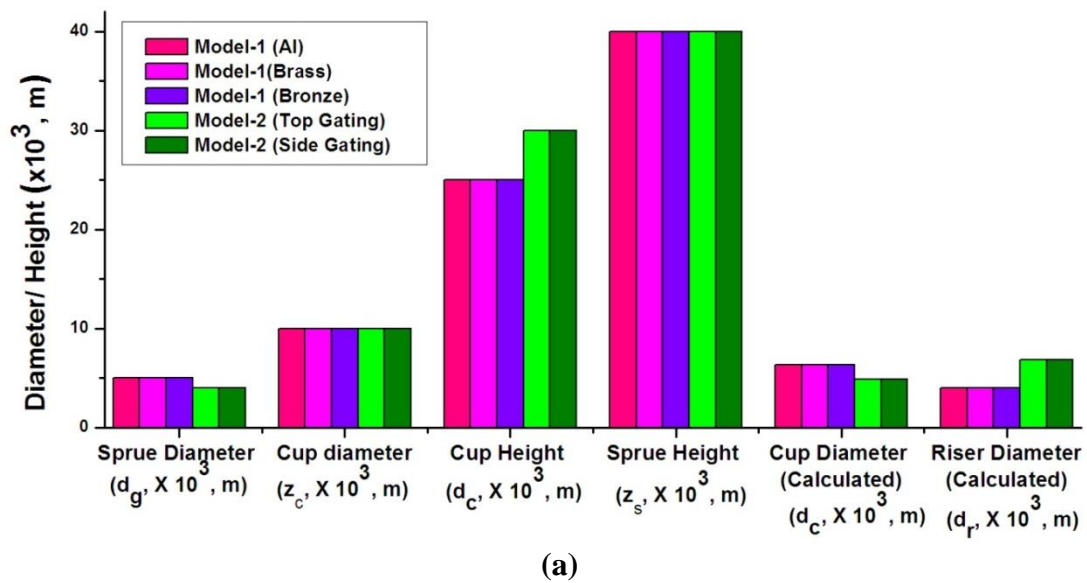


Figure- 7.5: Physical Parameters of the cast samples: (a) Effective Mold width (mm), (b) Weight of the casting (gm), (c) Mold Volume (m^3), (d) Mold height (m) and Length of path of liquid metal flow (m), (e) Inside and outside mold surface area



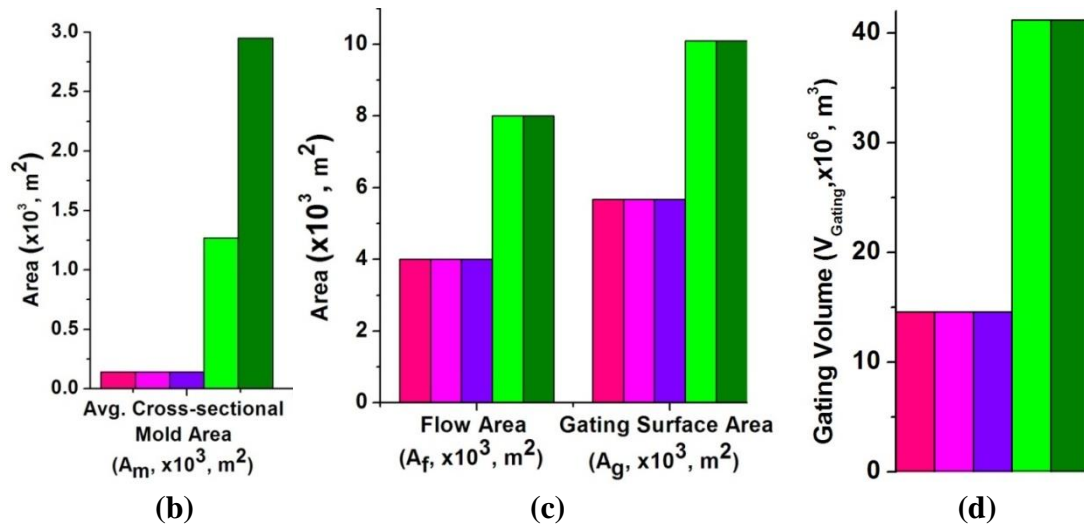
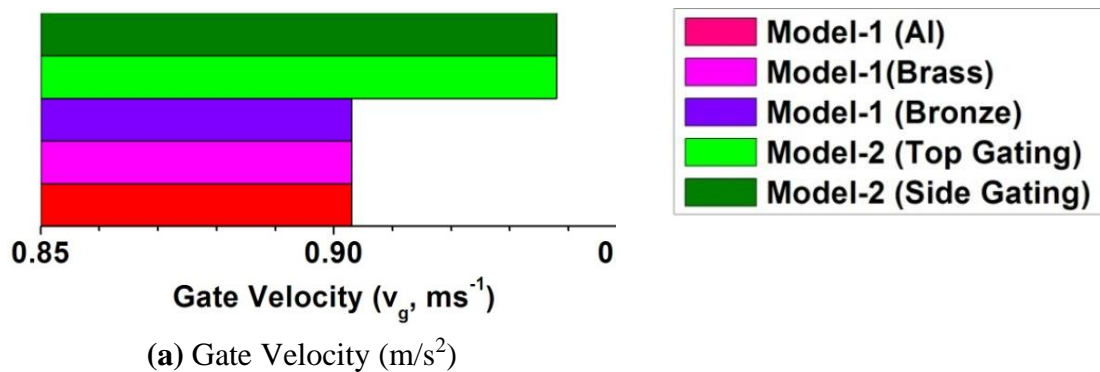
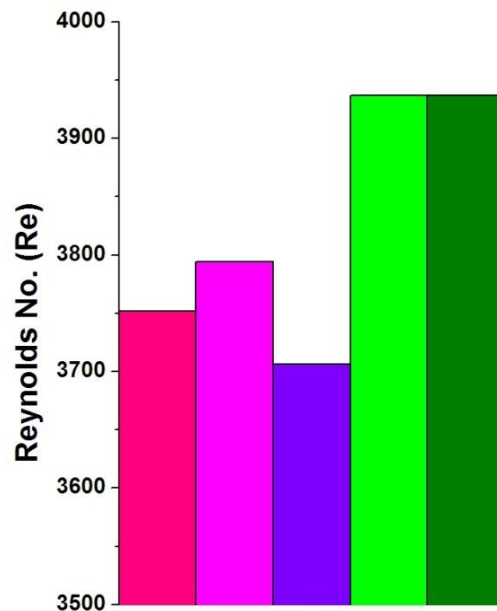


Figure- 7.6: Gating Details of the castings (a) Sprue Diameter (m), Cup Diameter (m), Cup Height (m), Sprue Height (m), Calculated Cup Diameter(m) and Calculated Riser Diameter (m), (b) Average cross-sectional mold area(m^2), (c) Flow area (Gate area) (m), Gating Surface Area, (d) Gating Volume

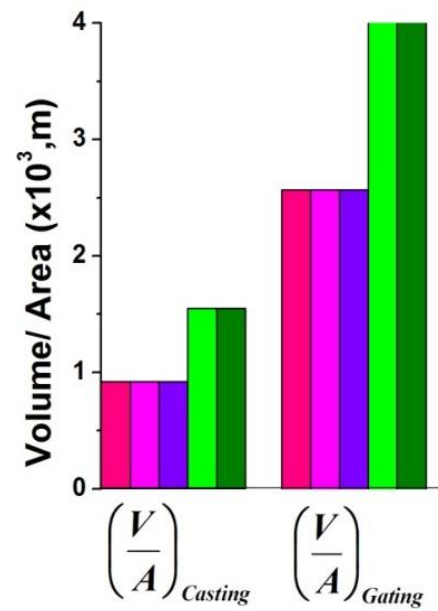
7.1.3. Result

The calculated parameters such as (i) Liquid metal Velocity at Gate (m/s^2), (ii) Reynolds Parameters (Re), (iii) Modulus (Volume/Area) of casting and gating system, (iv) Hot metal required (kg) for casting, and (v) Yield percentage of the castings were shown in figure 7.7. The actual (t_{act}) and calculated filling time (t_f) were shown along with the conventional filling time (t_{conv}) in the figure-7.8. The percentage of error for actual filling time (t_{act}) compared to calculated filling time (t_f) and conventional filling (t_{conv}) time were shown in Figure- 7.9.

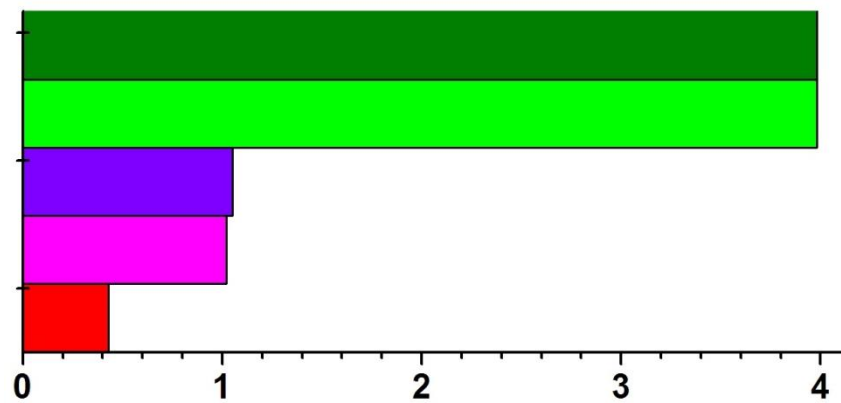




(b) Reynolds Parameters

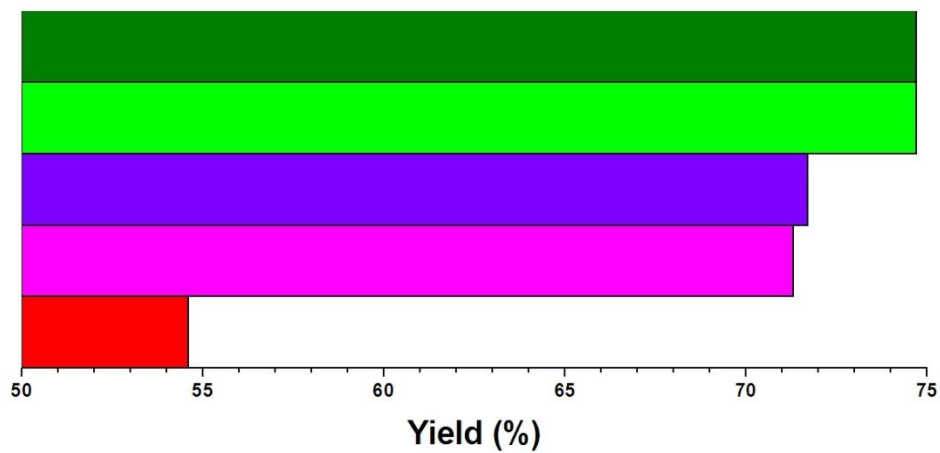


(c) Modulus (Volume: Area) of casting and gating system



Hot Metal Required (kg)

(d) Hot metal required (kg),



Yield (%)

(e) Yield (%)

Figure- 7.7: Calculated Parameters

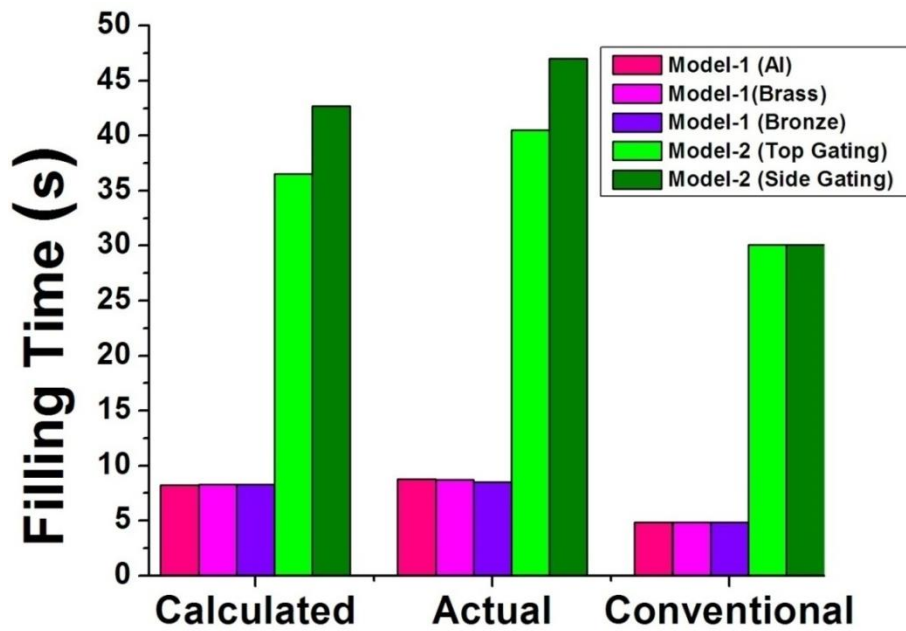


Figure- 7.8: Comparison among the calculated filling time, actual (experimented) filling time, and the conventional filling time

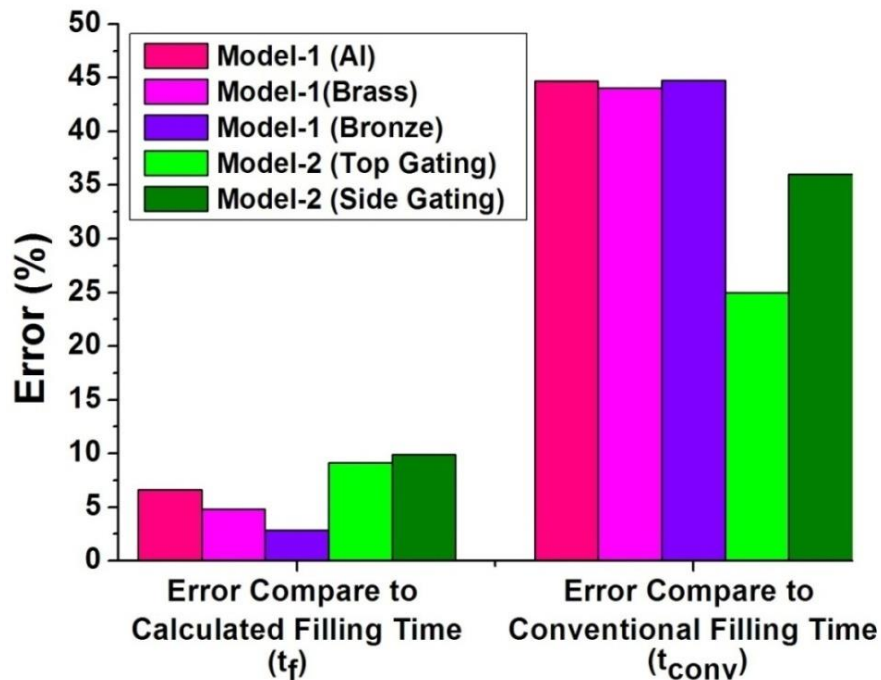


Figure- 7.9: Comparison of the error (%) between the calculated filling time and the actual filling time, as well as between the conventional filling time and the actual filling time

7.2.Metrological Analysis of Industrial Clay Molded Thin-Walled Investment

Casting

Metrological analyses were conducted for a Cosmetic case and cap. It was a Circular Section of Wax-Based Thin-Walled Investment Castings in a hot mold. The evaluations encompassed various products with distinct geometrical shapes [7.2] are as follows

- I. Cosmetics Case- Truncated Cone,
- II. Cosmetic Cap- Hemispherical Dome.

7.2.1 Experimental Framework

The details of experiments for Dimensional Analysis were tabulated in Table-7.2. Each sample was cast by a different type of gating system with different mold positions. Four gating systems were selected for this experiment followed by [7.4, 7.5]

- | | |
|--|-----------------|
| I. Central Axial Top Gating System- | TYPE-I |
| II. Peripheral Axial Top Gating System - | TYPE-II |
| III. Peripheral Radial Top Gating System - | TYPE-III |
| IV. Peripheral Radial Bottom Gating System - | TYPE-IV |

The schematic diagrams of the Cosmetic cap and case along with gating systems were provided in Figure 7.10. All materials used were the same as those mentioned in Chapter 6. The process, from pattern creation to clay mold making, was displayed in Figure 7.11, also featuring the chosen metal die's dimensions. The pictorial representations of the gating system with castings were shown in Figure 7.12. Cast samples, alongside observed defects, were depicted in Figure 7.13 for both the case and the cap.

Table-7.2: Experiments for Dimension Analysis

Type of Analysis	Shrinkage Analysis	Metrological Analysis
Classification	i. Radial (Diameter wise) ii. Longitudinal (Height wise) iii. Cast-wall Thickness (Metal width)	i. Eccentricity ii. Thickness Variation iii. Surface Quality iv. Surface Roughness (Ra)

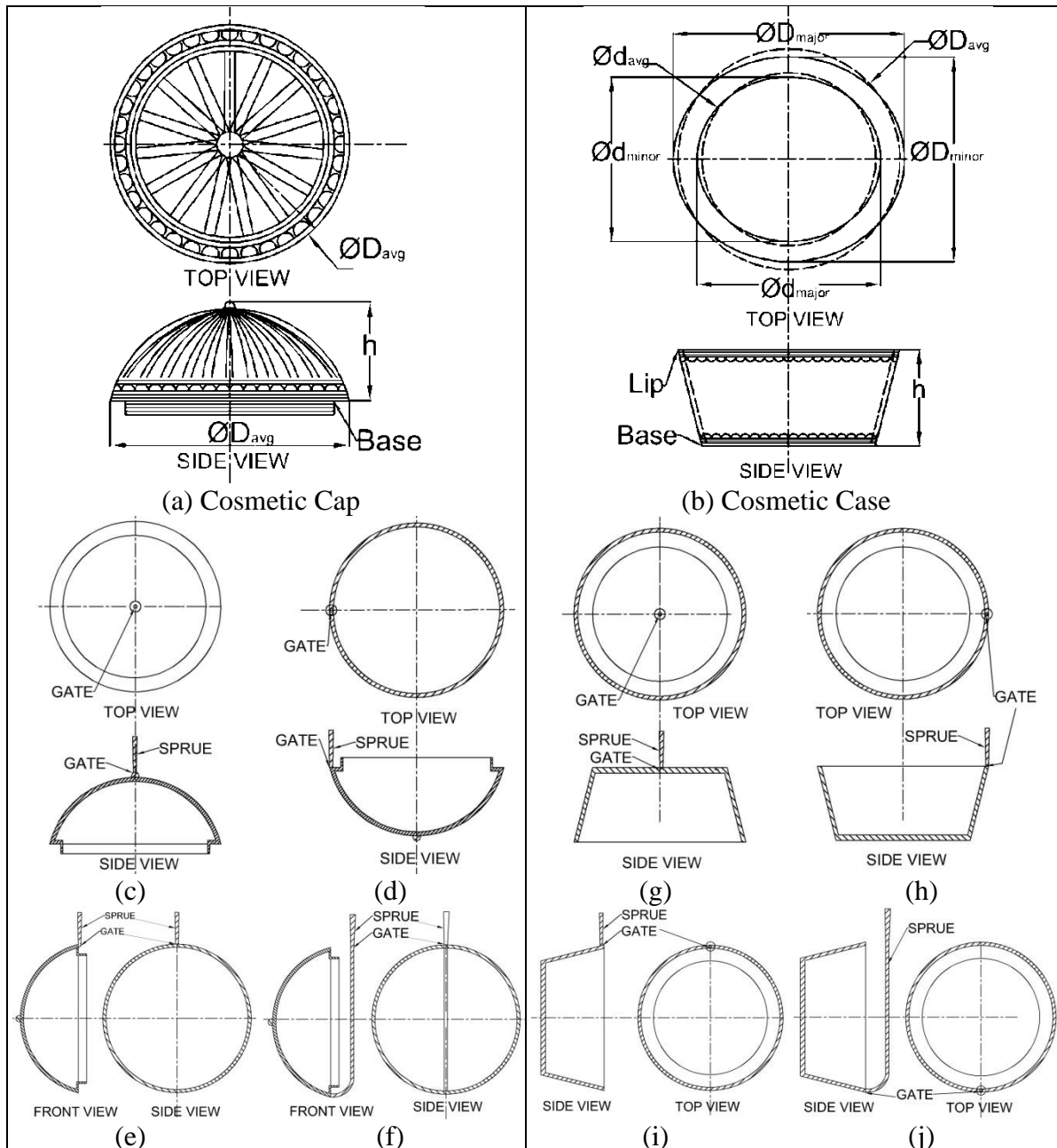


Figure- 7.10: Schematic diagram of (a) Cosmetic Cap and (b) case. Schematic diagram of gating system: Cosmetics Cap (c) Type-I, (d) Type-II, (e) Type-III, (f) Type-IV; and Case (g) Type-I, (h) Type-II, (i) Type-III, (j) Type-IV

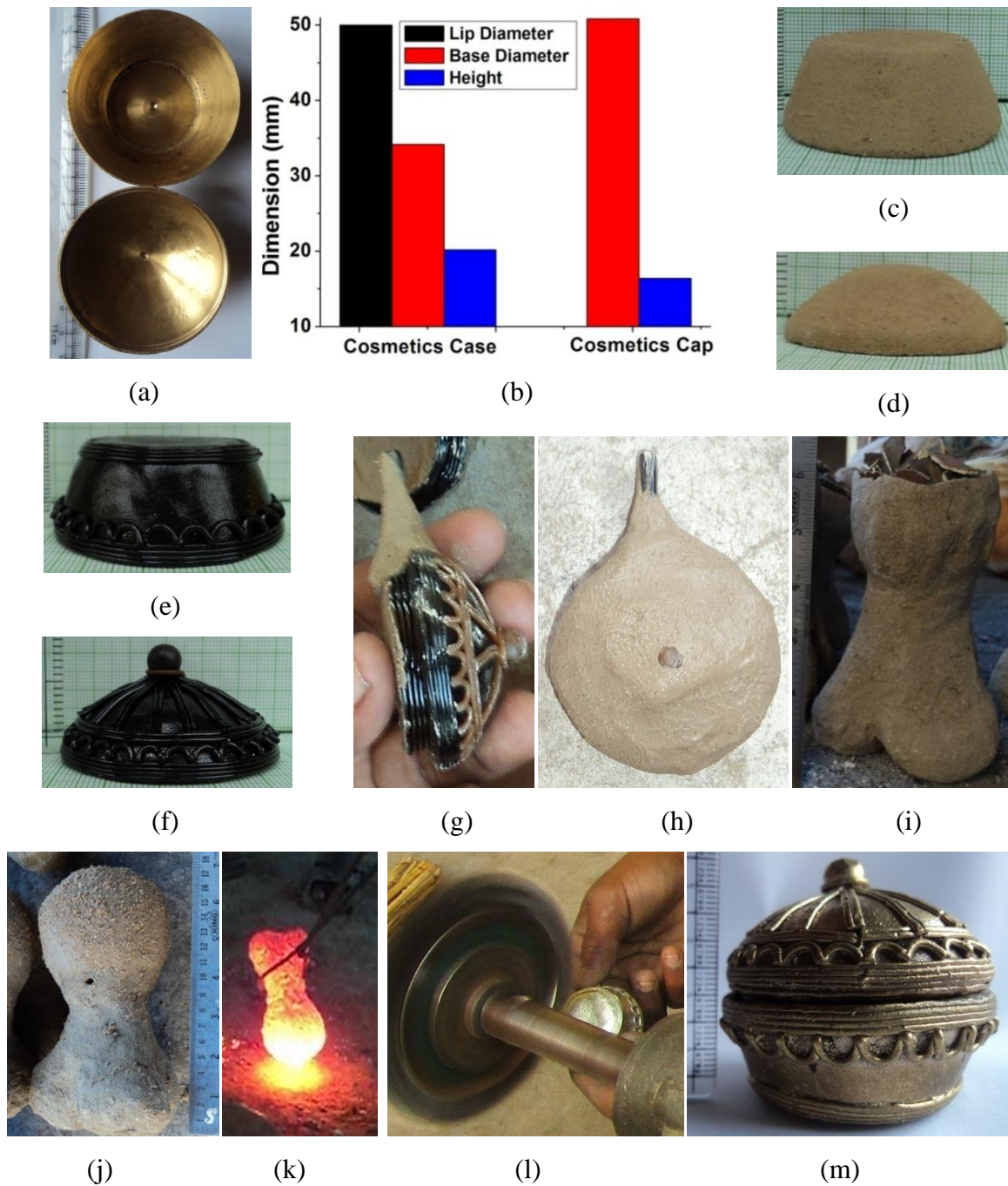


Figure- 7.11: Production Steps of Cosmetics Case and its Cap: (a) Die, (b) Dimension of the Dies, (c, d) Clay core, (e, f) Wax Pattern, (g) Gating on wax Pattern, (h) Primary Clay Coating, (i) clay mold with brass scrap, (j) Covered clay mold, (k) Fired mold- pouring of liquid metal also done, (n) Polishing, (m) Final product.



Figure- 7.12: Pictorial View of casting with gating system. Cosmetics Cap (a) Type-I, (b) Type-II, (c) Type-III, (d) Type-IV and Cosmetics Case (e) Type-I, (f) Type-II, (g) Type-III, (h) Type-IV



(a) Surface of Cosmetics Case of Type-I Gating System of two Opposite Surface



(b) Surface of Cosmetics Case of Type-II Gating System of two Opposite Surface



(c) Surface of Cosmetics Case of Type-III Gating System of two Opposite Surface



(d) Surface of Cosmetics Case of Type-IV Gating System of Two Opposite Surface



(e) Type-I



(f) Type-II



(g) Type-III



(h) Type-IV

Figure-7.13: Surface Quality of Finished Product. (a), (b), (c), (d) Cosmetic Case and (e), (f), (g), (h) Cosmetic cap

7.2.2 Shrinkage Analysis of Wax-Based Thin Walled Brass Castings in Hot Mold

The experiment was conducted on numerous samples of identical design to scrutinize the shrinkage behavior of Wax-Based Thin-Walled Casting in a Hot Mold. Shrinkage analysis for the diameters, height, and metal thickness of the cast samples along with the shrinkage percentage of the clay core was presented in Figure 7.14. Detailed dimensions were illustrated in appendix XVII. Additionally, figure 7.15 showcased the schematic diagram of the wax pattern and cast item. Furthermore, Table 7.3 summarizes the shrinkage analysis of the cast product concerning the wax pattern and the internal dimension shrinkage concerning the die.

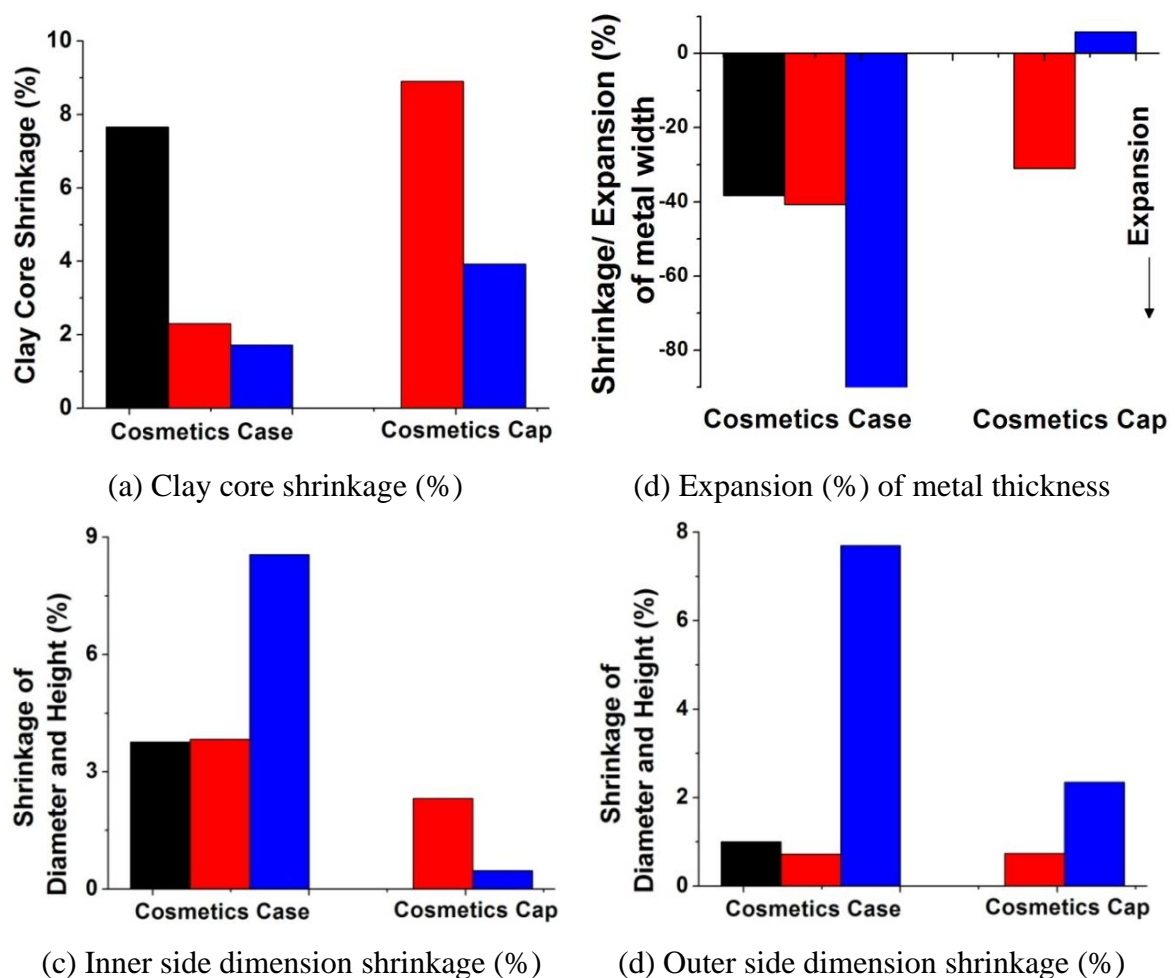


Figure-7.14: Dimensional Shrinkage (%)('+ve' is for shrinkage, '-ve' is for expansion)

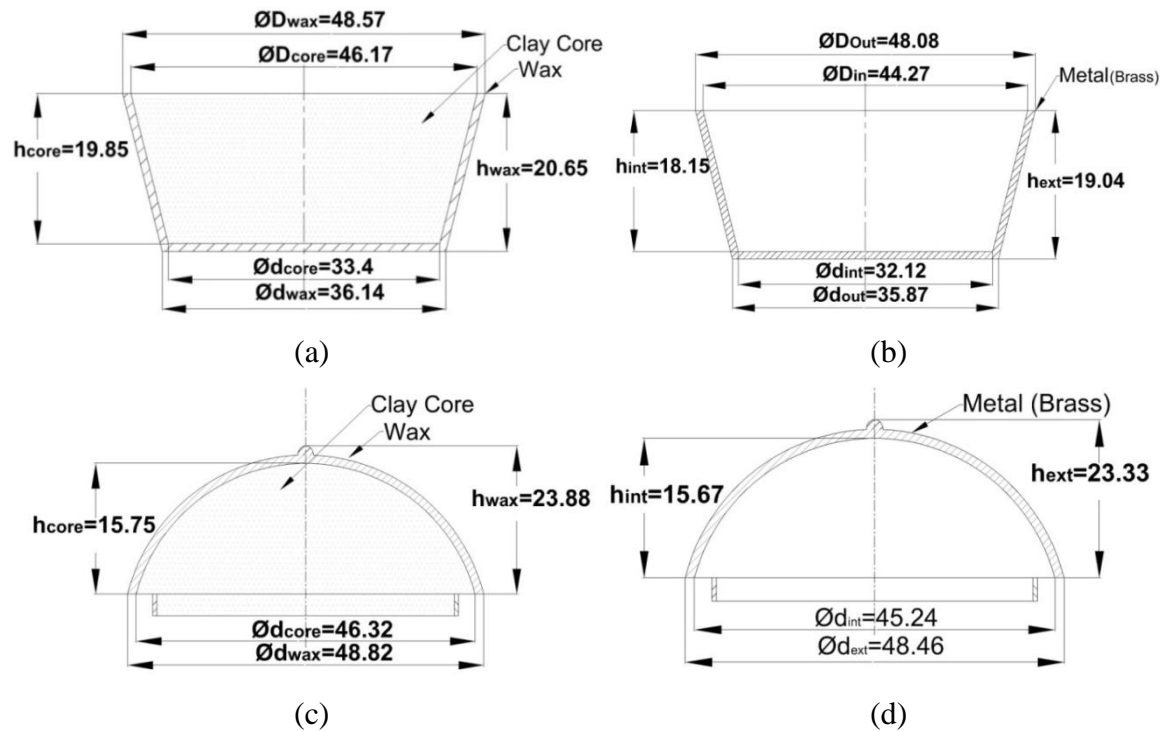


Figure-7.15: Schematic diagram of different Stage of the Product. Cosmetic Case: (a) Clay Core and Wax pattern, (b) Cast Sample (Internal and external); Cosmetics cap: (c) Clay Core and Wax pattern, (d) Cast Sample (Internal and external).

(All dimensions are in mm)

Table -7.3: Shrinkage Analysis of Cast Product with respect to Wax Pattern and Shrinkage of Internal dimensions with respect to Die

(‘+’ for Shrinkage, ‘-’ for Expansion)

			Lip Diameter (%)	Base Diameter (%)	Height (%)	Metal Width (%)
Shrinkage (%) compare to Wax Pattern	Cosmetics Case	External	1.0	0.72	7.7	-56.3
		Internal	3.76	3.83	8.56	
	Cosmetics Cap	External	X	0.74	2.35	- 31.0
		Internal	X	2.32	0.47	
Shrinkage (%) compare to Die	Case	Internal	11.14	6.08	9.25	X
	Cap	Internal	X	10.59	2.06	

7.2.3 Effect of Gating System for Thin Walled Investment Castings

To assess uniformity, wall thickness measurements were conducted based on designated planes and sections [Appendix-XVIII] for the Cosmetics Case and Cap. These measurements encompassed various properties across multiple samples of identical designs but employing different gating systems.

7.2.3.1.The Eccentricity of the Lip and Base

The calculated eccentricities of the Outer and Inner diameters of the Lip and Base positions were shown in figure-7.16.

7.2.3.2.Mean Variation (R.M.S) of Metal thickness

The data chart of the average variation of Metal width for different planes and a different section for the cosmetic cases and caps for different gating systems were shown in Appendix XVIII. A comparison of the Percentage of Mean Variation (R.M.S) of Metal thickness was calculated and was shown in Figure 7.17.

7.2.3.3.Surface Quality by Visual Inspection and Surface Roughness

The visible inspection was done by the images of the surface taken by an optical camera. The Pictures of the surfaces were shown according to different gating types in Figures-7.13 and the Surface and Sectional Quality of the Samples were tabulated in table-7.4.

7.2.3.4.Surface Roughness

The surface roughness (Arithmetic mean of departures-Ra) of the samples was measured using the same method as before. The sampling length (Lc) for the Cosmetics case and Cap was set at 0.8mm due to the presence of designs with less open surface available for measurement. Surface Roughness (Ra) was illustrated in Figure 7.18.

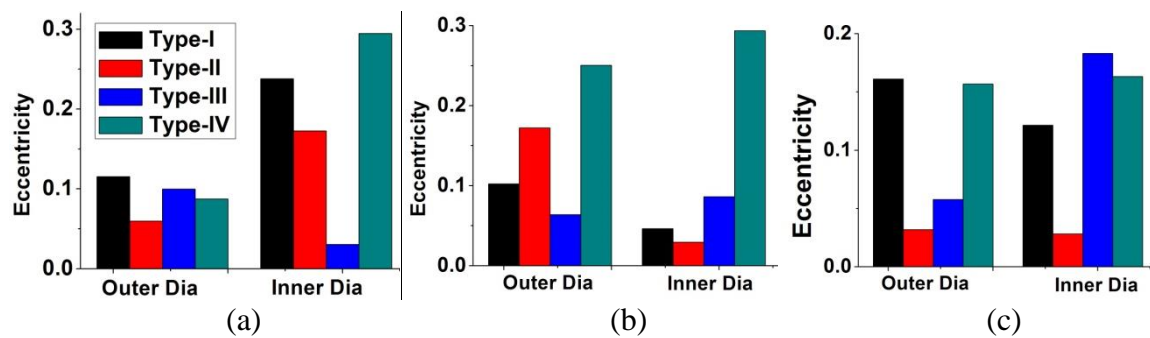


Figure-7.16: Eccentricity of Cosmetics Case and Cap: (a) Eccentricity of Base Diameter and (b) Lip Diameter of cosmetic case, (c) Eccentricity of Cap Base Diameter

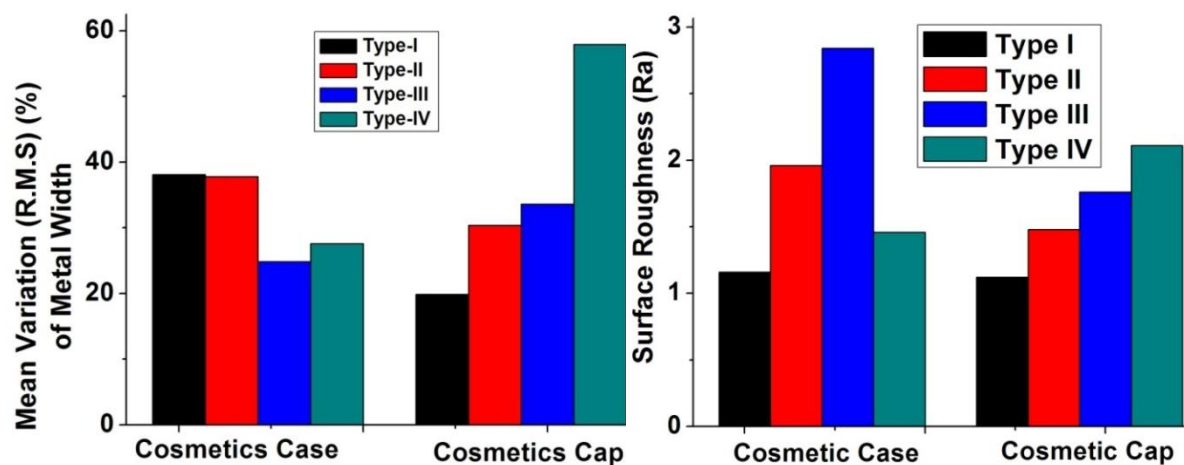


Figure-7.17: Percentage of Mean Variation (R.M.S) of Metal Thickness

Figure 7.18: Surface Roughness of Cosmetics Case and Cap

Table-7.4: Surface and Sectional Quality of the Cosmetics Case

	Gating Type	Surface Quality (%)			Un-Filled section (%)
		Accepted	Salvaged	Damaged	
Cosmetic Case	Type-I	100	0	0	0
	Type-II	99	1	0	0
	Type-III	98	2	0	0
	Type-IV	75	5	32	20
Cosmetic Cap	Type-I	100	0	0	0
	Type-II	97	3	0	0
	Type-III	85	5	10	10
	Type-IV	55	10	35	35

7.2.4 Ranking by TOPSIS

An MCDM tool, TOPSIS (Technique for Order Preference by Similarity to Ideal Solution), was employed. In Appendix XX and XXI detailed calculations were shown. Table 7.5 lists preferable gating systems [7.5] based on experimental analysis with rejected rates (%). The ‘Unfilled sections’ was the cause for rejection for every case.

Table-7.5: Preferable and Rejected Gating System with Ranking

Product	Gating Type	Ranking		Preferable Gating System (according to preference)	Rejected Gating System [Rejection (%)]
		Individual	Overall		
Cosmetics Cap	I	2	2	1. Type-II 2. Type-I	i. Type-IV (100% Rejected) ii. Type-III (40% Rejected)
	II	1	1		
	III	3	6		
	IV	4	8		
Cosmetics Case	I	1	4	1. Type-I 2. Type-II 3. Type-III	Type-IV (100% Rejected)
	II	2	3		
	III	3	5		
	IV	4	7		

7.3. Metallurgical Characterization of Castings Products

The characterization of Brass, Gunmetal and Aluminium castings produced by wax-base investment casting process in hot clay molds was investigated.

7.3.1. Chemical Compositions

The results of chemical analyses of the cast metals investigated have been given in Table-7.6. The chemical analysis of the brass casting indicates that copper (Cu) and zinc (Zn) are the primary constituents. Some alloys also contain trace amounts of tin (Sn), lead (Pb), and iron (Fe) as minor elements. With a Zn-equivalent value of 37.84 (~38%), the alloy is categorized as Muntz metal (Cu:Zn = 60/40) [7.6].

The chemical composition (wt. %) of the Bronze Casting has been assessed as, Cu: 84.4., Sn: 10.1, Zn:2.0, and Pb: 3.05 and so, this indicates the alloy is Gunmetal. The Chemical analysis (wt. %) of the Aluminium Casting has been assessed as, Al: 87.6%, Si: 10.2%, Fe 0.5%, Mn: 0.5% and other elements. The result confirms that the alloy is Al-LM6.

7.3.2. Hardness of the Cast Samples

The Bulk Hardness (HV 5/10) and Micro Hardness (HV 50/10) of Cast samples were illustrated in figure-7.19. Hardness results were similar to those of the corresponding metals.

In general, thickness of the metal specimen should be 1.5 times of the diagonal of the indentation [7.7]. The thickness of the castings was very low, 0.7mm to 3.2mm. So, there is a chance of error. Also, the micro-hardness was taken over the thin section cast structures which are a non-equilibrium phase as well as produces fine grains. The diagonal of the indentations are even larger than the grain sizes, therefore the micro-hardness values are close to the bulk hardness value.

7.3.3. Microstructures with SEM-EDX Analyses

The microstructure of aluminum (figure-7.20) LM6 alloy sample, Al-Si system, and shows typical cast aluminum structure exposes the visible silicon streaks over the aluminum matrix. being divorced-eutectic silicon separates itself from the metal phase (like graphite in cast iron) and the coarseness of the silicon indicates unmodified structure.

The SEM microstructure of the 60-40 Brass sample (Figure-7.21) exposes the visible dendrites with well-marked grain boundaries. The microstructures of the cast metal consist of copper rich α -Cu phase (grey colored) as the matrix and Zinc rich β -phase in the grain boundary region around the α -Cu phase.

The microstructure of Gunmetal (Figure-7.22) Sample, in chemical composition, as already stated can be pronounced as a Semi Red Brass having Cu-Zn-Sn-Pb system.

Table-7.6: Chemical Composition of Cast Samples

<u>60:40 Brass</u> (Muntz metal)			<u>Gun Metal</u> (Red Brass)			<u>Silumin Alloy</u> (Aluminium LM6)		
1.	Cu%	61.12	1.	Cu%	84.4	1.	Al	87.6
2.	Sn%	1.16	2.	Sn%	10.1	2.	Si	10.2
3.	Pb%	3.51	3.	Zn%	2.0	3.	Fe%	0.5
4.	Fe%	0.25	4.	Pb%	3.05	4.	Mn%	0.5
5.	Other (%)	0.33	5.	Fe%	0.04	5.	Pb%	0.1
6.	Zn%	33.63	6.	Ni%	0.2	6.	Cu%	0.1
Zn Equivalent		37.84	7.	Other%	0.21	7.	Other%	1.0

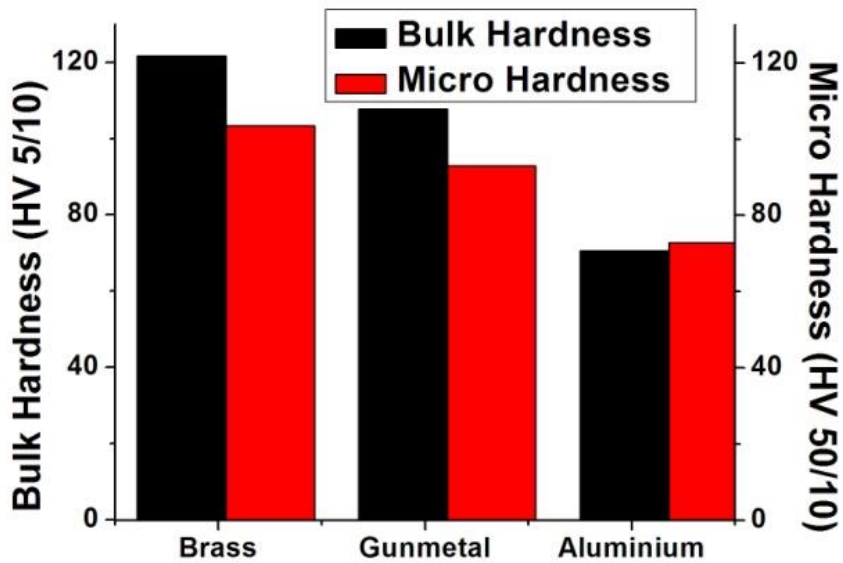


Figure- 7.19: Vickers (Bulk) Hardness (HV 5/10) and Micro Hardness (HV 50/10) of Cast Samples

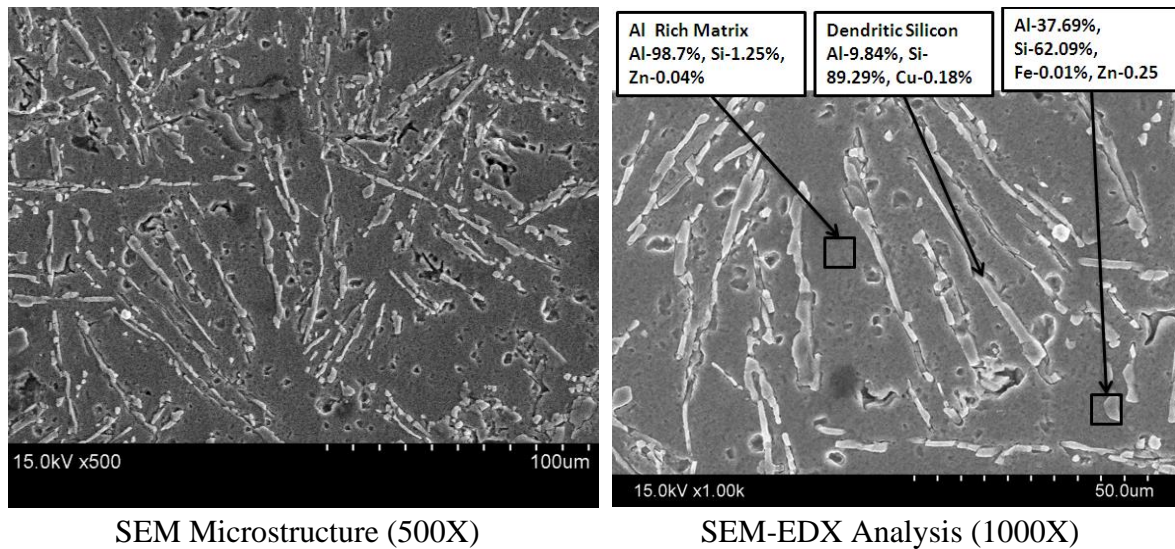


Figure-7.20: SEM Microstructure of Auminium Cast Sample (Etchant: Methanol, Hydrochloric acid, Nitric acid). Dendritic structure of Silicon (Whitish) is distributed in Aluminium Matrix (Gray) of the Cast sample.

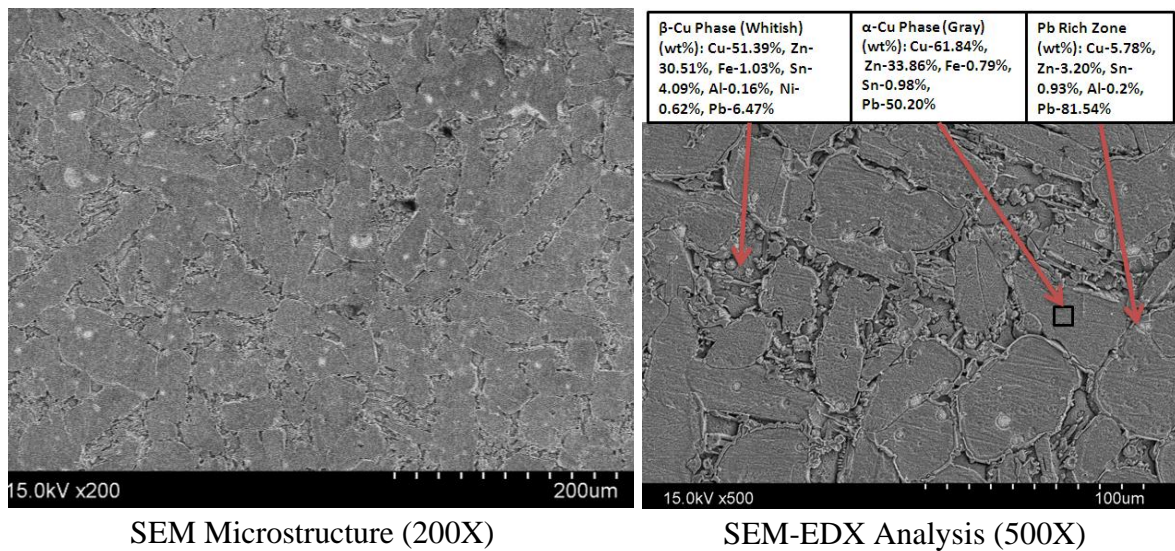


Figure-7.21: Microstructure (SEM) of Brass Casting (200X) (Etchant: FeCl_3 in HCl) with SEM- EDX analysis. Structure shows the single α -Cu phase with inter dendritic region solute rich β -Cu phase. Insoluble Lead is Distributed everywhere.

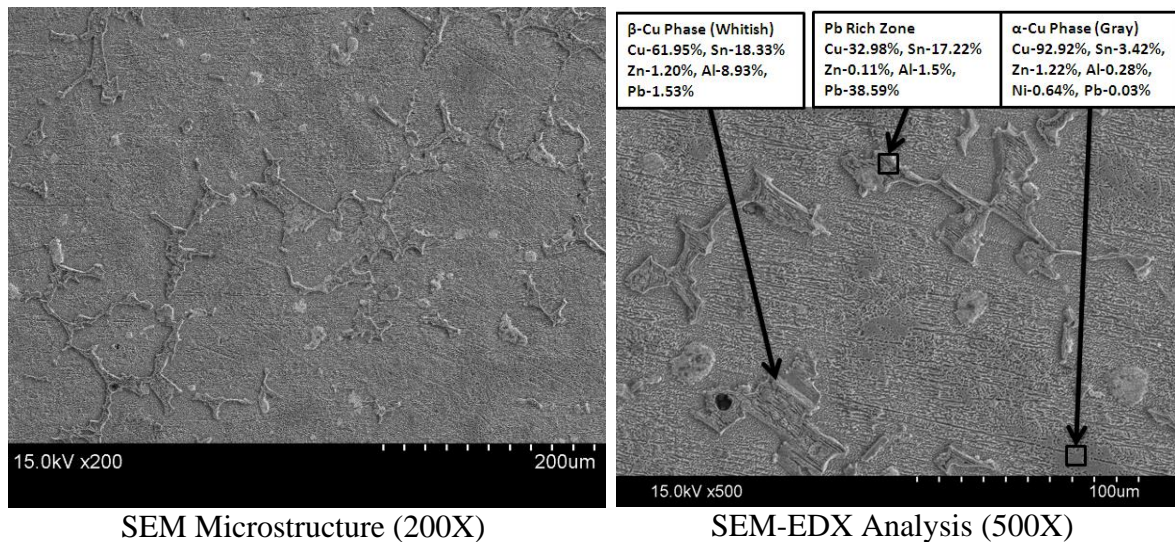


Figure-7.22: SEM Microstructure of Bronze (Gunmetal) Cast Sample (200X and 500X) (Etchant: FeCl_3 in HCl) highly distinctive cellular structure formed by α -Cu-Zn phase (whitish areas).

7.4.Discussion

The following observations from the actual Industrial casting are given below:

- i. **Gating Design:** During observation, it was noticed that the sprue diameters were sufficiently large compared to the calculated riser diameter. As a result, the sprues themselves functioned as risers. This finding indicates that there was no need for a separate sprue in the casting process. Also, the actual gate areas of all castings are as big as the calculated gate areas.
- ii. **Yield:** The yield of Copper alloy castings typically falls within the range of 70% to 75%. In contrast, Aluminum castings have a lower yield of approximately 55%.

iii. Filling time: The relatively minor variations in mold filling time among different metals can be attributed to the fact that the density differences among the metals being considered are within a range of 30%. It was observed that the mold filling time for the top gating system was less compared to the side gating system, even when considering the same metal (60/40 Brass) and gating system design. This observation provides validation for the accuracy of the mathematical model in predicting the mold filling time with precision.

iv. Shrinkage varied from 0.7% to 4% for restricted dimensions (base, lip) and from 0.4% to 8.5% for unrestricted dimensions (height), showing less variation in the former. Metal thickness expanded compared to wax pattern thickness for sections less than 3 mm. The reason was already discussed earlier. Notably, shrinkage was higher closer to the gate than in other sections. For most cases, sections nearest to the gate were the thinnest due to liquid metal supply during solidification.

v. The Central Axial Top Gating System (Type-I) exhibited uniform wall thickness in different sections and better surface roughness due to uniform liquid metal flow in all direction throughout the mold cavity.

vi. Surface roughness overall was better for the Cosmetics Cap-Hemispherical Geometrical Shape due to smoother metal flow. Smoother surfaces were observed in thinner sections compared to thicker ones; with defects like Metal Penetration and Scab found more in thicker sections.

vii. Unfilled section was the **main reason for rejection** for this product in this industry. Maximum unfilled sections were opposite side of the gate for the bottom gating system, showing larger dimension variations.

viii. Quality of Casting of Both macroscopic (good quality surface) and microscopic analyses confirm the high-quality nature of the castings.

The result of the experiment recognized that gating systems should be chosen based on product shape, size, and thickness, ensuring smoother metal flow for better quality casting.

Chapter-8

Conclusions

8. Conclusions

- I. Fluid flow through parallel plate encounters some physical constraints and mechanical engineers postulates some special consideration in case of Kinetic energy correction factor (α), Friction factor (f), surface energy factor (γ). Considering the above constraints a new fluid flow analytical model based on Bernoulli's theorem has been proposed for mold filling time calculation for investment molds having flat cavities of the order of microns ($\sim\mu\text{m}$). The new analytical model attempts to consider the resistance pressure due to Capillary action (ΔP_γ) along with frictional head loss (z_f). Torricellian vacuum in Pascal's multiplication inside a closed mold was also determined.
- II. To validate the analytical model derived using Bernoulli's equation for Investment mold filling time calculations, simulation experiments using fluids in form of Water and Mercury have been utilized. The results of the experiments validated the proposed model within the reasonable ($\pm 10\%$) assessment. Obviously the proposed model can be used for design purpose for the sake of filling time measurement.
- III. Further to evaluate the analytical model in actual industrial application some traditional clay molded investment casting production have been tried out and tested. The incorporated filling times of investment castings using the analytical model have been observed to be followed with a reasonable errors (6% to 12%) of judgment. All the calculated filling times of investment castings further confirms the utility of the proposed model.

- IV. To evaluate the dimensional accuracy investment casting produced by silica based mold from the metrological view point some experiments were conducted confirming through standard method. Results of the metrological experiments (for metal thickness dimensional variation<10% and other section dimensional variation<1%,) are very much encouraging for designers to achieve higher degree of dimensionally accurate thin ($\sim\mu\text{m}$) investment casting. The anomalous expansion of silica mold have been dealt with for better accuracy of investment castings when silica based molds are used.
- V. Some preliminary assessments of microstructural development studies have been attended to assess coarseness of the grain structure of the investment cast materials. As expected the coarseness of the grains and thick silicon streaks have been observed in case of Cu based and Silumin alloys respectively.

Bibliography

Bibliography

Chapter-1

- 1.1. Spurk JH, Aksel N (2008) Fluid mechanics. Springer, Berlin, pp 167–179
- 1.2. Schaschke C (2000) Fluid mechanics: worked examples for engineers. Institution of Chemical Engineers, Rugby, pp197–198
- 1.3. White FM (2006) Fluid mechanics, 4th edn. McGraw-Hill, New York, pp 170–171
- 1.4. Çengel YA, Cimbala JM (2014) Fluid mechanics, fundamentals and applications. McGraw Hill, New York, p 59
- 1.5. Stefanescu DM (2002) Science and engineering of casting solidification. Springer, New York, pp 65–67

Chapter-2

- 2.1. ASM Metals handbook: vol.-15-casting, (electronic version), pp-17-18, 57, 68 (1998)
- 2.2. ASM Metals handbook: vol.-15-casting, (electronic version), pp -446-447, 543, 565, (1998)
- 2.3. Maheta N, Sata A, Systematic Development of Cumulative Complexity Index for Investment Casting, Journal of Advanced Manufacturing Systems (June 2022)
- 2.4. Donga Y.W., et. al., Modeling of shrinkage during investment casting of thin-walled hollow turbine blades, Journal of Materials Processing Technology, pp-190–203 (2017)
- 2.5. Tiwary Vivek kumar. et al., Surface enhancement of FDM patterns to be used in rapid investment casting for making medical implants, Rapid Prototyping Journal, 25(2), (June 2019), DOI: 10.1108/RPJ-07-2018-0176
- 2.6. Pattnaik Sarojrani, et al., Developments in investment casting process—A review, Journal of Materials Processing Technology, 212, pp-2332-2348 (2012)
<http://dx.doi.org/10.1016/j.jmatprotec.2012.06.003>
- 2.7. Ripetskiy A.V., et al., The role of additive manufacturing in the investment casting process, E3S Web Conf., Volume 413, 2023, (August 2023) DOI: 10.1051/e3sconf/202341304015
- 2.8. Kumar Parlad, et al., Investigations on dimensional accuracy of the components prepared by hybrid investment casting, Journal of Manufacturing Processes 20 (2015) 525–533
- 2.9. Beeley Peter, Foundry Technology, Butterworth Heinemann, 2nd Edition, p-563, 591 (2001)
- 2.10. Campbell John, Casting Practice- The 10 Rules of castings, pp-75-78 (pdf-88)Elsevier Butterworth-Heinemann Linacre House, Jordan Hill, Oxford OX2 8DP 200 Wheeler Road, Burlington, (2004)
- 2.11. Hwang Weng-Sing, et. al., Molten metal flow pattern prediction for complete solidification analysis of near net shape castings, Materials Science and Technology, Vol. 4, 240-250 (March 1988)
- 2.12. Stefanescu D. M., Science and Engineering of Casting Solidification, , pp. 65-67. Springer Science, New York (2002)
- 2.13. Horáček M., Accuracy of Dimensional Analysis, Archives of Foundry, Volume 5, No. 15, pp-121-137 (2005)
- 2.14. Cannell N., et. al., Predicting Pattern Tooling and Casting, Dimensions for Investment Casting, Phase II, U.S. Department of Energy (DOE) Information Bridge (2005)
- 2.15. Cannell N., et. al., Predicting Pattern Tooling and Casting, Dimensions for Investment Casting, Phase III, U.S. Department of Energy (DOE) Information Bridge (2007)
- 2.16. Beeley P., Foundry Technology, Butterworth Heinemann, 2nd Edition, pp-426-427, (2001)

- 2.17. Clegg, A. J., Precision Casting Processes, Pergamon Press, Oxford (1991)
- 2.18. Oliff I. D., Lumby, R. J. and Kondic, V., Foundry Trade J., 119, 469 (1965)
- 2.19. Ragone D. V., Adams, C. M. and Taylor, H. F., Trans. Am. Foundry Soc. 64, 640 and 653 (1956)
- 2.20. Barlow G. and Beeley, P. R., Br. Foundrym., 63, 61 (1970)
- 2.21. Hoar T. P. and Atterton, D. V., J. Iron Steel Inst., 166, 1 (1950)
- 2.22. Baruch T. A. and Rengstorff, G. W. P., Trans. Am. Foundry Soc., 71, 595 (1963)
- 2.23. Flemings M. C., et. al., Trans. Am. Foundry Soc., 70, 1029 (1962)
- 2.24. Jeyakumar M., et.al., Rheology of liquid metals and alloys, Journal of Non-Newtonian Fluid Mechanics, pp. 831-838 (2011)
- 2.25. Nakayama Y., et.al., Introduction to Fluid Mechanics, Butterworth, Heinemann, pp. 88-91 (1999)
- 2.26. Spurk, Joseph H., et. al., Fluid Mechanics, Springer, pp. 168-169 (2008)
- 2.27. Bansal R.K., A textbook of Fluid Mechanics and Hydraulic Machines, Laxmi Publication, pp. 404-407 (2010)
- 2.28. Frank M. White, Fluid Mechanics, WCB McGraw-Hill Publication, New Delhi, p-170-171, (1998)
- 2.29. Frank M. White, Fluid Mechanics, WCB McGraw-Hill Publication, New Delhi, p- 357-360, (1998)
- 2.30. Bruce R. Munson, et. al., Fundamentals of Fluid Mechanics, Wiley, USA, 396-397 (2009)
- 2.31. Çengel Y. A., et. al., Fluid Mechanics, Fundamentals And Applications, , McGraw Hill, p.59 (2014)
- 2.32. Bullard J. W., Capillary rise between planar surfaces, Physical Review E, 79, pp-011604-1 - 011604-8, (2009)
- 2.33. Foundry Technology, Peter Beeley, Butterworth Heinemann, 2nd Edition, p-25-30, (2001)
- 2.34. Kalpakjian S., Schmid S. R., Manufacturing Engineering and technology, Pearson, pp. 266-269 (2001)
- 2.35. Jeyakumar M., et.al., Rheology of liquid metals and alloys, Journal of Non-Newtonian Fluid Mechanics, pp. 831-838 (2011)
- 2.36. Transport Phenomena in Materials Processing, D. R. Poirier, G. H. Geiger, Addison-Wesley, pp-13-22 (1973)
- 2.37. A textbook of Fluid Mechanics and Hydraulic Machines, R.K. Bansal, Laxmi Publication, pp. 265 (2010)
- 2.38. Yang X., Campbell J., Liquid metal flow in a pouring basin, International Journal of Cast Metals Research, 1998 10:5, 239-253 (1998)
- 2.39. Kharrazi Y. H. K., et. al., Mold filling behavior of double gating system in aluminum LFC process, Iranian Journal of Materials Science and Engineering, Vol. 2, No. 1, pp-47-54 (2005)
- 2.40. Raza Mohsin, et.al., Experimental study of the filling of thin-walled investment castings in 17-4PH stainless steel, Metallurgy and Foundry Engineering – Vol. 41, 2015, No. 2, pp. 85–98 (2015) <http://dx.doi.org/10.7494/mafe.2015.41.2.85>
- 2.41. Beeley Peter, Foundry Technology, Butterworth Heinemann, 2nd Edition, p-29 (2001)
- 2.42. Beeley Peter, Foundry Technology, Butterworth Heinemann, 2nd Edition, p-548 (2001)
- 2.43. Beeley Peter, Foundry Technology, Butterworth Heinemann, 2nd Edition, p-25-30 (2001)
- 2.44. Designers' Handbook for Investment Casting. British Investment Casting Trade Ass. Birmingham UK (1990)
- 2.45. Sabau Adrian S., Alloy Shrinkage Factors for the Investment Casting Process, Metallurgical and materials transactions B, Volume 37B, pp131-14 (February 2006)

- 2.46. Cannell Nick, Predicting Pattern Tooling and Casting Dimension for Investment Casting, Phase I, U.S. Department of Energy (DOE) Information Bridge (2008)
- 2.47. Mandal Barnali and Datta Prasanta Kumar, Hot mold casting process of ancient East India and Bangladesh, China Foundry, 7.2 May (2010), 171-177 (May 2010)
- 2.48. B. Mandal, Ph.D. dissertation, Jadavpur University, Kolkata, (2010)
- 2.49. B. K. Das, Ph.D. dissertation, Jadavpur University, Kolkata, (2017)
- 2.50. R. Mandal et al., Distortion Analysis of Thin-Walled Investment Castings, Archives of foundry engineering, Volume 2023, Issue 3/2023, pp-59 – 66, (2023)

Chapter-3

- 3.1. Spurk Joseph H., et. al., Fluid Mechanics, Springer, pp. 168-169 (2008)
- 3.2. Schaschke C, et al., Fluid mechanics: worked examples for engineers. Institution of Chemical Engineers, Rugby, pp-197–198 (2000)
- 3.3. Frank M. White, Fluid Mechanics, WCB McGraw-Hill Publication, New Delhi, (1998)
- 3.4. Çengel Y. A., Cimbala J. M., Fluid Mechanics, Fundamentals and applications, McGraw Hill, (2014)
- 3.5. Stefanescu D. M., Science and Engineering of Casting Solidification, pp. 65-67. Springer Science, New York, (2002)
- 3.6. Elliott R., Cast iron technology. Elsevier, Amsterdam, pp170–175 (1998)
- 3.7. Sylvia J. G., Cast metal Technology, Addison, p-194 (1972)
- 3.8. Flinn R. A., Fundamental of Metal Casting, , Addison-Wesley Pub. Co. inc., P-66-77 (1963)
- 3.9. Kalpakjian S., Schmid S. R., Manufacturing Engineering and technology, Pearson, pp. 266-269 (2001)
- 3.10. Rao P. N., Manufacturing Technology—Foundry, Forming and Welding, (Volume 1), 5th edition, McGraw Hill Education (India) Private Limited, pp-4.13-1.15, (2019)
- 3.11. Das B. K., Ph.D. dissertation, Jadavpur University, Kolkata, p-88 (2017)
- 3.12. Jeyakumar M., et.al., Rheology of liquid metals and alloys, Journal of Non-Newtonian Fluid Mechanics, pp. 831-838 (2011)
- 3.13. Poirier D. R., Geiger G. H., Transport Phenomena in Materials Processing, Addison-Wesley, pp-13-22 (1973)
- 3.14. Roy S., Maity U. K., Pramanick A. K., Datta P. K., Kinetics of liquid metal flow in gating design of investment casting production, Slevarenstvi 5–6:149–154 (2017)
- 3.15. White Frank M., Fluid Mechanics, WCB McGraw-Hill Publication, New Delhi, p-357–360 (1998).
- 3.16. Stefanescu D. M., Science and Engineering of Casting Solidification, pp. 65-67. Springer Science, New York, (2002)
- 3.17. Roy S., Pramanick A. K., Datta P. K., Precise Filling Time Calculation of Thin-Walled Investment Casting in Hot Mold, Journal of the Brazilian Society of Mechanical Science and Engineering , Springer Nature Publication, Vol.-42, issue 10, (2020),
Doi.org/10.1007/s40430-020-02634-6
- 3.18. Roy S., Das B. K., Pramanick A. K., Datta P. K., The Technology Inherent in Indian Traditional Craft Metal Casting Process, Indian Foundry Journal, Vol.- 65 Issue-8, (2019)
- 3.19. Cengel Y.A, Boles M.A., Thermodynamics: An Engineering Approach McGraw-Hill, 5th edition. P-137 (2006)

- 3.20. Cengel, Y.A, Boles, M.A. Thermodynamics: An Engineering Approach McGraw-Hill, 5th edition. P-22 (2006)

Chapter-4

- 4.1. Horáček M., Accuracy of Dimensional Analysis, Archives of Foundry, Volume 5, No. 15, pp-121-137 (2005)
- 4.2. Roy S., Pramanick A. K., Datta P. K., Precise Filling Time Calculation of Thin-Walled Investment Casting in Hot Mold, Journal of the Brazilian Society of Mechanical Science and Engineering, Springer Nature Publication, Vol.-42, issue 10, (2020) Doi.org/10.1007/s40430-020-02634-6
- 4.3. Das B. K., Ph.D. dissertation, Jadavpur University, Kolkata, (2017)
- 4.4. Rao P. N., Manufacturing Technology—Foundry, Forming and Welding, (Volume 1), 5th edition, McGraw Hill Education (India) Private Limited, p-4.24, (2019).
- 4.5. Prasad K.D.V et al., Statistical analysis on accuracy of wax patterns used in investment casting process, Journal of Materials Processing Technology, 138, pp-75–81 (2003)
- 4.6. Roy S., Pramanick A. K., Datta P. K., Characteristics of Dimensional Variation and Shrinkage Analysis of Wax- Based Thin Walled Investment Casting in Hot Clay Mold for Batch Production, International Journal of Computational Engineering Research (IJCER), Volume, 09, Issue, 3, pp.-43-52 (March 2019)
- 4.7. “Root-mean-square value” A Dictionary of Physics (6 ed.), Oxford University Press., ISBN 9780199233991 (2009)
- 4.8. Pontius, Robert; et al., of information for multiple resolution comparison between maps that share a real variable (PDF). Environmental Ecological Statistics. 15 (2): 111–142 (2008) doi:10.1007/s10651-007-0043-y
- 4.9. Thomas George B.; et al., Calculus and Analytic Geometry (5th ed.), Addison-Wesley, p. 434, (1979).
- 4.10. G. R. Prasad, Statistical Quality control and Operational Research, Indian Statistical Institute, Calcutta, pp 107-165 (1982)
- 4.11. Mardani Abbas, et al., Multiple criteria decision-making techniques and their applications – a review of the literature from 2000 to 2014, Economic Research-Ekonomska Istraživanja, Vol. 28, No. 1, pp 516–571 (2015)
- 4.12. Vimal Jyoti, et al., Application Of Topsis Method For Supplier Selection In Manufacturing Industry, IJREAS Volume 2, Issue 5, pp- 25-35 (May 2012)
- 4.13. Pavić Zlatko, et al., Notes on TOPSIS Method, International Journal of Research in Engineering and Science, Volume 1, Issue 2, pp-.05-12 (June. 2013)
- 4.14. Raju K. Srinavasa, et al., Multicriterion analysis in Engineering and management; PHI Learning Pvt. Ltd., New Delhi pp- 80-81 (2010)
- 4.15. Metrology & Measurement, A. K. Bewoor, V. A. Kullarni, Tata McGraw-Hill, pp-46-102 (2009)
- 4.16. Raju K. Srinavasa, et al., Multicriterion analysis in Engineering and management; PHI Learning Pvt. Ltd., New Delhi pp- 266-296 (2010)
- 4.17. Rollason E.C., “Metallurgy for Engineers”, ELBS, UK, p. 310 (1977)
- 4.18. Mandal B., et.al., Understanding Alloy Design Principles And Cast Metal Technology In Hot Molds For Medieval Bengal, Indian Journal of History of Science, 45.1, 101-140 (2010)

- 4.19. G. L. Kehl, "Principles of Metallographic Practice", Eurasia Pub. House, New Delhi, p. 264 (1965)
- 4.20. Bramfitt B. L., et al., Metallographer's Guide: Practice and Procedures for Irons and Steels, ASM International, p-132 (2002)
- 4.21. P. M. Kelley, The Structure and Hardness of Martensite, in Electron Microscopy and Strength of Crystals. (Ed.s) Thomas, G and J. Washburn, New York: Interscience Publishers, pp. 917-33 (1963).
- 4.22. William F. Smith, "Foundation of Material Science and Engineering", McGraw – Hill Int. Edt., 2nd Edition, p-392 (1993).
- 4.23. Mechanical Metallurgy, S. E. Dieter, McGraw-Hill, pp-331-332 (1988),
- 4.24. Cast metal Technology, J. G. Sylvia, Addison, pp- 79-81 (1972)
- 4.25. Fundamental of Metal Casting, R. A. Flinn, Addison-Wesley Pub. Co. inc., P-162 (1963)
- 4.26. Brandes EA, Brook GB (1993) Smithells metals reference book, Butterworth-Heinemann, Oxford, pp 14.14–14.16 (1998)
- 4.27. ASM handbook, volume-15: casting. ASM International, p 1691 (1998)
- 4.28. Valencia J. J., Quested P. N., Thermophysical properties, ASM handbook, volume 15: casting, pp 468–481 (2013)
- 4.29. Dan W., The wetting behavior of Fe–Si And Fe–Mn alloy with Al–10%Si coating. In: TMS 2016, Supplemental Proceedings: 145th Annual Meeting and Exhibition, The Minerals, Metals & Materials Society (TMS), pp 779–786 (2016)
- 4.30. Tan M., et al., Correlation between viscosity of molten Cu–Sn alloys and phase diagram. Physica B 387, pp-1–5 (2007)
- 4.31. Lee J et al., Surface tension and its temperature coefficient of liquid Sn-X (X = Ag, Cu) alloys. Mater Trans (The Japan Institute of Metals) 45(9), pp-2864–2870 (2004)
- 4.32. Eustathopoulos N., Wettability at high temperature. Pergamon, Oxford, p 206 (1999)
- 4.33. Gale W. F., Totemeier T. C., Smithells metals reference book, 8 edn, vol 14. Butterworth-Heinemann an imprint of Elsevier, pp 14–17 (2004)
- 4.34. Ruud C. O., et al., Copper and copper alloy viscosity. Met Trans 7B, pp-497–498 (1976)
- 4.35. Wang M., et al., Surface free energy of copper-zinc alloy for energy-saving of boiler. Rare Met 25:324 (2006)
- 4.36. Eustathopoulos N., Wetting by liquid metals-application in materials processing: the contribution of the Grenoble group. Metals 5, pp-350–370 (2015)
- 4.37. Gupta S. V., Practical density measurement and hydrometry. IoP, p 123 (2002)
- 4.38. Assael M. J., et al., Reference data for the density and viscosity of liquid cadmium.... mercury. J Phys Chem Ref Data 41(3):033101-1–033101-16 (2012)
- 4.39. Nakayama Y., Introduction to fluid mechanics. Butterworth, Oxford, p 13 (1999)
- 4.40. Frank M. White, Fluid Mechanics, WCB McGraw-Hill Publication, New Delhi, p 17 (1998)

Chapter-5

- 5.1. Roy S., Pramanick A. K, Datta P. K., Precise Filling Time Calculation of Thin-Walled Investment Casting in Hot Mold, Journal of the Brazilian Society of Mechanical Science and Engineering , Springer Nature Publication, Vol.-42, issue 10, (2020),
Doi.org/10.1007/s40430-020-02634-6
- 5.2. Frank M. White, Fluid Mechanics, WCB McGraw-Hill Publication, New Delhi, p 59-72, (1998)

- 5.3. Roy S., Pramanick A. K, Datta P. K., The Technology Inherent in Indian Traditional Craft Metal Casting Process, Indian Foundry Journal, Vol.- 65 Issue-8, (2019)
- 5.4. İlter Yasin Kaan, et. al., Large eddy simulations of the turbulent channel flow over dimpled surfaces, Journal of Turbulence, 24:3-4, 2186415, (2023) DOI: 10.1080/14685248.2023.2186415
- 5.5. Jyh-tong, et al., Fluid Dynamics in Microchannels, Fluid dynamics, computational modeling and applications, Publisher:In Tech, Croatia (2012)
- 5.6. The Engineering Tool Box (2003). Air - Density, Specific Weight and Thermal Expansion Coefficient vs. Temperature and Pressure. [online] Available at: https://www.engineeringtoolbox.com/air-density-specific-weight-d_600.html [Accessed date: 14th January 2024]

Chapter-6

- 6.1. ISO 1: 2022: Geometrical product specifications (GPS)—standard reference temperature for the specification of geometrical and dimensional properties. <https://www.iso.org/standard/80702.html>
- 6.2. Horáček M., Accuracy of Dimensional Analysis, Archives of Foundry, Vol.-5, No. 15, pp-121-137 (2005)
- 6.3. Roy S., Pramanick A. K, Datta P. K., The Effect of Gating System on Quality of Traditional Rural Metal Castings of India, Recent Trends in Industrial and Production Engineering, Lecture Notes in Mechanical Engineering, Book Series, Springer Publication, p-267-278 (July, 2021) Doi.org/10.1007/978-981-16-3135-1_27, Vol.- 1080, 2021
- 6.4. Austral Wright Metals-Ferrous, Non-Ferrous and High Performance Alloys (2008, August). Metal alloys-properties and applications of brass and brass alloys. Retrieved May, 30 2022
- 6.5. Extra High Leaded Brass UNS C35600. Retrieved May, 30 2022 <https://www.azom.com/article.aspx?ArticleID=6389>
- 6.6. Indian Minerals Yearbook 2015 (Part- III : Mineral Reviews), (2017, February) Retrieved May 28, 2022, from https://ibm.gov.in/writereaddata/files/02282017165033IMYB2015_Kaolin_28022015_Adv.pdf
- 6.7. Thampi, C.J., Soils Of Bankura District (West Bengal) For Land Use Planning. National Bureau of Soil Survey & Land Use Planning, India (2013)
- 6.8. RSP Green Development and Laboratories PVT. LTD, District Survey Report of Bankura District. India (July 2018)
- 6.9. Chakraborty A. K., Phase transformation of Kaolinite clay, (1st ed.), Springer (2014) DOI 10.1007/978-81-322-1154-9.
- 6.10. Hyslop A. M., The thermal expansion of some clay mineral. Transactions and journal of the British Ceramic Society, 37, pp-180-186 (1938).
- 6.11. Heindl, R.A., Meng, L.E., Length changes and endothermic and exothermic effects during heating of flint and aluminous clays. Journal of Research of the National Bureau of Standards. 23(9), 427-441 (1939)
- 6.12. Thiel. J., Thermal expansion of chemically bonded silica sands. AFS Transactions - American Foundry Society, 11-116, pp-1-10 (2011).

- 6.13.** Roy S., Pramanick A. K, Datta P. K., Negative Shrinkage of Thin-walled Investment Brass Castings, Archives of foundry engineering, Volume-2023, issue1/2023,- pp-17-24, (2023)
DOI:10.24425/afe.2023.144275
- 6.14.** Anggono, J., Mullite ceramics: its properties, structure, and synthesis. Jurnal Teknik Mesin. 7(1), pp.-1-10, (2005)..
- 6.15.** Cannell, N., Sabau, A.S. (2007). Predicting pattern tooling and casting, dimensions for investment casting, phase III. Final Technical Report, Oak Ridge National Laboratory, Oak Ridge, Tennessee.
- 6.16.** Standard Test Methods for Determining Average Grain Size [ASTM E112-13(2021)], (2021)
DOI:10.1520/E0112-13R21, <https://www.astm.org/e0112-13r21.html>

Chapter-7

- 7.1.** Roy S., Pramanick A. K, Datta P. K., Precise Filling Time Calculation of Thin-Walled Investment Casting in Hot Mold, Journal of the Brazilian Society of Mechanical Science and Engineering , Springer Nature Publication, Vol.-42, issue 10, (2020),
Doi.org/10.1007/s40430-020-02634-6
- 7.2.** Beeley Peter, Foundry Technology, Butterworth Heinemann, 2nd Edition, p-76 (2001)
- 7.3.** Roy S., Pramanick A. K, Datta P. K., Comparative Study of Dimensional Variation and Surface Characteristics of Thin Walled Investment Casting of Different Geometrical Shape for Different Gating System in Hot Clay Mold, IOSR Journal of Engineering, Vol. 09, Issue 3 17-23 (2019)
- 7.4.** Roy S., Pramanick A. K, Datta P. K., Characteristics of Dimensional Variation and Shrinkage Analysis of Wax- Based Thin Walled Investment Casting in Hot Clay Mold for Batch Production, International Journal of Computational Engineering Research (IJCER), Volume, 09, Issue, 3, pp-43-52. (2019)
- 7.5.** Roy S., Pramanick A. K, Datta P. K., Quality Analysis of Tribal Casting Products by TOPSIS for Different Gating System, IOP Conference Series: Materials Science and Engineering,, vol-1080, p.-1-5, IOP Publishing Ltd. (2021) doi:10.1088/1757-899X/1080/1/012014
- 7.6.** Mandal B., et.al., Understanding Alloy Design Principles And Cast Metal Technology In Hot Molds For Medieval Bengal, Indian Journal of History of Science, 45.1 pp.-101-140 (2010)
- 7.7.** Khel G. L., The Principles of Metallographic Laboratory Practice, Eurasia Publishing (Pvt.) Ltd., 3rd Ed., 1965.

List of symbols

Symbol	Meaning	Unit	Symbol	Meaning	Unit
A_g	Gate Area	m ²	v	Velocity	m/s
A_f	Flow Area of Liquid inside mold	m ²	V_{avg}	Average Velocity of fluid	m/s
A_m	Average Cross-sectional Area of Mold	m ²	v_g	Velocity of fluid at Gate	m/s
b	Breadth	m	V	Volume	m ³
C_D	Co-efficient of discharge		W	Mold width or Thickness	m
d	Diameter	m	Z_f	Friction head	m
d_h	Hydraulic diameter	m	z_m	Mold Height	m
d_g	Gate diameter	m	z_s	Sprue Height	m
f	Friction Factor		z_t	Total Height ($z_m + z_s$)	m
g	Gravitational acceleration	m/s ²	α	Energy correction Factor	
KE	Kinetic Energy		γ	Surface tension	N/m
L_m	Flow length of Liquid Inside Mold	m	γ_{LS}	Surface tension between liquid and solid phase	N/m
m	Mass	kg	ρ	Density	kg/ m ³
P	Pressure	N/ m ²	μ	Viscosity	mPa.s
ΔP_γ	Pressure drop due capillary action	N/ m ²	θ	Wetting angle	radian
Q	flow rate	m ³ /s	ξ	Wetted perimeter	m/s
R_C	Characteristics gas constant	kJ. kg ⁻¹ K ⁻¹	ϵ	Wall-roughness height	m
r_h	Hydraulic radius	m	τ	Shear stress	N/ m ²
t_{act}	Actual Filling Time	sec	μ	Viscosity	mPa.s
t_{conv}	Conventional Filling Time	sec	θ	Wetting angle	radian
t_f	Calculated Time of Filling	sec	ξ	Wetted perimeter	m/s
T	Temperature	°C and K	ϵ	Wall-roughness height	m
u	Velocity	m/s	τ	Shear stress	N/ m ²

Appendix

Appendix I.

Investigation details by researcher on Investment casting

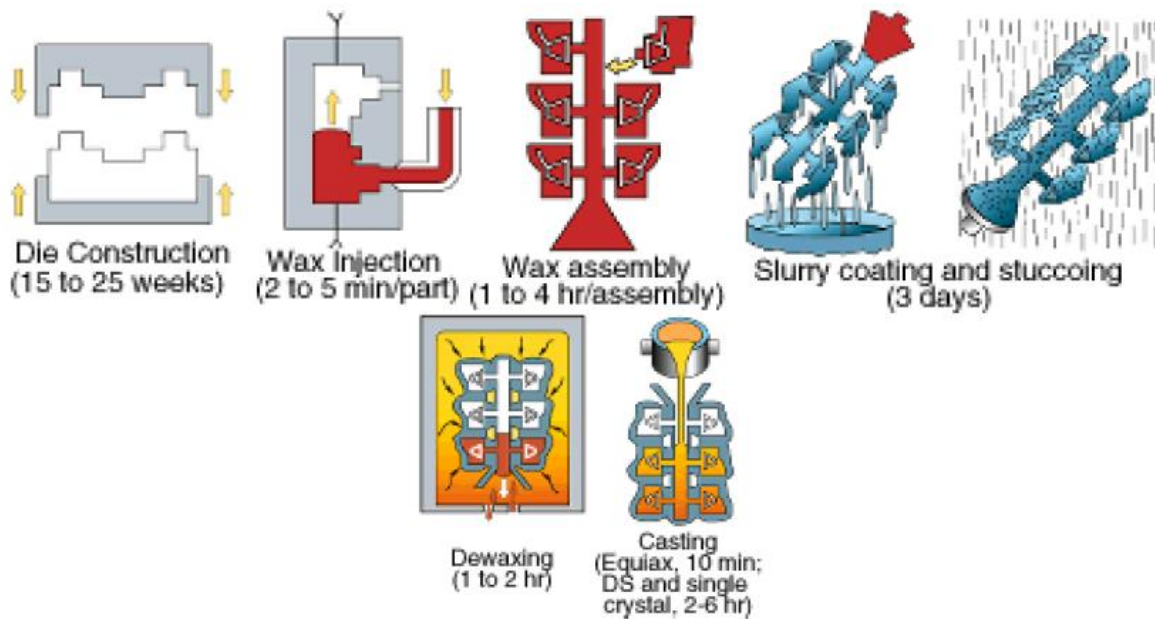


Figure: Sketches of the investment casting process [Nick Cannell, Adrian S. Sabau, 2007] [2.15]

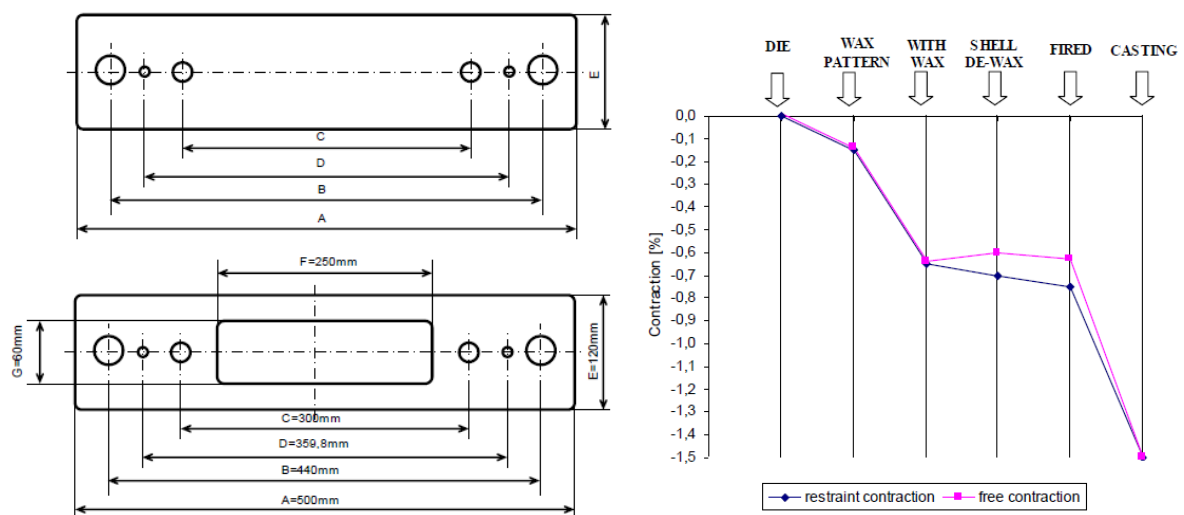


Figure: Dimensions of "Test Plate" casting – "free" and "restrained" type (Right), Changes of "D" dimension of "test plate" part during the process (Left) [M. Horáček] [2.13]

Appendix II.

Fluid flow patterns through the mold: Water Simulation

➤ Flow Pattern of Water for 0.7 mm thin Rectangular Plate



$t = 0.1s$

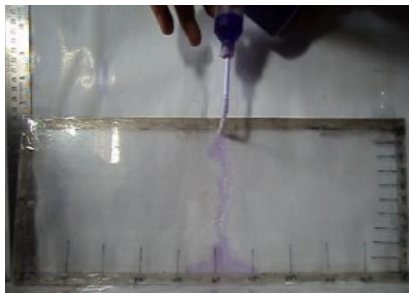


$t = 5s$



$t = 15s$

Fig.: Flow Pattern of Water for 0.7 mm thin Rectangular Plate in Vertical Position



$t = 0.5s$



$t = 5s$



$t = 15s$

Fig.: Flow Pattern of Water for 0.7 mm thin Rectangular Plate in Horizontal Position



$t = 1s$



$t = 5s$



$t = 20s$

Fig.: Flow Pattern of Water for 0.7 mm thin Rectangular Plate in Flat Position

➤ **Flow Pattern of Water for 1.8 mm thin Rectangular Plate**

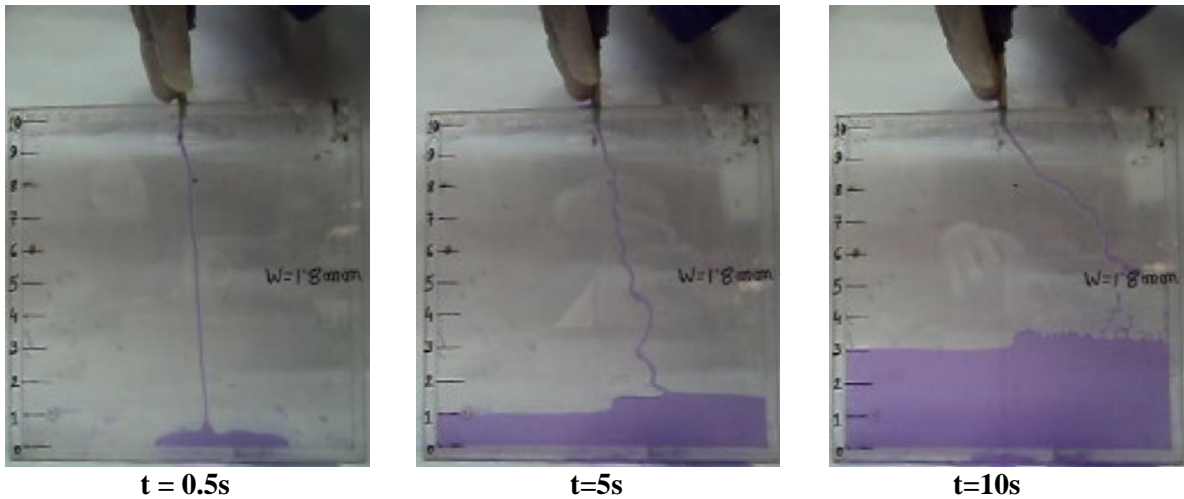


Fig.: Flow Pattern of Water for 1.8 mm thin Rectangular Plate in Vertical Position

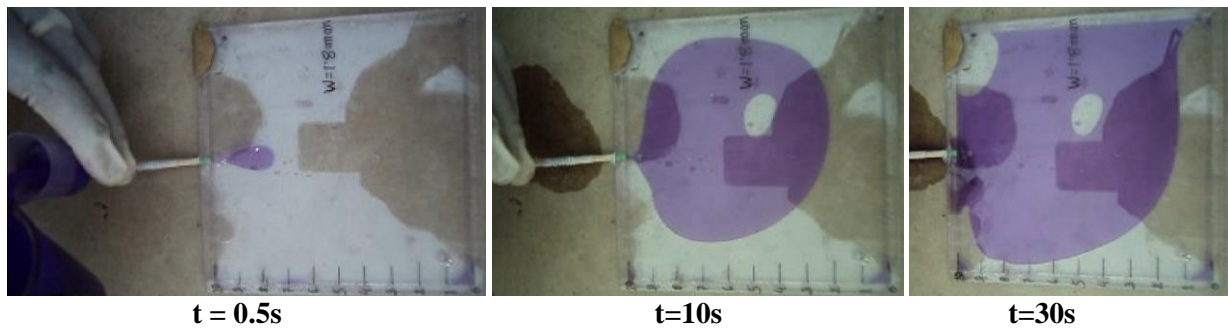


Fig.: Flow Pattern of Water for 1.8 mm thin Rectangular Plate in Flat Position

➤ **Flow Pattern of Water for 3.6 mm thin Rectangular Plate**

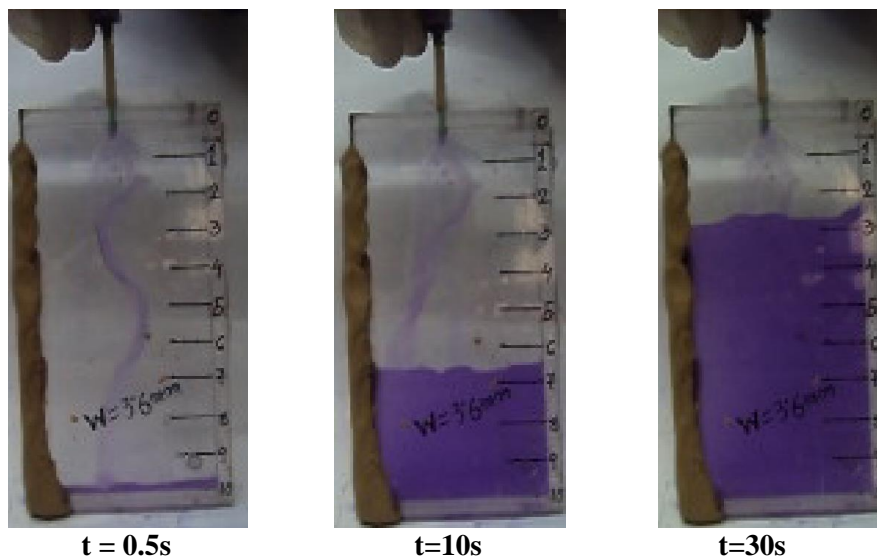


Figure: Flow Pattern of Water for 3.6 mm thin Rectangular Plate in Vertical Position

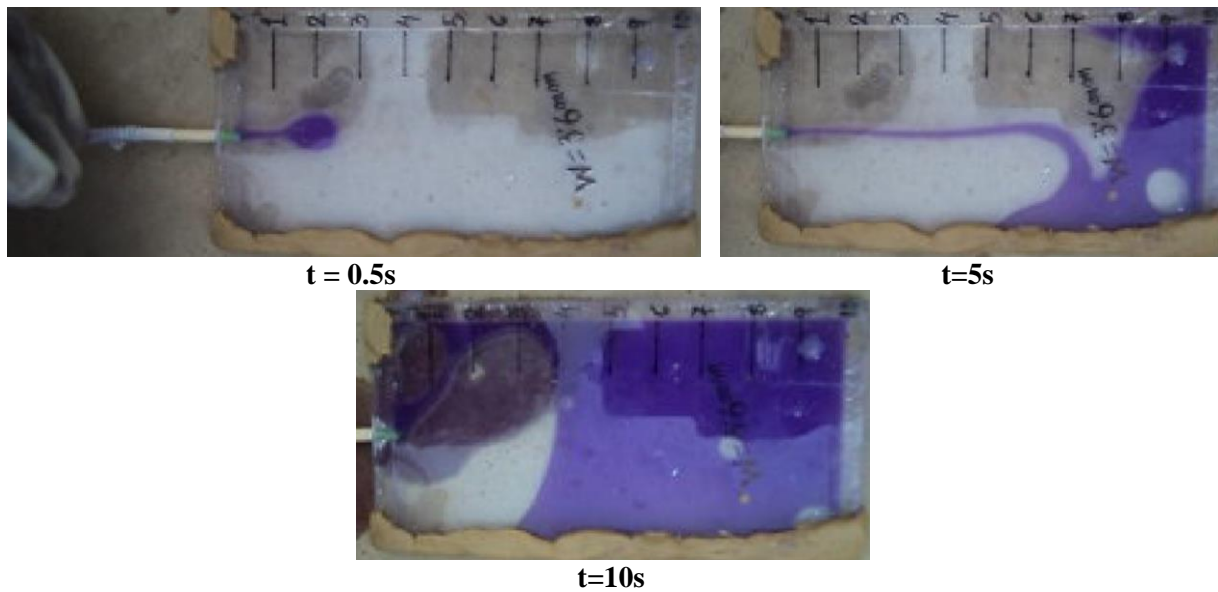


Figure: Flow Pattern of Water for 3.6 mm thin Rectangular Plate in Flat Position

Appendix III.

Fluid flow patterns through the mold: Mercury Simulation

➤ Flow Pattern of Liquid Mercury for 0.7 mm thin Rectangular Plate

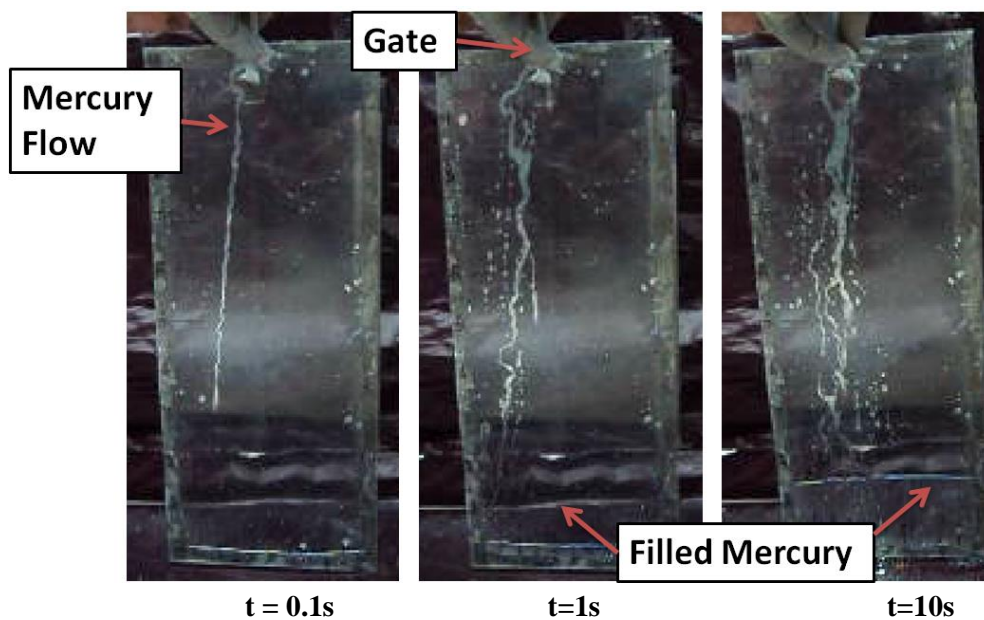


Figure: Flow Pattern of Liquid Mercury for 0.7 mm thin Plate in Vertical Position

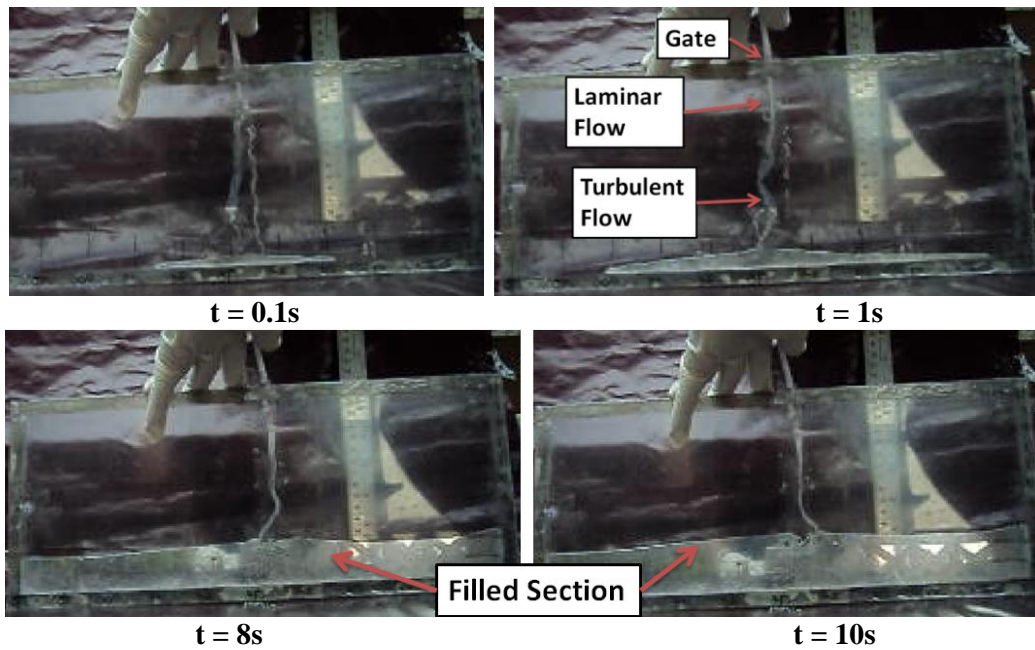


Figure: Flow Pattern of Liquid Mercury for 0.7 mm thin Plate Mold in Horizontal Position

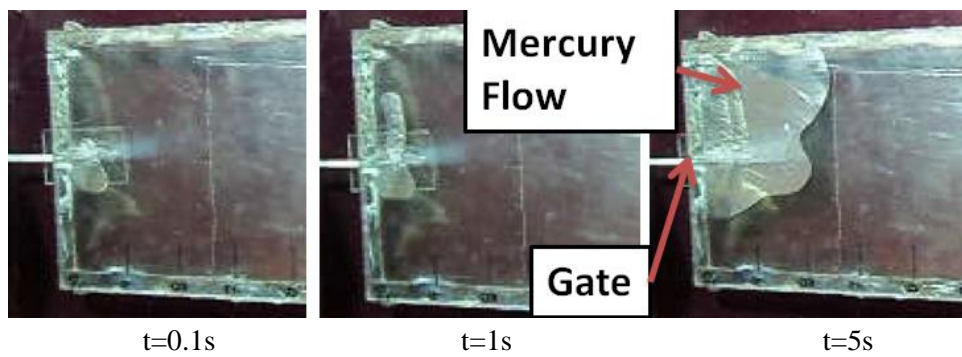


Figure: Flow Pattern of Liquid Mercury for 0.7 mm thin Rectangular Plate Mold in Flat Position

➤ **Flow Pattern of Liquid Mercury for 1.8 mm thin Rectangular Plate**

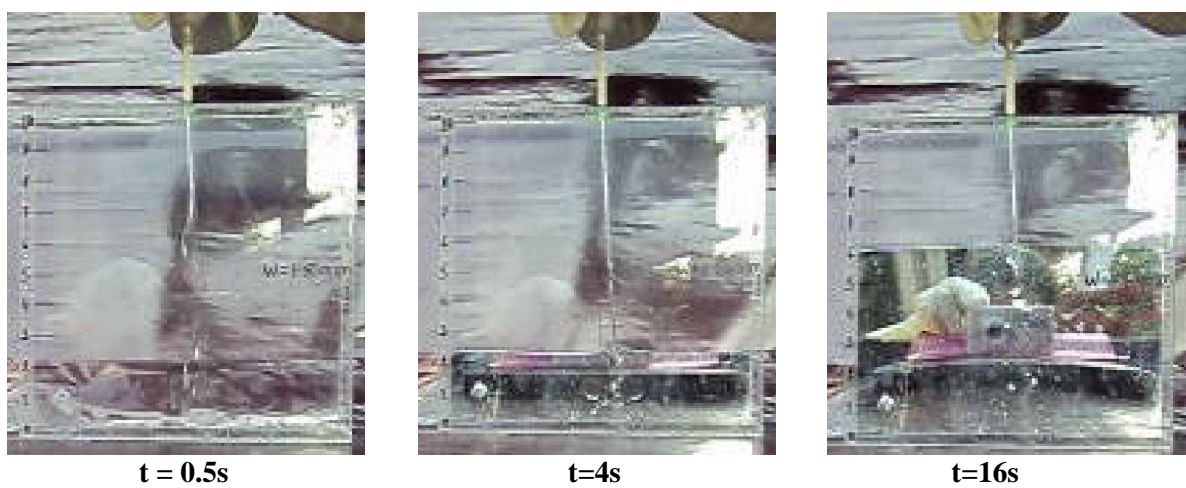
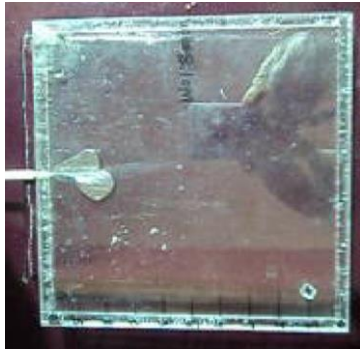
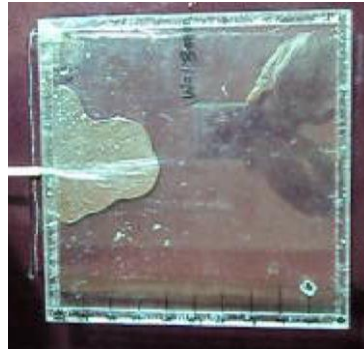


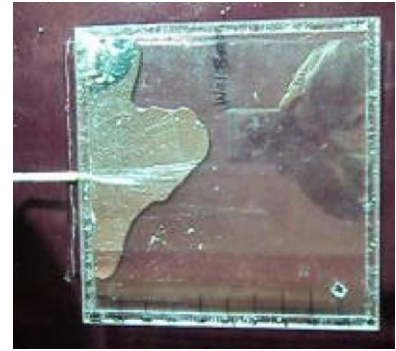
Figure: Flow Pattern of Liquid Mercury for 1.8 mm thin Plate in Vertical Position



$t = 0.2 \text{ s}$



$t = 1 \text{ s}$



$t = 5 \text{ s}$

Figure: Flow Pattern of Liquid Mercury for 1.8 mm thin Plate in Flat Position

➤ **Flow Pattern of Liquid Mercury for 3.6 mm thin Rectangular Plate**



$t = 0.2 \text{ s}$



$t = 1 \text{ s}$

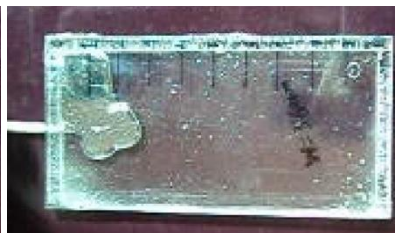


$t = 4 \text{ s}$

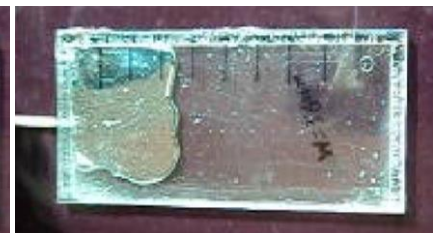
Figure: Flow Pattern of Liquid Mercury for 3.6 mm thin Rectangular Plate in Vertical Position



$t = 0.2 \text{ s}$



$t = 1 \text{ s}$



$t = 5 \text{ s}$

Figure: Flow Pattern of Liquid Mercury of 3.6 mm thin Rectangular Plate in Flat Position

Appendix IV.

Calculation of Simulation experiment using Mercury for 0.7mm Thick plate at vertical position ($z_m=140\text{mm}$)

Volume of the mold, $\times 10^6, \text{ m}^3 = 35.3;$

Width of the mold, $w \times 10, \text{ m} = 0.7 \text{ mm},$ **Mold Height,** $z_m=140\text{mm}$

$z_s=(\text{Sprue} + \text{cup Height}) = (0.04+0.03) \text{ m}, C_D=0.8$

Velocity entered into the cavity (at gate):

$$v_g = C_D \sqrt{gz_s} = 0.8 \sqrt{9.81 \times (0.04 + 0.03)} = 0.938 \text{ m/s}$$

Effect of resistance due to surface tension:

$$\gamma = 486 \text{ mN/m}, \theta = 140^\circ, w = 0.7 \text{ mm}$$

$$\Delta P_\gamma = -\frac{2\gamma}{w} \cos \theta = -\frac{2 \times 486 \times 10^{-3}}{0.0007} \cos(140) = 1063.7 \text{ N/m}^2$$

Gas Pressure: $\Delta P_{\text{gas}}=0$

Calculation of Constants:

$$L_m=140\text{mm}, \mu=0.016 \text{ poise}, \rho=13510\text{kg.m}^3, d_H=2w=0.0014\text{m},$$

$$b = \frac{24\mu L_m}{\rho d_H^2} = 0.2 \text{ k} = \frac{1}{g} [b^2 + gz_m + v_g^2 - \frac{\Delta P_\gamma}{\rho_{\text{liq}}}] = 0.23$$

Flow area:

$$A_f = d_g \times w \Rightarrow 0.0007 \times 0.00135 = 0.945 \times 10^{-6} \text{ m}^2$$

Average Mold Area:

$$A_m = \frac{\text{Casting Volume}(V)}{\text{Mold Height}(Z_m)} = \frac{35.3 \times 10^{-6}}{140 \times 10^{-3}} = 0.25 \times 10^{-3} \text{ m}^2$$

Filling Time:

$$t_f = \frac{A_m}{A_f} \left[\frac{2}{\sqrt{g}} (\sqrt{k} - \sqrt{k - Z_m}) + \frac{2b}{g} \ln \left(\frac{\sqrt{k} - \frac{b}{\sqrt{g}}}{\sqrt{k - Z_m} - \frac{b}{\sqrt{g}}} \right) \right] = 36.32 \text{ s}$$

Actual Filling Time= 38.2s

Error Calculation:

$$\text{Error} = \left(\frac{t_{\text{actual}} - t_{\text{calculated}}}{t_{\text{actual}}} \right) \times 100\% = \left(\frac{38.2 - 36.32}{38.2} \right) \times 100\% = 5.18\%$$

Appendix V.

Calculated Data Chart for Simulation Experiments and Actual Metal casting

➤ Data Chart for Physical Parameters of Mold

Mold	Position	$V_{\text{mold}} \times 10^6 \text{ m}^3$	$Z_m, \times 10^3 \text{ m}$	$w \times 10^3 \text{ m}$	$A_m \times 10^6 \text{ m}^2$	$L_m \times 10^3 \text{ m}$	$d_H \times 10^3 \text{ m}$	$A_f \times 10^6 \text{ m}^2$
Plate/0.7	Upright	35.3	360	0.7	98	360	1.4	0.945
Plate/0.7	Vertical	35.3	140	0.7	252	140	1.4	0.945
Plate/0.7	Flat	35.3	0.7	0.7	50400	0.7	1.4	0.945
Plate/1.8	Vertical	35.3	140	1.8	252	140	3.6	1.43
Plate/1.8	Flat	35.3	0.7	1.8	19600	0.7	3.6	1.43
Plate/3.6	Vertical	35.3	140	3.6	252	140	7.2	1.43
Plate/3.6	Flat	35.3	0.7	3.6	9800	0.7	7.2	1.43

➤ Data Chart for Water and Mercury Simulation

Mold	Position	Water			Mercury		
		$\Delta P\gamma \text{ N/m}^2$	b	k	$\Delta P\gamma \text{ N/m}^2$	b	k
Plate/0.7	Vertical	205.714	39.23	0.0559	1060.6	0.52	0.476
Plate/0.7	Horizontal	205.714	15.26	0.073	1060.6	0.202	0.233
Plate/0.7	Flat	205.714	39.23	0.011	1060.6	0.001	0.089
Plate/1.8	Vertical	80	2.31	0.4437	412.46	0.03	0.2294
Plate/1.8	Flat	80	2.31	0.1851	412.46	0.00	0.0911
Plate/3.6	Vertical	40	0.58	1.0297	206.23	0.01	0.2294
Plate/3.6	Flat	40	0.58	0.538	206.23	0.00	0.093

➤ Data Chart for Metal Castings

Mold	Type	$V_{\text{mold}} \times 10^6 \text{ m}^3$	$Z_m, \times 10^3 \text{ m}$	$w, \times 10^3 \text{ m}$	$A_m, \times 10^6 \text{ m}^2$	$L_m, \times 10^3 \text{ m}$	$d_H, \times 10^3 \text{ m}$	$A_f, \times 10^6 \text{ m}^2$	$\Delta P\gamma \text{ N/m}^2$	b	k
Mann	Al	86.3	104	2	830	118	4	1.35	344	0.086	0.188
	Gun Metal	86.3	104	2	830	118	4	1.35	788	0.085	0.185
	Brass	86.3	104	2	830	118	4	1.35	1434	0.084	0.186
Ganesha	Top Gating	354	278	2	1273	290	4	8	1434	0.207	0.37
	Side Gating	354	1200	2	2950	210	4	8	1434	0.15	0.21

Appendix VI.

Mercury Simulation experiments using in Annular Cylindrical glass mold with two different position

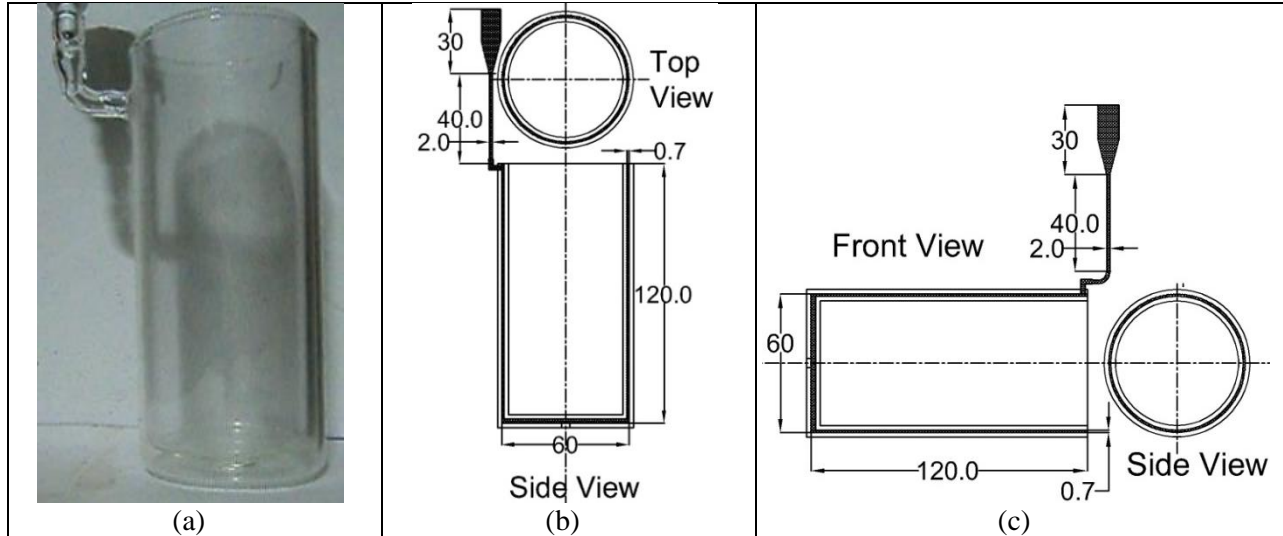


Figure: Schematic diagram of Annular Cylindrical mold (M-4) at (a) vertical and (b) Horizontal position with (c) Pictorial view (All dimensions are in mm)

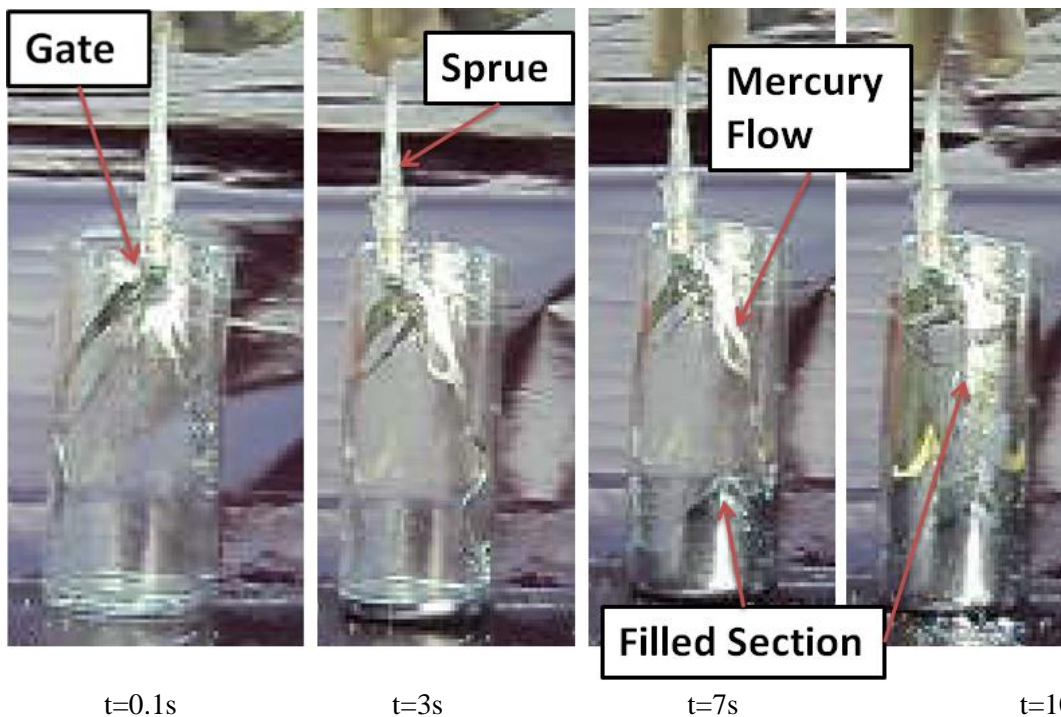


Figure: Flow Pattern of Liquid Mercury of annular cylindrical Glass mold in Vertical Position

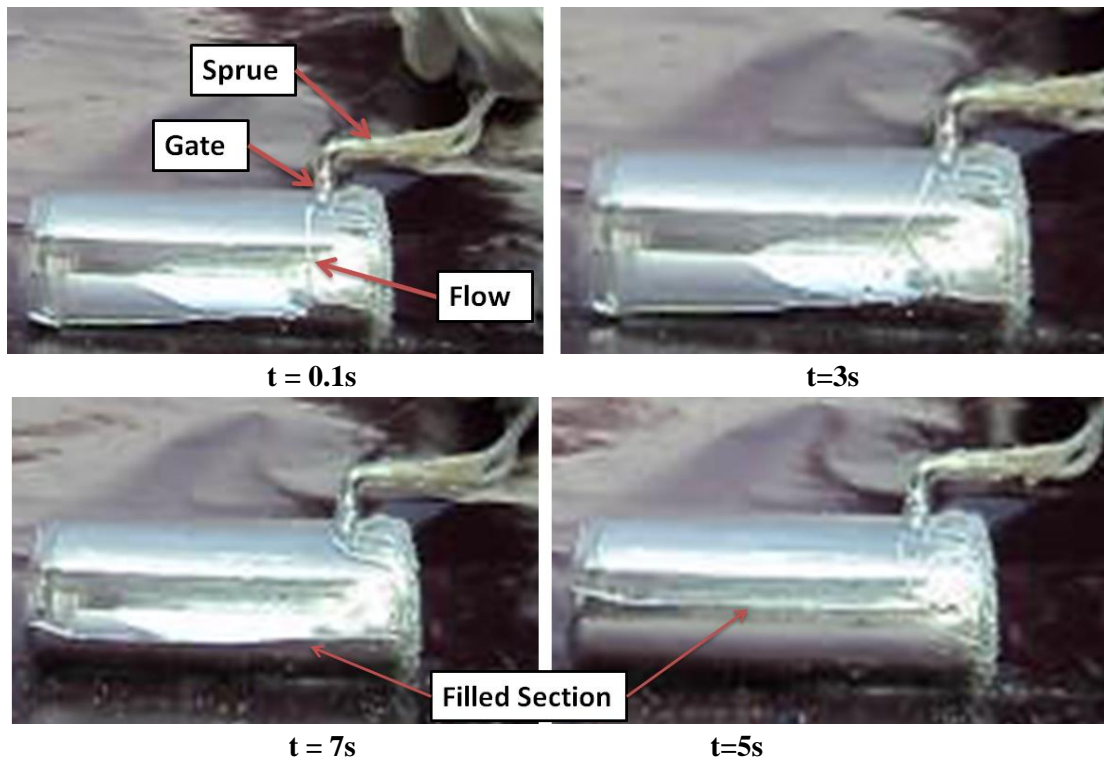


Figure: Flow Pattern of Liquid Mercury through annular cylindrical Glass mold in Horizontal Position

Filling Time and Error (%)

Position	Actual Filling Time t_{Act} , s	Proposed Model		Conventional Filling Time (t_{conv}), sec	
		t_f , sec	Error (%)	t_{conv} , s	Error (%)
Vertical	10	9.09	10.07	6.79	32.06
Horizontal	12	9.92	20.96	6.79	43.38

Appendix VII.

Comparison of Calculated and Actual Filling Time and Gating Design of Few other thin-walled investment castings in hot clay mold

Many other thin walled investment castings in hot clay mold were done to validate the analytical model further. Actual Filling Time of the castings were compared to the proposed mold filling time. Gating Design of the castings was also done and Validated.

➤ Comparison of Calculated and Actual Filling Time and Gating Design of Brass Icon- Peacock



Wax Pattern

Cast model with Gating



Figure: Finished Model

Physical Parameters of the casting

Weight of Casting	Vol. of Casting	Outside Area of Cast	Inside area of cast	Heat dissipat- ing Area	Height	Path length of Flow	Width
$W_{Casting}, kg$	$V_{Casting}, \times 10^6, m^3$	$A_{outside} \times 10^3, m^2$	$A_{inside} \times 10^3, m^2$	$A_{Total} \times 10^3, m^2$	$z_m \times 10^3, m$	$L_m, \times 10^3, m$	$W_{Effective}, \times 10^3, m$
201	23.9	26.3	2.3	28.6	168	175	1

Gating Details

Number of Sprue	Gate Diameter,	Sprue Height	Cup diameter.	Cup Height	Gating Vol.	Gating Surface Area
n	$d_g, \times 10^3, m$	$z_s, \times 10^3, m$	$d_c, \times 10^3, m$	$z_c, \times 10^3, m$	$V_{Gating}, \times 10^6, m^3$	$A_{Gating}, \times 10^3, m^2$
1	4.0	30	6	25	4.83	2.0

Calculated Filling Time

Gate Vel.	Avg. Cross- sectional Mold Area	Flow Area	Calculated Filling Time	Actual Filling Time	Error	Re. no,
v_g, ms^{-1}	$A_m, \times 10^3, m^2$	$A_f \times 10^6, m^2$	t_f, sec	t_{actual}, sec	%	
0.831	0.142	4.0	7.9	7.6	-3.97	1745

Calculated Riser Parameter

Calculated Cup Diameter	Calculated Riser Diameter	Hot metal required	Yield	$\left(\frac{V}{A}\right)_{Casting}$	$\left(\frac{V}{A}\right)_{Gating}$
$d_c, \times 10^3, m$	$d_R, \times 10^3, m$	W_l, kg	(%)		
4.9	3.68	0.290	69.3	0.84×10^{-3}	2.41×10^{-3}

➤ Comparison of Calculated and Actual Filling Time and Gating Design of Brass Icon- Ganesha



Wax Pattern



Cast model with Gating



Figure: Finished Model

Physical Parameters of the casting

Weight of Casting	Vol. of Casting	Outside Area of Cast	Inside area of cast	Total Heat dissipating Area	Height	Path length of Flow	Effective Width
$W_{Casting}, kg$	$V_{Casting}, \times 10^6, m^3$	$A_{outside}, \times 10^3, m^2$	$A_{inside}, \times 10^3, m^2$	$A_{Total}, \times 10^3, m^2$	$z_m \times 10^3, m$	$L_m, \times 10^3, m$	$w, \times 10^3, m$
449	53.48	32.35	14.75	47.1	135	155	1.5

Gating Details

Number of Sprue	Gate Diameter,	Sprue Height	Cup diameter.	Cup Height	Gating Vol.	Gating Surface Area
n	$d_g, \times 10^3, m$	$z_s, \times 10^3, m$	$d_c, \times 10^3, m$	$z_c, \times 10^3, m$	$V_{Gating}, \times 10^6, m^3$	$A_{Gating}, \times 10^3, m^2$
1	4.5	40	6	25	5.38	2.38

Calculated Filling Time

Gate Vel.	Avg. Cross-sectional Mold Area	Flow Area	Calculated Filling Time	Actual Filling Time	Error	Re. no,
v_g, ms^{-1}	$A_m, \times 10^3, m^2$	$A_f, \times 10^6, m^2$	t_f, sec	t_{actual}, sec	%	
0.903	0.396	6.75	8.01	8.3	3.55	2845

Calculated Riser Parameter

Calculated Cup Diameter.	Calculated Riser Diameter.,	Hot metal required,	Yield	$\left(\frac{V}{A}\right)_{Casting}$	$\left(\frac{V}{A}\right)_{Gating}$
$d_c, \times 10^3, m$	$d_R, \times 10^3, m$	W_l, kg	(%)		
5.7	5.0	0.593	75.7	1.14×10^{-3}	2.26×10^{-3}

➤ Comparison of Calculated and Actual Filling Time and Gating Design of Brass Icon- Laxmi



Wax Pattern

Cast model with Gating



Figure: Finished Model

Table-5.2.3.1: Physical Parameters of the casting

Weight of Casting	Vol. of Casting	Outside Area of Cast	Inside area of cast	Total Heat dissipating Area	Height	Path length of Flow	Effective Width
$W_{Casting}, kg$	$V_{Casting}, \times 10^6, m^3$	$A_{outside}, \times 10^3, m^2$	$A_{inside}, \times 10^3, m^2$	$A_{Total}, \times 10^3, m^2$	$z_m \times 10^3, m$	$L_m, \times 10^3, m$	$w, \times 10^3, m$
402	47.8	32.27	16.25	48.52	148	160	1.5

Table-5.2.3.2: Gating Details

Number of Sprue	Gate Diameter,	Sprue Height	Cup diameter.	Cup Height	Gating Vol.	Gating Surface Area
n	$d_g, \times 10^3, m$	$z_s, \times 10^3, m$	$d_c, \times 10^3, m$	$z_c, \times 10^3, m$	$V_{Gating}, \times 10^6, m^3$	$A_{Gating}, \times 10^3, m^2$
1	4.5	40	6	25	5.38	2.38

Table-5.2.3.3: Calculated Filling Time

Gate Vel.	Avg. Cross-sectional Mold Area	Flow Area	Calculated Filling Time	Actual Filling Time	Error	Re. no,
v_g, ms^{-1}	$A_m, \times 10^3, m^2$	$A_f, \times 10^6, m^2$	t_f, sec	t_{actual}, sec	%	
0.903	0.323	6.75	7.05	7.5	6.07	2845

Table-5.2.3.4: Calculated Riser Parameter

Calculated Cup Diameter.	Calculated Riser Diameter.,	Hot metal required,	Yield	$\left(\frac{V}{A}\right)_{Casting}$	$\left(\frac{V}{A}\right)_{Gating}$
$d_c, \times 10^3, m$	$d_R, \times 10^3, m$	W_l, kg	(%)		
5.7	4.33	0.536	74.9	0.985×10^{-3}	2.26×10^{-3}

➤ Comparison of Calculated and Actual Filling Time and Gating Design of Brass Icon-Saraswati



Wax Pattern

Cast model
with Gating



Figure: Finished Model

Physical Parameters of the casting.

Weight of Casting	Vol. of Casting	Outside Area of Cast	Inside area of cast	Total Heat dissipating Area	Height	Path length of Flow	Effective Width
$W_{Casting}, kg$	$V_{Casting}, \times 10^6, m^3$	$A_{outside}, \times 10^3, m^2$	$A_{inside}, \times 10^3, m^2$	$A_{Total}, \times 10^3, m^2$	$z_m \times 10^3, m$	$L_m, \times 10^3, m$	$w, \times 10^3, m$
360	42.89	24.8	10.47	35.27	157	185	1

Gating Details.

Number of Sprue	Gate Diameter,	Sprue Height	Cup diameter.	Cup Height	Gating Vol.	Gating Surface Area
n	$d_g, \times 10^3, m$	$z_s, \times 10^3, m$	$d_c, \times 10^3, m$	$z_c, \times 10^3, m$	$V_{Gating}, \times 10^6, m^3$	$A_{Gating}, \times 10^3, m^2$
2	4.5	35	6	25	5.16	2.21

Calculated Filling Time.

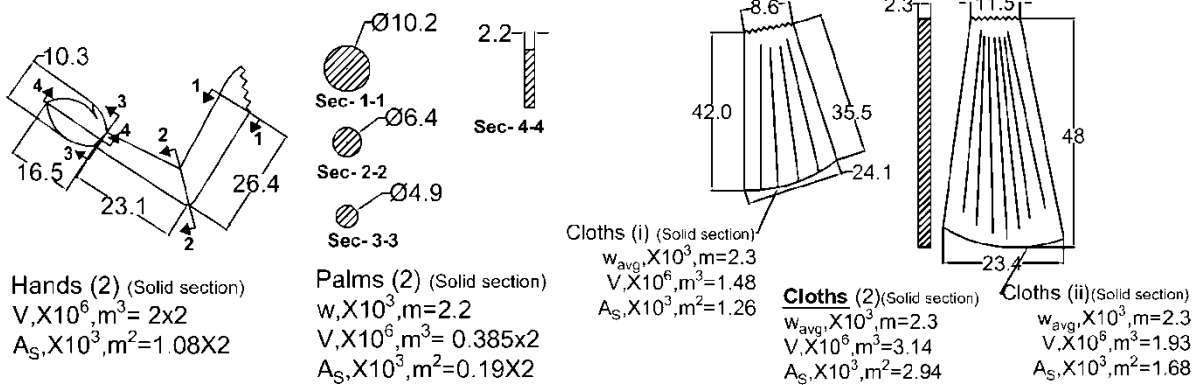
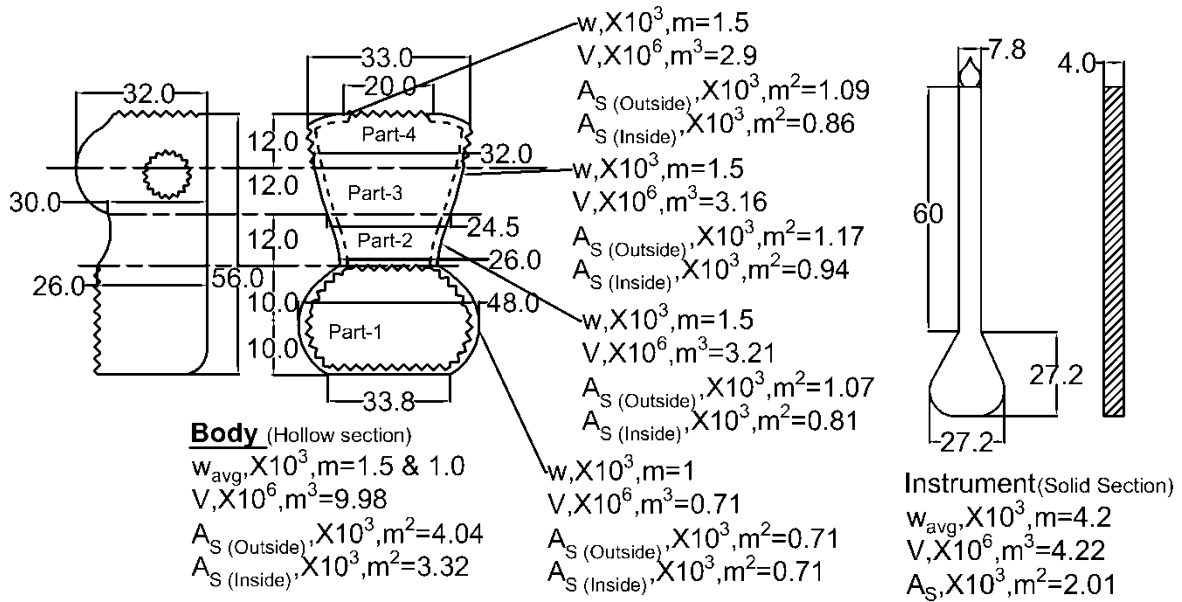
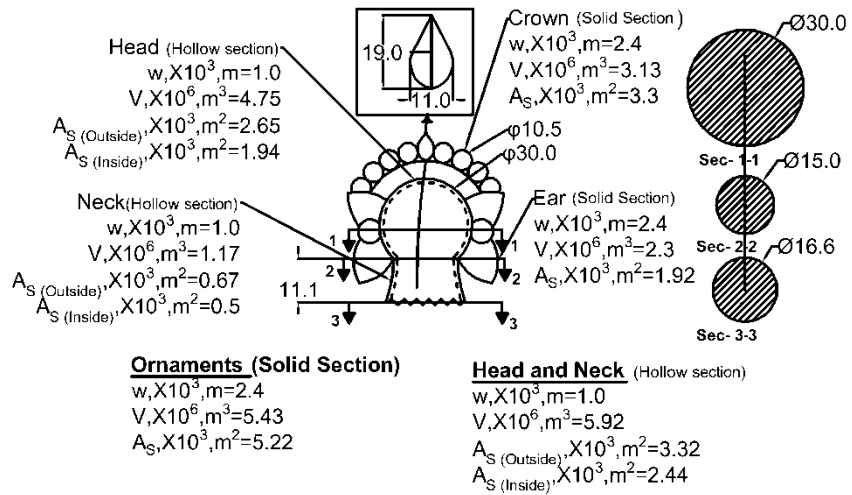
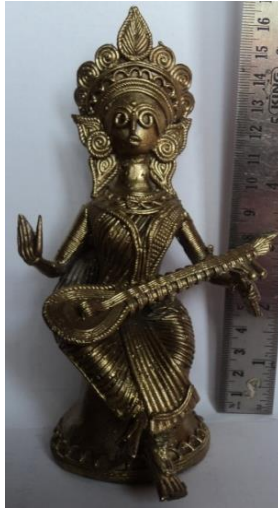
Gate Vel.	Avg. Cross-sectional Mold Area	Flow Area	Calculated Filling Time	Actual Filling Time	Error	Re. no,
v_g, ms^{-1}	$A_m, \times 10^3, m^2$	$A_f, \times 10^6, m^2$	t_f, sec	t_{actual}, sec	%	
0.86	0.273	9.0	7.14	7.6	6.05	1822

Calculated Riser Parameter

Calculated Cup Diameter	Calculated Riser Diameter	Hot metal required	Yield	$\left(\frac{V}{A}\right)_{Casting}$	$\left(\frac{V}{A}\right)_{Gating}$
$d_c, \times 10^3, m$	$d_R, \times 10^3, m$	W_I, kg	(%)		
5.6	5.36	0.484	74.4	1.22×10^{-3}	2.33×10^{-3}

Appendix VIII.

Detailed Dimension, Volume and Area of Model “Saraswati” part by part



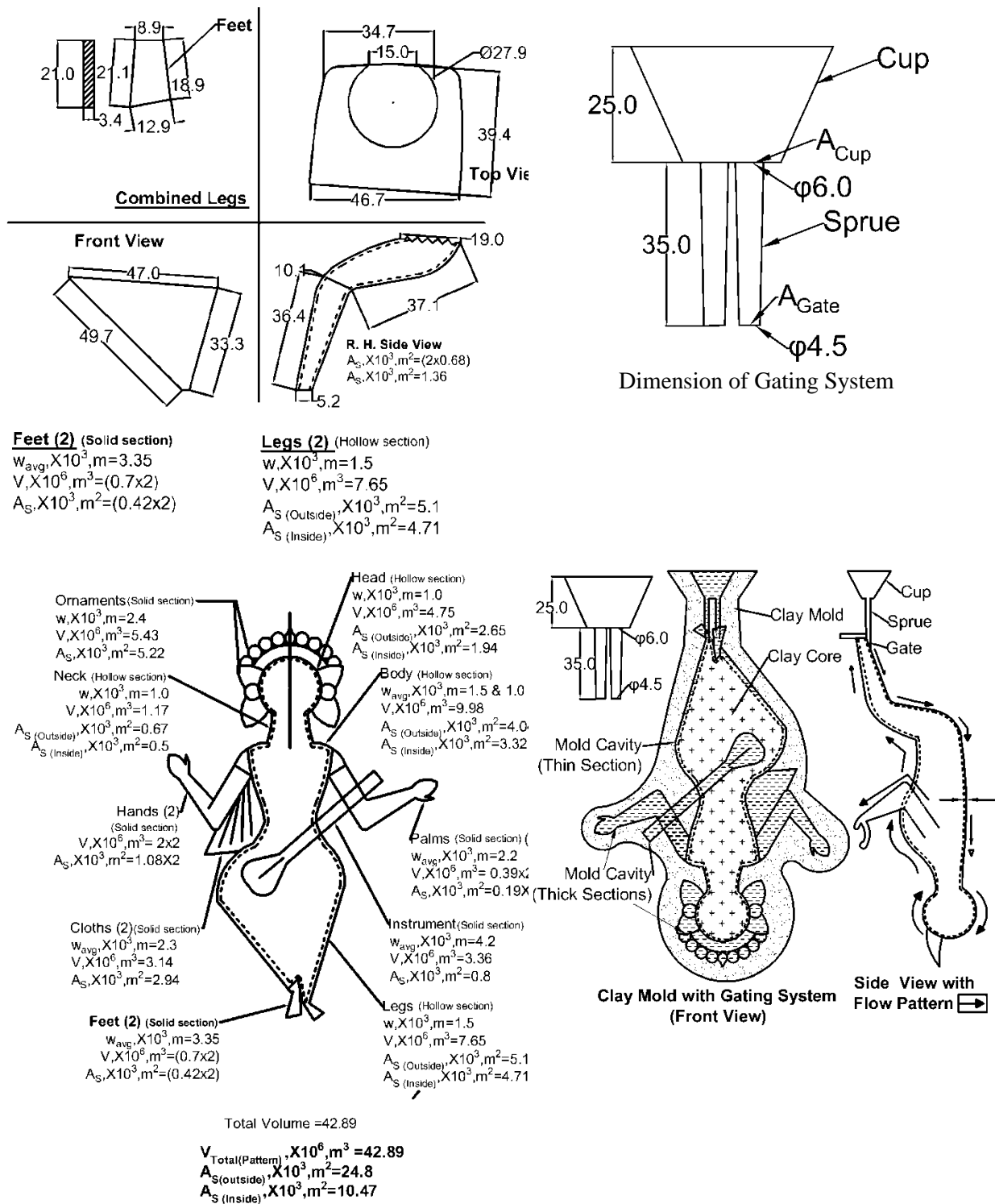


Figure: Detailed Dimension, Volume and Area part by part (All dimensions are in mm)

Appendix IX.

Calculation of Filling Time and Gating Design of Brass Icon SARASWATI

➤ Calculation of Filling Time

Details of casting as received,

Volume of the casting, $\times 10^6, m^3 = 42.9$;

Width of the casting, $w \times 10, m = 1.0 \text{ mm}$, Mold Height (z_m) = 157mm

z_s = (Sprue + cup Height) = (0.04 + 0.03) m, $C_D = 0.8$

♦ **Velocity at gate:** $v_g = C_D \sqrt{gz_s} = 0.8 \sqrt{9.81 \times (0.04 + 0.03)} = 0.938 m/s$

♦ **Effect of resistance due to surface tension:** [$\gamma = 2 \text{ N/m}$, $\theta = 135.790$, $w = 1.0 \text{ mm}$]

$$\Delta P_\gamma = -\frac{2\gamma}{w} \cos \theta = -\frac{2 \times 2 \times 10^{-3}}{0.001} \cos(135.79) = 2867 \text{ N/m}^2$$

♦ **Effect of gas pressure:** At 300K temperature, pressure of air is (considered as ideal gas):

$$P_{atm} = \rho_{atm} R_C T_{atm} = 1.177 \times 287 \times 300 = 101339 \text{ N/m}^2$$

Let, pressure inside mold at 1250 is P_2

$$P_h = \rho_{air(1273K)} R_C T_h = 0.2773 \times 287 \times 1273 = 101311 \text{ N/m}^2$$

$$\therefore \Delta P_{gas} = P_h - P_{atm} = -28.7 \text{ N/m}^2$$

Gas pressure is negative here; create a suction pressure, i.e., accelerating the flow.

♦ **Calculation of Constants:** [Now, $L_m = 185 \text{ mm}$, $\mu = 0.04 \text{ poise}$, $\rho = 8400 \text{ kg/m}^3$, $d_H = 2w = 0.002 \text{ m}$]

$$b = \frac{24\mu L_m}{\rho d_H^2} = 0.53 \quad k = \frac{1}{g} [b^2 + gz_m + v_g^2 - \frac{\Delta P_\gamma}{\rho_{liq}}] = 0.26$$

♦ **Flow area Calculation:** Number of Sprue (n) = 2; and as, $d_g < w$, therefore

$$A_f = n \times d_g \times w \Rightarrow 2 \times 0.004 \times 0.001 = 8 \times 10^{-6} \text{ m}^2$$

♦ **Avg. Mold Area:** $A_m = \frac{\text{Casting Volume}(V)}{\text{Mold Height}(Z_m)} = \frac{42.9 \times 10^{-6}}{157 \times 10^{-3}} = 0.273 \times 10^{-3} \text{ m}^2 = 74.4\%$

♦ **Filling Time:** $t_f = \frac{A_m}{A_f} \left[\frac{2}{\sqrt{g}} (\sqrt{k} - \sqrt{k - Z_m}) + \frac{2b}{g} \ln \left(\frac{\sqrt{k} - \frac{b}{\sqrt{g}}}{\sqrt{k - Z_m} - \frac{b}{\sqrt{g}}} \right) \right] = 7.14 \text{ s}$

♦ **Actual Filling Time** = 7.6s

♦ **Error Calculation:** $\text{Error} = \left(\frac{t_{actual} - t_{calculated}}{t_{actual}} \right) \times 100\% = \left(\frac{7.6 - 7.14}{7.6} \right) \times 100\% = 6.05\%$

➤ Gating Design Calculation of Brass Castings

Sprue Design:

Cup Diameter, d_c , m; Gate Diameter, d_g , m; Cup Height, z_c , m; Total Sprue Height, z_t , m

$$\text{Aspiration Correction, } \frac{d_g}{d_c} = \sqrt[4]{\frac{z_c}{z_t}} \Rightarrow \frac{4.5}{d_c} = \sqrt[4]{\frac{25}{60}} \Rightarrow d_c = 5.6 \text{ mm}$$

Actual Cup Diameter, $d_c = 2 \times 6 \text{ mm}$

Riser Design:

Riser diameter, d_r , m; Modulus of Riser, M_r , m; $M_r = 1.1 \times M_c$

$$\text{Modulus of the casting, } M_c, \quad M_c = \left(\frac{\text{Vol}}{\text{Area}} \right)_{\text{Casting}} = \left(\frac{42.89 \times 10^{-6}}{35.27 \times 10^{-3}} \right) = 1.216 \times 10^{-3}$$

Assume, Cylindrical Riser, $d_r = h_r$ so, $M_r = \frac{d_r}{4} \Rightarrow d_r = 4.87 \text{ mm}$,

Actual Riser Diameter (Sprue act as Riser), $d_c = 2 \times 4.5 = 9 \text{ mm}$

Hot metal required [considering, 20% extra metal for drossing and spilling]

$$W_1 = (V_{\text{Casting}} + V_{\text{Gating}}) \times \rho_{\text{Brass (Liquid)}}, \text{ kg} = 0.484 \text{ kg}$$

$$\text{Yield of the Casting, } (\%) = \frac{W_{\text{Casting}}}{W_{\text{Required}}} \cdot 100 (\%) = \frac{0.36}{0.484} \cdot 100 \% = 74.4\%$$

Appendix X.

Variation of length, breadth and width of the plates

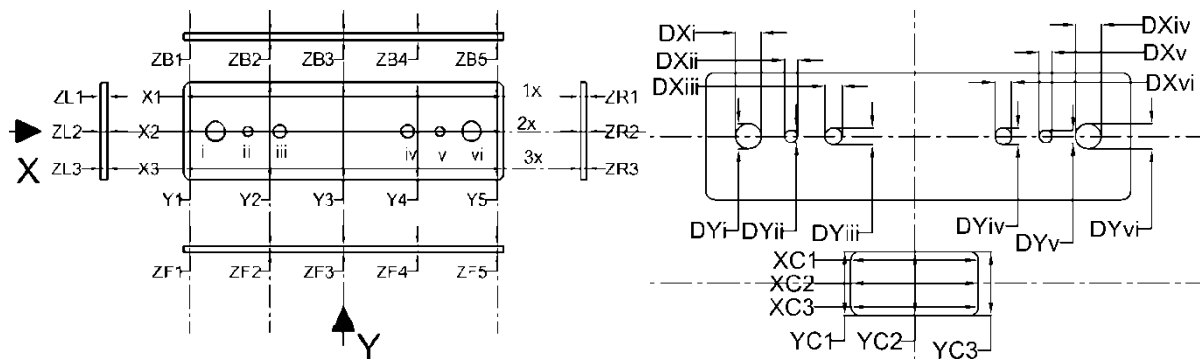


Figure: Dimension Nomenclatures of Cast Plate

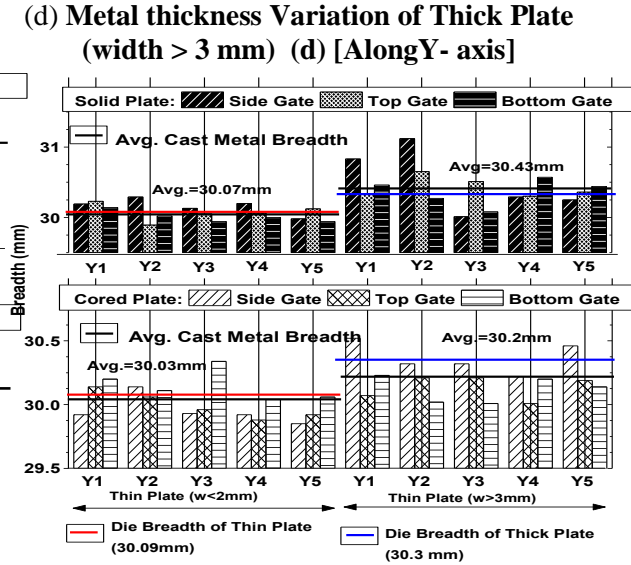
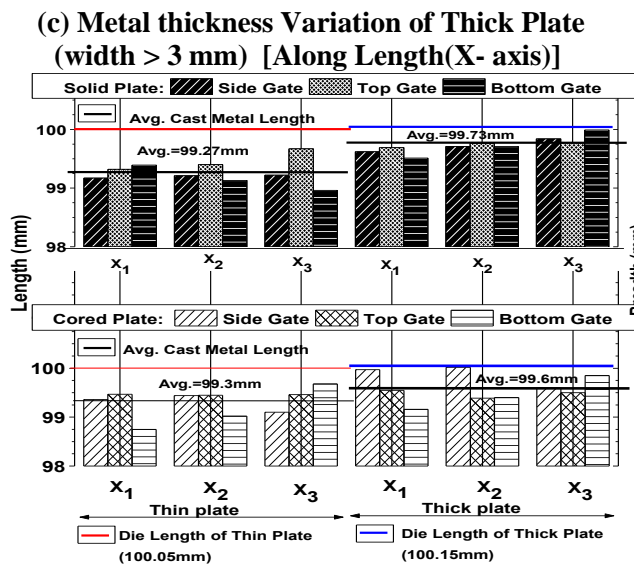
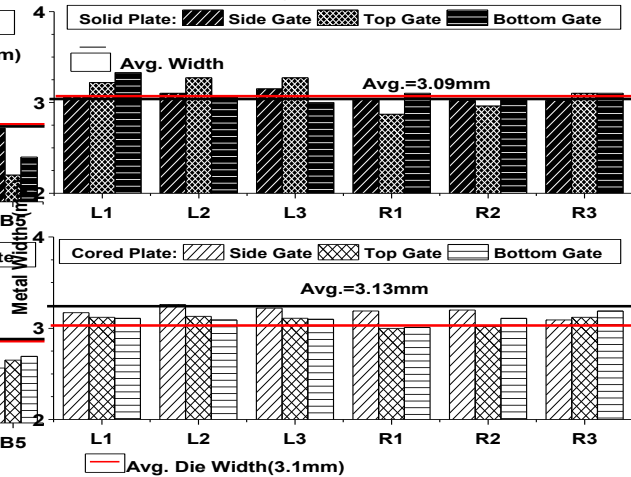
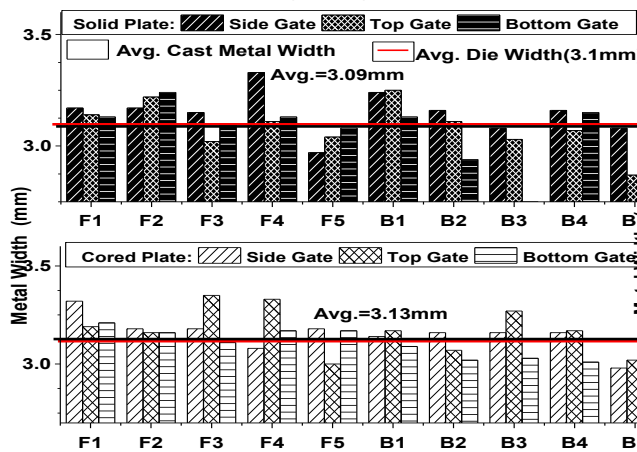
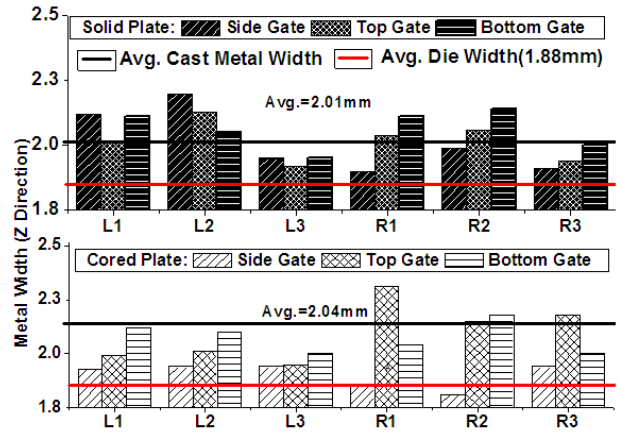
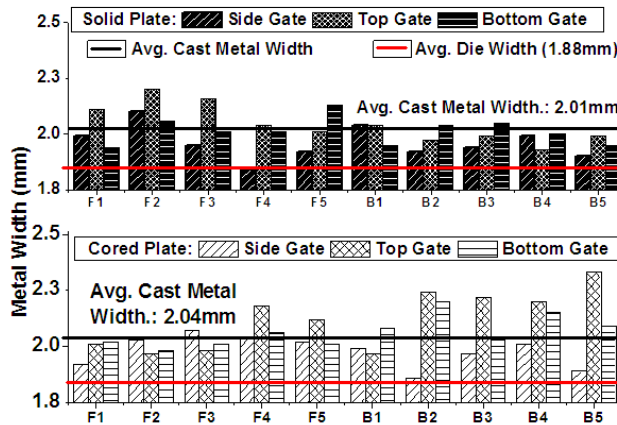
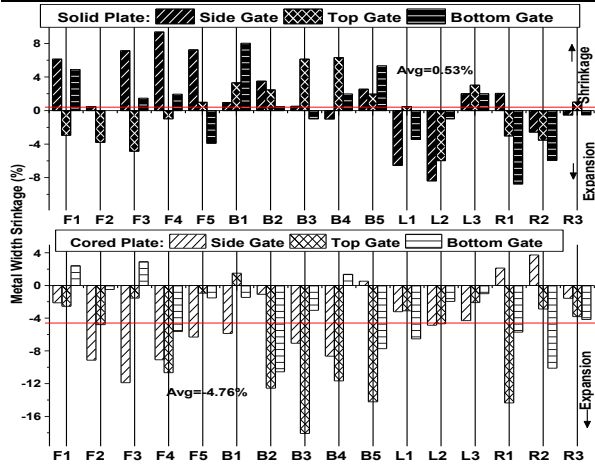


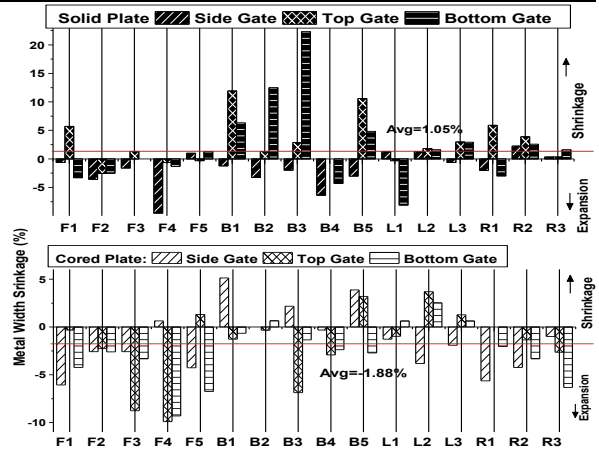
Figure: Variation of length, breadth and width of the plates

Appendix XI.

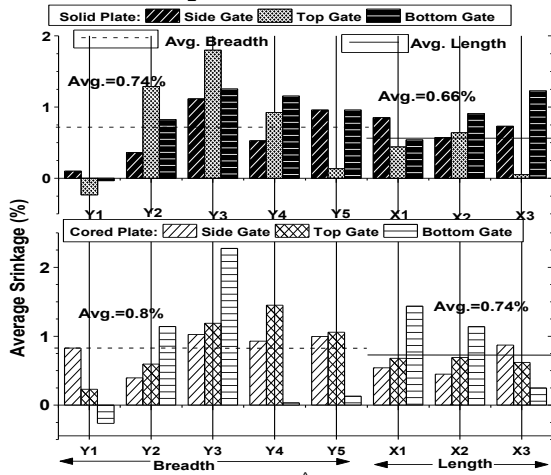
Shrinkage/ Expansion of length, breadth, metal thickness and the holes



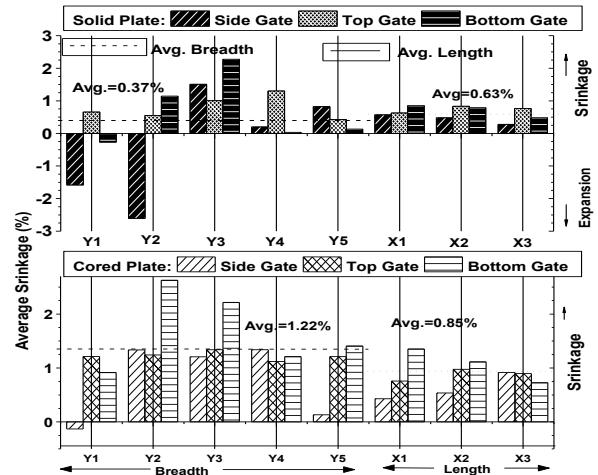
(a) Shrinkage/ Expansion of metal thickness of thin plate (width < 2 mm)



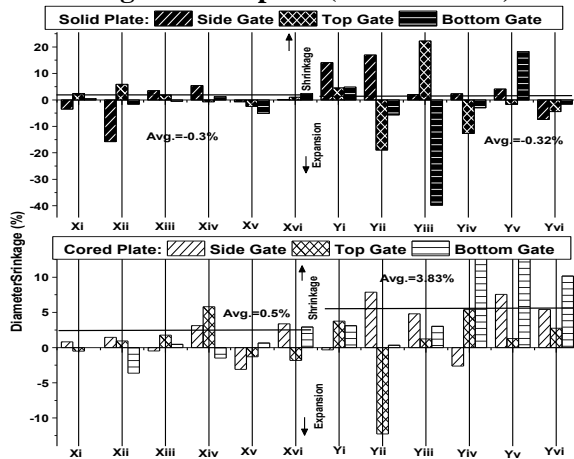
(b) Shrinkage/ Expansion of metal thickness of thin plate (width > 3 mm)



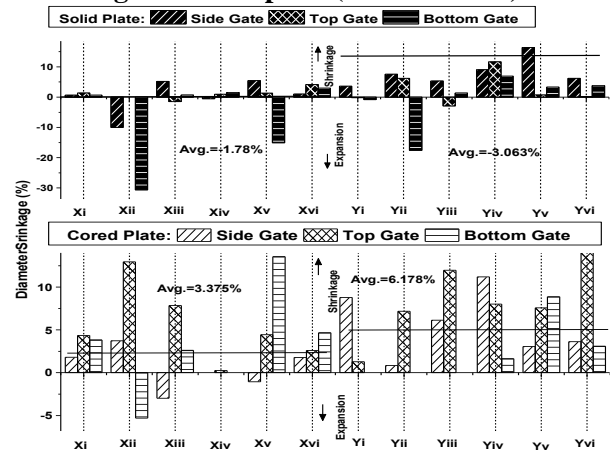
(c) Shrinkage/ Expansion of Breadth and Length of thin plate (width < 2 mm)



(d) Shrinkage/ Expansion of Breadth and Length of thick plate (width > 3 mm)



(e) Shrinkage/ Expansion of the hole diameter in 'X' and 'Y' direction of thin plate



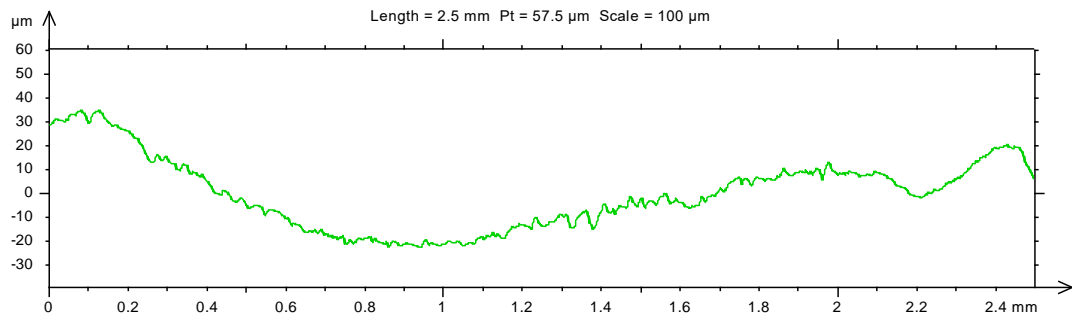
(f) Shrinkage/ Expansion of the hole diameter in 'X' and 'Y' direction of thick plate

Figure: Shrinkage/ Expansion of length, breadth, metal thickness and the holes

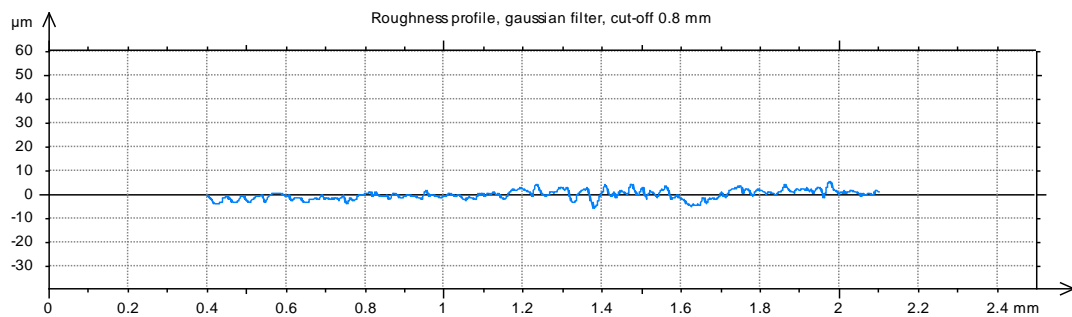
Appendix XII.

Surface roughness graphs of Thin ($w < 2\text{mm}$) Rectangular Plate Castings (Ref. Fig.-6.3)

➤ **Thin, Solid Plate, Top Gating, Location: Nearest Position From Gate**

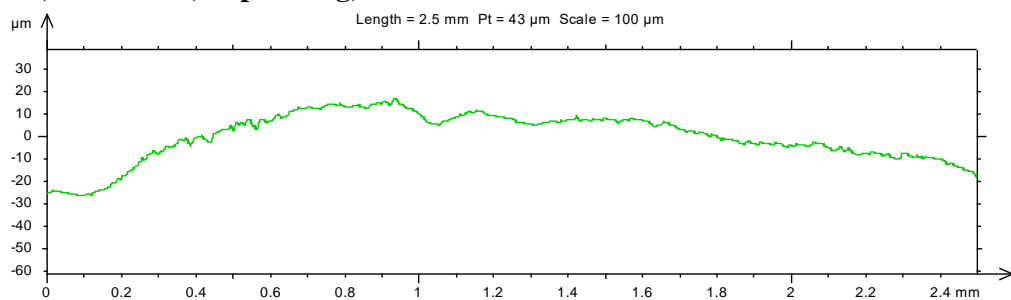


Surface Profile

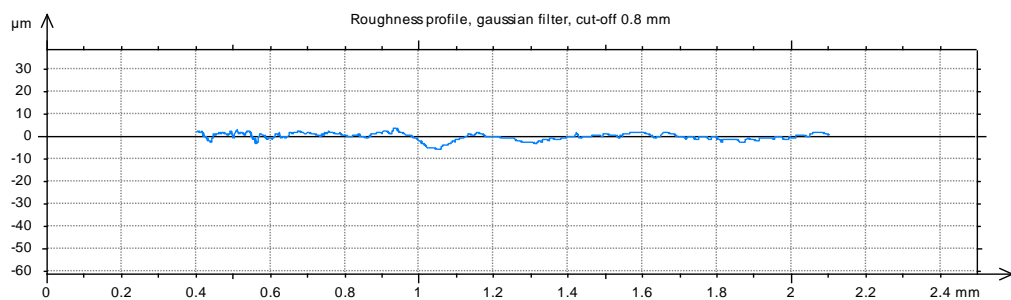


Roughness profile

➤ **Thin, Solid Plate, Top Gating, Location: Furthest Position From Gate**

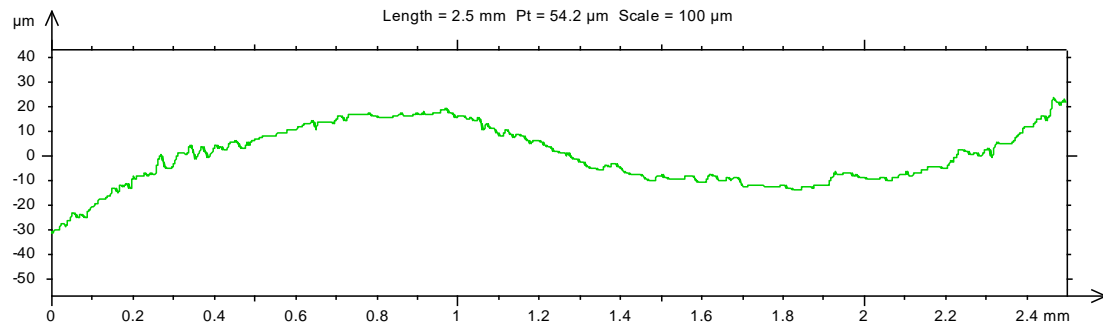


Surface Profile

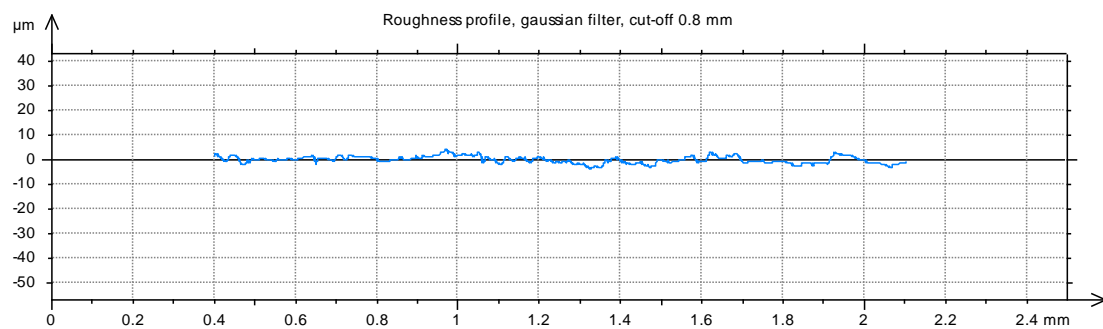


Roughness profile

➤ **Thin, Solid Plate, Side Gating, Location: Nearest Position From Gate**

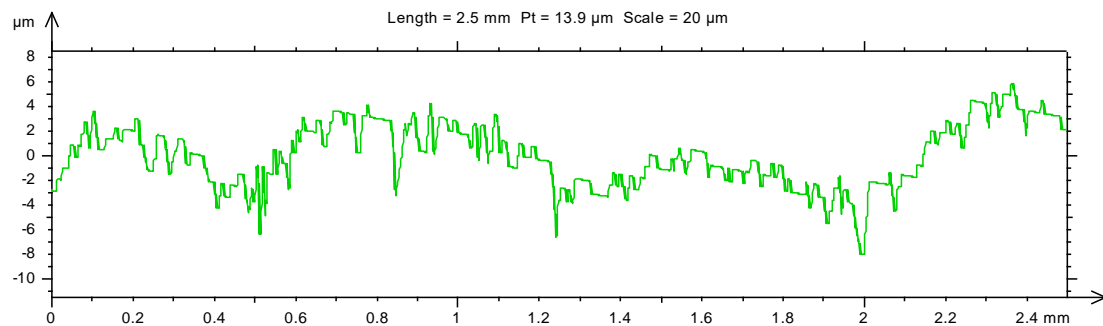


Surface Profile

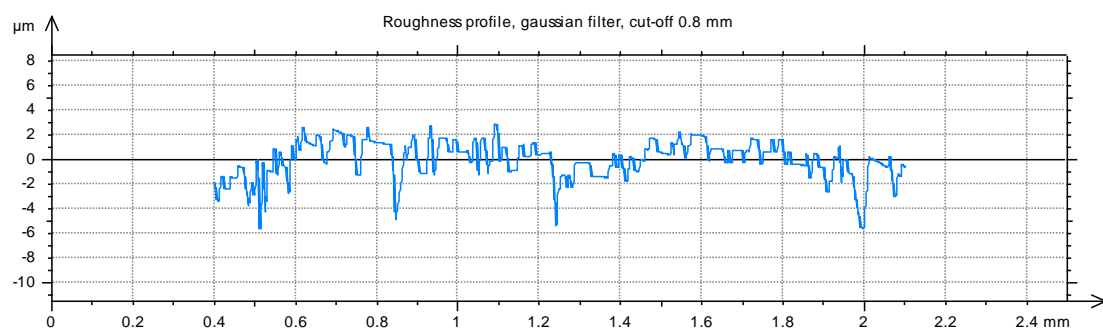


Roughness profile

➤ **Thin, Solid Plate, Side Gating, Furthest Position from Gate**

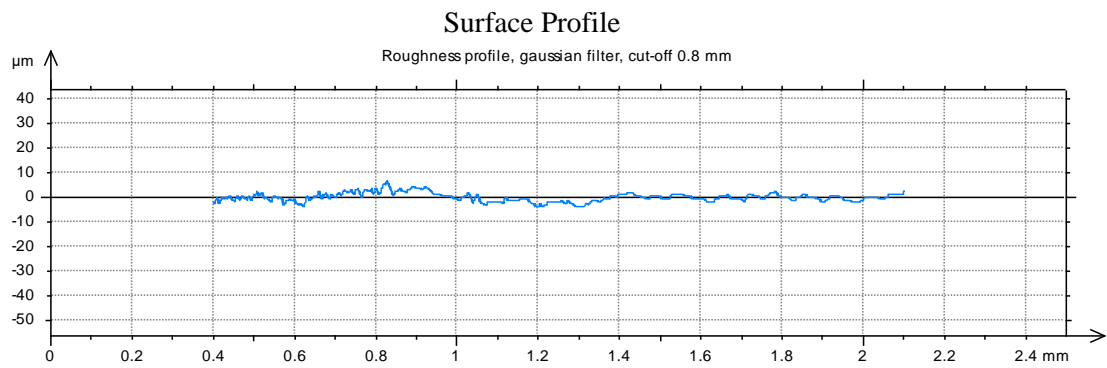
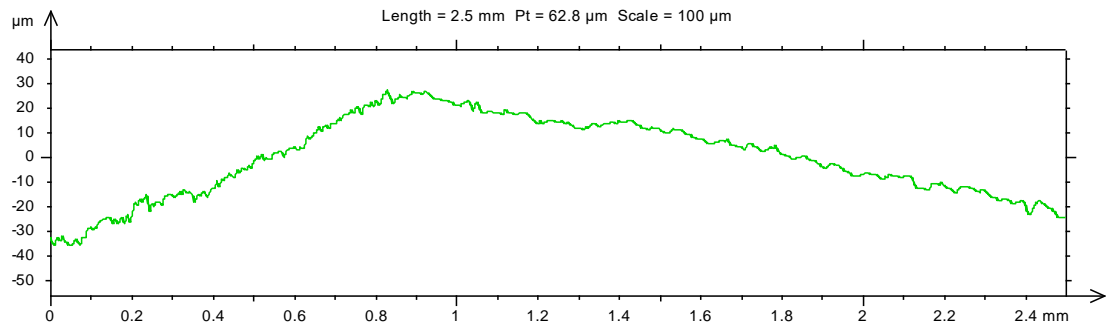


Surface Profile

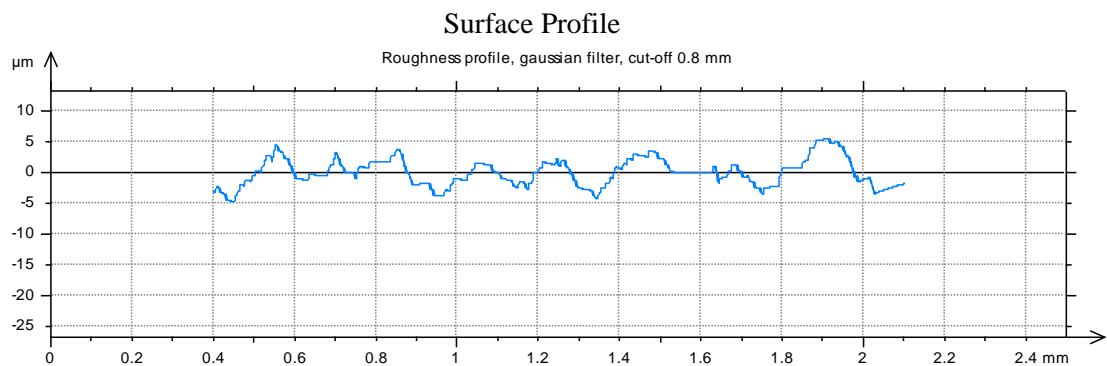
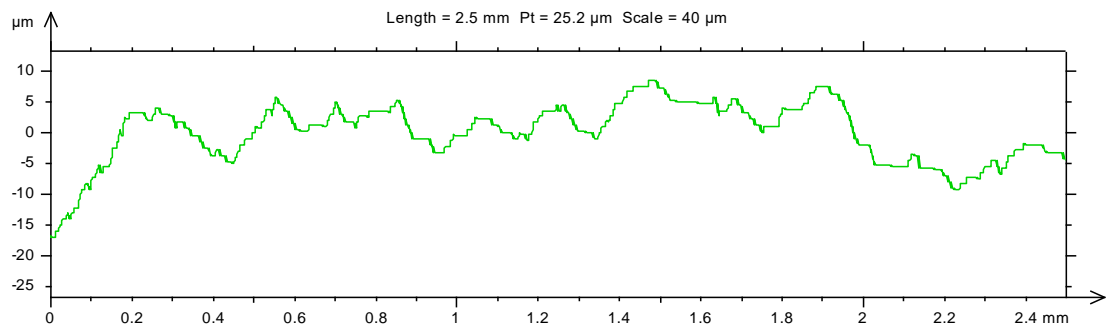


Roughness profile

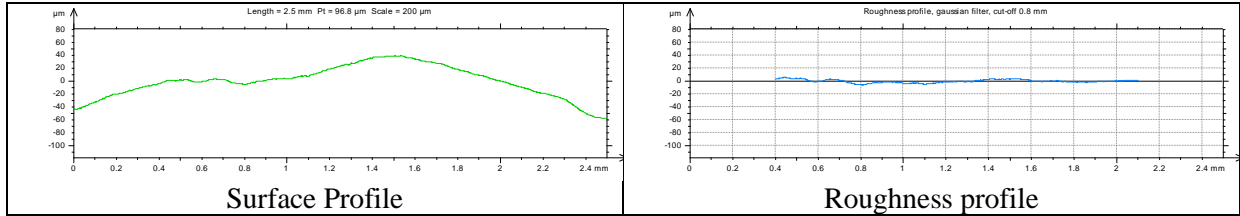
➤ **Thin, Solid Plate, Bottom Gating, Location: Nearest Position from Gate**



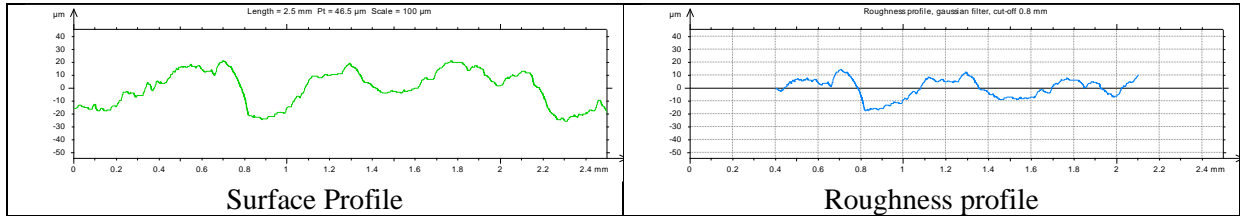
➤ **Thin, Solid Plate, Bottom Gating, Location: Furthest Position from Gate**



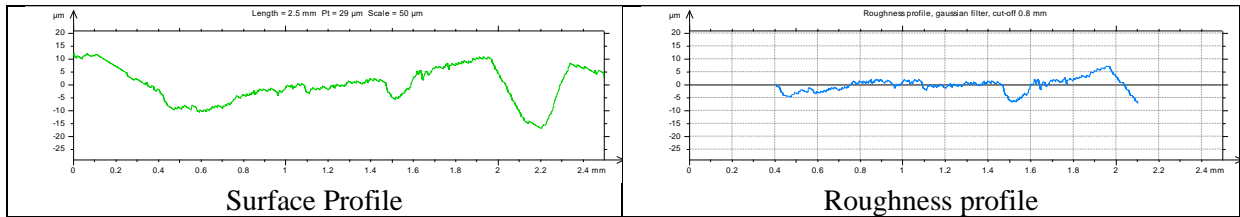
➤ **Thin, Cored Plate, Top Gating, Location: Nearest Position from Gate**



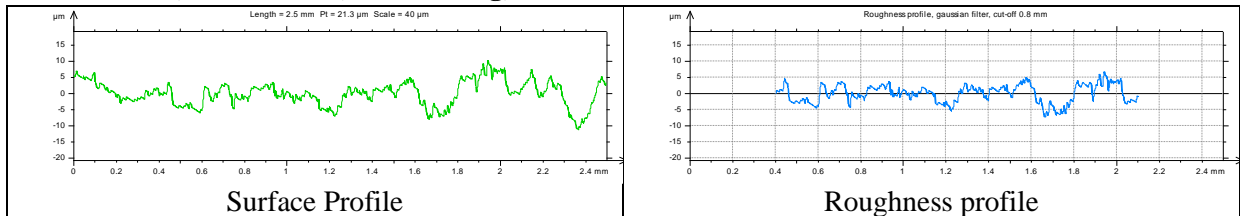
➤ **Thin, Cored Plate, Top Gating, Location: Furthest Position From Gate**



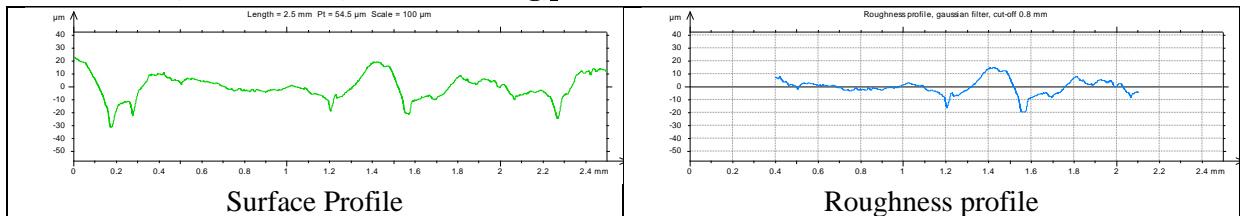
➤ **Thin, Cored Plate, Side Gating, Location: Nearest Position from Gate**



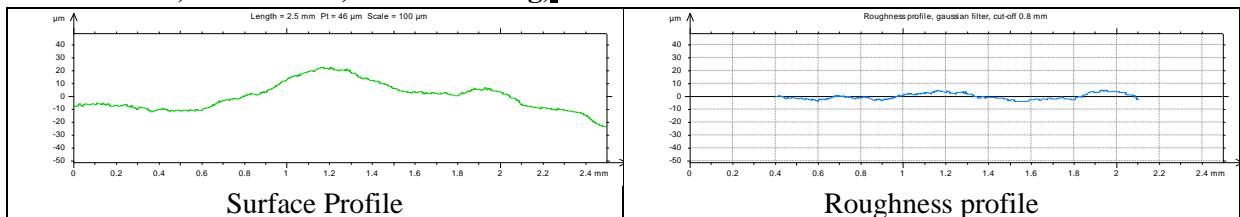
➤ **Thin, Cored Plate, Side Gating, Furthest Position From Gate**



➤ **Thin, Cored Plate, Bottom Gating, Location: Nearest Position from Gate**



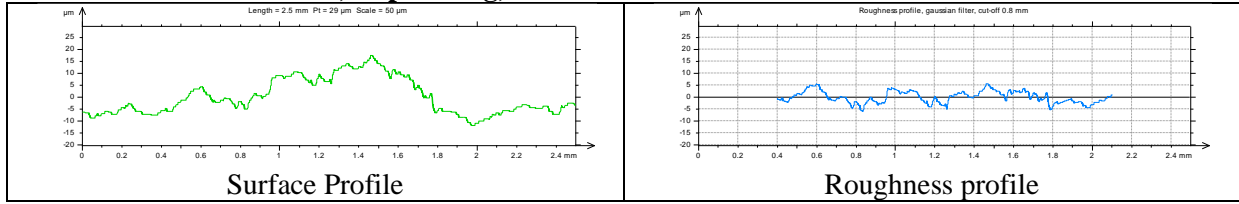
➤ **Thin, Cored Plate, Bottom Gating, Location: Furthest Position from Gate**



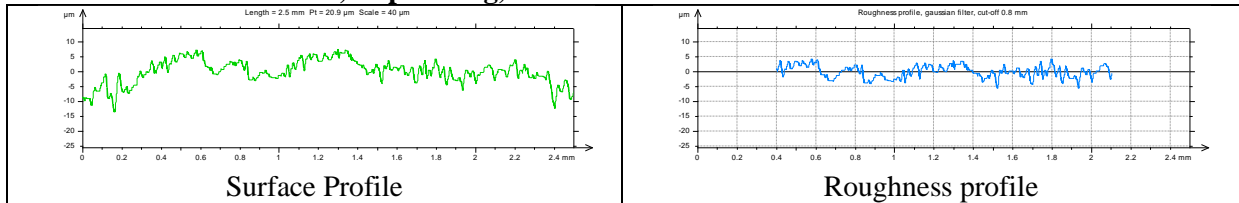
Appendix XIII.

Surface roughness graphs of Thick ($w > 3\text{mm}$) Rectangular Plate Castings

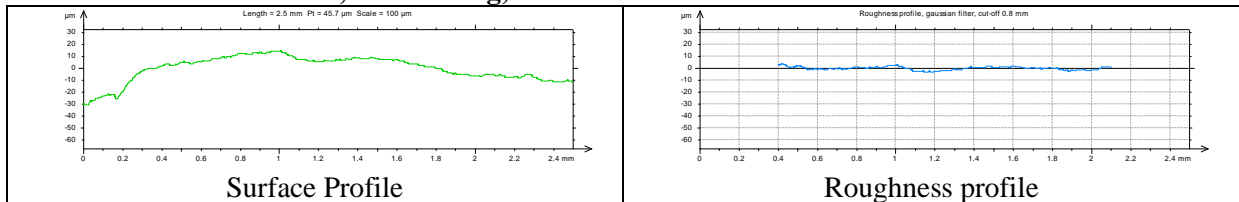
➤ Thick. Solid Plate, Top Gating, Location: Nearest Position from Gate



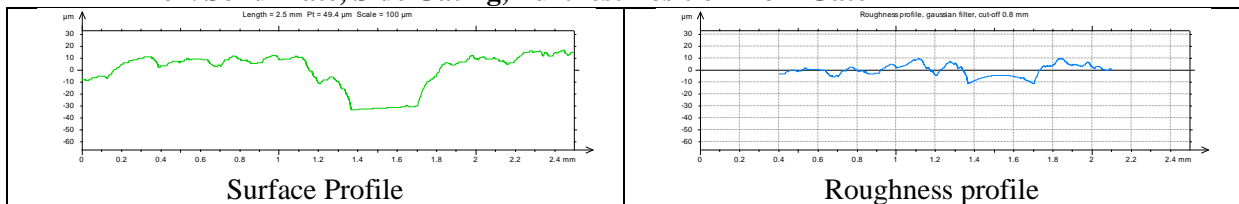
➤ Thick. Solid Plate, Top Gating, Location: Furthest Position from Gate



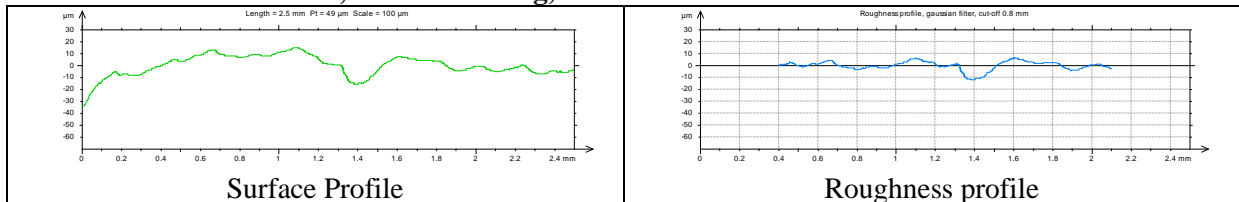
➤ Thick. Solid Plate, Side Gating, Location: Nearest Position from Gate



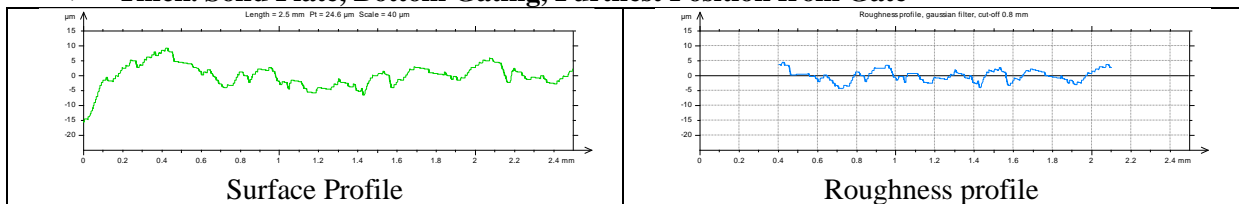
➤ Thick. Solid Plate, Side Gating, Furthest Position from Gate



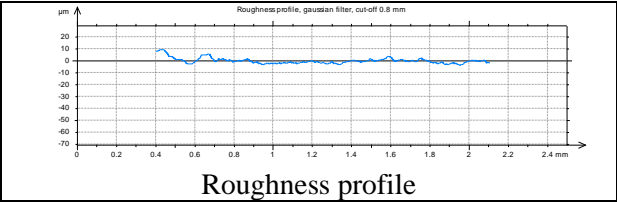
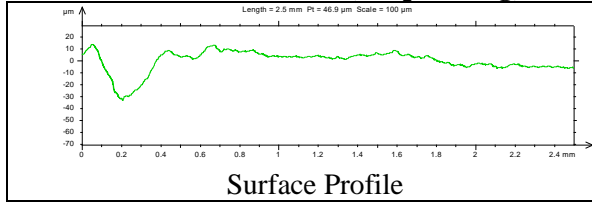
➤ Thick. Solid Plate, Bottom Gating, Location: Nearest Position from Gate



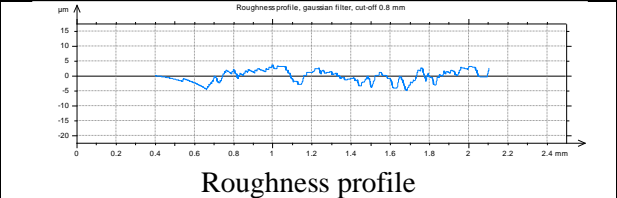
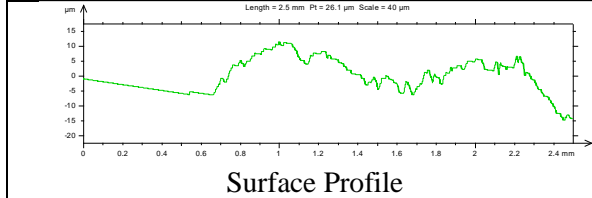
➤ Thick. Solid Plate, Bottom Gating, Furthest Position from Gate



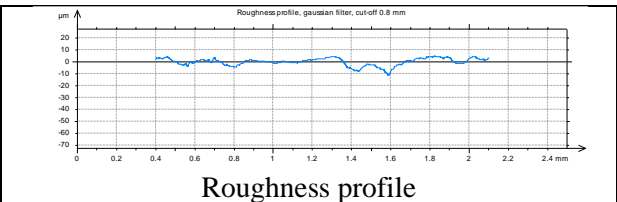
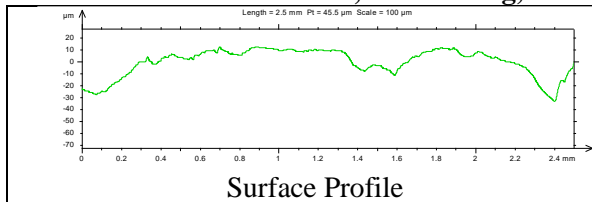
➤ **Thick. Cored Plate, Top Gating, Location: Nearest Position from Gate**



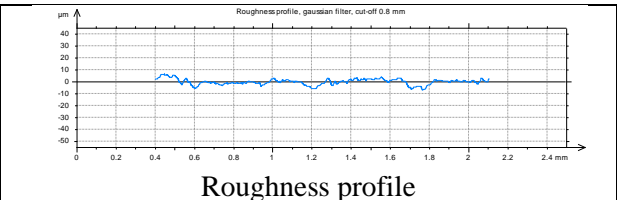
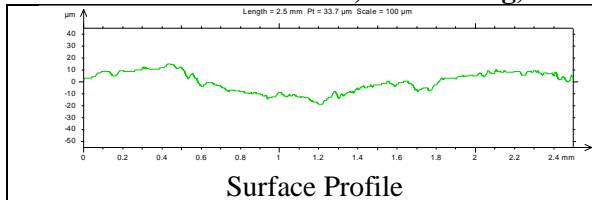
➤ **Thick. Cored Plate, Top Gating, Furthest Position from Gate**



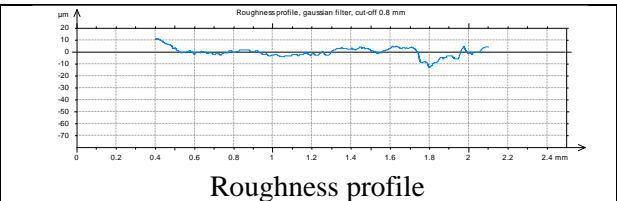
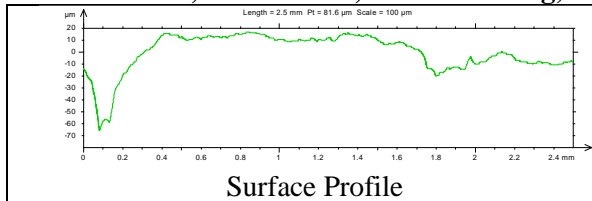
➤ **Thick. Cored Plate, Side Gating, Location: Nearest Position from Gate**



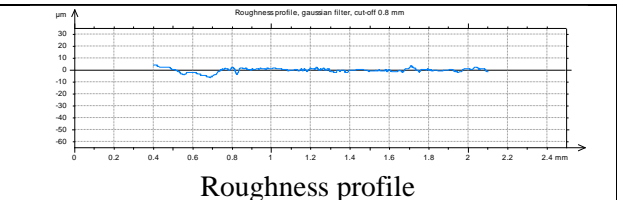
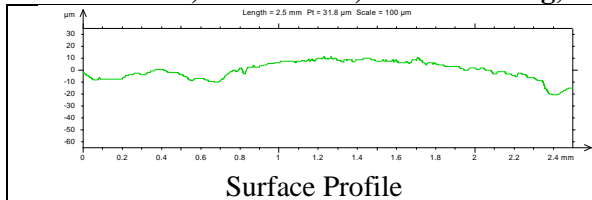
➤ **Thick. Cored Plate, Side Gating, Furthest Position from Gate**



➤ **Thick, Cored Plate, Bottom Gating, Location: Nearest Position from Gate**

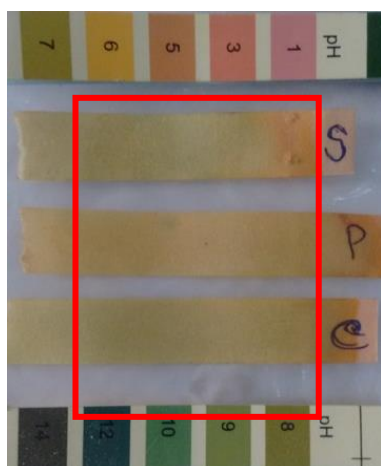


➤ **Thick, Cored Plate, Bottom Gating, Location: Furthest Position from Gate**

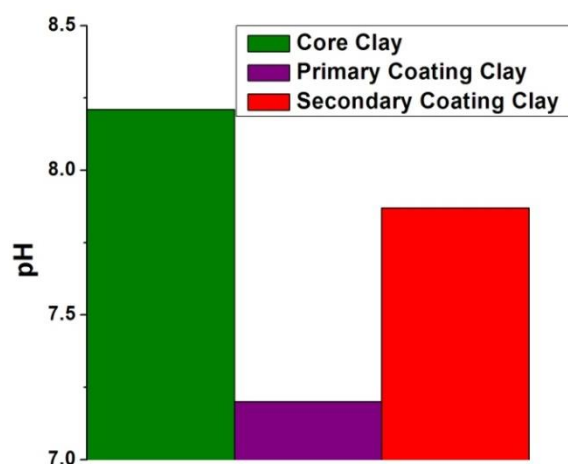


Appendix XIV.

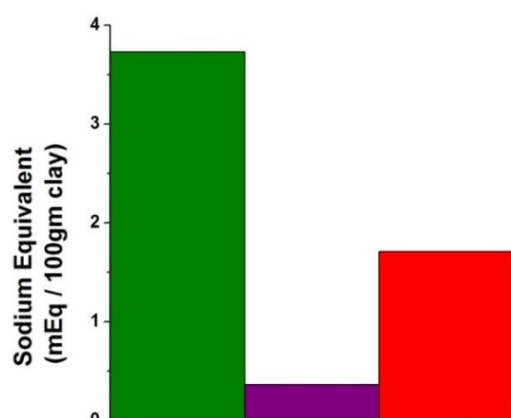
Analysis of Clay



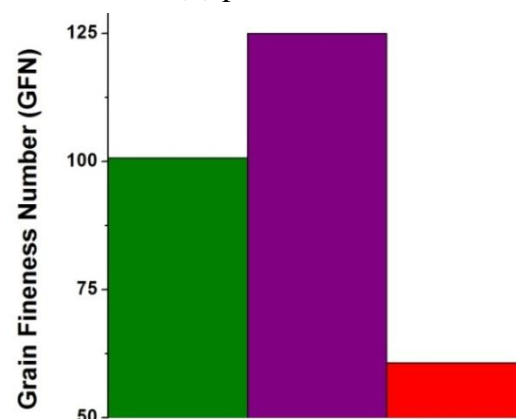
(a) Color change of litmus paper



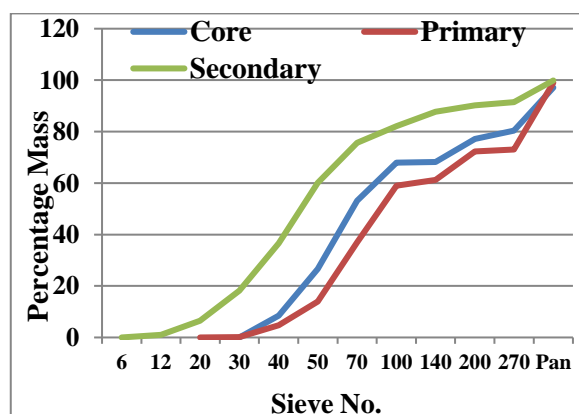
(b) pH



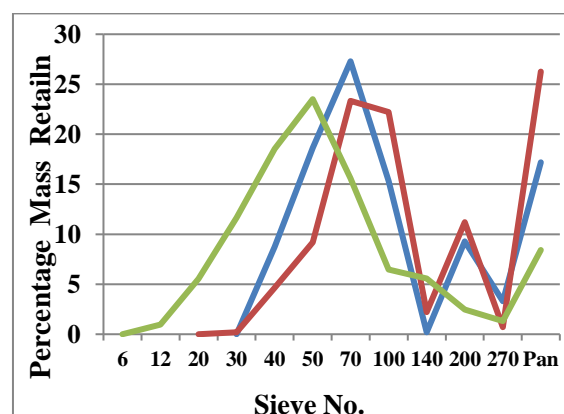
(c) Base Exchange Capacity in Sodium Equivalent (miliEquivalent /100 gm clay)



(d) Grain Fineness Number (GFN)



(d) Cumulative graphs for GFN



(e) Distribution graph for GFN (Mass % Retain)

Figure: Analysis of clay

Detailed Calculation of Base Exchange capacity (Ref. Table-6.2)

	40 ml					80 ml				
	pH	pOH	[OH-]	Na ⁺	For 100gm	pH	pOH	[OH-]	Na ⁺	For 100gm
Core Clay	8.1	5.94	1.15×10^{-6}	2.64×10^{-5}	2.64×10^{-3}	8.2	5.79	1.62×10^{-6}	3.73×10^{-5}	3.73×10^{-3}
Primary Coating Clay	7.2	6.84	1.45×10^{-7}	3.32×10^{-6}	3.32×10^{-4}	7.2	6.8	1.58×10^{-7}	3.65×10^{-6}	3.65×10^{-4}
Secondary Coating Clay	7.8	6.2	6.31×10^{-7}	1.45×10^{-5}	1.45×10^{-3}	7.9	6.13	7.41×10^{-7}	1.71×10^{-5}	1.71×10^{-3}

Appendix XV.

Procedure of Calculation Zn Equivalent (Ref. Table-6.3 and Figure-7.26)

Detailed Chemical composition of a brass sample (Ref. Figure-7.26)

Cu%	Zn%	Pb%	Fe%	Sn%	Ni and other Elements (%)
61.12	33.63	3.51	0.25	1.16	0.33

For example, in icon , percentage of Lead insoluble and outside the system: $3.51 \times 0.8 = 2.808$ wt.%,
percentage of Lead: $3.51 \times 0.2 = 0.702$ wt. % soluble in the system.

Total elements remaining in the solid

$\text{Cu} + \text{Sn} + \text{Pb} + \text{Fe} + \text{Ni} + \text{Zn} = 61.12 + 1.16 + 0.702 + 0.25 + 0.33 + 33.63 = 97.192$ wt.%

In weight percentage, the actual composition achieved by the alloy is,

$$\text{Cu} = \frac{61.12}{0.9719} \% = 62.88\%; \quad \text{Sn} = \frac{1.16}{0.9719} \% = 1.19\%; \quad \text{Pb} = \frac{0.702}{0.9719} \% = 0.722\%;$$

$$\text{Fe} = \frac{0.25}{0.9719} \% = 0.257\%; \quad \text{Ni} = \frac{0.33}{0.9719} \% = 0.3395\%; \quad \text{Zn} = \frac{33.63}{0.9719} \% = 34.6\%;$$

With this alloy for calculation[#] of Zn-Equivalent¹⁴, the zinc will be,

$34.6 (\text{Zn}) + 2 \times 1.19 (\text{Sn}) + 0.9 \times 0.257 (\text{Fe}) + 1 \times 0.722 (\text{Pb}) + 1 \times 1.19 + 1 \times 0.3395 (\text{Ni}) = 38.28\%$

For Zn-Equivalent calculation the total comes to $38.28 + 61.12 (\text{Cu}) = 101.167$

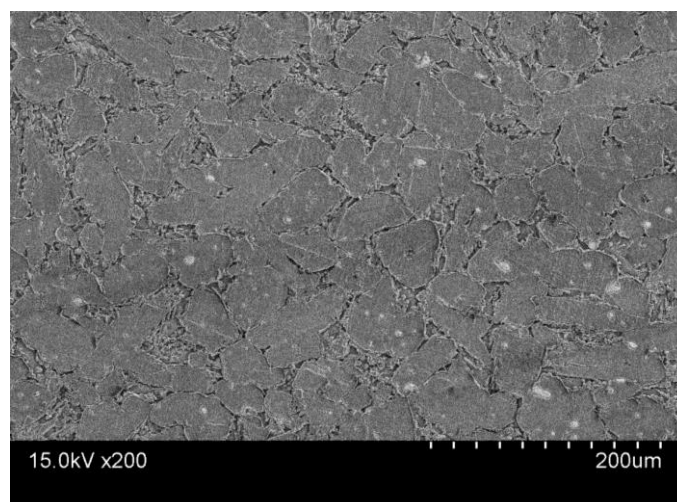
Zn-Equivalent will be $\frac{38.28}{101.03} = 37.84$ wt.% and Cu – will be $\frac{61.12}{101.03} = 62.16$ wt.%.

The equivalents, due to Guillet,

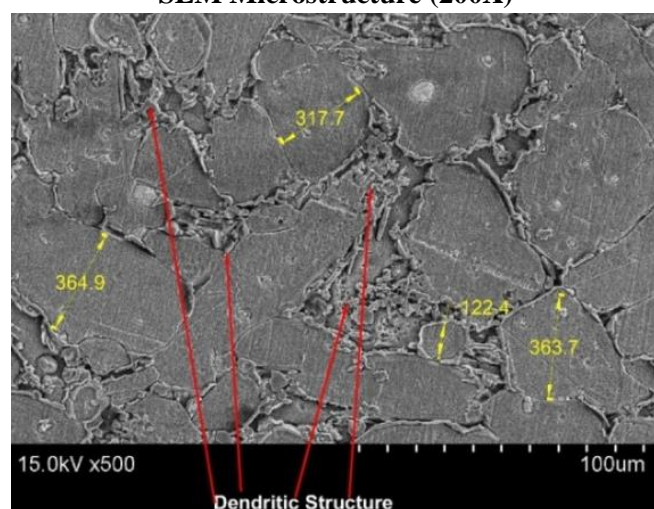
Element	Sn	Pb	Fe
Equivalent Zn	2	1	0.9

Appendix XVI.

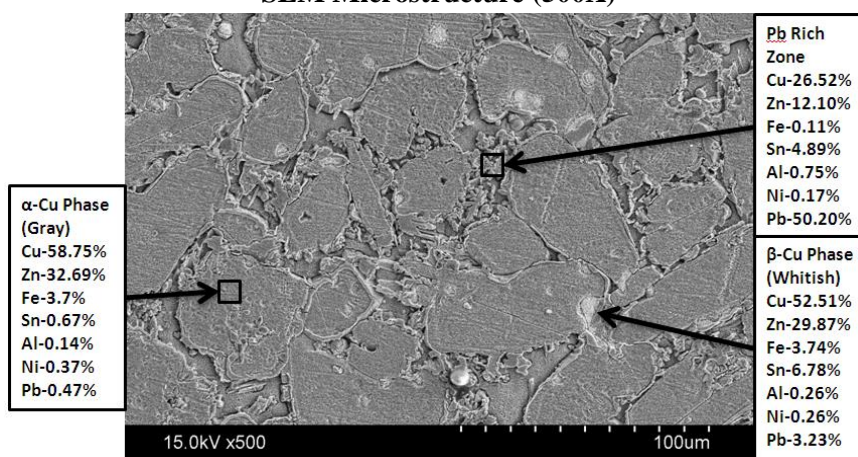
SEM-EDX Analysis of Thick and Thin plate followed by Horacek Model



SEM Microstructure (200X)

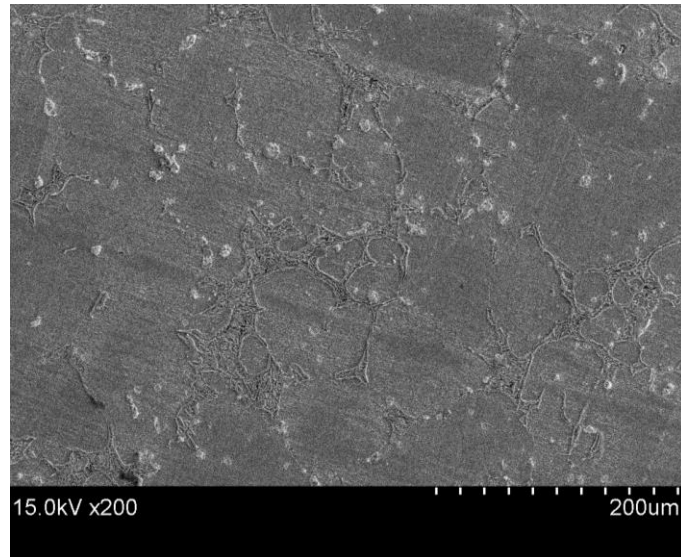


SEM Microstructure (500X)

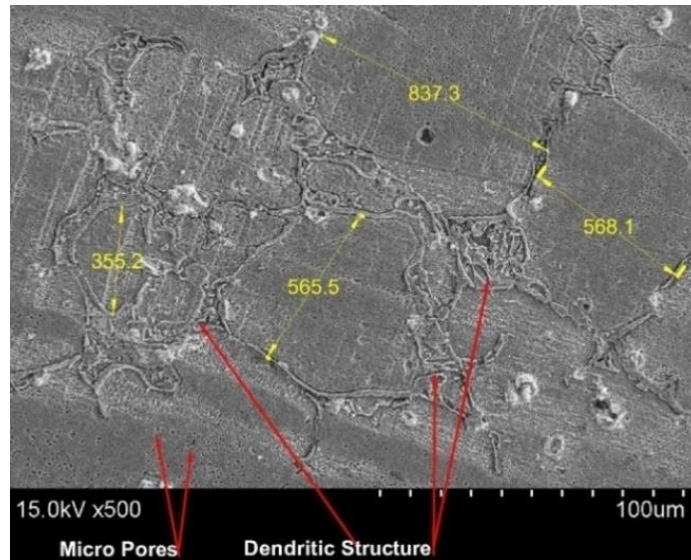


SEM-EDX Analysis (500X)

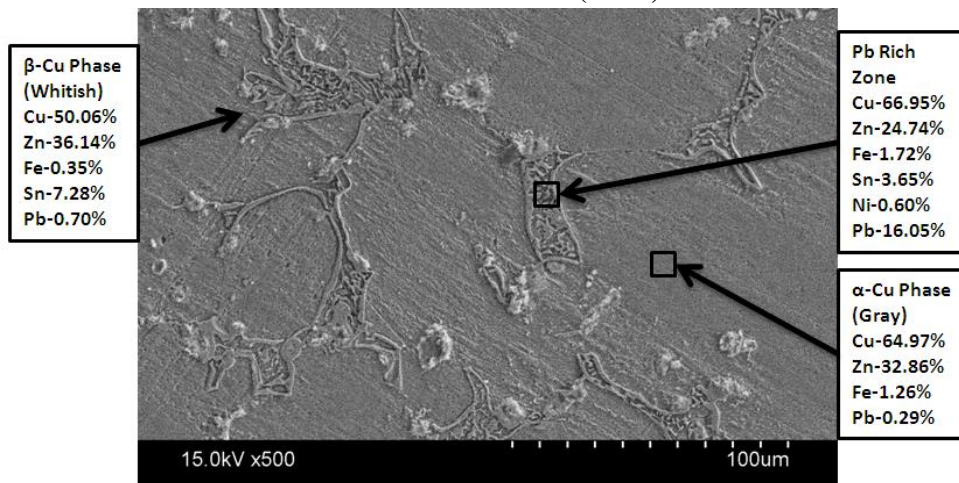
Figure: SEM Microstructure of Thin ($w < 2$) Cast Plate (200X and 500X) (Etchant: FeCl_3 in HCl) with SEM-EDX Analysis. The single α -Cu phase with inter dendritic region solute rich β -Cu phase is present with Insoluble Lead.



SEM Microstructure (200X)



SEM Microstructure (500X)

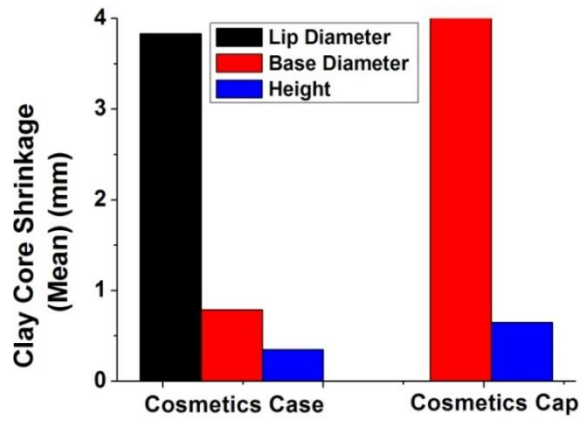


SEM-EDX Analysis (500X)

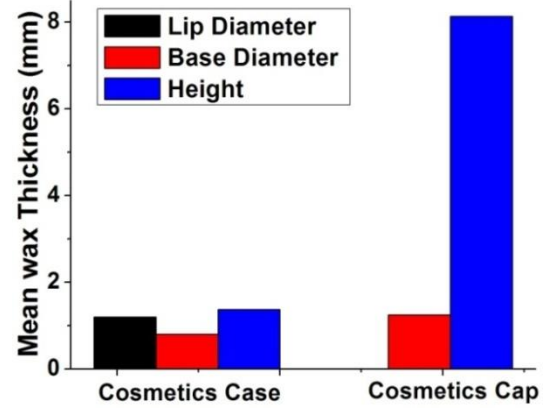
Figure: SEM Microstructure of Thick($w > 3$) HORÁČEK Cast Plate (200X and 500X) (Etchant: FeCl_3 in HCl). The single α -Cu phase with inter dendritic region solute rich β -Cu phase is present. Distributed Pb is everywhere.

Appendix XVII.

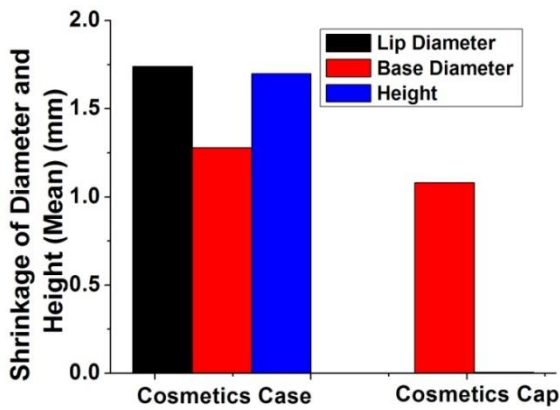
Data chart of Dimensional Shrinkage (%) of Cast Samples at different stages



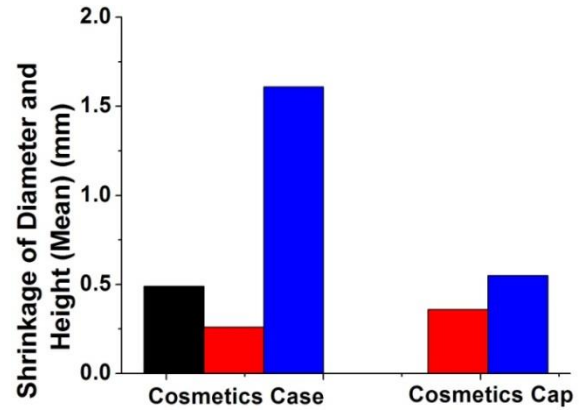
(a) Mean Clay Core Shrinkage (mm)



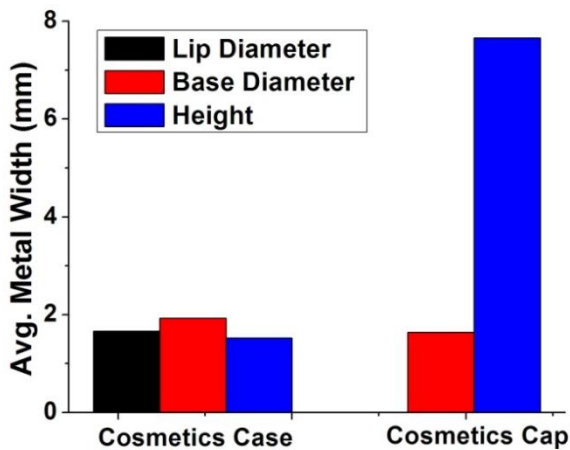
(b) Mean wax Thickness



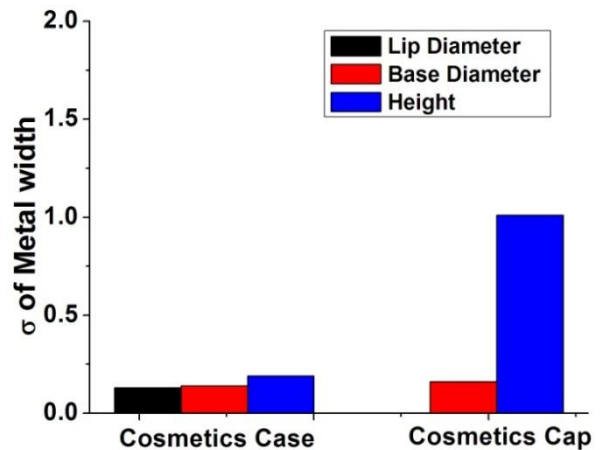
(c) Inner Side Dimension



(d) Outer Side Dimension



(e) Avg. Metal Thickness



(f) σ of Metal Width

Figure: Dimensional Shrinkage (%) of Cast Samples at different stages

Appendix XVIII.

Data chart of average variation of Metal width for different plane and different section for cosmetic case and cap for different gating system

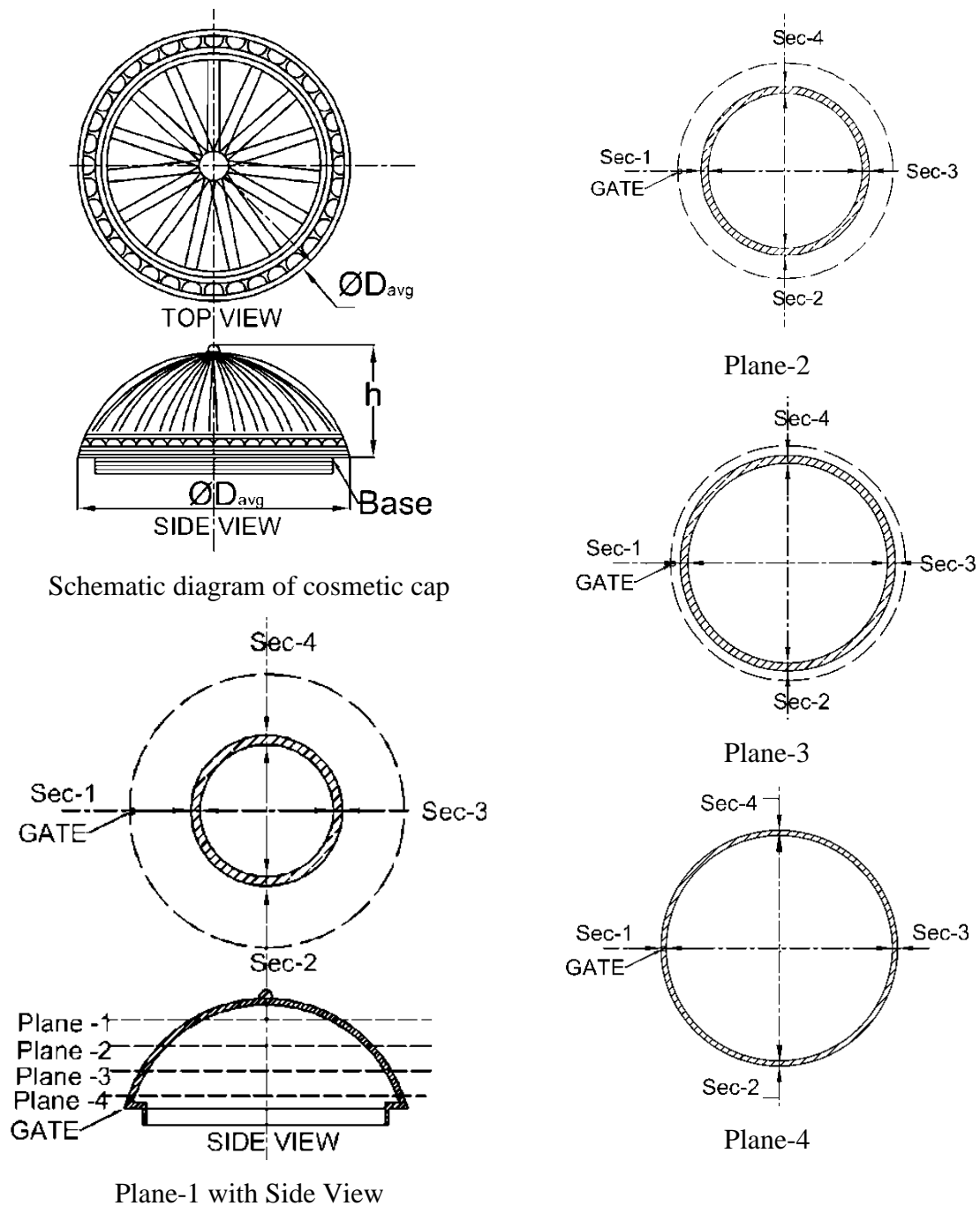


Figure: Plane-wise schematic diagram of the cross-section of the Cosmetic Cap

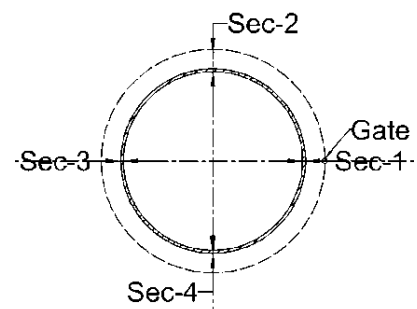
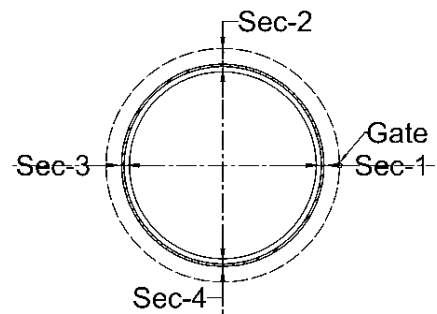
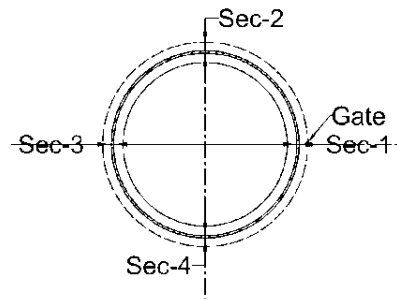
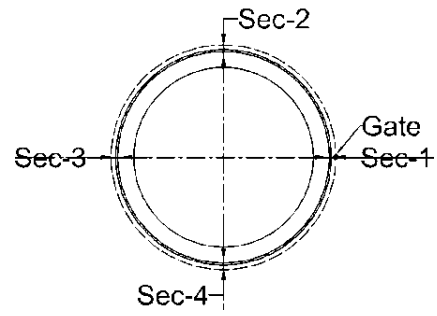
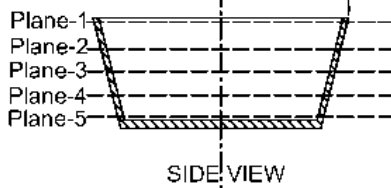
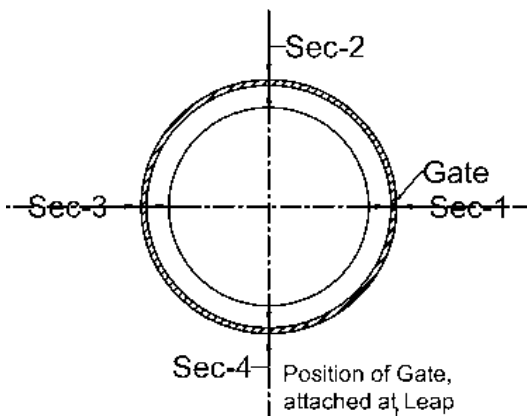
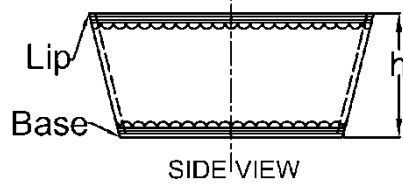
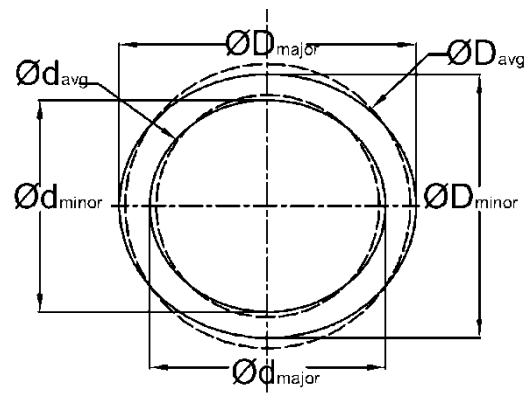
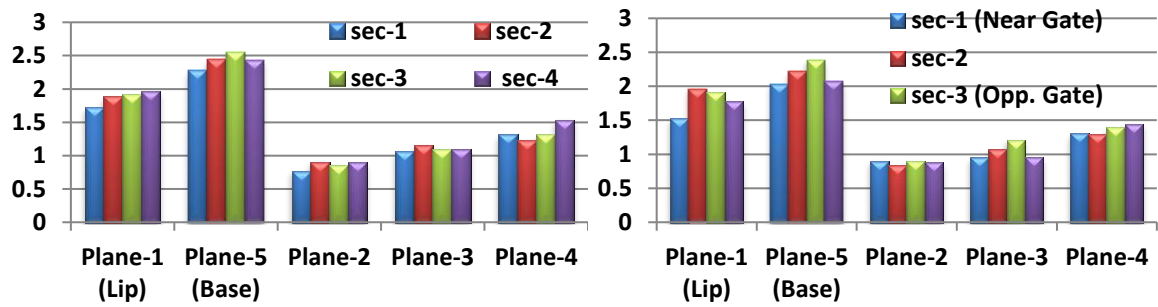
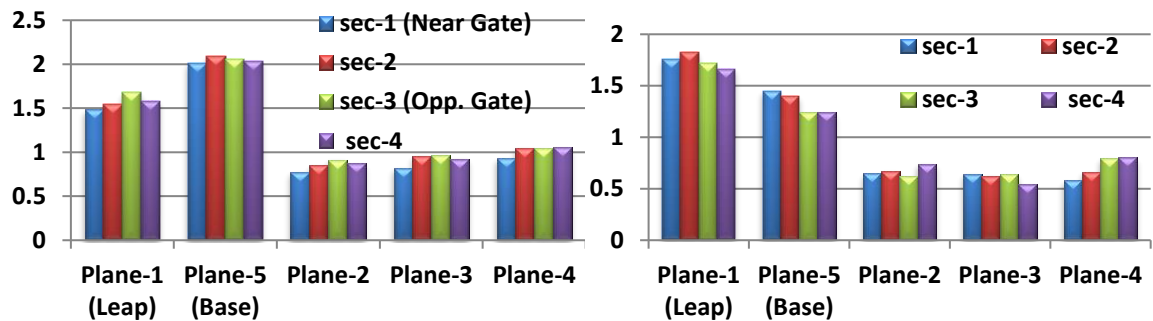


Figure: Schematic diagram of cosmetic case (Top Left Corner), Plane-wise schematic diagram of the cross-section of the Cosmetic Case



(a) Gating Type-I

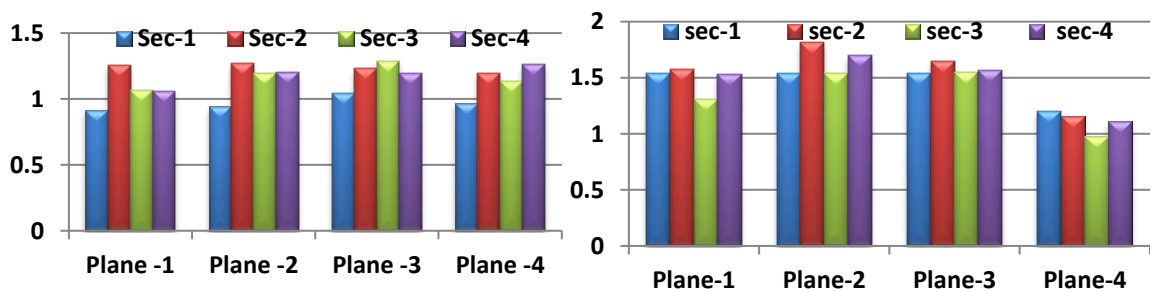
(b) Gating Type-II



(c) Gating Type-III

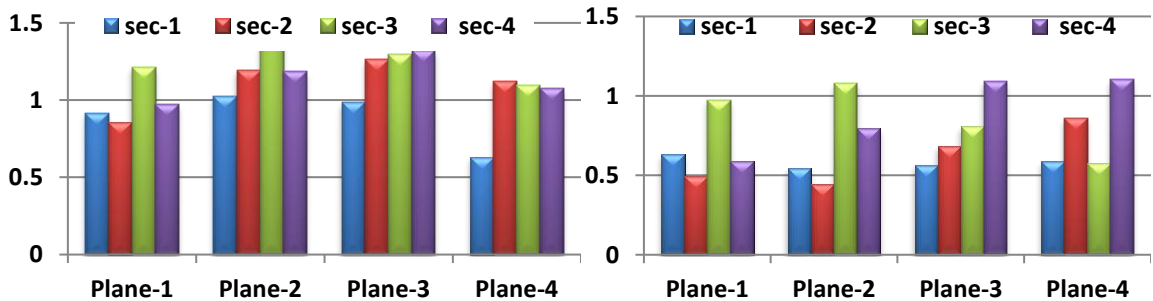
(d) Gating Type-IV

Figure: Metal Thickness of Cosmetics Case at Different Sections at Different Plane



(a) Gating Type-I

(b) Gating Type-II



(c) Gating Type-III

(d) Gating Type-IV

Figure: Metal thickness of Cosmetics Cap at Different Sections at different Plane

Appendix XIX.

Calculation to determine the Rank of the Casting using TOPSIS of Thin ($w < 2$) Plate

The Criteria taken to determine the Rank of the Casting is given by

- i. Variation (RMSD) of Metal Thickness
- ii. Variation (RMSD) of Length and Breadth
- iii. Surface Quality: Percentage of unaccepted surface was taken into account.
- iv. Surface Roughness (Ra)

- All the criteria chosen such a way, that lowest value are the best for each one.
- Equal Weight (0.25) was chosen to determine the rank of the castings.

Payoff Matrix

Payon Matrix							
Criterion		Gating Type	Sample No.	Mean Variation (RMSD) of Metal Thickness (C ₁)	Mean Variation (RMSD) of Length and Breadth (C ₂)	Surface Quality [un-accepted surface (%)] (C ₃)	Surface Roughness (Ra) (C ₄)
Weights				C ₁ = 0.25	C ₂ = 0.25	C ₃ = 0.25	C ₄ = 0.25
2mm	Solid	Top	1	0.1562	0.0054	0	1.415
	Solid	Side	2	0.1852	0.004	0	1.29
	Solid	Bottom	3	0.127	0.0108	1.55	2.275
	cored	Top	4	0.238	0.01025	0	4.265
	cored	Side	5	0.147	0.00925	0	4.92
	cored	Bottom	6	0.1274	0.0133	5.05	3.185
3mm	Solid	Top	7	0.162	0.0112	0	2.16
	Solid	Side	8	0.1134	0.01895	0.07	2.44
	Solid	Bottom	9	0.282	0.01255	2.57	2.265
	cored	Top	10	0.1338	0.01065	2.55	1.55
	cored	Side	11	0.927	0.00965	0.01	1.89
	cored	Bottom	12	0.823	0.05135	5.16	4.475

Normalized Payoff Matrix

Criterion			Sample No.	C_1	C_2	C_3	C_4
Weights				0.25	0.25	0.25	0.25
2mm	Solid	Top	1	0.11959	0.094588	0	0.153496
	Solid	Side	2	0.141793	0.070065	0	0.139936
	Solid	Bottom	3	0.097234	0.189175	0.209899	0.246787
	cored	Top	4	0.182218	0.179541	0	0.462657
	cored	Side	5	0.112546	0.162025	0	0.53371
	cored	Bottom	6	0.09754	0.232966	0.683866	0.345501
3mm	Solid	Top	7	0.124031	0.196182	0	0.234312
	Solid	Side	8	0.086822	0.331932	0.009479	0.264685
	Solid	Bottom	9	0.215905	0.219829	0.348027	0.245702
	cored	Top	10	0.10244	0.186548	0.345318	0.16814
	cored	Side	11	0.709732	0.169032	0.001354	0.205023
	cored	Bottom	12	0.630107	0.899458	0.698762	0.485438

Weighted Normalized Payoff Matrix, ideal (f_i^*), negative ideal (f_i^{}) values**

Criterion				C_1	C_2	C_3	C_4
Weights				0.25	0.25	0.25	0.25
2mm	Solid	Top	1	0.029898	0.023647	0	0.038374
	Solid	Side	2	0.035448	0.017516	0	0.034984
	Solid	Bottom	3	0.024309	0.047294	0.052475	0.061697
	cored	Top	4	0.045555	0.044885	0	0.115664
	cored	Side	5	0.028137	0.040506	0	0.133428
	cored	Bottom	6	0.024385	0.058241	0.170966	0.086375
3mm	Solid	Top	7	0.031008	0.049045	0	0.058578
	Solid	Side	8	0.021705	0.082983	0.00237	0.066171
	Solid	Bottom	9	0.053976	0.054957	0.087007	0.061425
	cored	Top	10	0.02561	0.046637	0.08633	0.042035
	cored	Side	11	0.177433	0.042258	0.000339	0.051256
	cored	Bottom	12	0.157527	0.224865	0.17469	0.121359
		f_j^*		0.177433	0.224865	0.17469	0.133428
		f_j^{**}		0.021705	0.017516	0	0.034984

Decision matrix

			Da+	Da-	Ca	Individual Rank	Overall Rank
2mm	Solid	Top	0.319072	0.010779	0.032679	1	1
	Solid	Side	0.321498	0.013743	0.040994	2	2
	Solid	Bottom	0.273972	0.066035	0.194217	3	4
	cored	Top	0.283931	0.088471	0.237569	4	6
	cored	Side	0.294608	0.101297	0.255861	5	8
	cored	Bottom	0.231116	0.183129	0.442079	6	11
3mm	Solid	Top	0.297442	0.040464	0.119748	1	3
	Solid	Side	0.280355	0.072555	0.20559	2	5
	Solid	Bottom	0.238711	0.103501	0.302448	4	9
	cored	Top	0.266412	0.091465	0.255576	3	7
	cored	Side	0.265511	0.158518	0.373839	5	10
	cored	Bottom	0.023279	0.315307	0.931247	6	12

Appendix XX.

Calculation to determine the Rank of the Casting using TOPSIS of Cosmetics Case

The Criteria taken to determine the Rank of the Casting of Cosmetics Case is given by

- i. RMS (Mean Variation of Metal width): Root Mean Square of Variation of Metal width was considered.
- ii. Eccentricity: The calculated average eccentricity was taken for calculation.
- iii. Surface Quality: Percentage of unaccepted surface was taken into account.
- iv. Surface Roughness (Ra): Measures Ra value was taken.
 - All the criteria chosen such a way, that lowest value are the best for each one.
 - Equal Weight (0.25) was chosen to determine the rank of the castings.

Payoff Matrix

Criterion		RMS (Mean Variation of Metal width) (C ₁)	Eccentricity (C ₂)	Surface Quality [un-accepted surface (%)] (C ₃)	Surface Roughness (Ra) (C ₄)
Weights		C ₁ = 0.25	C ₂ = 0.25	C ₃ = 0.25	C ₄ = 0.25
Alternatives Gating Types	Type-I	0.381	0.1255	0	1.16
	Type-II	0.378	0.1085	1	1.96
	Type-III	0.248	0.07	2	2.84
	Type-IV	0.276	0.2315	25	1.46

Normalized Payoff Matrix

	C ₁	C ₂	C ₃	C ₄
Type-I	0.583929	0.427915	0	0.295745
Type-II	0.579332	0.36995	0.039841	0.499707
Type-III	0.380091	0.238678	0.079682	0.724066
Type-IV	0.423004	0.789341	0.996024	0.372231

Weighted Normalized Payoff Matrix, ideal (f_i^{*}), negative ideal (f_i^{**}) values

	C ₁	C ₂	C ₃	C ₄
Type-I	0.145982	0.106979	0	0.073936
Type-II	0.144833	0.092488	0.00996	0.124927
Type-III	0.095023	0.059669	0.01992	0.181016
Type-IV	0.105751	0.197335	0.249006	0.093058
f _j [*]	0.145982	0.197335	0.249006	0.181016
f _j ^{**}	0.095023	0.059669	0	0

Decision matrix

	Da+	Da-	Ca	Rank
Type-I	0.285717	0.101497	0.262121	1
Type-II	0.266989	0.138795	0.342041	2
Type-III	0.272083	0.182109	0.400952	3
Type-IV	0.096723	0.299551	0.755919	4

Appendix XXI.

Calculation to determine the Rank of the Casting using TOPSIS of Cosmetics Cap

The Criteria taken to determine the Rank of the Casting of Cosmetics Case is given by

- i. RMS (Mean Variation of Metal width): Root Mean Square of Variation of Metal width was considered.
- ii. Eccentricity: The calculated average eccentricity was taken for calculation.
- iii. Surface Quality: Percentage of unaccepted surface was taken into account.
- iv. Surface Roughness (Ra): Measures Ra value was taken.
 - All the criteria chosen such a way, that lowest value are the best for each one.
 - Equal Weight (0.25) was chosen to determine the rank of the castings.

Payoff Matrix

Criterion		RMS (Mean Variation of Metal width) (C ₁)	Eccentricity (C ₂)	Surface Quality [un-accepted surface (%)] (C ₃)	Surface Roughness (Ra) (C ₄)
Weights		C ₁ = 0.25	C ₂ = 0.25	C ₃ = 0.25	C ₄ = 0.25
Gating Types	Type-I	0.198	0.1413	0	1.12
	Type-II	0.304	0.02995	3	1.48
	Type-III	0.336	0.1205	15	1.76
	Type-IV	0.579	0.16	45	2.11

Normalized Payoff Matrix

	C ₁	C ₂	C ₃	C ₄
Type-I	0.260041	0.572187	0	0.337777
Type-II	0.399255	0.121281	0.063119	0.446348
Type-III	0.441282	0.487958	0.315597	0.530793
Type-IV	0.760424	0.647912	0.946792	0.636348

Weighted Normalized Payoff Matrix, ideal (f_i^{*}), negative ideal (f_i^{**}) values

	C ₁	C ₂	C ₃	C ₄
Type-I	0.06501	0.143047	0	0.084444
Type-II	0.099814	0.03032	0.01578	0.111587
Type-III	0.110321	0.12199	0.078899	0.132698
Type-IV	0.190106	0.161978	0.236698	0.159087
f _j [*]	0.190106	0.161978	0.236698	0.159087
f _j ^{**}	0.06501	0.03032	0	0.084444

Decision matrix

	Da+	Da-	Ca	Rank
Type-I	0.278576	0.112727	0.28808	2
Type-II	0.276672	0.046872	0.144872	1
Type-III	0.183198	0.137876	0.429421	3
Type-IV	0	0.307539	1	4

Appendix XXII.

The Indian Traditional Investment Casting Technology

➤ Location:

Two important centers were visited and comparative studies of the technology were done. The sites which were visited for understanding the technology are positioned as under (Figure-3.1):

- Dariapur, Guskara, Burdwan District, West Bengal ($23^{\circ}29'1''\text{N}$ $87^{\circ}44'6''\text{E}$) India.
- Bikna Shilpa Danga, Bankura District, West Bengal ($23^{\circ}15.3''\text{N}$ $87^{\circ}5.9''\text{E}$), India.



(a) Location of Dariapur and Bikna, West Bengal, India



(b) Entrance of Dariapur, Guskara



(c) Entrance of Bikna, Bankura

Figure.: Location of the craft village with the Main Gate (right)

Table: Materials used for Core and Mold

	Type of Clay and Sand		Components
1.	Core Clay	Core remained within Castings- Ex: Hollow Models	Fine Kaolinite + Sand
		Core extracted (Ex: Utensils)	Kaolinite + Rice husk + Cow Dung + Jute Cuttings + Sand
2.	Primary Mold Coating Clay		Very fine Kaolinite
3.	Secondary Mold Coating Clay		Kaolinite + Rice husk + Cow Dung + Jute Cuttings + Sand
4.	Sand		Silica Sand (Medium/Fine)

Table: Materials used for Pattern

	Mixture- 1	Mixture- 2	Mixture- 3
Materials Used	Petroleum tar (Pitch) (65%) + Sal Dammar resin (35%)	Sal Dammar resin (40%) + Bees wax (60%)	Sal Dammar resin (40%) + Bees wax (20%) + Paraffin wax (40%)
Use	Primary coating over Clay core, Simple designs	Making solid extended section, like legs, hands	Making threads, Complicated designs

➤ Core and Pattern Making

Clay core and Wax Pattern Preparation were shown in the following figure.

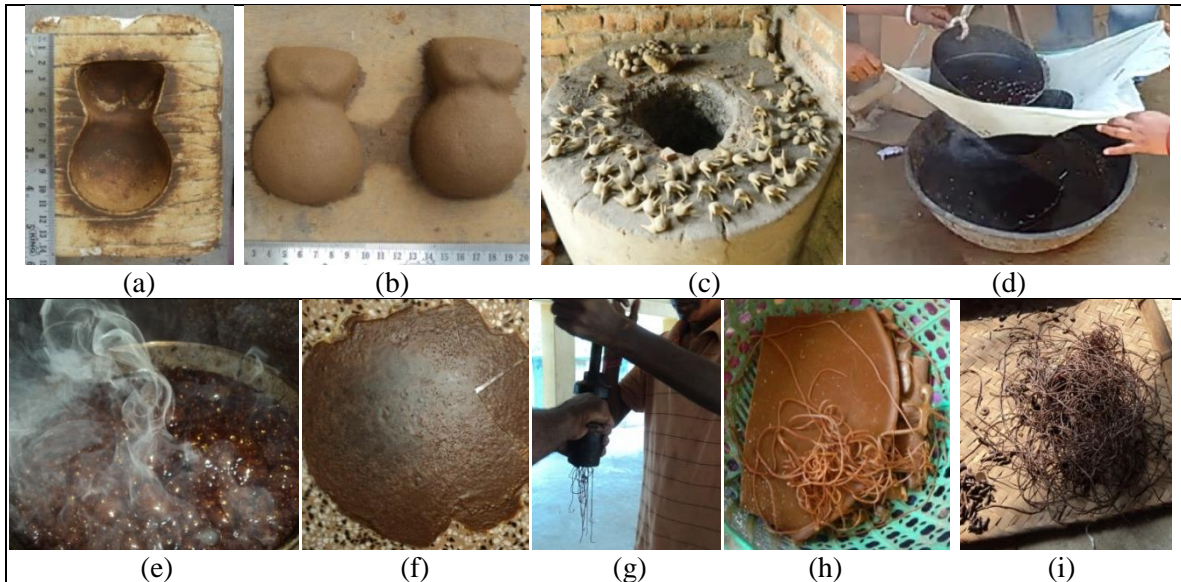


Figure: Preparation of Clay core and Wax Pattern Material: (a) Die, (b) Clay Core, (c) Handmade cores,

(d) Pitch + Bee's Wax mixture making, (e) (f) Sal Dammar Resin + Bee's Wax mixture, (g) Wax thread production by Extrusion, (h) (i) Wax Thread and Thin Strip of Wax mixture

➤ **Process of the Casting**

Table: Production stages of investment casting

Clay Core making (For Hollow casting): Clay cores are generally produced by handmade but for batch production and less complicated shape cores are often made using Die.



Wax pattern making: Utilizing thin wax sheets (0.7 to 2mm), fine and coarse wax threads (1-3mm), as well as diverse wax designs, patterns are crafted. In hollow casting, patterns stick to the clay core; in solid casting, patterns are coreless or attached to a clay base.



Gating: A wax thread is attached to make a gate.



Mold making: Very Fine clay is pasted over the pattern as primary coating clay of facing clay. Then secondary coating clay or backing clay is pasted layer by layer over the primary coating. Then it is assembled with the gating system containing a funnel and it is left under sunlight for drying.

Another technique: Metal scraps are put into the funnel and covered with clay.



Mold firing: The dried mold is pre-heated before putting into the furnace. The mold is heated as red hot at 1000°C temperature (approx.) into the furnace.



Melting and pouring: (i) Metal is melted (950°C-1000°C) in a separate furnace and is poured into the red hot mold outside the furnace.
(ii) Other technique: The combined mold metal arrangement heated until the metal melted. Mold is inverted for melted metal to fill up the vacant mold cavity.



Fettling and Finishing: After cooling mold is broken down and is made ready after fettling and polishing.



(a)



(b)



(c)



(d)



(e)



(f)



(g)



(h)



(i)



(j)



(k)



(l)



(m)

Figure: Production Steps of a Model of Tribal Couple: (a) Clay core, (b) Part of Wax Pattern of the Model, (c) Primary Wax Pattern over core, (d) Wax Pattern with Design, (e) Primary Clay Coating , (f) mold, (g) funnel attached to the mold, (h) metal scrap filled crucible, (i) Covered clay mold with fixed crucible, (j) pouring of liquid metal, (k) fired mold tilting for liquid metal pouring (l) Model with Gating System, (m) Final product.

➤ Divergence in Furnace Design and Firing Mechanism

Different type of furnace was used in two places for a different purpose. The schematic diagrams and pictorial view of both the furnaces are shown in following figures. In Bikna, Bankura; a cylindrical permanent closed furnace is used, but in Dariapur, Guskara temporary open type furnace is used. Natural convection and electrical fan supply the air for burning in Bikna but in Guskara only Natural convection is the only way. In Bikna only good quality coal is used as Fuel, but in Guskara Coal is used with cow dung cake. The temperature inside the furnaces was measured using thermocouple and it was found that the furnace temperature at Bikna was much more than Guskara. So, it can be concluded that the liquid metal is more superheated as well as the mold temperature is so high in Bikna.

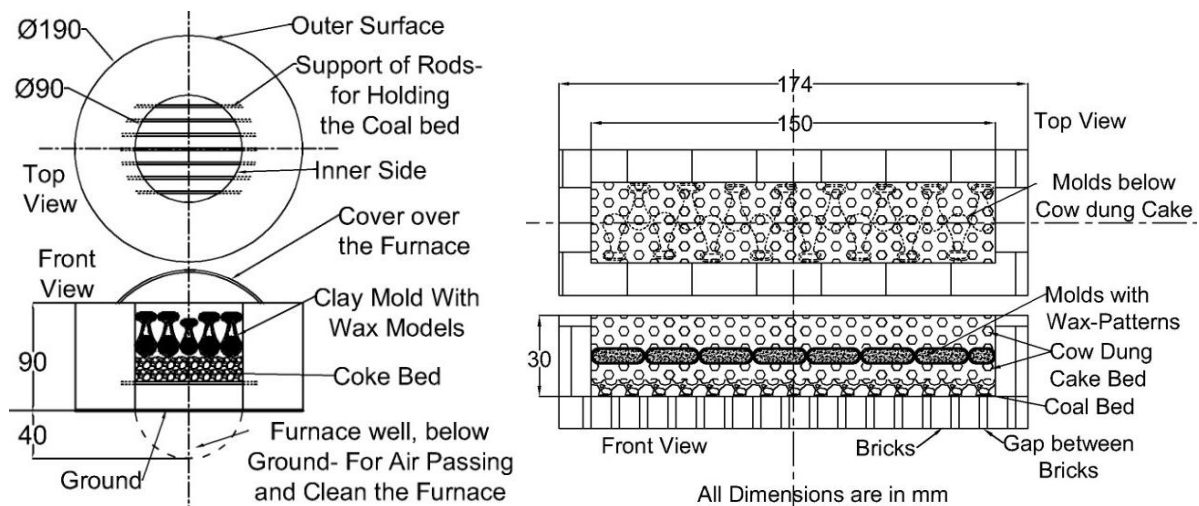


Figure: Schematic diagram of Permanent Furnaces made by clay and Brick at Bikna-Bankura (left) and Temporary Furnace made by only brick at Dariapur- Guskara (Right) (All dimensions are in mm)



Figure: Permanent Furnace at Bikna (left), Temporary Furnace at Guskara, (Right)

➤ Contrast in Mold Creation and Firing Process

Mold preparation and firing stand as pivotal factors influencing casting quality. A hole is pierced in the clay crucible, allowing the escape of Zinc vapor. This aids artisans in determining the metal's melting status.

In Bikna a 2-3 mm hole was present initially in the mold. For the same purpose, in Guskara a large hole (30 - 40 mm diameter) is made. In Bikna the hole is closed very fast using clay just after withdrawing from the furnace. Then the turning of the mold (which is actually pouring of liquid metal) is done. But in Guskara the hole is remained open.

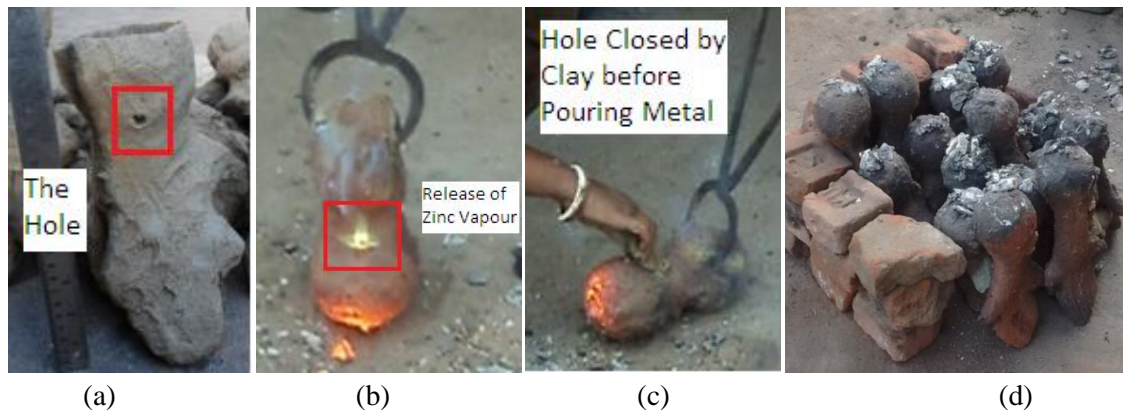


Figure: Bikna-Bankura: (a) Hole in the mold, (b) the mold, just after withdrawn from furnace, (c) closing the hole using clay before tilting the mold for pouring liquid metal in the mold, (d) All the molds are waiting for cooling

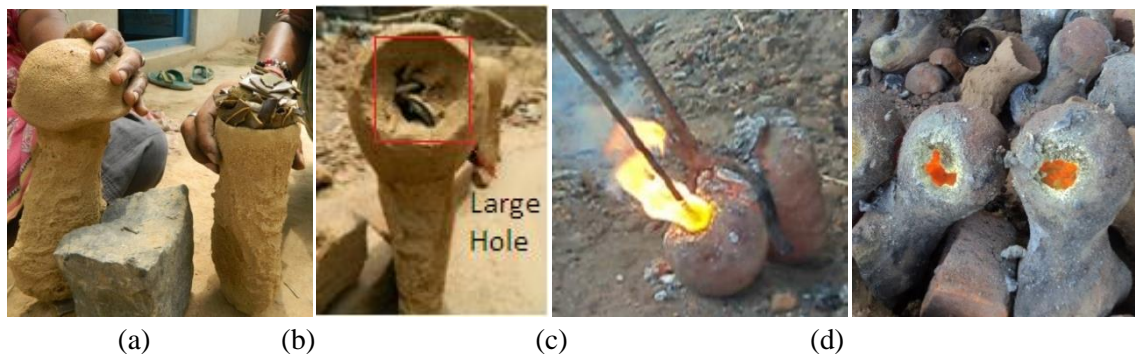


Figure: Dariapur- Guskara: (a) Crucible of mold Making, (b) A large passage made on crucible, (c) Pricking the hole after withdrawn and before tilting the mold for pouring liquid metal in the mold, (d) All the mold are resting for cooling

➤ Type of Gating System

Different types of gating system, which controls the liquid metal flow, are used in both Guskara and Bikna were shown in figure-3.9 and 3.10 respectively. Diameters of the Gate attached to the Castings at Bikna are 4mm to 5mm but at Guskara Gate Diameters were generally 2 mm to 3 mm. For very small casting, it may differ. In Bikna the gates are always attached in the thicker section of the pattern, so that liquid metal flow is smoother. Multiple Gates are used for large size or complicated casting both places.

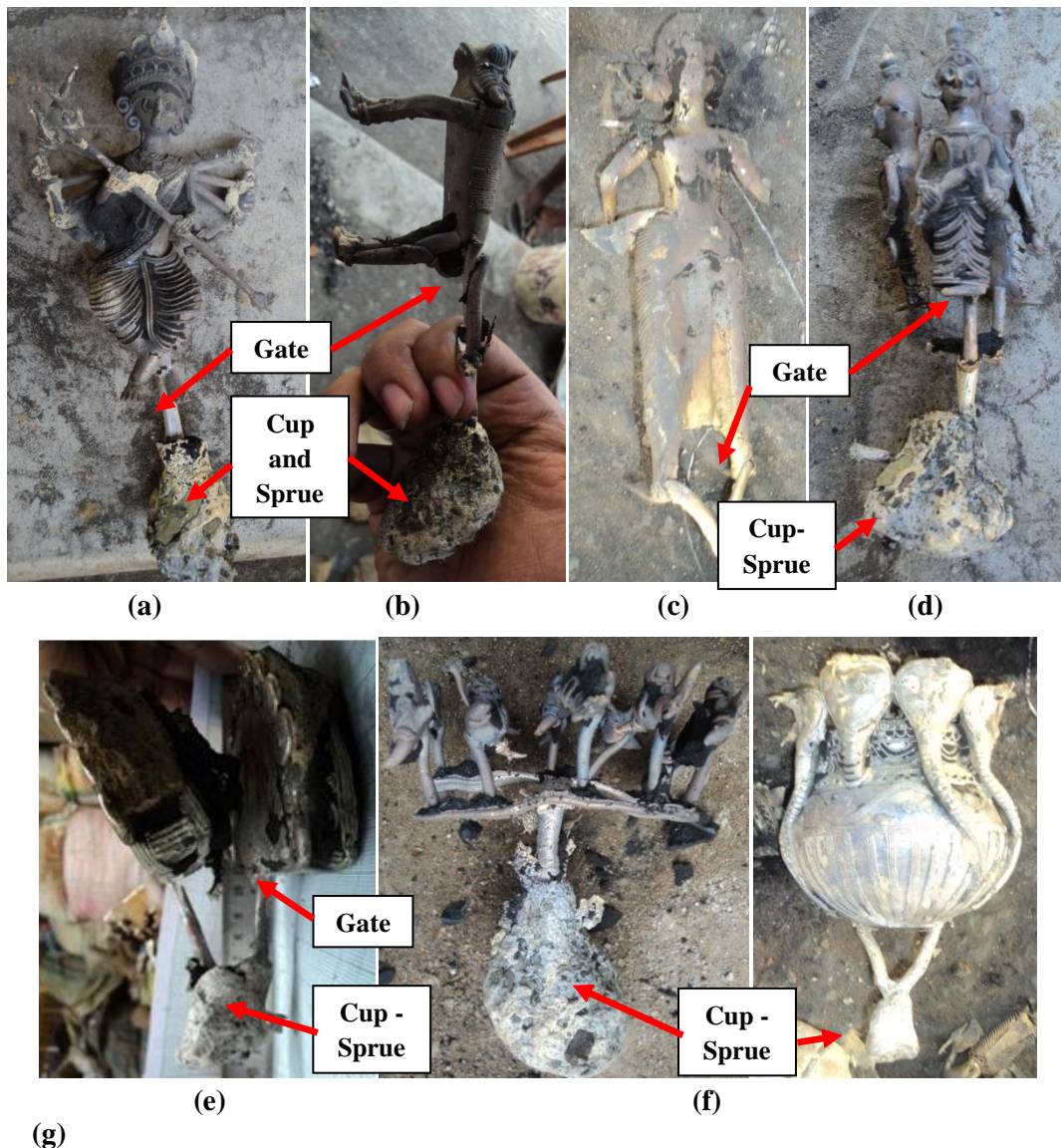


Figure: Few Casting With Gating System at **Bikna-Bankura:** (a) (b) Simple Gating, (c) Multiple Gating for a Single Mode, (d) (e) and (f) Multiple Gating for few small size casting having single Cup-Sprue, (g) Multiple Gating of a large size Casting

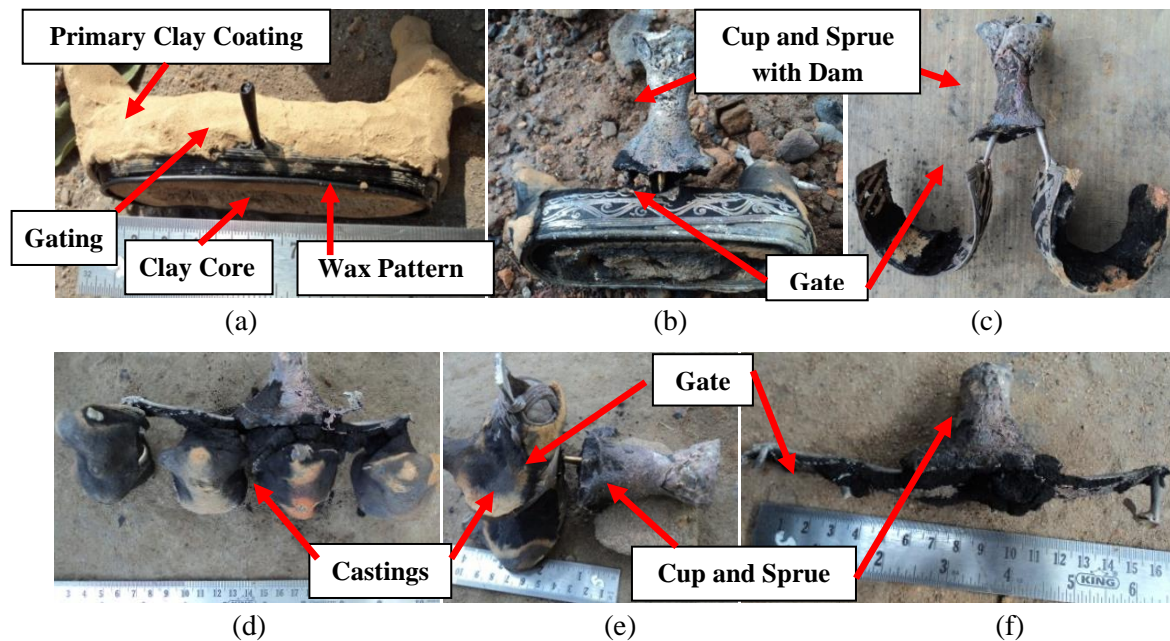


Figure: Few Casting With Gating System at **Dariapur- Guskara:** (a) Sprue attached on wax pattern, (b) A Model with Gate and Sprue, (c) A Horn Gate with Cast Sample, (d) Multiple gating System with models (Front View), (e) Side View, (f) The Gating System separately

➤ Defects of Casting

The defects are generally found in cast products were shown here. It was seen that the castings are more defect free and hence very low rejection rate in Bikna compared to the products of Guskara.

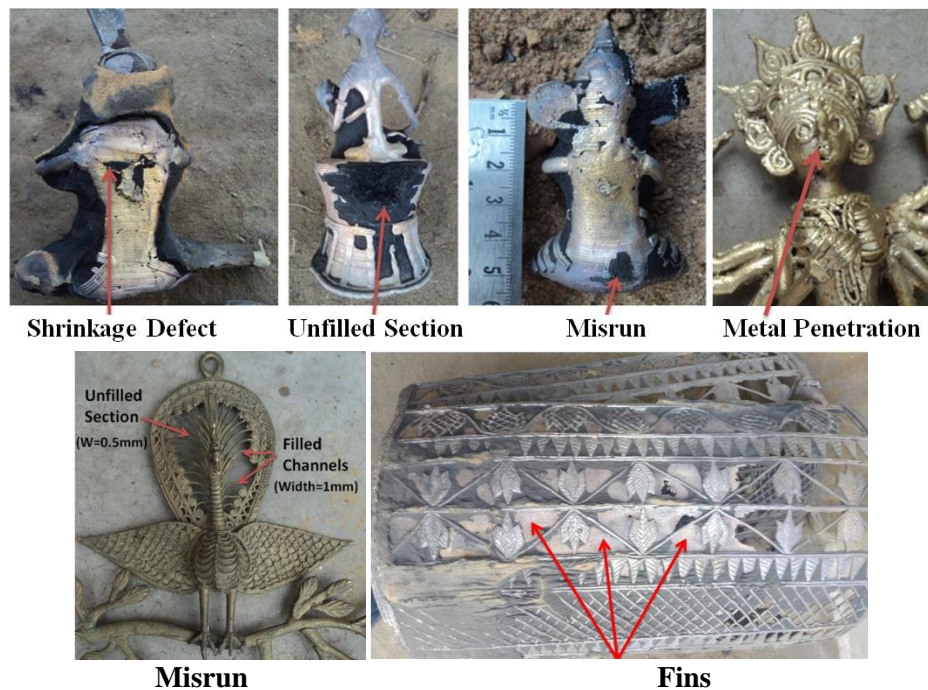


Figure: Few Casting defects at Dariapur (Top) and Bikna (Bottom)

➤ Premium-quality castings



(a)



(b)



(c)



(d)



(e)



(f)



(g)



(h)



(i)



(j)



(k)

Figure: Premium-quality castings from Guskara and Bikna. (a) (b) (c) Models and divine sculpture, (d) (e) Wall hooks, (f) Oil Lamp, (g) (h) Pen stand, (i) Book holder, (j) Napkin holder, (k) Basket

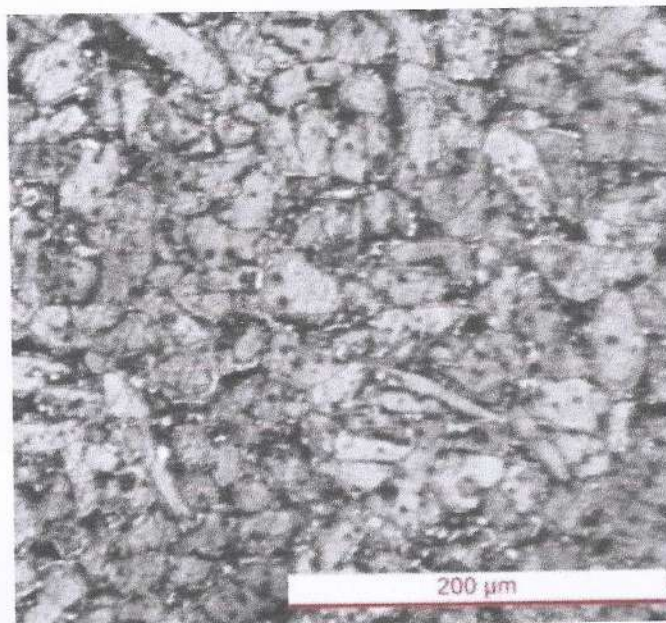
➤ Characterization

Table: Chemical Analysis and Hardness of Brass metals used for Casting

	Chemical Analysis (%)						Bulk Hardness (HV 5/10)
	Cu	Zn	Pb	Sn	Fe	Other	
Guskara	62.5	30.39	4.18	1.39	1.04	0.5	72.6
Bikna	61.12	33.63	3.51	1.16	0.25	0.33	82.3



Bikna (100X)



Guskara (100X)

Figure: Microstructure of Cast Sample, (Etchant: FeCl_3 in HCl) Typical α - β cast brass with coarse dendrites are seen. Pb is distributed.

Soumyajit Ray
21/03/2024

Ajman
21/03/24

Dr. Akshay K. Pramanick
Professor
Department of Metallurgical &
Material Engineering
Jadavpur University, Kolkata-700 032